

## **General Disclaimer**

### **One or more of the Following Statements may affect this Document**

- This document has been reproduced from the best copy furnished by the organizational source. It is being released in the interest of making available as much information as possible.
- This document may contain data, which exceeds the sheet parameters. It was furnished in this condition by the organizational source and is the best copy available.
- This document may contain tone-on-tone or color graphs, charts and/or pictures, which have been reproduced in black and white.
- This document is paginated as submitted by the original source.
- Portions of this document are not fully legible due to the historical nature of some of the material. However, it is the best reproduction available from the original submission.

(NASA-CR-145125) DEVELOPMENT OF TECHNOLOGY  
FOR THE FABRICATION OF RELIABLE LAMINAR FLOW  
CONTROL PANELS ON SUBSONIC TRANSPORTS  
(Douglas Aircraft Co., Inc.) 214 p  
HC A10/MF A01

N77-17038

Unclas  
16265

CSCI 01C G3/25

# DEVELOPMENT OF TECHNOLOGY FOR THE FABRICATION OF RELIABLE LAMINAR FLOW CONTROL PANELS ON SUBSONIC TRANSPORTS



PREPARED UNDER CONTRACT NO. NAS 1-14408

BY

MCDONNELL DOUGLAS CORPORATION  
DOUGLAS AIRCRAFT COMPANY  
LONG BEACH, CALIFORNIA

FOR



National Aeronautics and  
Space Administration



DEVELOPMENT OF TECHNOLOGY FOR THE  
FABRICATION OF RELIABLE LAMINAR FLOW CONTROL  
PANELS ON SUBSONIC TRANSPORTS

OCTOBER 1976

PREPARED UNDER CONTRACT NO. NAS1-14408

FOR



LANGLEY RESEARCH CENTER  
NATIONAL AERONAUTICS AND SPACE ADMINISTRATION  
LANGLEY STATION, HAMPTON, VIRGINIA

MCDONNELL DOUGLAS CORPORATION  
DOUGLAS AIRCRAFT COMPANY  
LONG BEACH, CALIFORNIA

## FOREWORD

This document reports the contract study results performed for NASA, "Development of Technology for the Fabrication of Reliable Laminar Flow Control Panels on Subsonic Transports", by the Douglas Aircraft Company, McDonnell Douglas Corporation. The work included is closely allied to the current on-going study "Evaluation of Laminar Flow Control System Concepts for Subsonic Commercial Transport Aircraft", NASA Contract No. NAS1-14632.

The NASA technical monitor for the study was W. E. Howell, Materials Division, Composites Section, Langley Research Center, Hampton, Virginia.

Douglas task leaders on the study are as follows:



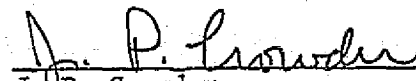
I. M. Goldsmith  
Principal Investigator



W. D. Nelson  
Structures

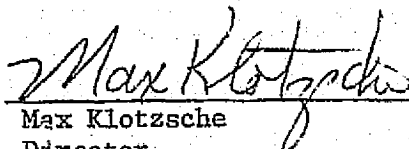


E. M. Kunreuther  
Materials and Producibility



J. P. Crowder  
Aerodynamics Testing & Analysis

Approval



Max Klotzsche  
Director  
Program Engineering - ACEE

# TABLE OF CONTENTS

	Page
List of Figures . . . . .	vii
List of Tables . . . . .	xi
List of Symbols . . . . .	xiii
Abstract . . . . .	xvii
Introduction . . . . .	1
Summary and Conclusions . . . . .	5
Recommendations . . . . .	9
General . . . . .	9
Detailed Materials . . . . .	10
LFC Panel Structural Concepts . . . . .	11
Functional Design Approach . . . . .	11
General Criteria and Considerations . . . . .	14
Major Maintenance Period Design Life Criteria . . . . .	14
Other Criteria . . . . .	15
Panel Design . . . . .	16
Surface Material Selection . . . . .	16
Stiffened Panel Concepts . . . . .	18
Test Panel Descriptions . . . . .	21
Candidate Surface Materials . . . . .	21
Doweave . . . . .	21
Leno No. 205 Weave Kevlar/Epoxy . . . . .	28
Dynapore Monolayer . . . . .	34
Microperforated Plate on a Substrate . . . . .	43
No. 143 Weave Kevlar/Epoxy . . . . .	48
Electron Beam Perforation of No. 143 Weave Kevlar/Epoxy Panels . . . . .	48
Lock Core Test Panel . . . . .	60
Isogrid Test Panel . . . . .	64
Reproducibility of Composite Panel Porosity . . . . .	67
Airflow Test Results . . . . .	71
General . . . . .	71
Derivation of Target Airflow Range . . . . .	73
Airflow Data Correlations . . . . .	75
Woven Laminates . . . . .	75
Dynapore . . . . .	89
Electron Beam Perforations . . . . .	91
Stiffened Panels . . . . .	99

TABLE OF CONTENTS (continued)	Page
Effective Porosity . . . . .	103
Contamination Tests . . . . .	117
Summary of Test Results . . . . .	119
Analytical Prediction of Flow Characteristics Through Porous Material . . . . .	121
Structural Test Results . . . . .	125
Doweave Strength Test Results . . . . .	125
Leno No. 205 Weave Kevlar/Epoxy Strength Test Results . . . . .	130
Dynapore Monolayer . . . . .	130
Structural Assessment . . . . .	139
Load/Skin Analysis . . . . .	139
Thermal Strain Analysis . . . . .	142
Perforated Panel Stress Concentrations . . . . .	145
Cost and Weight Comparison . . . . .	145
Preliminary Design Sketches . . . . .	147
References . . . . .	153
Appendix A - Airflow Test Apparatus . . . . .	155
Appendix B - Airflow Test Procedure . . . . .	161
Appendix C - Data Reduction Procedures . . . . .	163
Appendix D - Basic Airflow Pressure Drop Test Data and Panel Descriptions . . . . .	167



## LIST OF FIGURES

FIGURE		Page
1	LFC Transport Study General Arrangement Conventional Base Case (3 Engines -200 Passengers)	2
2	Typical Pressure Drop/Velocity Relationship for the Several Materials Tested	5
3	Demonstrated Reproducibility of Composite Panels Using Specific Resin Control	7
4	Basic Schemes for Pressure Drop Panels	12
5	Doweave Panel With Mat	22
6	Doweave Panel Without Mat	22
7	Doweave Panel - No. 23 - No Mat	23
8	Doweave Panel No. 24 With Mat	24
9	Doweave Panel No. 73 - Face Sheet for Stiffened Panels	25
10	Doweave Panels - Comparator Views	26
11	Doweave and Layup Panel Variations	27
12	Leno Weave Panel	29
13	Leno Weave Panel	29
14	Leno Weave Panel No. 88 - No Mat	30
15	Leno Weave Panel No. 89 - With Mat	31
16	Leno Weave Panels - Comparator Views	32
17	Typical Effects of Material and Layup	33
18	Dutch Weave Wire Cloth Construction	34
19	Dynapore Mesh Flat Surface Smoothness After Calendaring	35
20	Dynapore 316L Stainless Mesh	36
21	Dynapore 50 X 250 Mesh Typical Air Flow Paths Through the Material	38
22	Dynapore 50 X 250 Mesh Typical Thickness Deformation at Cross Sections of Mesh	39
23	Dynapore 50 X 250 Mesh Broken Bond Interface Region (Pt. A) Typical Dimple Rupture Evidence	40
24	Dynapore 50 X 250 Mesh Broken Bond Interface Region (Pt. B) Typical Dimple Rupture Evidence	41
25	Dynapore 24 X 110 Mesh - Surface Deformation and Evidence of Unbonded Mesh Wires	42
26	Leno with Microperforated Plate Facing	45
27	Leno with Microperforated Plate Facing	45
28	MPP on Substrate Concept	47

# LIST OF FIGURES (continued)

	Page
29 Electron Beam Perforated Panel and Panel No. Index	50
30 Electron Beam Drilled Composite Panels	51
31 Electron Beam Drilled Composite Panel (No. 149)	52
32 Electron Beam Drilled Composite Panel (No. 49)	53
33 Hole Spacing .243" Hole Size .008 Electron Beam Drilled Panels + .007 Ti Plate	55
34 Electron Beam Drilled Panels	56
35 Electron Beam Drilled Panels	57
36 Electron Beam Drilled Panels	58
37 Lock Core Basic Panel Definition	61
38 Backface Hole Patterns, Specimens 92 and 93	62
39 Face Sheet of Lock Core Panel	63
40 Lock Core Stiffened Panel	63
41 Scheme for No. 94 Grid Panel	65
42 Isogrid Stiffened Panel	66
43 Demonstrated Reproducibility of Composite Panels Using Specific Resin Control	69
44 Relationship Between Pressure Drop vs Flow Rate and Effective Porosity at Standard Conditions	72
45 Effect of Specimen Reproducibility on Airflow Characteristics	76
46 Effect of Specimen Reproducibility on Effective Porosity	77
47.1 Pressure Drop Variations with Flow Rate	78
47.2 Pressure Drop Variations with Flow Rate	79
47.3 Pressure Drop Variations with Flow Rate	80
47.4 Pressure Drop Variations with Flow Rate	82
47.5 Pressure Drop Variations with Flow Rate	83
47.6 Pressure Drop Variations with Flow Rate	84
47.7 Pressure Drop Variations with Flow Rate	85
47.8 Pressure Drop Variations with Flow Rate	86
47.9 Pressure Drop Variations with Flow Rate	87
47.10 Pressure Drop Variations with Flow Rate	88
47.11 Pressure Drop Variations with Flow Rate	90
48.1 Electron Beam Drilled Specimens Pressure Drop Variations with Flow Rate	93

# LIST OF FIGURES (continued)

48.2	Electron Beam Drilled Specimens Pressure Drop Variations with Flow Rate	94
48.3	Electron Beam Drilled Specimens Pressure Drop Variations with Flow Rate	95
49.1	Electron Beam Drilled Specimens Discharge Coefficient Variations with Hole Reynolds Number	96
49.2	Electron Beam Drilled Specimens Discharge Coefficient Variations With Hole Reynolds Number	97
49.3	Electron Beam Drilled Specimens Discharge Coefficient Variations with Hole Reynolds Number	98
49.4	Electron Beam Drilled Specimens Discharge Coefficient Variations with Hole Reynolds Number	100
50	Pressure Drop Variation with Flow Rate	101
51	Pressure Drop Variations with Flow Rate	102
52.1	Effective Porosity Variations with Reynolds Number	104
52.2	Effective Porosity Variations with Reynolds Number	105
52.3	Effective Porosity Variations with Reynolds Number	106
52.4	Effective Porosity Variations with Reynolds Number	107
52.5	Effective Porosity Variations with Reynolds Number	108
52.6	Effective Porosity Variations with Reynolds Number	109
52.7	Effective Porosity Variations with Reynolds Number	110
52.8	Effective Porosity Variations with Reynolds Number	111
52.9	Effective Porosity Variations with Reynolds Number	112
52.10	Effective Porosity Variations with Reynolds Number	113
52.11	Effective Porosity Variations with Reynolds Number	114
53	Effective Porosity Variations with Reynolds Number	115
54	Effective Porosity Variations with Reynolds Number	116
55	Effects of Contamination on Porosity	118
56	90-Degree Doweave Beam Tension Test Failures	127
57	Doweave Beam Compression Specimen	128
58	Trend Effect of Doweave Plies on Airflow	129
59	No. 205 Leno Compression Beam Failures	132
60	No. 205 Leno Compression Beam Failures	133
61	Extent of Wire Deformation During Compaction, Dynapore Monolayer	137
62	Required LFC Panel Limit Strains and Strengths	140
63	Sandwich LFC Panel on Blade-Stiffened Wing Cover	148

# LIST OF FIGURES (continued)

64	Skin and Stringer with Double Grid Concept	149
65	Double Sandwich Panel on Corrugated Primary Structure	151
A-1	Douglas Flow Resistance Test Rig - Front View	156
A-2	Douglas Flow Resistance Test Rig - Rear View	157
A-3	Schematic Diagram of Airflow Test Apparatus	158
D-1	Airflow Test Results	168
D-2	Airflow Test Results	169
D-3	Airflow Test Results	170
D-4	Airflow Test Results	171
D-5	Airflow Test Results	172
D-6	Airflow Test Results	173
D-7	Airflow Test Results	174
D-8	Airflow Test Results	175
D-9	Airflow Test Results	176
D-10	Airflow Test Results	177
D-11	Airflow Test Results	178
D-12	Airflow Test Results	179
D-13	Airflow Test Results	180
D-14	Airflow Test Results	181
D-15	Airflow Test Results	182
D-16	Airflow Test Results	183
D-17	Airflow Test Results	184
D-18	Demonstrated Reproducibility of Composite Panels Using Specific Resin Control	185



# LIST OF TABLES

Table No.		Page
I	Matrix of LFC Surface Concepts . . . . .	6
II	LFC Candidate Surfaces List . . . . .	17
III	Initial Screening of LFC Surface Concepts . . . . .	19
IV	Micro-Perforated Plate Characteristics . . . . .	44
V	No. 143 Kevlar/200 Denier Doweave Laminates . . . . .	49
VI	As Inspected Properties of E.B. Perforations . . . . .	59
VII	Strength and Stiffness of 200-Denier Doweave Kevlar 29/Epoxy . . . . .	126
VIII	Strength and Stiffness of #205 Leno Kevlar/Epoxy . . . . .	131
IX	Dynapore <sup>TM</sup> Monolayer - Thickness Versus Airflow . . . . .	134
X	Tensile Strength and Stiffness of 316L Dynapore Monolayer . . . . .	135
XI	Yield Strain Data - Dynapore Monolayer . . . . .	141
XII	Thermal Strain Compatibilities of Dissimilar Materials (1) . . . . .	143
XII	Continued from Page 1 . . . . .	144
XIII	Relative Costs and Weights - Kevlar Doweave Versus 316L Dynapore . . . . .	146
D-1	Description of Panel Construction . . . . .	186
D-II	Development of the Technology for the Fabrication of Reliable Laminar Flow Control Panels . . . . .	194
D-III	Panels Associated with Typical Comparisons . . . . .	199
D-IV	Panel Fabrication Description . . . . .	201

# LIST OF SYMBOLS

## Symbols

$A$	Specimen flow area
$E$	Elastic modulus
$E_i$	Elastic modulus, initial
$E_s$	Elastic modulus, second
$E_i/\rho$	Specific modulus, initial
$EI$	Bending stiffness (wing box)
$F$	Stress
$F^{tu}/\rho$	Specific strength
$GJ$	Torsional stiffness (wing box)
$M$	Air flow Mach number
$P_1$	Specimen upstream pressure (Appendix C)
$P_2$	Flow meter upstream pressure (Appendix C)
$\Delta P_1, \Delta P_2$	Flow meter differential pressure
$P_a$	Flow meter upstream pressure
$Q_1, Q_2$	Flow meter uncorrected flow rate
$Q$	Volumetric flow rate
$Re$	Unit Reynolds number
$T$	Air flow temperature (Appendix C)
$V_s$	Standard velocity
$V_i$	Ideal velocity
$t$	Thickness
$t_o$	Initial thickness

# LIST OF SYMBOLS (continued)

$t_f$	Final thickness
$q$	Mass flow rate
$q_i$	Ideal mass flow rate
$\alpha$	Thermal expansion coefficient
$\Delta\alpha$	Difference in thermal expansion coefficients
$\epsilon_{lim}$	Allowable limit strain
$\mu$	Strain in micro-inches
$\mu$	Air viscosity
$\rho$	Air density
$\sigma$	Effective porosity

## Subscripts

c	Compression
D	Doweave ply
f	Facing
L	Leno weave ply
s (s)	Symmetrical about laminate midplane
T	When used, total no. of directional plies are in brackets.
x	In the laminate 0-degree direction.
143, 120, 181	Fabric ply weave designation.

## Superscripts

cl	Compression limit
cu	Compression ultimate
tl	Tension limit
tu	Tension ultimate
ty	Tension yield

## LIST OF SYMBOLS (continued)

### Prefixes

k	Kilo
M	Mega
G	giga
c	Centi

### Materials

316L	316L low carbon 316 stainless
17-7	PH 17-7 stainless steel
Al	Aluminum
B/E	Boron/epoxy
Gr <sub>s</sub> /E	High-Strength Graphite/Epoxy
Kv/E	Kevlar/epoxy
MPP 21	Micro-perforated plate, Cat. No. 21
MPP 24	Micro-perforated plate, Cat. No. 24
Ti	Titanium

### Miscellaneous

$[0/90]_n$	Degree orientations of ply pattern, per ply. Number subscript indicates pattern repeats in total laminate. See T, s subscripts above.
------------	---



## ABSTRACT

The study described herein is in response to NASA Langley Contract NAS1-14408 and is an initial step in the necessary research required for development of a lightweight, efficient LFC surface material. The study is exploratory, is preliminary in nature, and concentrates on the feasibility of porous composite materials (Kevlar, Doweave and Leno Weave) as compared to the metallic 316L stainless Dynapore surfaces and electron beam drilled composite surfaces. Areas of investigation are

- selection of the LFC-suitable surface materials, structural materials, and fabrication techniques for the LFC aircraft skins;
- aerodynamic static air flow test results in terms of pressure drop through the LFC panel and the corresponding effective porosity;
- structural design definition and analyses of the panels;
- contamination effects on static pressure drop and effective porosity.

The practical goal to which the LFC surface panel characteristics are directed is simulation of the amount of suction required to maintain laminar flow for the flight operational conditions compatible with a 200 passenger commercial transport aircraft designed for  $M_{\text{cruise}} = .8$ , 5500 nautical mile range (10,160 km) operating at 30,000 feet to 40,000 feet (91.2 to 122.0 km).

General conclusions from the study are as follows:

- Woven composites, Dynapore, and electron beam drilled panels all show promise as an LFC surface material. Further development is definitely warranted.
- Repeatable porosity in woven composite panels is considered an achievable production goal.
- Dynapore is a definite contender provided contamination of the pores is not a limiting factor.
- Transverse flow tests of these materials is a requirement to satisfy aerodynamic smoothness criterion question.
- Detailed structural analysis of the panels and their integration into an aircraft configuration is required.
- Preliminary comparative cost evaluations of the several concepts should be initiated.

Recommendations are included for developmental follow-on work in the areas of aerodynamic testing, structural concept design and test; and materials characteristics and fabrication.

## INTRODUCTION

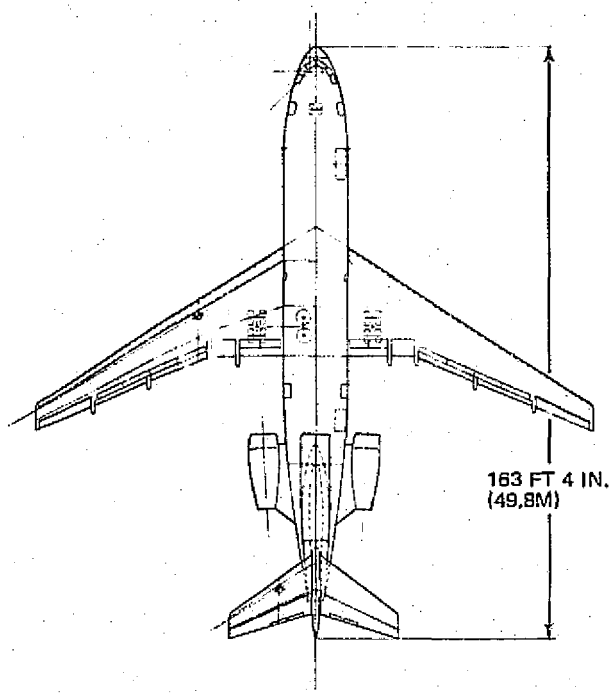
Current long range planning for either commercial or military aircraft has placed emphasis on fuel conservatism and/or the attainment of long range/long endurance. The incorporation of laminar flow control (LFC) in the aircraft design, with its possibilities for large zero lift drag reduction, is thus of particular interest for the next generation aircraft development. Of all the drag reduction concepts, LFC represents the largest single potential improvement. Consequently, the development of a light weight laminar flow control surface material, which is efficient aerodynamically, competitive from the points of view of fabrication and maintenance, and environmentally practical is definitely worthwhile. This particular study, described herein, is in response to NASA Langley Contract NAS1-14408, and is an initial step in the necessary research required for development of a LFC surface material. It is to be emphasized that this study is exploratory and preliminary in nature. The results of the study confirm the feasibility of the concept and are the basis of the recommendations for further study.

The scope of the study, which concentrates on the feasibility of porous composite material as compared to the metallic 316L stainless Dynapore surfaces, and electron beam drilled composite surfaces, includes

- selection of the LFC-suitable surface materials, structural materials, and fabrication techniques for the "C aircraft skins;
- aerodynamic static air flow test results in terms of pressure drop through the panel and the corresponding effective porosity;
- structural design definition and analyses of the panels;
- contamination effects on static pressure drop and effective porosity.

The goal, to which the LFC surface panel static airflow characteristics are directed, is simulation of the amount of suction required to maintain laminar flow for the flight operational conditions compatible with a 200 passenger commercial transport aircraft designed for a 5500 nautical mile range at  $M_{\text{cruise}} = .8$  and cruise altitudes between 30,000 ft to 40,000 ft. A typical aircraft configuration is as shown in Figure 1.

Relating these general flight conditions to the corresponding static flow rates and pressure drop conditions of the tests results in the following variations in pressure distribution and suction quantities.



**PAYLOAD CAPACITY**

• BASE CASE - MIXED CLASS			
FIRST CLASS	=	6 ABREAST AT 35 IN. PITCH	= 20 (10 PERCENT)
ECONOMY CLASS	=	8 ABREAST AT 34 IN. PITCH	= 180 (90 PERCENT)
TOTAL		200 SEATS	

• CONVENTIONAL GALLEY

• CARGO VOLUME -			
FORWARD BAY	=	12 LD-3 CONTAINERS AT 158 CU FT	= 1896 CU FT (53.7 CU M)
AFT BAY	=	6 LD-3 CONTAINERS AT 160 CU FT	= 948 CU FT (26.8 CU M)
	=	BULK	= 380 CU FT (10.8 CU M)
TOTAL		3224 CU FT (91.3 CU M)	

CHARACTERISTICS DATA			
ITEM	WING	HORIZONTAL STABILIZER	VERTICAL STABILIZER
AREA, SQ FT (SQ M)	2400 (223)	575 (53)	554 (51)
ASPECT RATIO	10.0	4.0	0.69
TAPER RATIO	0.39	0.40	0.609
SWEEP, C/4	30 DEG	32 DEG	45 DEG
DIHEDRAL	4 DEG AT C/4	-3 DEG	
TAIL VOLUME		1.058	0.037

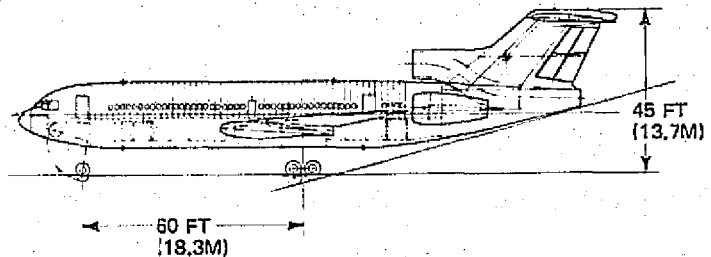


FIGURE 1. PROPOSED LFC TRANSPORT STUDY GENERAL ARRANGEMENT - CONVENTIONAL BASE CASE (3 ENGINES - 200 PASSENGERS)

	High Flow Condition	Low Flow Condition
$C_Q$	$\approx .0010$	$\approx .0003$
Mass Flow	0.025 lb/sec/ft <sup>2</sup> (0.12 kg/sec/m <sup>2</sup> )	0.005 lb/sec/ft <sup>2</sup> (0.024 kg/sec/m <sup>2</sup> )
$\Delta P_{\text{across surface}}$	1 lb/ft <sup>2</sup> $\rightarrow$ 100 lb/ft <sup>2</sup> (48 Pa $\rightarrow$ 4.8 kPa)	5 lb/ft <sup>2</sup> $\rightarrow$ 100 lb/ft <sup>2</sup> (.24 kPa $\rightarrow$ 4.8 kPa)

These ranges are based on flight conditions at  $M_{\text{cruise}} = .8$  at altitudes between 30,000 ft to 40,000 ft. These ranges of pressure drop account for the conditions where -

- all of the desired pressure drop is taken across the face sheet, or where
- only a portion of the pressure drop is taken across the face sheet to the collector duct.

These brackets, representing the operational flight conditions, are shown on the air flow plots as a means of orienting each LFC surface panel.

The 107 test panels fabricated during the program represent effects of surface material, construction, processing, panel thickness, ply orientation, surface treatment such as mat titanium or microperforated plate. The consideration of metal surfaces on the composite panel is in deference to environmental protection which may be required. In the learning process of finding the material thicknesses and porosity of interest for airflows, the panels tended to be too open for the particular operational regions of interest. Those results are included on the data analysis; however, all of such panels were not transmitted to NASA Langley for their structural testing.

The test panel description in subsequent sections of the report includes photographs at a high degree of magnification, utilizing reflected lighting, scanning electron microscope and the comparator. The detail of the material fabrication, made possible by the scanning electron microscope, is of particular interest. The comparator affords a means of obtaining an accurate correlation between the actual geometric porosity and the effective porosity, particularly in the case of the electron beam drilled panels. The question of capability of composite panel reproducibility is addressed.

Discussion, analysis, and correlation of aerodynamic test data and structural test analyses follows. An assessment of the structural feasibility of the LFC surface panels investigated, in a practical design application, is included.

The description of the aerodynamic airflow test facility, the airflow test procedure, the data reduction procedure, and the detailed test data and panel construction descriptions are included in Appendices A, B, C, and D, respectively.



## SUMMARY AND CONCLUSIONS

Emphasis of this program, NASA Contract NAS1-14408, is placed on the exploration of the feasibility of porous woven composite materials, using Dynapore 316L stainless mesh and electron beam drilled panels as bases of comparison, for laminar flow control (LFC) surfaces for aircraft. Materials and panel constructions taken into account in this study are summarized in the following matrix, Table I; off-the-shelf composite materials, the resin, and the impregnation processes are used in the study. Fabrication of all porous composite panel face sheets as well as the stiffened panels are done by Douglas. The Dynapore laminate is an experimental material by Michigan Dynamics to Douglas' specifications. The composite panels for electron beam drilling are fabricated by Douglas and supplied to Farrel Company (U.S. representative of Steigerwald Strahltechnik) for drilling to Douglas' specifications. With the exception of the Leno weave which did require a surfacing mat for smoothness, all of the panels felt smooth to the touch. It is to be emphasized that the airflow tests performed in this study provide static pressure drop data. Any final conclusions as to the aerodynamic smoothness evaluation of the panels must await transverse flow testing.

A general summary of the airflow test results is shown in Figure 2.

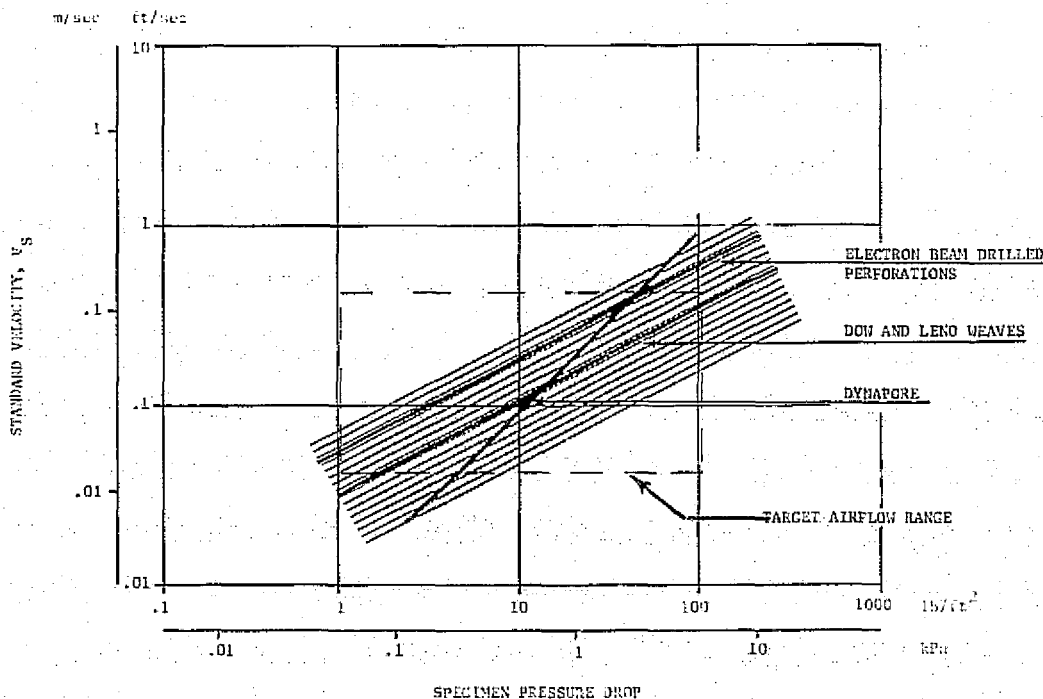

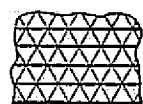


Figure 2. Typical Pressure Drop/Velocity Relationship for the Several Materials Tested

TABLE I  
MATRIX OF LFC SURFACE CONCEPTS\*

PANEL CONSTRUCTION					
LFC SURFACE CONCEPT	THICKNESS		NO. PLIES	LAY-UP	PROCESSING
	IN.	(MM)			
<b>POROUS WOVEN COMPOSITES</b>					
• DOWEAVE PANEL	0.010 → 0.060	(0.25 → 1.52)	2 → 12	VARIABLE DIRECTION PLY PATTERN AND USE OF MISC FABRICS.	120 MIN AT 250°F (394°K) OR 90 MIN AT 170°F (350°K) + 120 MIN AT 250°F (394°K)
• LENO PANEL	0.030 → 0.108	(0.76 → 2.74)	2 → 8		
• MISCELLANEOUS FABRICS			1 ↓		
120	0.005	(0.13)			
143	0.01	(0.25)			
181	0.01	(0.25)			
0.7 OZ/SQ YD CEREX NYLON RANDOM FIBER SURFACING MAT	0.003	(0.08)			
<b>DYNAPORE</b>					
<b>316L STAINLESS</b>					
• 24 x 110 MESH	0.0117 → 0.0120	(0.297 → 0.305)	MONOLAYER	PLAIN DUTCH WEAVE	COMPACTION/DIFFUSION BONDED/COMPACTION ↓
• 50 x 250 MESH	0.0062 → 0.0065	(0.157 → 0.165)	MONOLAYER	PLAIN DUTCH WEAVE	
			<u>HOLE SIZE</u>	<u>HOLE SPACING</u>	
			IN. (MM)	IN. (MM)	
<b>ELECTRON BEAM DRILLED</b>	0.028 → 0.072	(0.74 → 1.83)	0.004 → 0.026 (0.102 → 0.650)	0.135 → 0.243 (3.43 → 6.17)	EB DRILLED KEVLAR PANELS
<b>MICROPERFORATED PLATE ON SUBSTRATE</b>					
• NO. 24 316L STAINLESS	0.0013	(0.033)	0.0024 (0.061)	SQUARE WEAVE.	BONDED TO COMPOSITE OR EB DRILLED SURFACE ↓
• NO. 21 316L STAINLESS	0.0029	(0.074)	0.0046 (0.117)	SQUARE WEAVE.	
• TITANIUM FOIL	0.007	(0.178)			
			<u>NO. PLIES</u>	<u>LAY-UP</u>	
<b>STIFFENED PANELS</b>					
• LOCK CORE	0.456 → 0.475	(11.58 → 12.07)	8 (FACE SHEETS) 6 (WEB)		180 MIN AT 250°F (394°K) OR AUTOCLAVE 90 MIN AT 170°F (350°K) + 120 MIN AT 250°F (394°K) AT 50 PSI.
• ISOGRID	0.140 → 0.160	(3.56 → 4.06)	8 (FACE SHEETS) 0.05 x 0.05 IN. (1.27 x 1.27MM) GRID		GRID -- 240 MIN AT 350°F (450°K) 6 FACE SHEETS 120 MIN AT 250°F (394°K) 2 FACE SHEETS USED FOR BONDING ISOGRID -- 120 MIN AT 250°F (394°K)

NOTE (\*) 107 PANELS CONSTRUCTED.

ORIGINAL PAGE IS  
OF POOR QUALITY

Of course, the bands of data are much broader than indicated in Figure 2, however, the slopes of the results and the relative placement of the several LFC surface concepts are consistent throughout the study. Both the electron beam drilled and the woven composite panels exhibit the same slope of pressure drop versus velocity. The Dynapore exhibits a somewhat steeper slope. The significance of these slopes are

- the flatter slopes allow a wider range of efficient LFC operation for a given design;
- the steeper slopes permit a greater variation of velocity for a given pressure drop requirement.

The selection of one type variation over another may be dependent on the specific aircraft design and operational requirements.

Use of off-the-shelf materials and material supplier's impregnation procedures, with their higher resin content, for composite panel fabrication resulted in difficulty in duplicating panels which have the same airflow characteristics. This high resin content also tends to reduce the net strength of the fabricated panels. However, the results of Douglas' research on a suitable, thinner, resin system confirm that the woven composite panels may be reproducible with a high degree of accuracy. Figure 3 shows the results of three composite panels which were fabricated at three completely different times. The results show that satisfactory duplication of the panels is achievable.

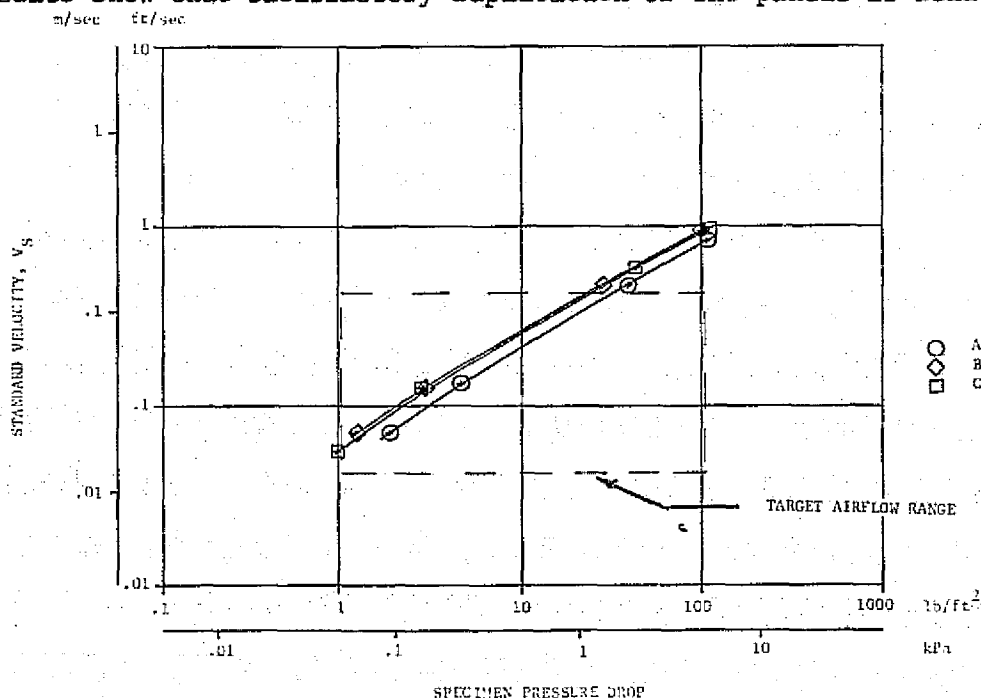


Figure 3. Demonstrated Reproducibility of Composite Panels Using Specific Resin Control  
[0/90]<sub>4</sub>, 120, [0/90]<sub>4</sub> Doweave

General conclusions forthcoming from the study are:

- Further development work is required before a definite selection of one material concept over the other can be made with confidence. All three, woven composites, Dynapore, and electron beam drilled panels show promise as an LFC surface material.
- The woven composite LFC surface is a feasible concept and definitely warrants further development. At this preliminary stage, the Doweave appears preferable over the Leno weave; however, adequate work has not been done to make a definite selection of one over the other.
- Repeatable porosity in woven composite panels is considered an achievable production goal.
- Dynapore is a definite contender as a suitable LFC surface material provided the indicated problem of contamination of the pores is not a definite limiting factor.
- Transverse flow tests of these materials are a requirement to satisfy the aerodynamic smoothness criterion question for a satisfactory LFC surface.
- Further detailed structural analysis of the panels and their integration into an aircraft configuration is required.
- Preliminary comparative cost evaluations of the several concepts should be initiated.

## RECOMMENDATIONS

This program is an exploratory investigation which has verified the initial feasibility of the three basic concepts included in the study. The broad general approach highlights the definite need for follow-on work. Recommendations for this incorporated developmental work are as follows:

### GENERAL

- Determine aerodynamic smoothness requirements, or criteria, by test; transverse flow tests are recommended as an initial step in further development of a suitable LFC surface material.
- Verify pressure drop panel design formula.
- Investigate "glove" versus "integral" design solutions to the overall LFC panel design problem (consider that the panels are adequately attached to strain with the structure, but are still removable for major maintenance and inspection cycles of the airframe).
- Determine surface collection duct area requirements to enable integrated surface panel/primary structure design.
- Obtain sufficiently reliable strength, stiffness and environmental resistance data on porous materials studied herein to perform detailed design evaluation.
- Obtain thermal expansion coefficients by test and perform two-dimensional thermal strain and load compatibility analysis to confirm feasible panel and primary structure materials combinations.
- Investigate LFC surface design for minimum remove and/or replace panel life, of the order of 8000 flight hours, to accommodate primary structure major inspection cycle.
- Continue to explore the continuous fiber joint isogrid panel stiffening concept for producibility and performance in the LFC design environment.
- Continue to explore the Lock Core porous panel concept for producibility to LFC requirements.
- Compare the following three basic types of pressure drop panel designs on the bases of weight, airflow management, manufacturing cost and structural reliability.
  - honeycomb or truss-core sandwiches,
  - grid or parallel solid stiffened single porous sheet,
  - corrugated or integrally stiffened porous multi-sheet design.

## DETAILED MATERIALS

### Doweave-Basic Weave

- Investigate the use of greater thickness per ply than the 200-denier, say 500-denier, to reduce layup labor and material cost for given airflow values. This basic weave appears adequate for the intended use on bases of uniformity of weave, stability of the fabric, relative ease of pre-pregging and handling during layup.

### Leno No. 205 Weave or Thinner Unidirectional Lenos

- Obtain unidirectional and  $[0/+45/90]_n$  laminate strength and stiffness, at correct resin content. Leno is attractive as a potential directional reinforcement to provide anisotropy when used in conjunction with the isotropic Doweave or to increase laminate thickness in those design situations requiring strength with higher mass flow/less pressure drop.

### Dynapore Monolayer

- Improve static strength and test for fatigue life.
- Obtain pressure drop with less compaction and larger pores, if compatible means can be determined to have both at once without also increasing weight and cost.
- Determine nature of "water-only" clogging result from the contamination test reported herein.

### Electron Beam Perforated Panels

- Improve small hole size uniformity in Kevlar/epoxy panels with Ti foil, plated or painted surfaces.

### Cure-in-Place, Peel Ply Concept

- Continue to look for materials solutions for the LFC surfaces.

### Fused Fiber

- Continue to consider the fused thermoplastic fiber concept as a means to improve cost, weight and porosity control over the thermoset resin/fiber laminate concepts.

### Resin

- Define resin impregnation parameters for porous Kevlar reinforced plastic laminates.
- Define resin properties unique to such Kevlar porous laminates for optimum structural properties.
- Coordinate with the manufacturers in order to establish a "production type" resin system suitable for porous composite LFC surface impregnation.

## LFC PANEL STRUCTURAL CONCEPTS

### FUNCTIONAL DESIGN APPROACH

The main functional design problems associated with LFC panels addressed in this program are how to achieve required pressure drop, suitable configurations to achieve both pressure drop and resistance to structural loads/requirements, and surface smoothness.

The primary function of the LFC panel in this program is to provide removal of boundary layer air by means of a static pressure drop through the panel or through the outer surface. The design approach is to provide pressure drop through the entire panel, since a porous surface by itself is not a structural entity in most cases. The structural function of a load-bearing LFC panel is to strain with the aircraft structure to which it is attached and not fail under any conditions of induced strains or environments over some life defined from the life of the primary structure. A structural load and stiffness contribution to the primary structure may be provided accordingly to panel design and attachment. In contrast to the above-described design concept, the LFC panels considered in this study will share the loads in proportion to its cross-sectional area and stiffness relative to primary structure. If a non-load bearing panel may be designed, it must still resist normal pressures and service/maintenance environments.

Three primary design concepts for airflow design of a panel that must achieve given strains without buckling are: (1) a single outer surface with an open pattern of stiffening on the underside, (2) some form of sandwich construction where two parallel facings are held apart by a core, or (3) two porous facings, one of which is configured (corrugated) and attached to the outer face to provide integral stiffening. Figure 4 is a schematic of these options.

It must further be assumed that the air drawn through the panel is collected, either by a series of channels running parallel to the surface and directly under the panel (attached to or integral with it) or the air is drawn entirely through the underlying primary structure and then conducted to the air collection manifold system. It is noted that each of these schemes has some airflow blockage on the surface due to attachment of stiffening.

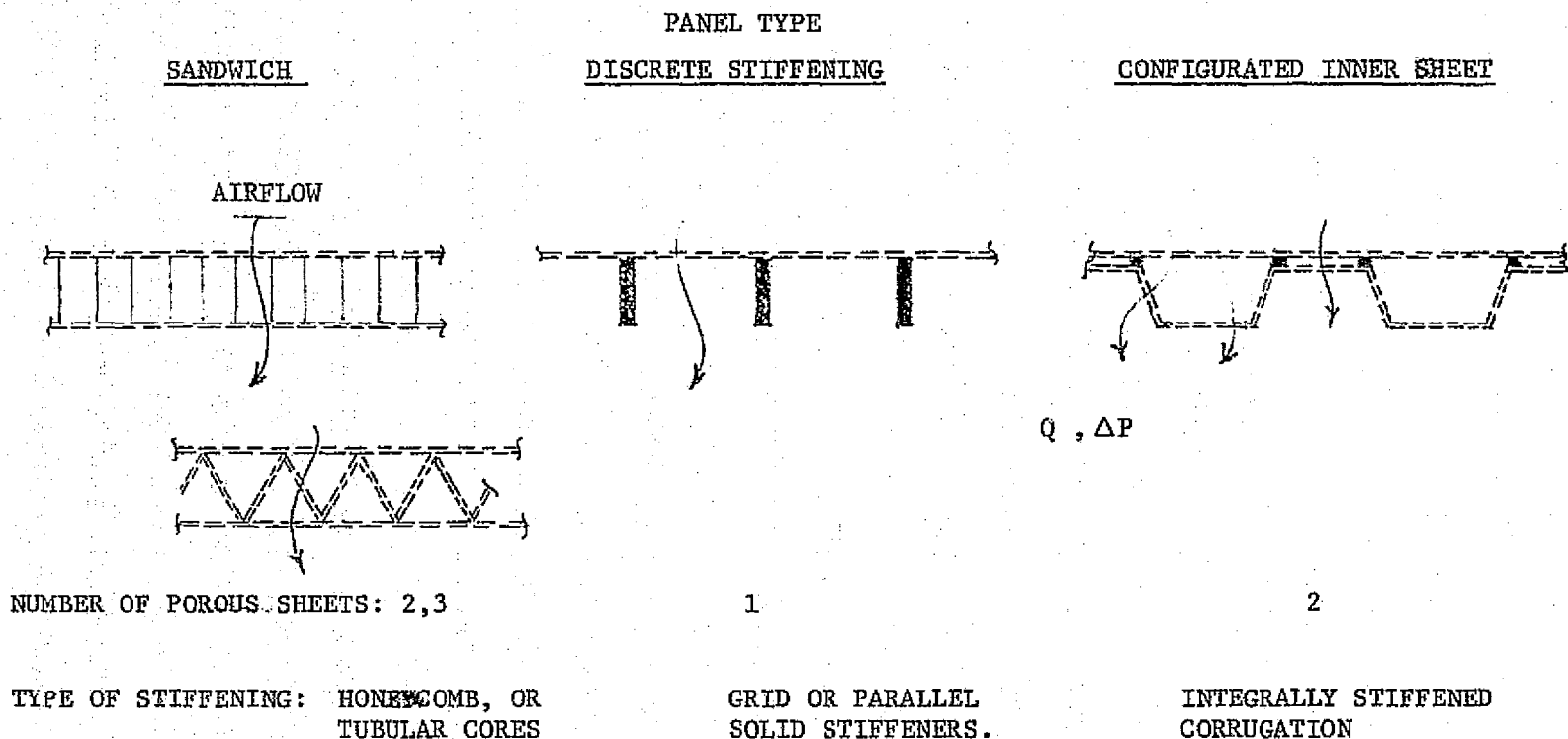


Figure 4. Basic Schemes for Pressure Drop Panels



Pressure drop design of the discretely stiffened single porous sheet, Figure 4 , is straightforward. Whatever airflow,  $Q$  , is achieved through the unstiffened sheet is reduced by the percent of geometric blockage provided by the stiffening attached to the surface. In cases where the stiffening is molded or bonded to the porous face, the size of adhesive fillet or amount of resin/adhesive intrusion into the facing must be known.

The cases of two or three porous sheets in series were approached using an analogy with series resistance of electric current. The analogous formula for airflow/pressure drop would be

$$\frac{\Delta P}{Q} = \sum \frac{\Delta P_i}{Q} \quad , \text{ where } \Delta P \text{ is total pressure drop, } Q \text{ is}$$

total flow, and  $\Delta P_i$  is individual element pressure drop at the same  $Q$ .  $\Delta P_i$  could be adjusted for each layer according to percent blockage of required joints or other non-porous areas. Attempts to check this formula against panel airflow test results were inconclusive due to insufficient data. See page 131, Panels No. 92 and 93.

Alternatives for pressure drop design of two-layer panels are to take the greatest pressure drop at the outside surface, at the inside surface or share the pressure drop relatively equally. A general principle appears to be to compartment the space between the sheets, particularly when the outer face is more porous than the inner, to prevent intercommunication of air sucked from the surface while it is between the sheets. In this respect, the honeycomb sandwich design is a direct solution. The tubular Lock Cores, where the truss webs must be porous to allow air passage through to the inside facing, are designs which must be examined for compartmentation. The isogrid stiffening is naturally compartmented while the parallel stiffened sheet and corrugated inner porous sheet designs are longitudinally compartmented. Extent of allowable longitudinal airflow communication within the panel must be studied.

Panel edge treatments and attachment schemes could only be addressed superficially in this program although such questions may become crucial to the successful performance of such panels. Although the non-loaded panel (or "glove") concept seems attractive -- allows the panel to be just a fairing that floats

above structure and doesn't pick up any loads -- it is doubtful if it can be achieved. Consider the 5000 micro-inch strain typically achieved in aluminum primary wing structure at ultimate load. A non-loaded LFC panel system with only 30-inch panel widths on such a wing must have capability of absorbing 0.15 inch at each joint. This exceeds the capability of oversize holes and standard fastener systems. For this reason the load-sharing panel, which is still removable for major inspection and maintenance, is recommended.

Actual strain levels required will be subject not only to primary structure strains but to additive thermal strains due to temperature changes in the case of dissimilar materials, i.e., Kevlar panels on an aluminum wing. These questions will be further analyzed in the Structural Assessment section.

#### General Criteria and Considerations

Ultimate guidelines for aircraft safety and performance are FAR-25 regulations and such documents as MIL-A-8860 Specifications and the AFSCM 80-1 Design Handbook, however these documents do not yet include any recognition of LFC-peculiar problems, and in fact only now are the FAR regulations for advanced composite structures being developed. Development of a structural design criteria for LFC panels is thus required. In general, it will state that no degradation of safety or reliability of the airframe due to LFC modifications shall occur. Thus a panel that is permanently attached as structure must have a structural reliability equal to or better than conventional design. This may place a severe requirement on porous/perforated materials. As considered in this study, the LFC panel is removable and interchangeable; thus the following discussed criteria becomes feasible.

#### Major Maintenance Period Design Life Criteria

In accordance with standard commercial/FAA practice, the LFC panels should not require removal prior to the structural inspection and assessment interval, approx. 8000 hours of flight service. At this time, if structural cracks are detected, the primary structure must be capable of sustaining at least limit load until the major inspection interval of 16,000 hours is reached, at which time repair action could be taken. It thus appears that, if the LFC panels are removable for structural inspections, the remove and replace cycle (design life) for such LFC panels should be not less than 8000 flight hours. This means the panels must be cleanable without removal from the aircraft as

required by probable contamination affecting LFC performance.

#### Other Criteria

Other than design life, an LFC panel design criteria will include the following requirements:

- Design philosophy
- Porous material requirements
- Environmental
- Strength and stiffness
- Fail safe and damage tolerance
- Thermal compatibility
- Acoustic damping
- Smoothness and waviness
- Maintainability/repairability

The general problem areas visible at this time which prevent definitive criteria from being written are lack of proven information in the following areas:

- Extensive knowledge of porous materials properties versus LFC-peculiar requirements.
- Environmental effects (humidity effects, fuel wetting, adverse chemical composition effects, lightning protection, elevated temperature effects, hail and ablation).
- Reproducibility of fabrication processes and quality controls.
- Static ultimate and fatigue evaluations under safe-life concepts.
- Inspectability of structure.
- Detail design of load transfer areas (joints).
- Thermal stress/load strain compatibility.
- Reliable NDT methods.
- Acoustic strength and vibration amplitudes.
- Smoothness and waviness effects (unique).
- Damage tolerance of porous materials.

The present program, which explores a few porous materials and design configurations is, then, a beginning on the road towards establishing a comprehensive LFC/structure design criteria.

## PANEL DESIGN

### Surface Material Selection

The initial survey of potential surface materials considered the following factors:

- Smoothness potential
- Weight
- Cost
- Environmental resistance
- Potential for pressure drop design
- Porosity control in material
- Strength/Stiffness

Although lack of data prevents quantification of properties for an entirely rationale selection procedure, engineering judgement is applied in anticipation of such properties. For instance, Dynapore mesh is high on the list because stainless steel, although heavy, is strong, tough, relatively low cost, non-corrosive, impact resistant, weathering resistant and erosion resistant, and the fabrication procedure and available fine mesh sizes promise adequate aerodynamic smoothness and control of porosity.

Table II lists the initial surface material candidates. Selection of materials for work in this program was strongly influenced by availability on a short lead time rather than theoretical potential; therefore it is fortunate that several of the promising materials were indeed available. By contrast, the stretched, cure-in-place fabric and fused thermoplastic cloth laminate concepts (S2.4, S7, S8 - Table II) were subsequently dropped because of unavailability and necessity for excessive fabrication feasibility effort for proper evaluation. Thermoplastic fibers under consideration were Dacron and Nylon.

All available fiber-reinforced/thermoset laminates utilized Kevlar 29 fiber because of its availability in the 200-denier triaxial fabric, Leno #205 fabric, and other fabrics used in this program. Kevlar 29 was a priori selected over graphite fabric because of cost, weavability, density and toughness. The low compressive strength of Kevlar appeared to be adequate for this application since low modulus is expected in the porous laminate and the LFC surface load

TABLE II  
LFC CANDIDATE SURFACES LIST

CODE	NAME	COMMENT
<u>S1.</u>	<u>Dynapore</u>	<u>316L Stainless Steel Mesh</u>
S1.1	Dynapore Laminate	• Multi-Layer, Standard Product
S1.2	Dynapore Monolayer	• Single Layer, Product Line Extension
S1.3	Dynapore Micro-Perforated Plate (MPP)	• Fine Square Mesh
<u>S2.</u>	<u>MPP on a Substrate</u>	<u>Fine Scale Surface on a Coarser Underlying Open Sheet</u>
S2.1	MPP on Perforated Stainless Sheet	• Brazed Joining
S2.2	MPP on Perforated Laminate	• Bonding Required
S2.3	MPP on Open Mesh Fiber/Resin Laminate	• Cocure or Bond
S2.4	MPP and Thermoplastic Fiber Cloth	• No Wet Resin, Heat Bond
<u>S3.</u>	<u>Perforated Aluminum Sheet</u>	• Hard to Anodize Against Hole Corrosion
<u>S4.</u>	<u>Solid Laminate</u>	<u>Fabrication Provides Porosity, Needs Surface Protection</u>
S4.1	Molded Holes in Solid Laminate	• Minimum Stress Concentrations
S4.2	Perforated Laminates	• Electron Beam or Laser Perforate
S4.3	Dissolving or Subliming Threads in Fabric	• Controlled Hole Size
<u>S5.</u>	<u>Perforated Titanium Sheet</u>	• EB, Laser Perforate, No Environmental Protection Needed
<u>S6.</u>	<u>Porous Reinforced Plastic</u>	<u>Concepts Need Environmental Protection</u>
S6.1	Leno Weave - Polyimide Resin	• Resin Naturally Porous
S6.2	Leno Weave - Foamed Epoxy	• Added Porosity Through Foaming
S6.3	Doweave - Epoxy, Controlled Flow	• Tri-axial Fabric
<u>S7.</u>	<u>Cure-in-Place Porous Fabric</u>	• Peel-ply Application on a Permanent Perforated Surface. Probably UV-cured Resin.
<u>S8.</u>	<u>Fused Thermoplastic Cloth Laminate</u>	• No Resin Flow Control Necessary. Porosity Control in the Weave.

pickup should therefore be minimal. Dupont 5134 controlled flow resin was used for the Kevlar laminates.

Tables II and III summarize the initial screening evaluation of the candidate surface concepts. It will be noted that the items evaluated on a 1 to 10 basis (10 is best) are weighted towards fabrication concerns. Materials are included with labor in the cost column. The comments concern contraindications to the apparent ranking of concepts from the summation column, Table III. Weights represent equal porosity on a unit area basis. The highest ranked surfaces, anodized aluminum and the perforated titanium, are not selected for the program since experimental work was proposed in this study for only one representative perforated concept, to free limited funds for porous panel work. Perforated aluminum may be difficult to protect from corrosion. The other high-valued concepts in the initial screening are carried into the program, except S6.1 Leno weave, in which epoxy rather than polyimide resin was chosen. Polyimide is naturally porous but epoxy is a lower cost system if controlled flow epoxy can attain the required porosity.

#### Stiffened Panel Concepts

An initial set of concept sketches were drawn for a producibility evaluation of stiffened LFC panel concepts. These panel configurations were based on the basic schemes described earlier, Figure 4. As the program progressed, it became apparent that many of them could be judged overly complex from a fabrication standpoint or were unsuitable from an airflow management aspect; and, of course, none were designed for strength. As material strengths and stiffnesses are obtained and airflows achievable through various materials are known, as well as sharper definition of basic structural and aerodynamic design requirements, it becomes possible to devise more definitive design concepts that contain member sizes and spacings, thicknesses, numbers of plies, etc.

Four types of stiffened panel design utilizing porous materials were considered:

(1) Honeycomb panel, (2) Lock Core sandwich panel, (3) a tubular core similar to the Lockheed glove panel, and (4)  $\pm 60^\circ$  or  $0/90^\circ$  grids. The general order of preference for producibility of the four types show the Honeycomb, Lock Core (truss-core) and Lockheed concepts all of equal preference but grid stiffened concepts about 75 percent as producible.

The lower valued assessment of the interlocked continuous fiber grids concept

TABLE III  
INITIAL SCREENING OF LFC SURFACE CONCEPTS  
10 = BEST

CODE	FABRICATION FEASIBILITY	EASE OF FABRICATION	ENVIRONMENTAL RESISTANCE (MOISTURE)	COST TO FABRICATE	WEIGHT AT EQUAL AIRFLOW	SUM	CONTRAINDICATIONS AND COMMENTS
S1.1	10	8	9	8	1	36	Heavy
S1.2	10	8	9	8	8	43	Practical
S1.3	---	---	9	---	---	---	Not Recommended by Itself. (fragile)
S2.1	9	6	7	6	4	32	S2.1, S2.2 may act as exposed perfora- tions to crossflow S2.3, S2.4 appear promising.
S2.2	8	5	4	5	8	30	
S2.3	8	9	4	6	7	34	
S2.4	2	---	---	---	8	---	
S3.	10	10	9	10	9	48	Hole Corrosion
S4.1	9	5	9	6	9	38	Development Needed.
S4.2	9	7	9	5	9	39	Needs Protection.
S4.3	5	5	9	5	9	33	Surface Smoothness.
S5.	10	7	10	6	7	40	Non-Corroding
S6.1	9	10	9	7	8	43	Needs Protection.
S6.2	2	3	5	7	8	27	Impractical.
S6.3	9	10	9	7	8	43	Needs Protection.
S7.	---	---	---	---	10	---	Insufficient Data.
S8.	---	---	---	---	9	---	Insufficient Data.

is based chiefly on uncertainty regarding cost and method to produce large flat area grids and how to join them. This uncertainty does not exist for such grids produced as surfaces of revolution. For instance, a study for the Air Force, Reference 1, and a follow-on IRAD producibility study at Douglas, Reference 2, portrayed the low cost potential and fabrication ease of this method.

A greater amount of in-house work has been accomplished regarding the truss core (Lock Core) panel concept, and it is relatively easy to extrapolate thinking to porous material construction. It is also easier to evaluate Honeycomb and bonded plate and stiffener constructions, based as they are on known techniques. The grid, however, is retained in the continuing selection process because of its natural compartmentation of airflow through a panel, and its ability to accept loads and strains independently of the porous surface which may be attached to it. The grid bondlines to a porous facing, however, will create blockage to airflow on a regular pattern, the same as a honeycomb bond. Specific Lock Core and grid panels will be discussed in the Test Panel Description Section of this report.



## TEST PANEL DESCRIPTIONS

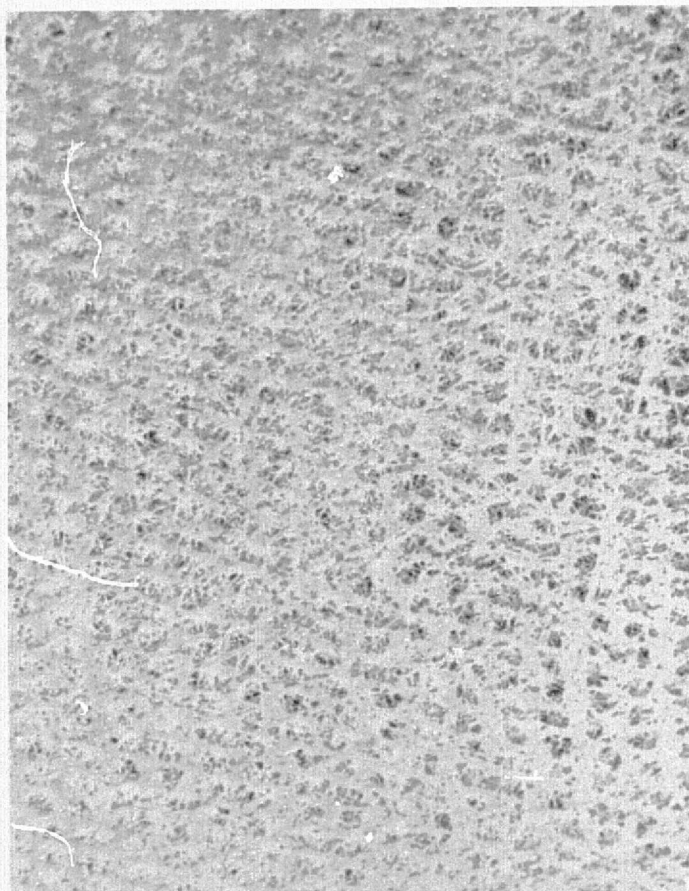
### CANDIDATE SURFACE MATERIALS

#### Doweave

The Industrial Products Division of E. I. DuPont de Nemours & Co., Inc., is producing fabrics utilizing a triaxial weaving system invented by N. F. Dow, hence the name, Doweave. The system produces fabrics with three sets of yarns, achieving stability in the bias, or roughly isotropic strength and stiffness properties. The basic weave utilized in the present program produces locked intersections and hexagonal openings as illustrated in Figures 5 & 6, showing the surface of a laminate made with this fabric. 200-denier Kevlar 29 yarns at the standard weaving pitch of 18-1/2 yarns per inch produced a fabric, when preimpregnated with DuPont 5134 epoxy (controlled flow) resin, making laminates with 0.0045 inches/ply thickness.

Superposition of two plies with various angles between them produces interesting and changing moire patterns suggestive of varying porosities, however, practical layup considerations led us to consider only the  $[0/90]_n$  laminate family, after initial experimentation. Structural stability, layup simplicity and uniformity of porosity distribution is achieved by this paired stacking sequence.

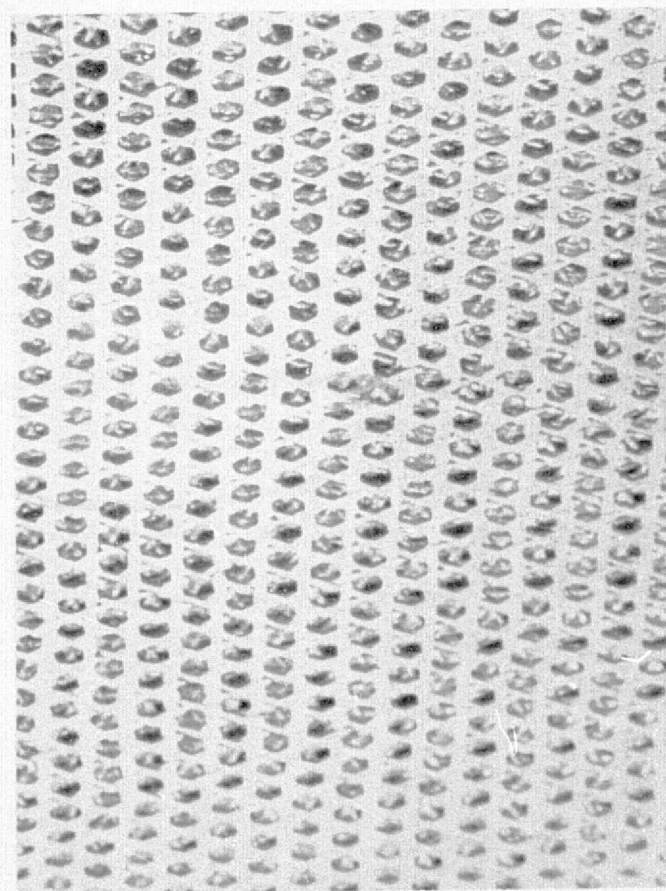
Figures 7 , 8 , and 9 from the scanning electron microscope show very clearly the make-up of typical Doweave panels. It is to be noted that the air passages completely through the panel are denoted by the very black spots on the pictures. Figures 10 and 11 from the comparator present, by means of light transmission, the airflow passages in several representative Doweave panels. Panel number and magnification are noted in the left hand corner of the picture. The photographs shown are taken at random locations on the panels.



PANEL NO. 20

$\left[ \begin{smallmatrix} 0_D/90_D \end{smallmatrix} \right]_T^M$ 
 THICKNESS .013 INCH  
 (.33 mm)

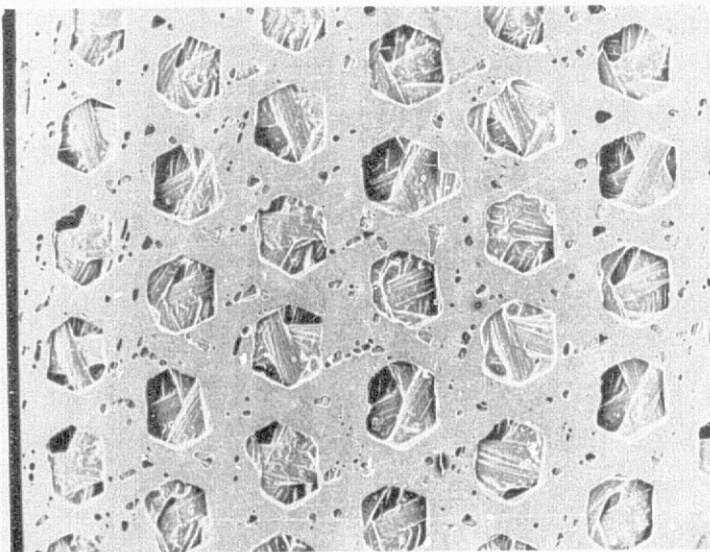
Figure 5. Doweave Panel With Mat



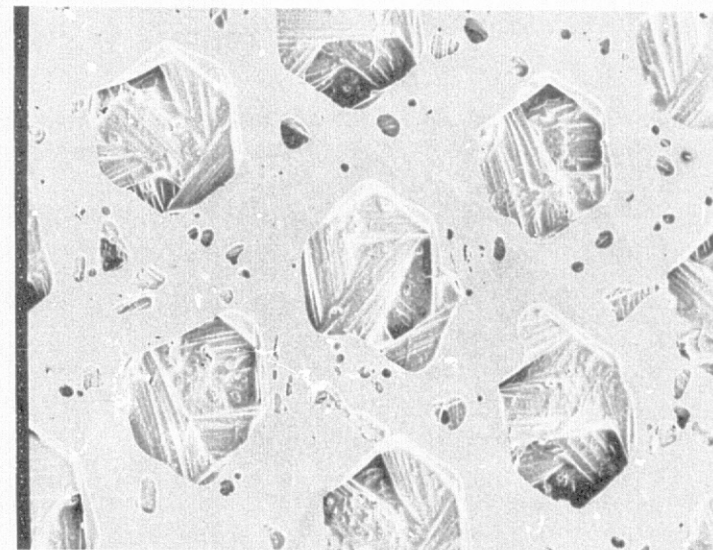
PANEL NO. 21

$\left[ \begin{smallmatrix} 0_D/90_D \end{smallmatrix} \right]_2$ 
 THICKNESS .020 INCH  
 (.51 mm)

Figure 6. Doweave Panel Without Mat



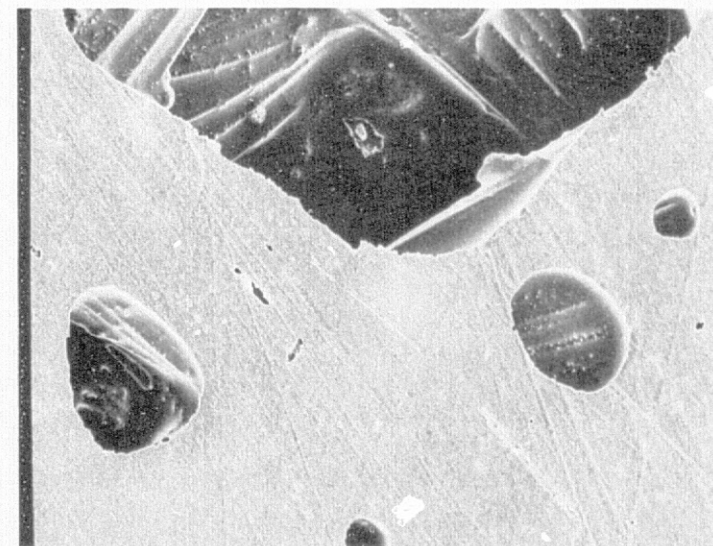
10X



20X



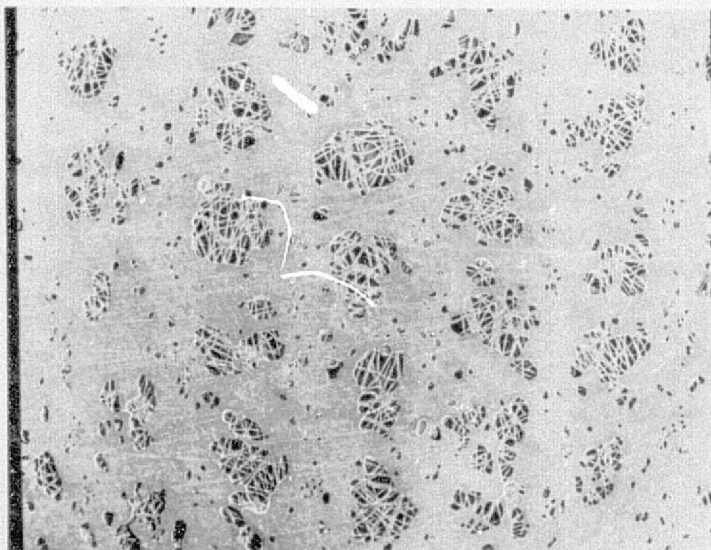
100X



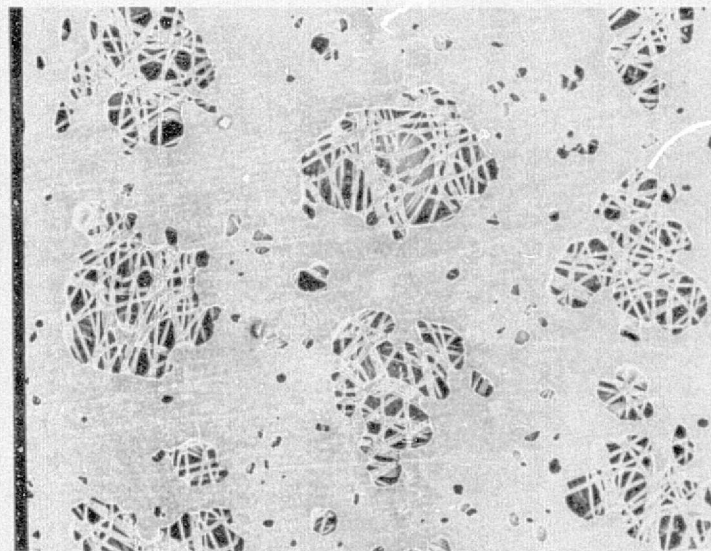
100X

Figure 7. Doweave Panel No. 23 - No Mat  
 $[0_D/90_D]_4$  Thickness - .038 Inch  
 (.97 mm)

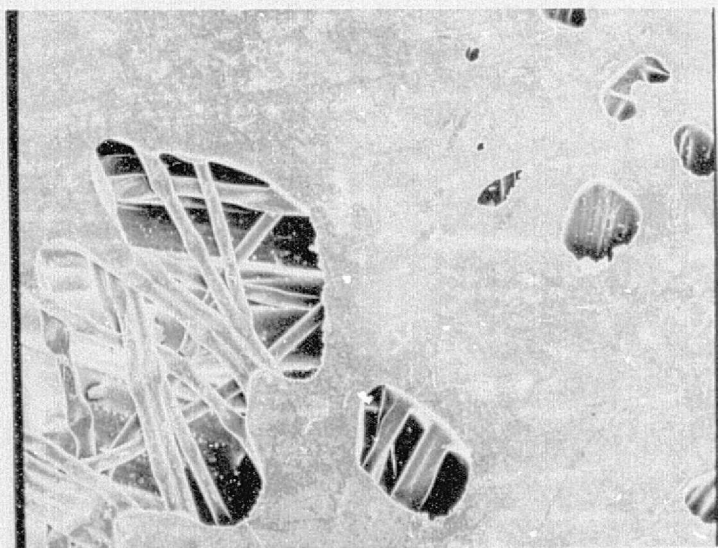




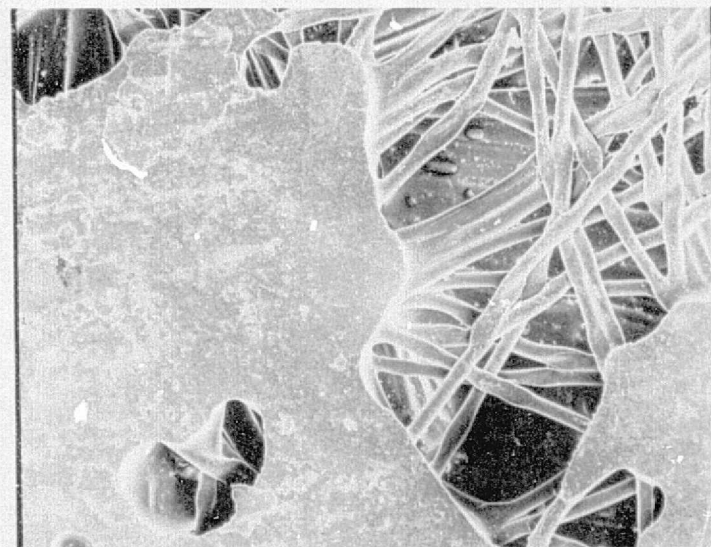
10X



20X

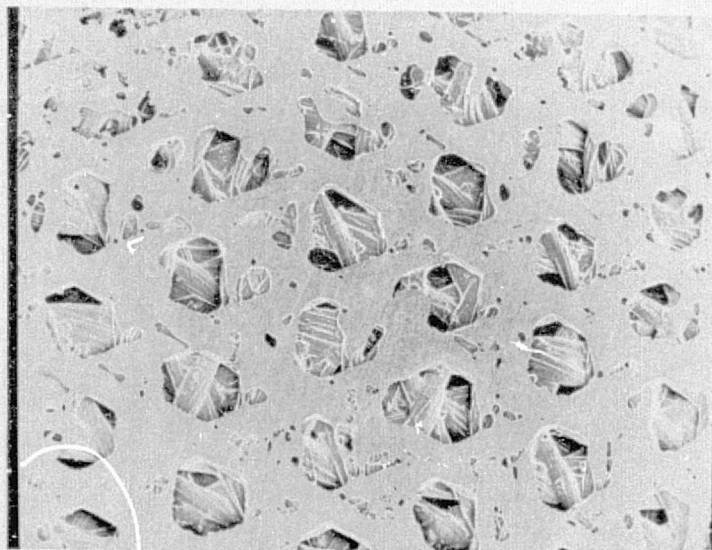


100X

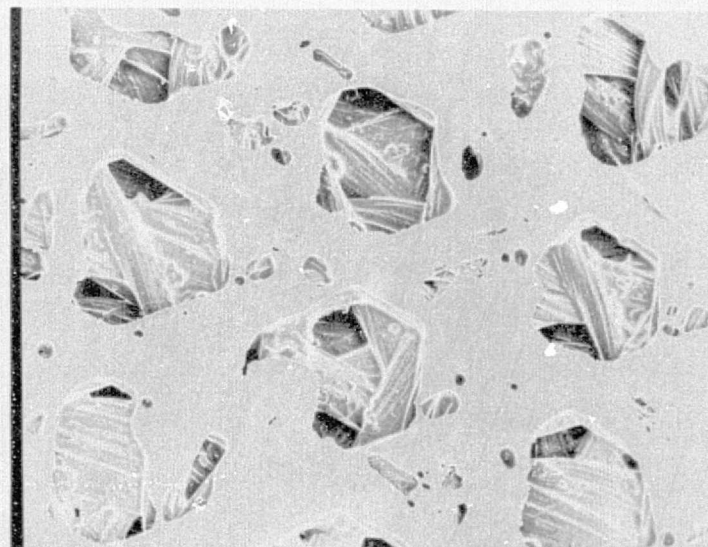


100K

Figure 8. Doweave Panel No. 24 With Mat  
 $[0_D/90_D]_4^M$  Thickness - .040 Inch  
 (1.02 mm)



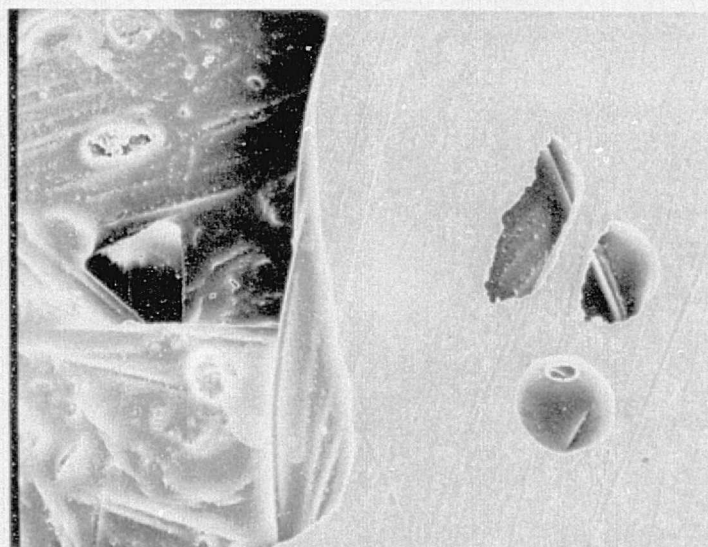
10X



20X



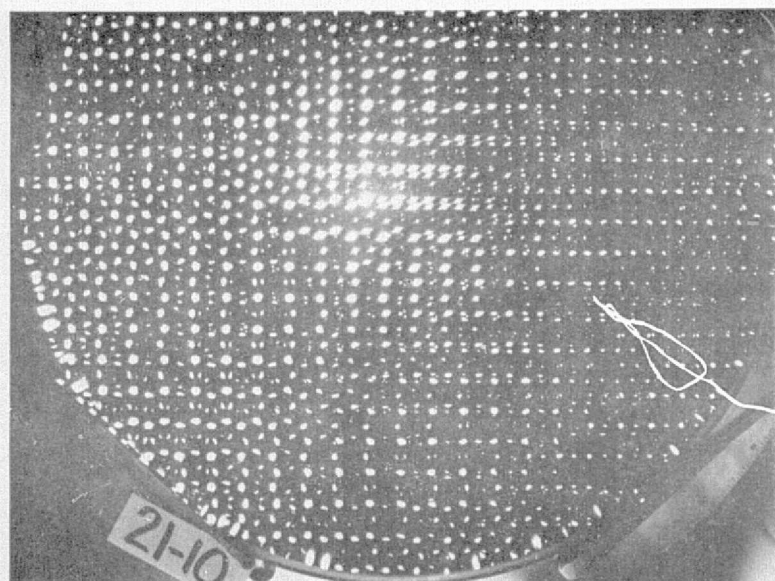
100X



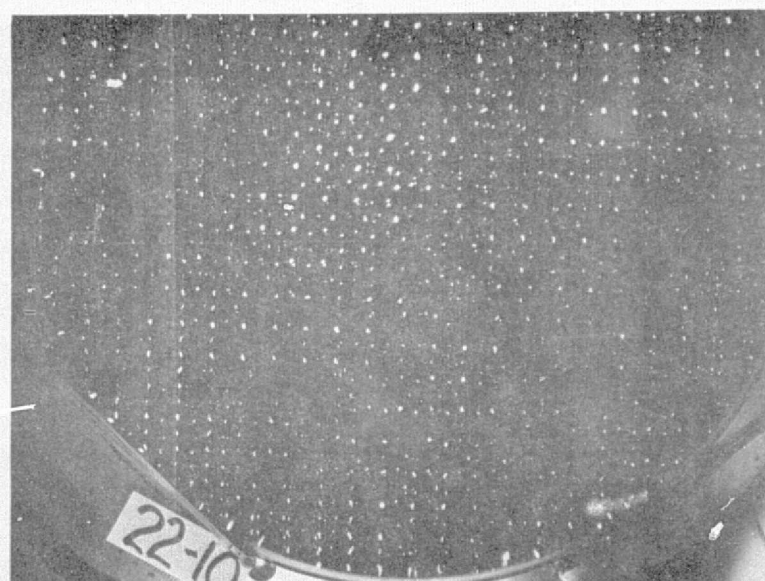
100X

Figure 9. Doweave Panel No. 73 - Face Sheet for Stiffened Panels  
 $\left[ \begin{smallmatrix} 0 & 90 \\ D & D \end{smallmatrix} \right]_4$  Thickness - .036 Inch  
 (.86 mm)

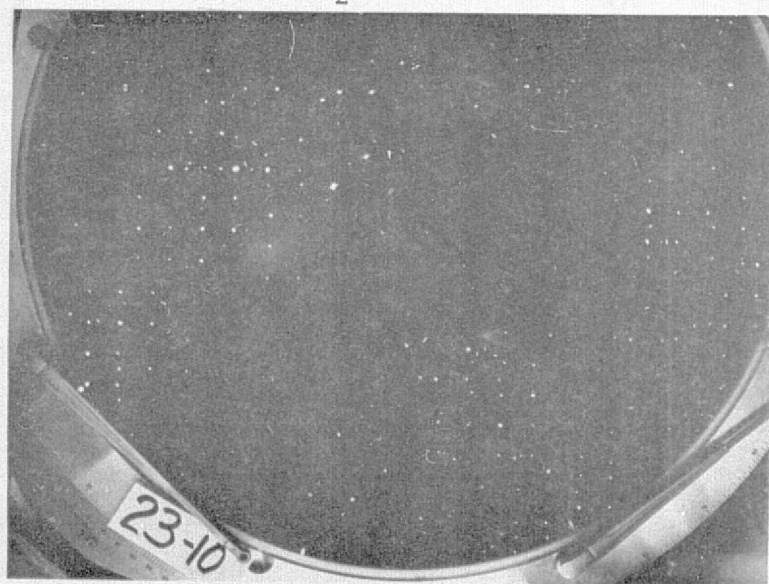




$[0_D/90_D]_2$



$[0_D/90_D]_2^M$



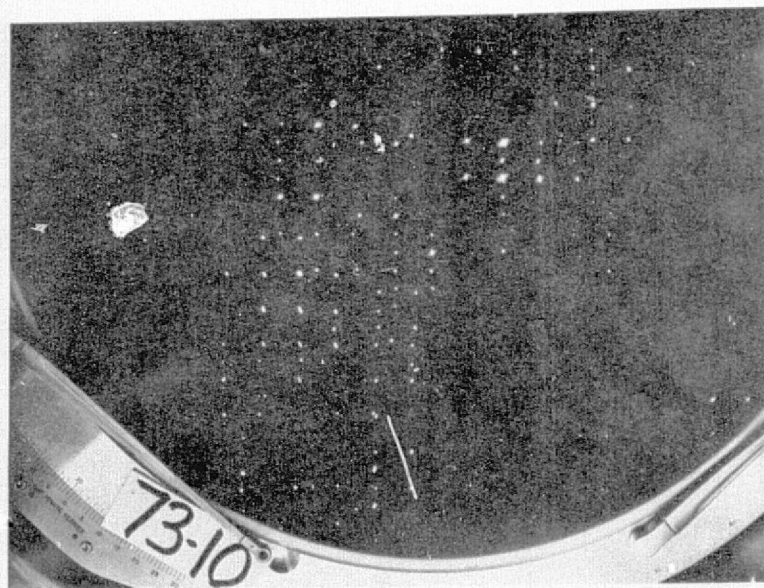
$[0_L/90_D]_4^D$



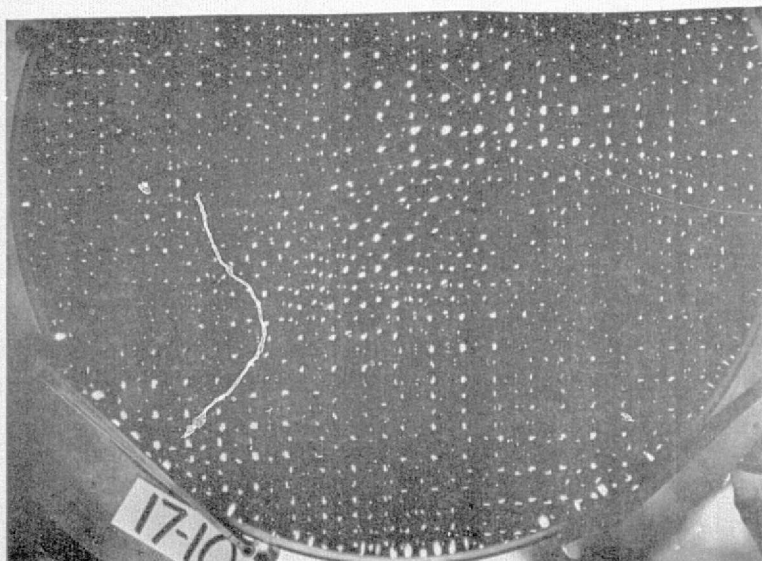
$[0_L/90_D]^M$

Figure 10. Doweave Panels - Comparator Views  $D$

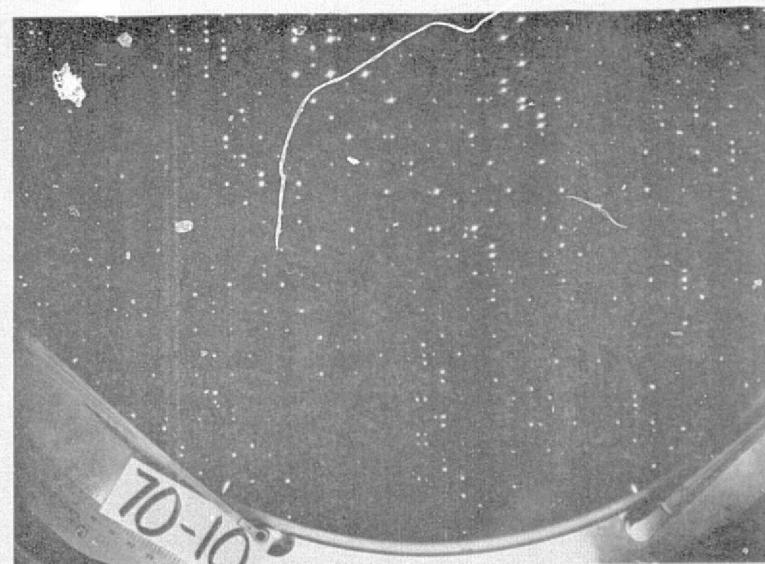
ORIGINAL PAGE IS  
OF POOR QUALITY



$[0_D/90_D]_4$  (Face Sheet Used on Stiffened Panels)



$[0_D/90_D]_2$  + MPP #21



$[90_D / 45_L / 90_{120}]_T$

Figure 11. Doweave and Lay-up Panel Variations

#### Leno No. 205 Weave Kevlar/Epoxy

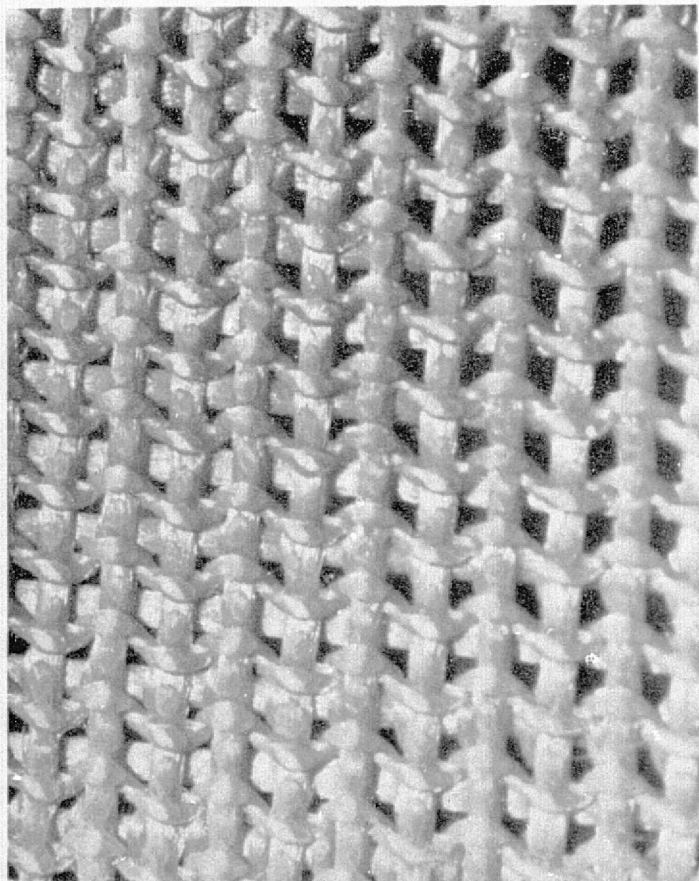
Leno Weave No. 205 is a predominantly unidirectional-woven fabric in which the warp fiber yarns are held apart approximately their own width by the twisted fill yarns. Preimpregnation was with Dupont 5134 controlled flow epoxy. Both 0/90 and 0  $\pm$  45/90 laminate patterns of varying numbers of plies were produced for airflow testing. Some thick laminate patterns with eight and greater numbers of plies had little, if any airflow. Also the porosity variation of laminates with fewer numbers of plies visually appeared irregular. This was attributed to uneven resin impregnation and excessive resin content. Attempts to vary cure cycle and to bleed more resin from the thicker laminates were only partially successful, all of which limited the amount of investigation with this material.

The thickness per ply of Leno #205 in laminate is 0.014-0.016 inches. Since for a balanced symmetrical laminate containing 0,  $\pm$  45 and 90 degree plies, 1/8 inch thick is minimum, it would appear that .008-inch/ply material would offer greater design flexibility in structural applications. Figures 12 and 13 show surface appearance of a Leno laminate.

Corresponding photographs to the Doweave, Figures 7 through 9, are presented in Figures 14 and 15. In the scanning electron microscope photographs, note the irregularity of the Leno panel construction as compared to the Doweave. Figure 16 shows comparator views of the Leno weave.

The effects of composite material and lay-up pattern on the surface appearance are exemplified in Figure 17.

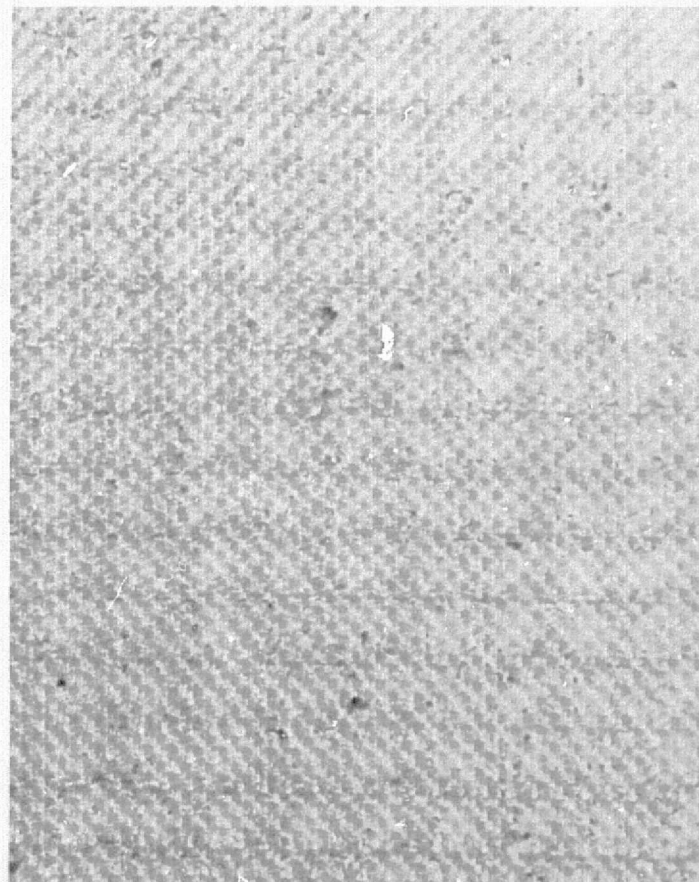




PANEL NO. 7  
 $\left[ \begin{smallmatrix} 0 \\ L \end{smallmatrix} / \begin{smallmatrix} 90 \\ L \end{smallmatrix} \right]_T$

Figure 12. Leno Weave Panel

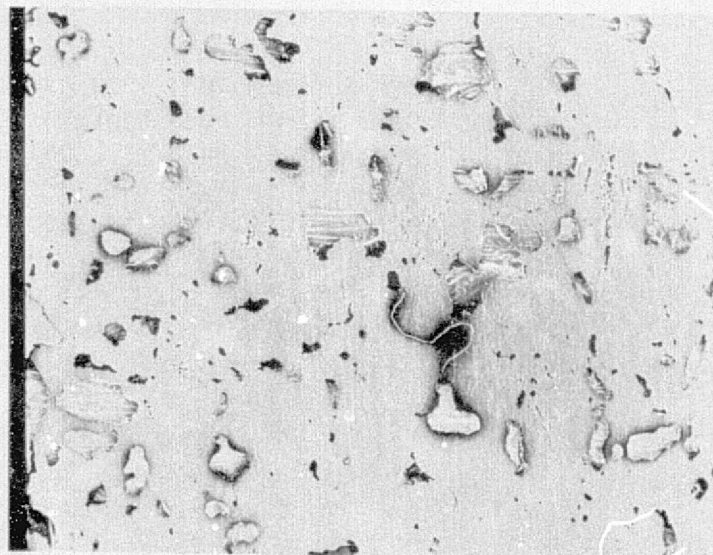
~ 4.0X  
 THICKNESS .030 INCH  
 (.76 mm)



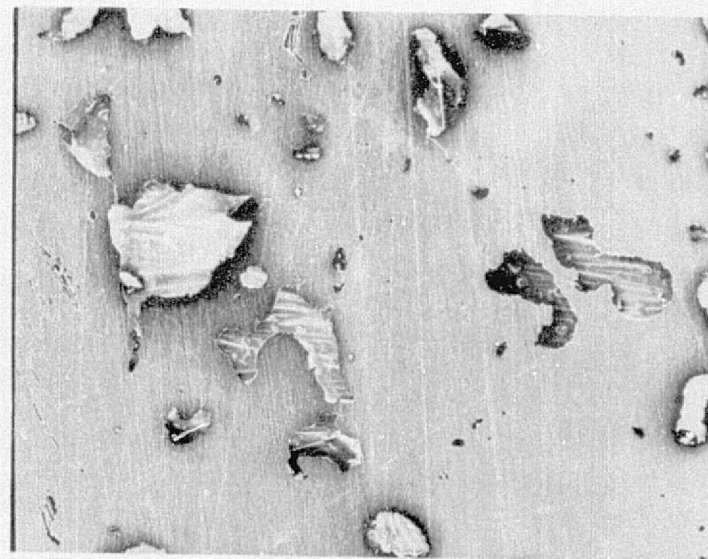
PANEL NO. 68  
 $\left[ \begin{smallmatrix} 0 \\ L \end{smallmatrix} / \begin{smallmatrix} 90 \\ L \end{smallmatrix} \right]_2$

Figure 13. Leno Weave Panel

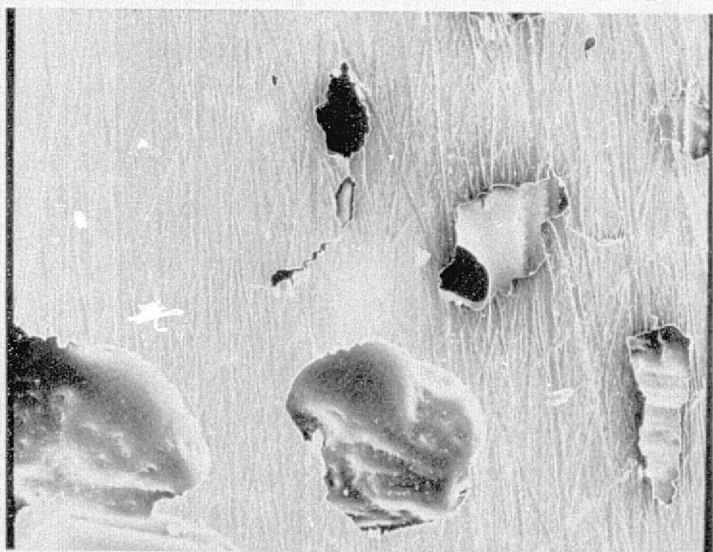
~ 4.0X  
 THICKNESS .059 INCH  
 (1.50 mm)



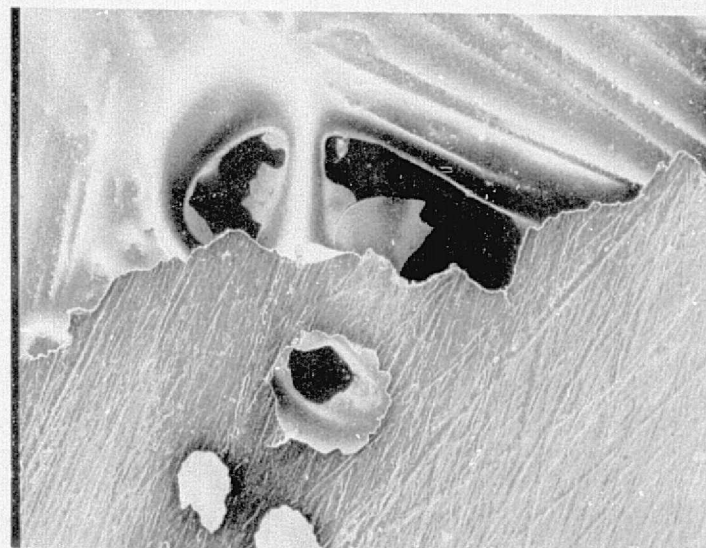
10X



20X



100X



100X

Figure 14. Leno Weave Panel No. 88 - No Mat  
 $[0_L/90_L]_2$  Thicknesses - .059 Inch  
 (1.50 mm)



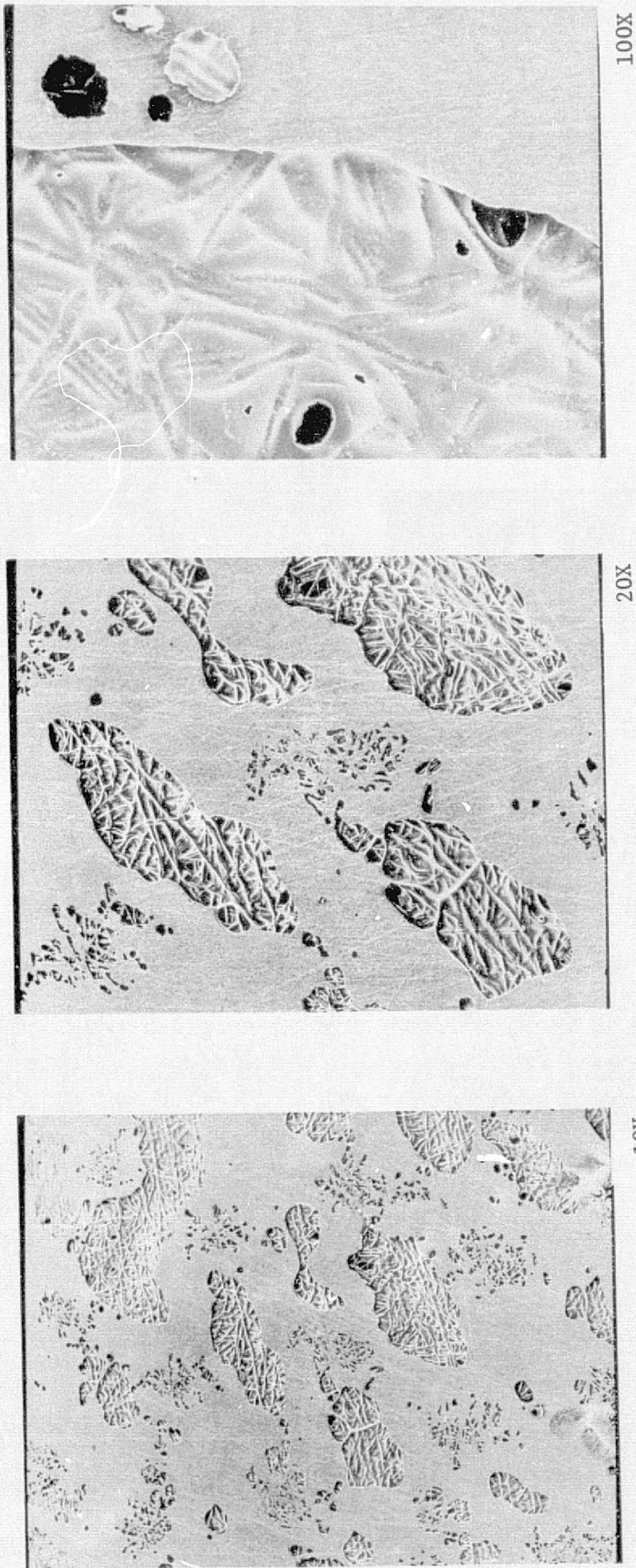
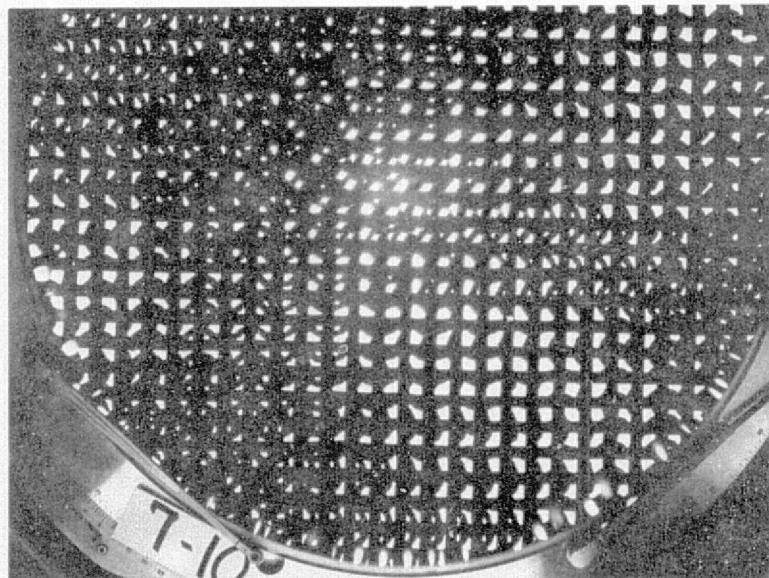
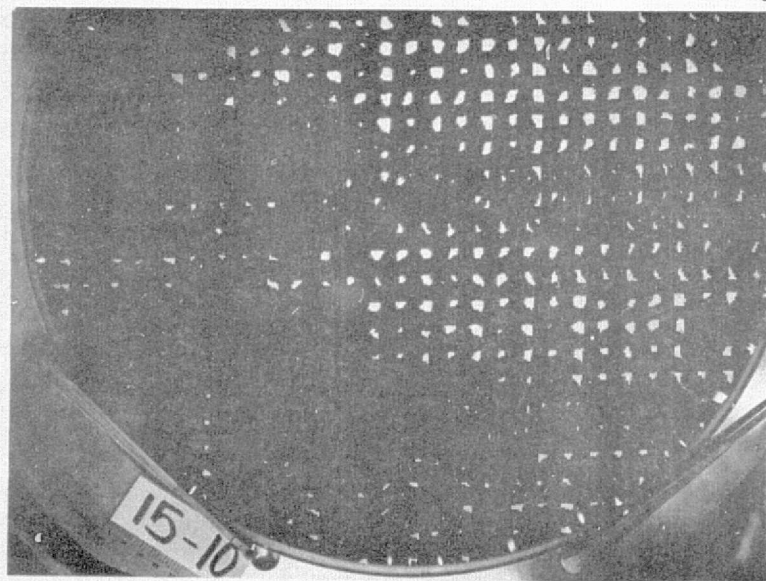


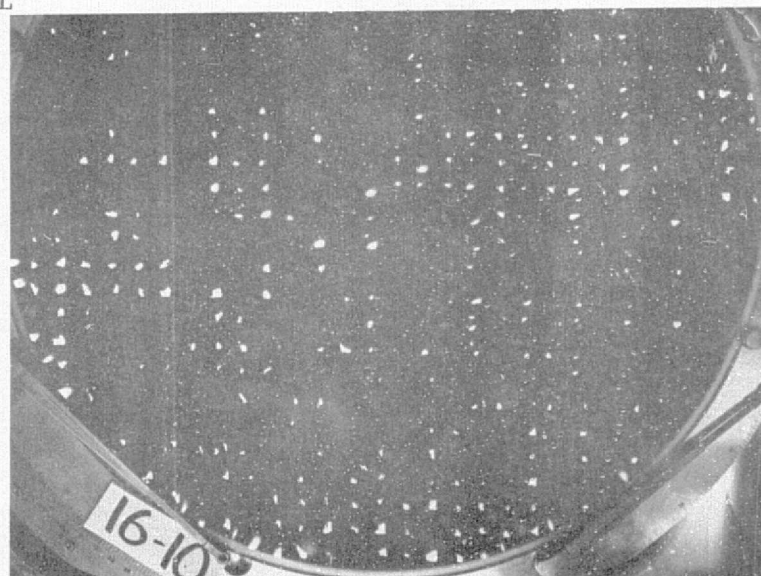
Figure 15. Leno Weave Panel No. 89 - With Mat  
 $[0_L/90_L]_2$  M Thickness - .060 Inches  
 (1.52 mm)



$[0_L/90_L]$



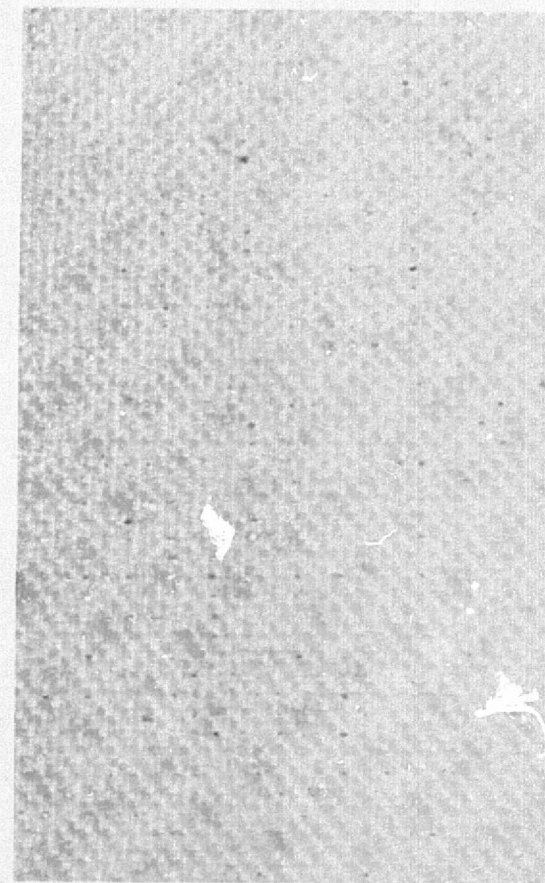
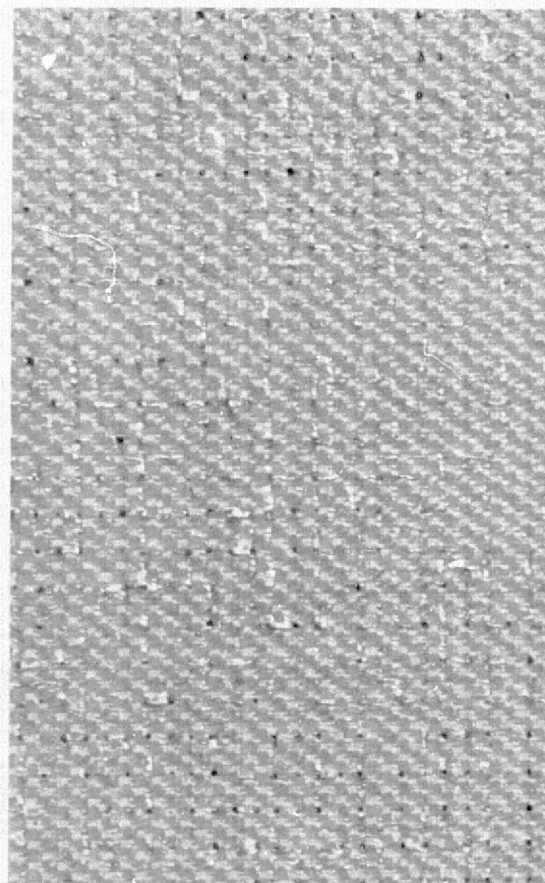
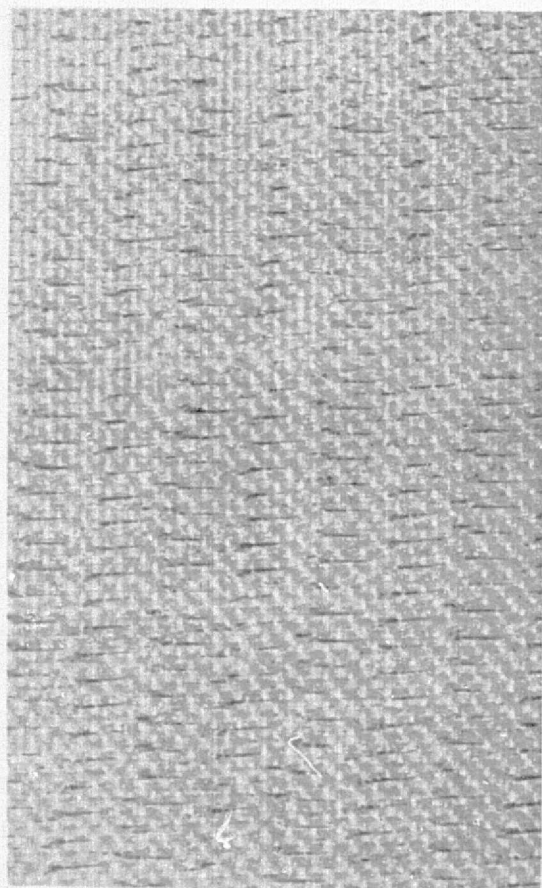
$[0_L/90_L] + \text{MPP \#21}$



$[0_L/90_L] + \text{MPP \#24}$

Figure 16. Leno Weave Panels - Comparator Views





PANEL NO. 71

$[0_D/90_D]_{143}$

THICKNESS .023"  
(.58 mm)

PANEL NO. 65

$[0_{120}/90_D/0_D]$

THICKNESS .016"  
(.41 mm)

PANEL NO. 64

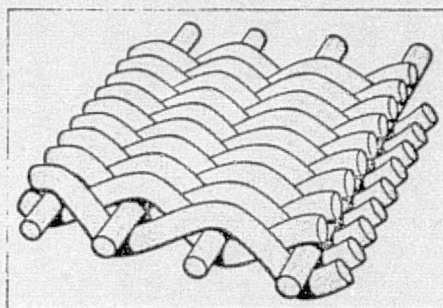
$[0_L/+45_L/90_{120}]$

THICKNESS .037"  
(.94 mm)

Figure 17. Typical Effects of Material and Lay-Up ~4.0X

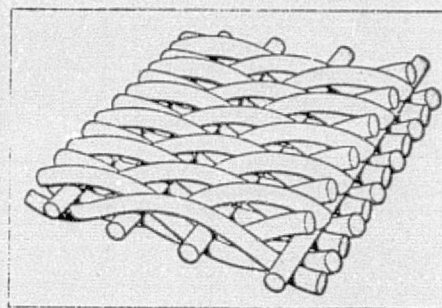
### Dynapore Monolayer

This designation was given by Michigan Dynamics Division of AMBAC Industries, Inc., to a single layer of their standard line of Dynapore<sup>TM</sup> diffusion-bonded laminates and composites. Two such monolayers were produced and characterized for the present program. One is made from a 24 X 110 inch plain dutch weave 316L stainless steel wire mesh, and the other from a 50 X 250 plain dutch weave of the same material, Figure 18. The twilled dutch weave, Figure 18B, was not considered in this study because of the more tortuous pore path.



A. Plain Dutch weave (1WP)

Plain Dutch weave is woven with warp and fill wires passing "over one/under one" in both directions. Compared to plain square weave with the same particle retention, plain Dutch weave has greater density, two to three times more mechanical strength and approximately one-third the flow rate. Plain Dutch weave is normally woven with a micronic retention as fine as 40 microns.



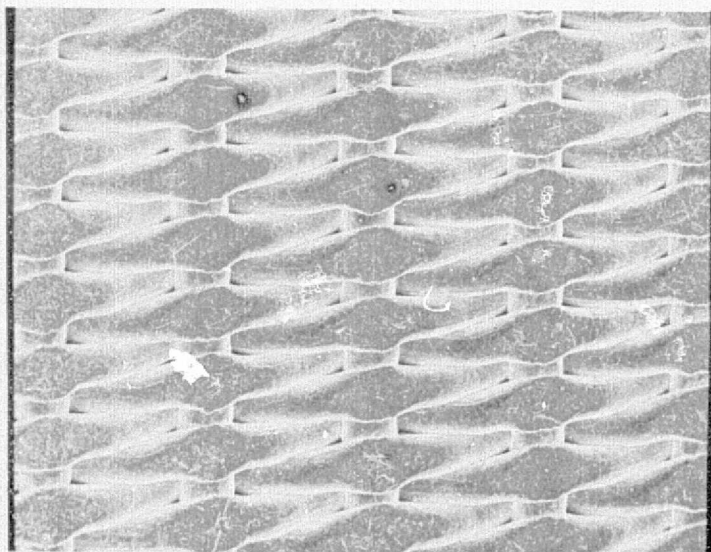
B. Twilled Dutch weave (1WT)

Twilled Dutch weave is woven with warp and fill wires passing alternately "over two/under two" in each direction. This type of metal filter cloth has five to eight times more strength than a plain square weave with the same hole size. Because of its denser and stronger construction, twilled Dutch weave has approximately half the flow rate of plain Dutch weave and is available with a micronic retention down to the range of two microns.

Figure 18. Dutch Weave Wire Cloth Construction

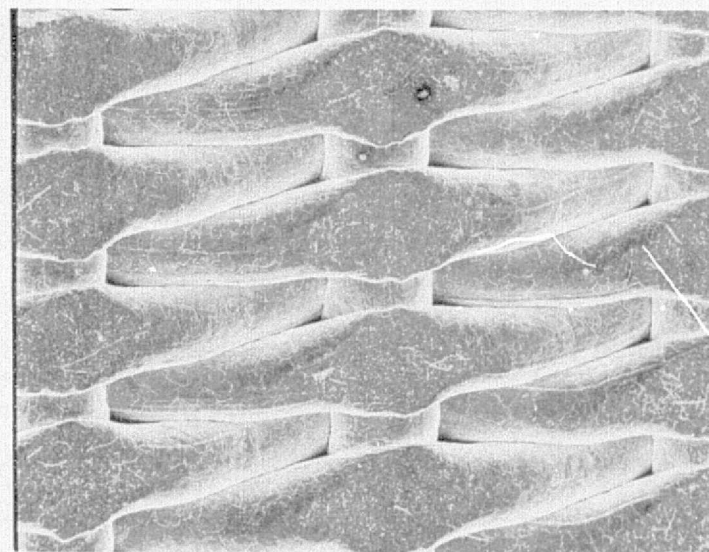
The numbers 24 X 110 refer to the number of wires per inch in the base material in the warp and fill directions, respectively. The base meshes were compacted, diffusion bonded in a hydrogen atmosphere furnace at approximately 2050°F., and then compacted to final thicknesses for specified airflow. The yield strength properties are achieved during the final compacting, i.e., cold working, since the furnace treatment leaves the 316L in a dead soft condition. After final calendaring, the material appears as in Figure 19 under a scanning electron microscope. Surface comparison under reflected light is shown in Figure 20 for the two materials.





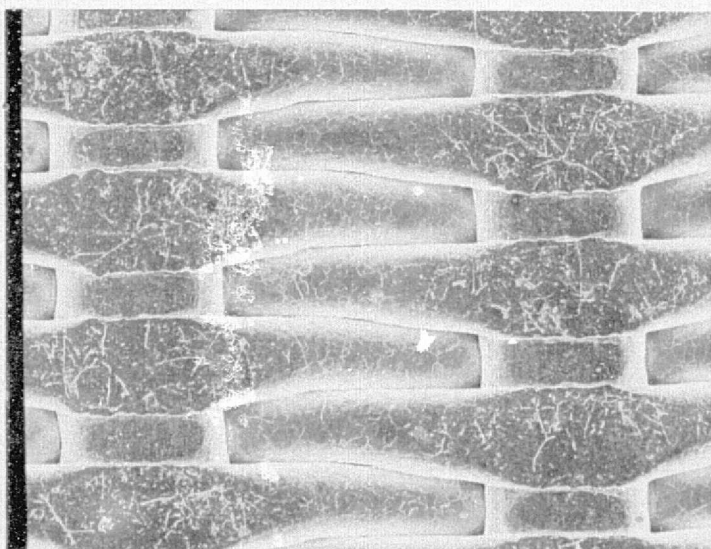
50 X 250 MESH

40X



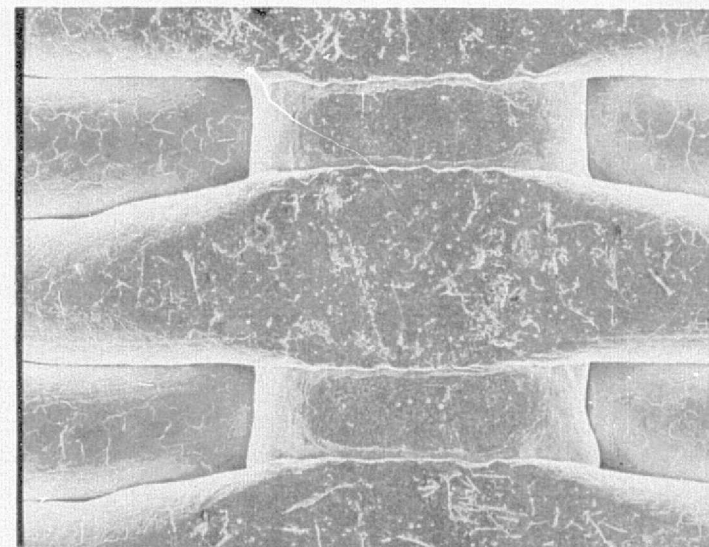
50 X 250 MESH

80X



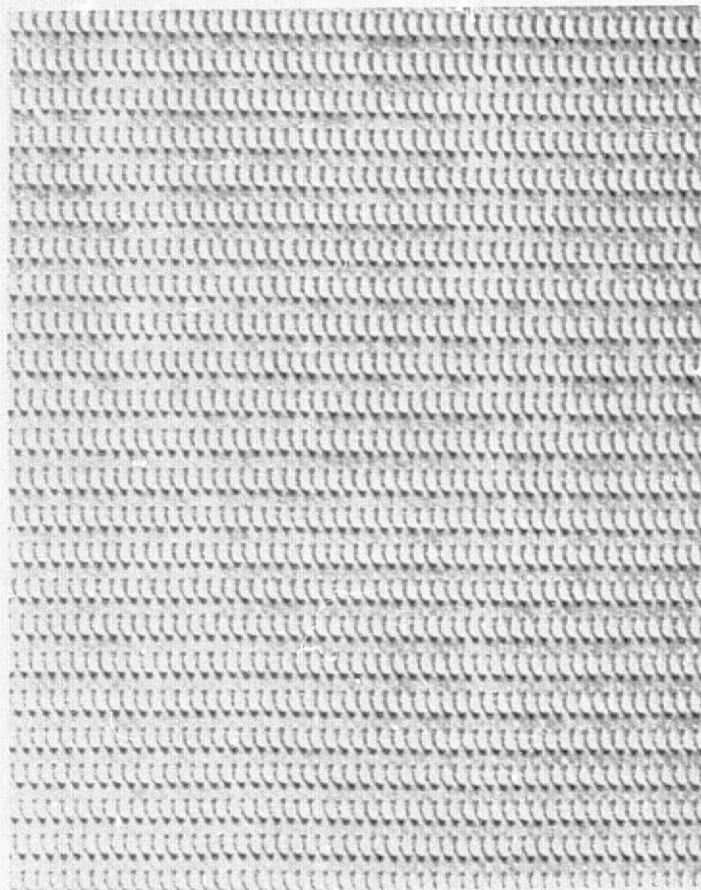
24 X 110 MESH

40X

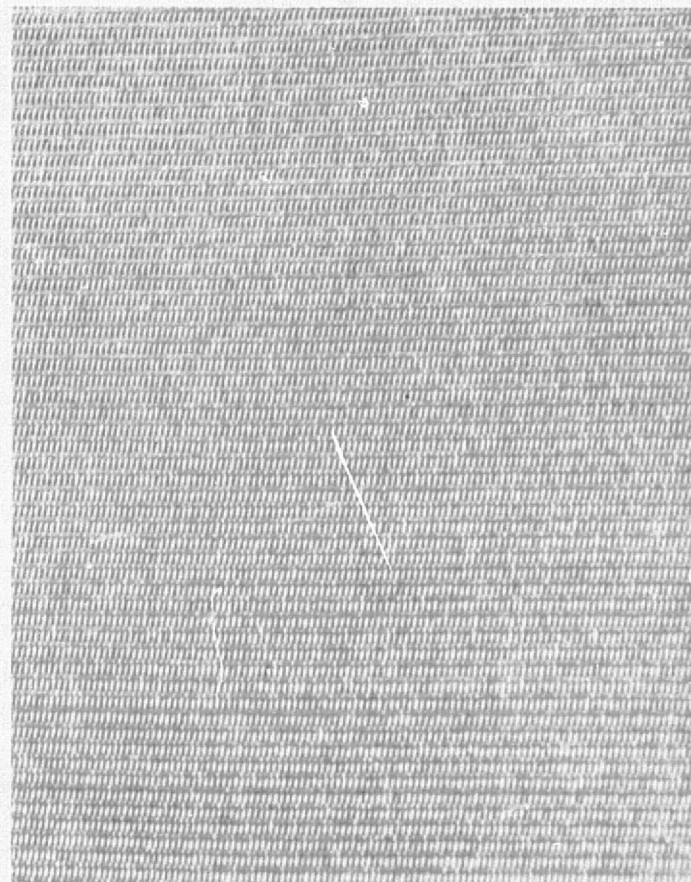


80X

Figure 19. Dynapore Mesh Flat Surface Smoothness After Calendaring



24 X 110 MESH



50 X 250 MESH

Figure 20. Dynapore 316L Stainless Mesh

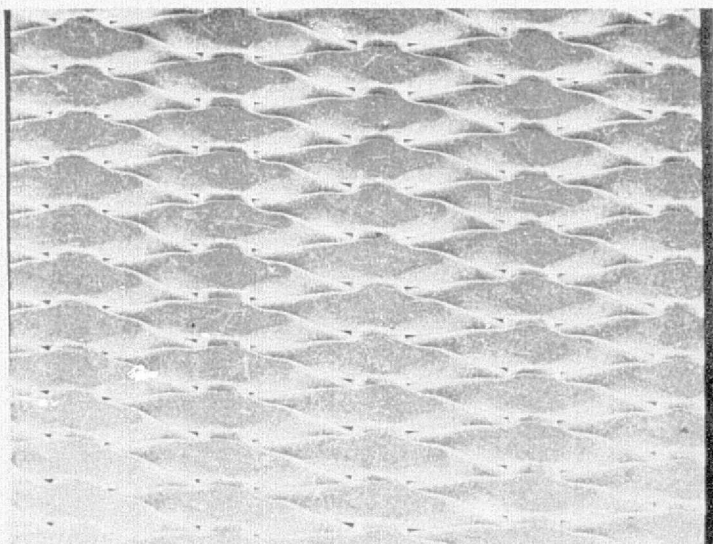


Figure 21 presents an oblique view of the fine mesh (50 X 250) Dynapore under the scanning electron microscope which shows the airflow paths through the material. Note the regularity of passages as shown under high magnification.

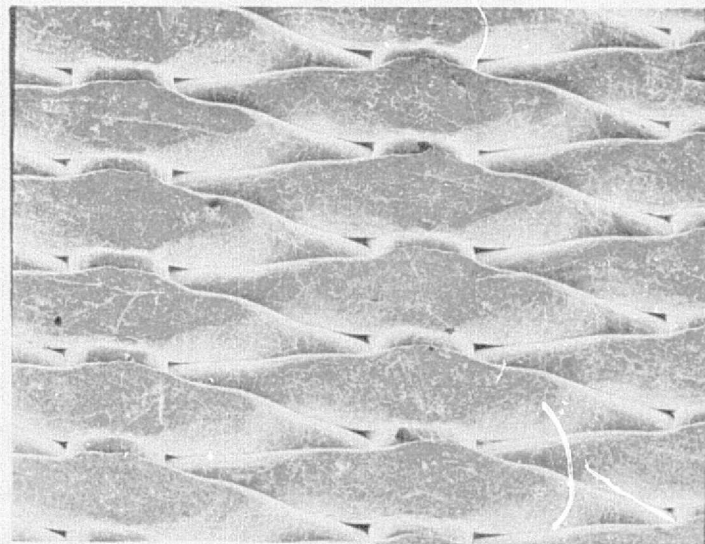
A second point of particular interest is the deformation of the wires which occurs during the calendaring. This deformation is a major factor in obtaining an LFC-suitably smooth surface. Figure 22 illustrates the point. Judgement as to the adequate smoothness of the surface for satisfactory LFC performance, although quite smooth to the touch, is dependent on transverse flow aerodynamic tests.

The diffusion bonding of stainless steel is not easily accomplished. However, random checks of the 50 X 250 mesh Dynapore confirms the fact that diffusion bonding has definitely been accomplished in this material, Figures 23 and 24. However, similar check of the heavier mesh (24 X 110) Dynapore showed that the material was not diffusion bonded, Figure 25, as the "fill" wires were easily removed from the mesh. Possible explanation of this difficulty, based on Douglas experience, may be due to the fact that

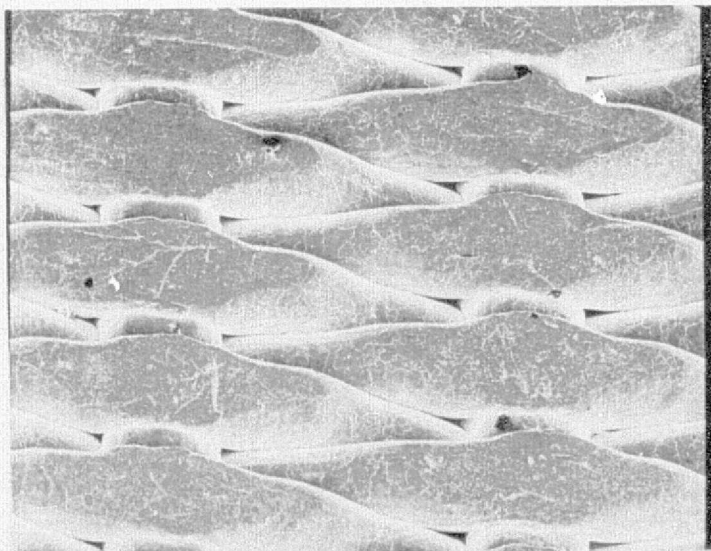
- The surfaces were not sufficiently clean (as the material is compacted, new surface is exposed to the areas to be diffusion bonded); or
- the diffusion bond may have been broken during the final compaction (Figure 25).



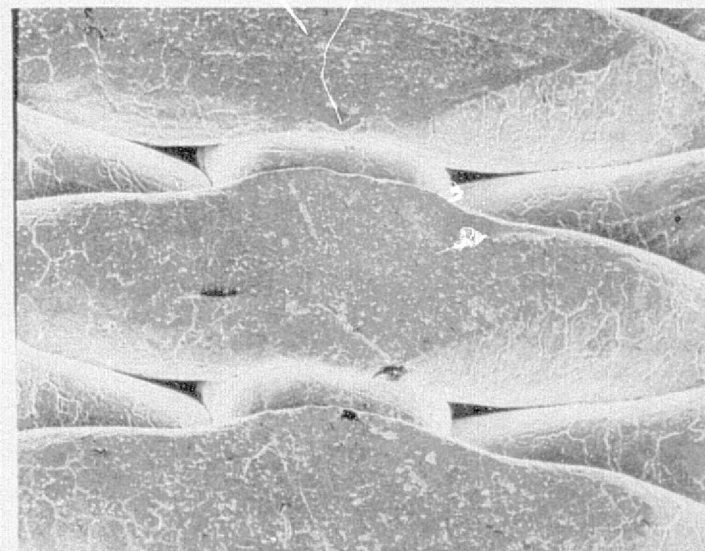
40X



80X

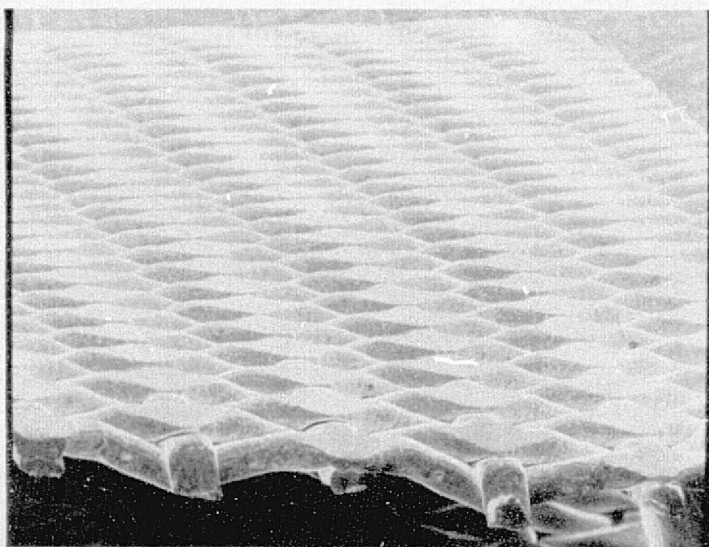


100K

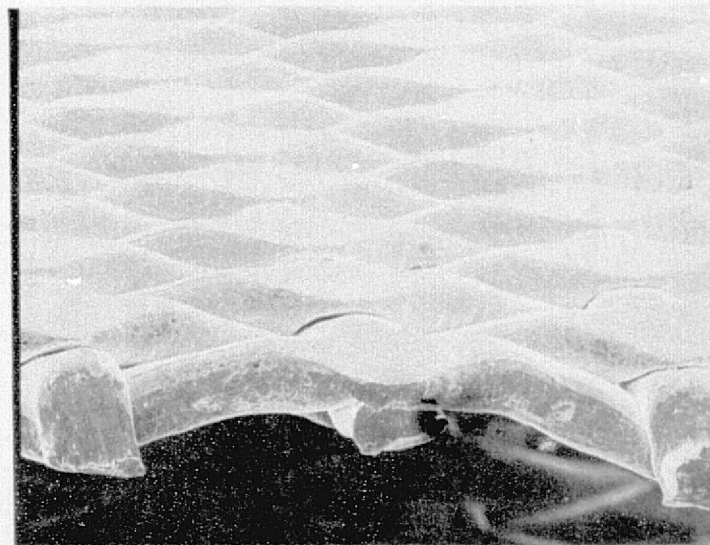


200X

Figure 21. Dynapore 50 X 250 Mesh Typical  
Air Flow Paths Through the Material



40X



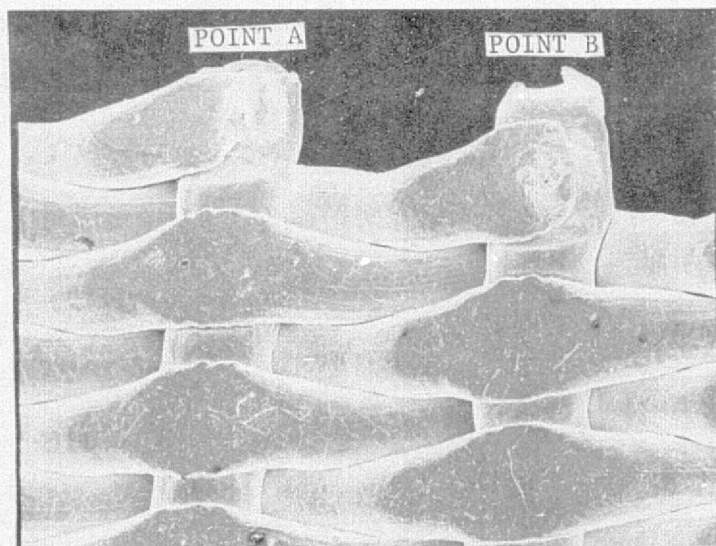
80X



200X

Figure 22. Dynapore 50 X 250 Mesh Typical Thickness  
Deformation at Cross Sections of Mesh

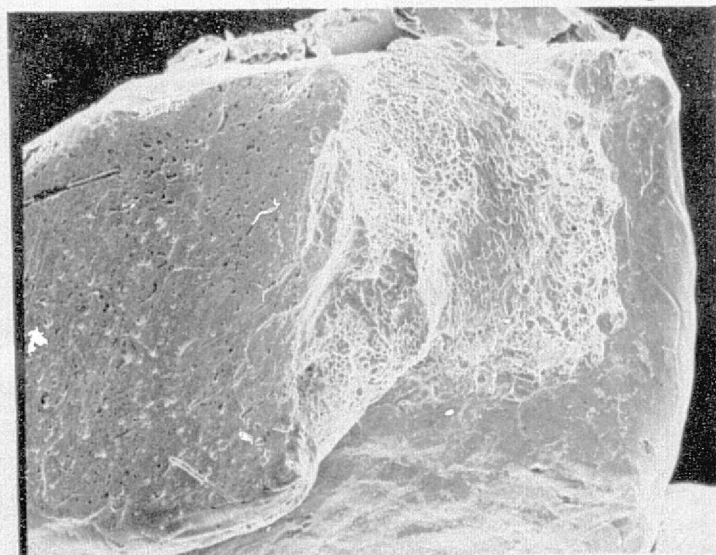




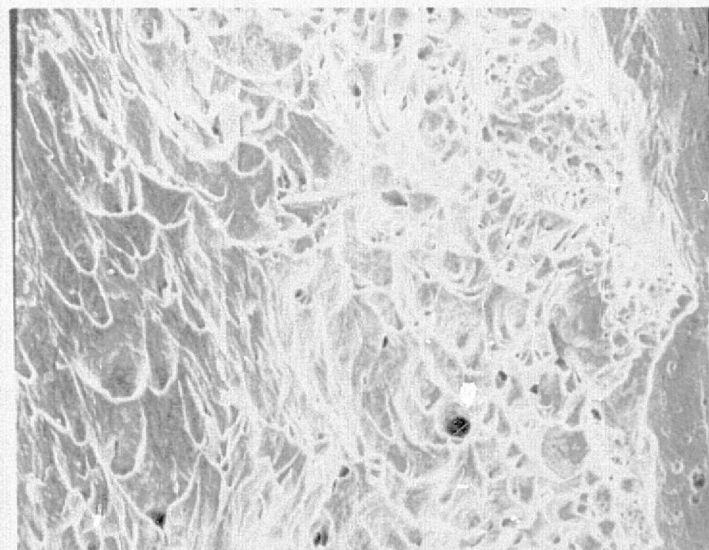
80X



200X

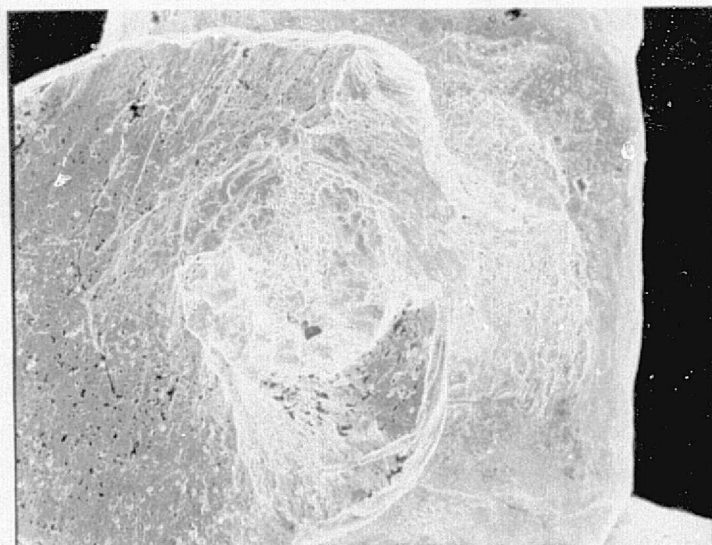


400X

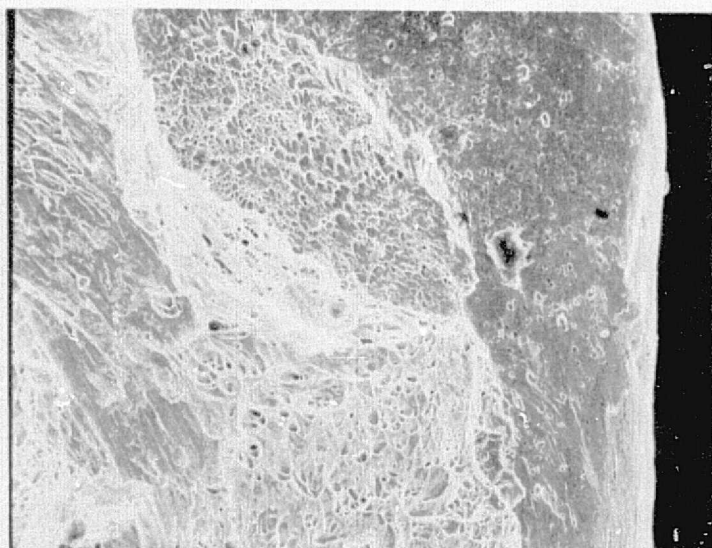


2000X

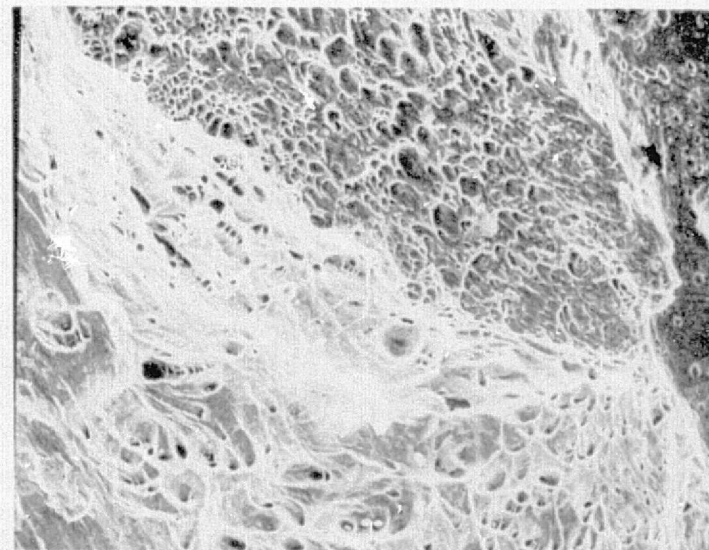
Figure 23. Dynapore 50 X 250 Mesh Broken Bond Interface Region (Point A)  
Typical Dimple Rupture Evidence of Diffusion Bonding



400X



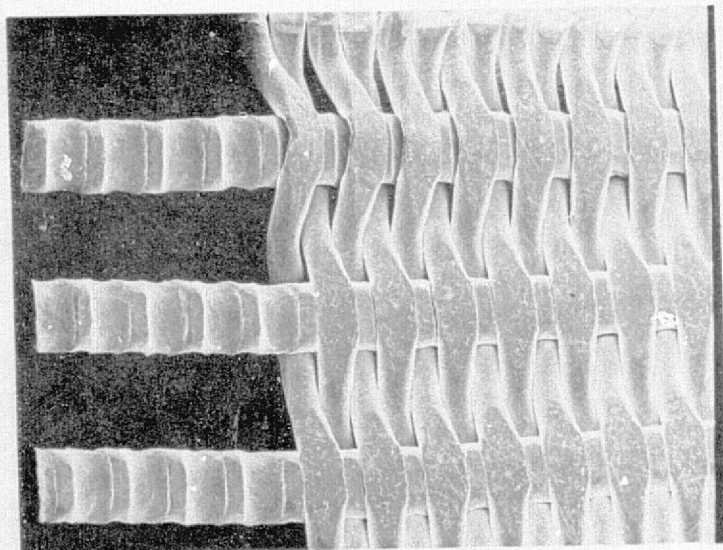
1000X



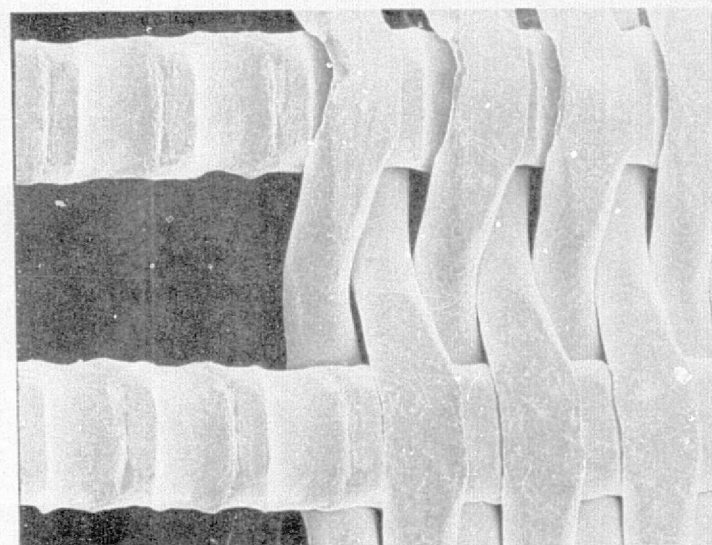
2000X

Figure 24. Dynapore 50 X 250 Mesh Broken Bond Interface Region  
(Point B) Typical Dimple Rupture Evidence of Diffusion Bonding

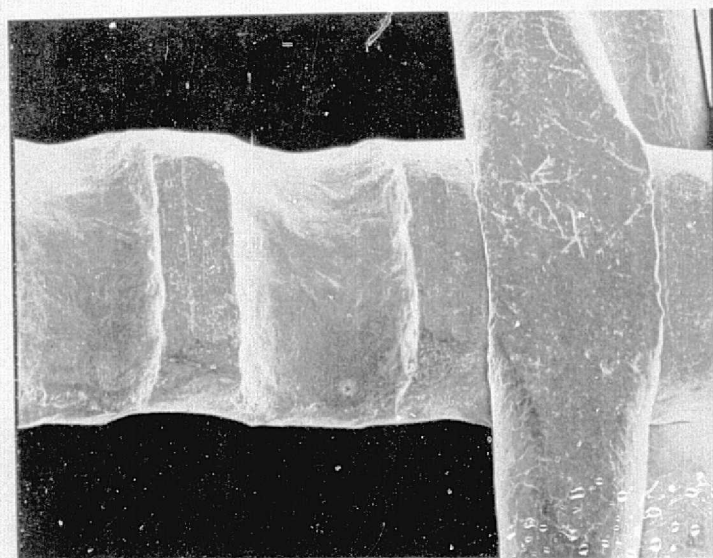




20X



40X



80X

Figure 25. Dynapore 24 X 110 Mesh - Surface Deformation and Evidence of Unbonded Mesh Wires

### Microperforated Plate on a Substrate

Besides the Dynapore Monolayer being developed as a special product, Michigan Dynamics manufactures as a standard product a fine scale, sintered and compacted square weave wire mesh called Dynapore Microperforated Plate<sup>TM</sup> (MPP). Two such 316L stainless steel meshes were utilized on airflow samples for this program; however, no strength properties were obtained. Available physical properties of the #21 and #24 meshes are listed in Table IV. The meshes were selected for minimal weight and for differences in pore size which might have an influence on allowable smoothness, contamination retention, and bonding characteristics when joined to a substrate. MPP is considered useful to provide aerodynamic surface smoothness, electrical conductivity, and environmental protection for reinforced composites, but are too thin to be considered a structural material by themselves.

One drawback in their use is the difference in thermal expansion coefficient between the stainless and some substrates, notably Kevlar. This causes warpage or locked-in stresses for panels bonded at common processing temperatures. The #24 MPP has the least thickness and therefore caused less warpage however, its fragility made it difficult to handle and bond without wrinkling (specimens 16 and 18). The #21 MPP with 3-mil thickness provided smoother surfaces (Panels 15, 17 and 19). Figures 26 and 27 show the microperforated plate facings on Panels 15 and 17.

Cocuring the MPP to Kevlar composite with 5134 controlled flow laminating resin presented no problem and no resin bleed-through to the outside surface to destroy the manufactured smoothness of the microperforated plate.

An alternate substrate for MPP is a solid sheet containing relatively large perforations. This concept offers positive porosity control since MPP pores and the large perforations can be produced to known sizes. A fabrication feasibility panel was produced but not airflow tested, since it was judged too open. Relatively few of the 1/8-inch perforations in the aluminum backing plate were contaminated with adhesive. There were adhesive fillets inside all perforations against the MPP, and the adhesive bled through the MPP providing a deposit on the outside which would require fine sanding to remove; however, the concept remains promising and invites processing development.

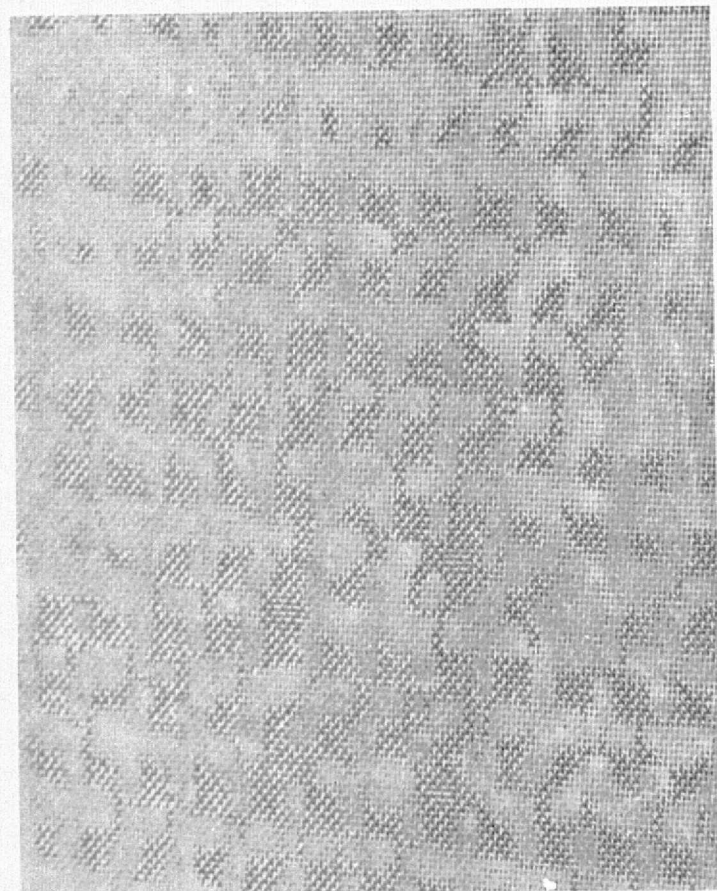
TABLE IV

## MICRO-PERFORATED PLATE CHARACTERISTICS

ITEM	PART NO.	MATERIAL	MESH PER INCH	HOLE INCH (mm)	THICKNESS INCH (mm)	OPEN AREA PERCENT	WEIGHT lb/ft <sup>2</sup> (kg/m <sup>2</sup> )	COST \$/ft <sup>2</sup> \$/m <sup>2</sup>
21	406121	316SS	120	(.117) .0046	(0.74) .0029	30.7	(.566) .116	(1) (78.90) 7.33
24	406251	316SS	250	(.061) .0024	(.033) .0013	36.0	(.224) .046	(92.89) 8.63

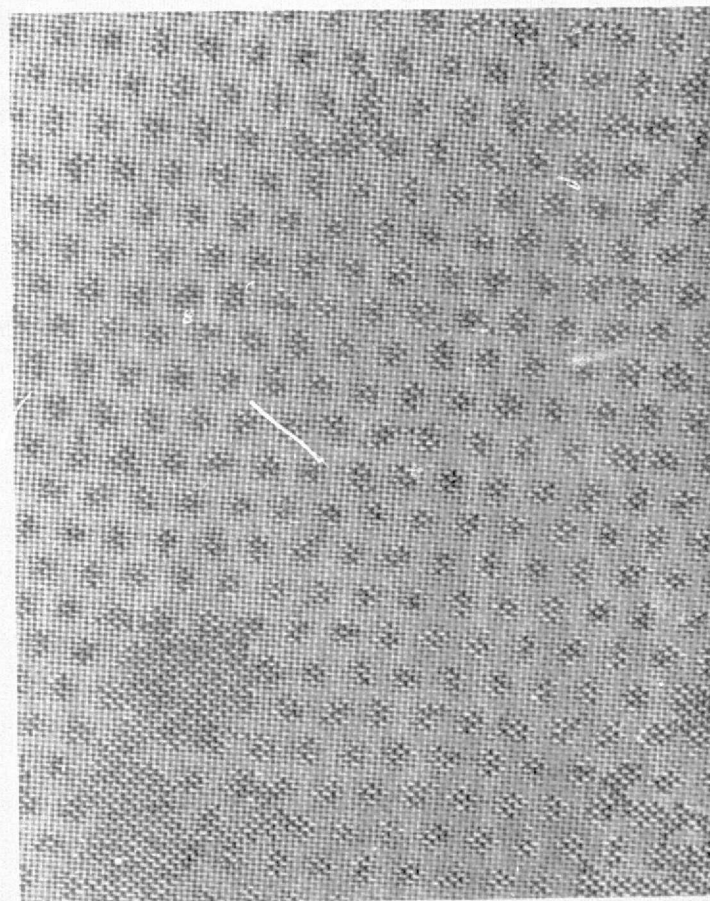
Note: (1) Small Quantity, 1976.





PANEL NO. 15 4.5X  
 $[0_L/90_L]_{MPP \#21}$  THICKNESS .039 INCH  
 $L_T$  (.99 mm)

Figure 26. Leno With Microperforated  
Plate Facing



PANEL NO. 17 4.5X  
 $[0_D/90_D]_{MPP \#21}$  THICKNESS .025 INCH  
 $_2$  (.64 mm)

Figure 27. Doweave with Microperforated  
Plate Facing

The thermal expansion coefficient differentials for 316L/Aluminum are approximately one-half those of 316L/Kevlar.

Figure 28 indicates the MPP-on-Substrate concept with typical dimensions for 0.5-percent open. For a square pattern, 0.5-percent requires holes spaced at  $12.53 d$ , where  $d$  is hole diameter. Such a large (practical) spacing could well appear as roughness to the boundary layer during LFC suction performance. Also, the large spacing implies a parallel stiffener or rectangular grid discrete stiffening pattern to avoid the hole blockage probable with a random stiffening pattern, such as honeycomb core. Smaller holes at closer spacing, i.e., 0.040 inch diameter and 0.30 inch spacing, would minimize these difficulties, but greatly increase the chance of hole blockage with adhesive. In the case of aluminum panels under MPP, it is felt the aluminum should be treated to preclude hole contamination from corrosion. For anodizing, the hole diameter is effectively limited to twice the sheet thickness to assure plating the inside of the perforations.

Calculation of thermal contraction stresses of MPP relative to Kevlar panels after bonding revealed that stresses between 9.5 and 12 ksi probably exist in the MPP at  $-60^{\circ}\text{F}$ . These stresses depend on whether initial bonding occurs at  $350^{\circ}\text{F}$  or  $250^{\circ}\text{F}$ , on relative areas and stiffnesses of the dissimilar materials and, of course, their relative thermal expansion coefficient. For 316L/Kevlar, the  $\Delta\alpha$  used was  $8.9 \times 10^{-6}$  in/in/ $^{\circ}\text{F}$ . Strength and stiffness of #21 MPP is not known, but on the basis of tests performed on the thicker Dynapore Monolayers, the above stresses may be a significant proportion of its yield strength. Assuming the microperforated plate to be made from Ph 17-7 stainless ( $\Delta\alpha = 5.8 \times 10^{-6}$  in/in/ $^{\circ}\text{F}$ ) reduced the stresses to 4.5 to 7.6 ksi. This analysis was done on a one-dimensional basis (bi-material bar, 1 inch wide) rather than the true 2-dimensional basis, to assess the feasibility of the Kevlar/steel material combinations. These preliminary results suggest that the MPP may not be feasible on Kevlar in loaded panels unless some stress relieving procedure after bonding is worked out. A more detailed thermal analysis is recommended, based on experimental strength, stiffness, and thermal data. The combination of 316L Microperforated Plate bonded to Kevlar panels that are non-load-bearing appears eminently feasible, provided some design or processing means is devised to avoid panel warpage.

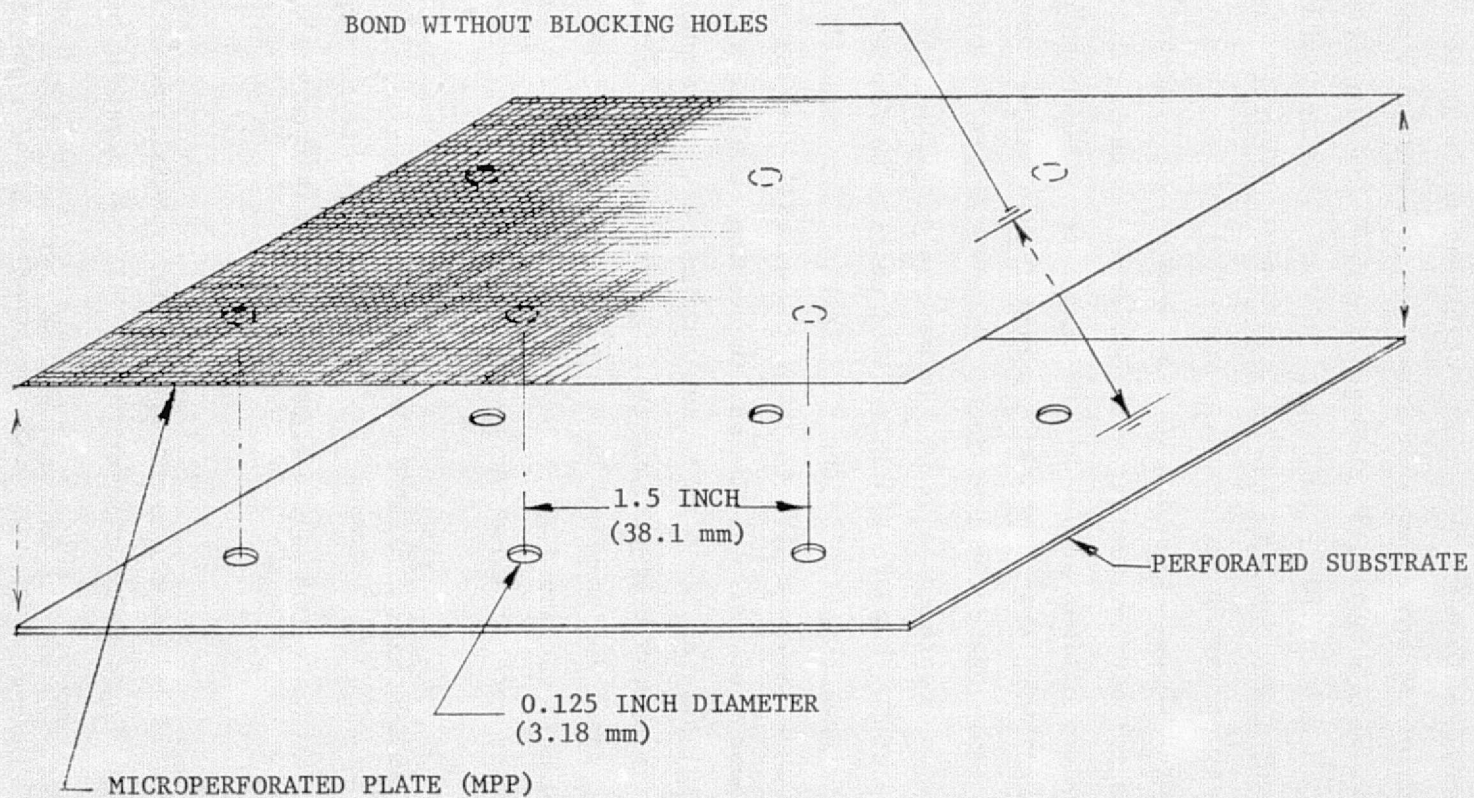


Figure 28. MPP On Substrate Concept



#### No. 143 Weave Kevlar/Epoxy

This weave is identical to the same numbered weave utilized in fiberglass reinforced plastic design. It has 90 percent unidirectional fibers (10 percent fill) and nominally provides 0.010 inch per ply thickness in laminates. This fabric, impregnated with 5134 resin, was utilized for the electron beam (EB) perforated panels, specimens numbered 39 through 62 and 76-79. In these panels, the ply thickness varied around .012 - .013 inch, perhaps because Doweave plies were integrated into the laminates with the No. 143. The ply pattern desired, to correlate with the  $60^{\circ}$ -array EB perforation, was  $[0, \pm 60]_n$ . This pattern should minimize the strength reduction due to open hole stress concentrations. A range of thicknesses for airflow testing with perforations was desired but, with the given material, a minimum achievable thickness for a balanced ply laminate was 0.060 inch. With the  $[0/\pm 45/90]_s$  pattern, this minimum would have been 0.080, four times the desired minimum. Unbalanced ply laminates were therefore accepted as representative of the materials system in the thickness range .020 - .060. Doweave was introduced chiefly to provide  $0^{\circ}$  fibers where there were none supplied by the #143 fabric. Conceptually, Doweave could be used as a laminate core to lower the overall density and increase solid panel moment of inertia, thereby increasing buckling allowable strength. Table V illustrates layup patterns, thicknesses, and densities of the panels made for electron beam perforation. A more amenable material for thin, balanced-ply panel design would have a ply thickness of 0.006 inch, similar to some of the unidirectional graphite fabrics now available. No other physical properties were obtained for these laminates.

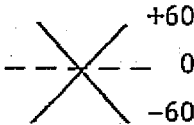
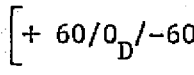
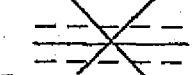
#### Electron Beam Perforation of #143 Weave Kevlar/Epoxy Panels

Figure 29 is an index showing the electron beam perforation patterns requested in the 3 basic panels fabricated and the specimen numbers cut from each panel section.

Figure 30 shows photographs of two electron beam drilled panels, one of which is .007 inch Ti plated. It is to be emphasized that all the electron beam drilled panels were very smooth to touch. As a matter of interest, a sampling of the drilled holes, Figures 31 and 32, are examined with the scanning electron microscope. Views are taken with both perpendicular to the panel and at an angle to show the interior surface of the hole. Effort was made to present

TABLE V

NO. 143 KEVLAR/200 DENIER DOWEAVE LAMINATES, 5143 RESIN

PATTERN (1)	PANEL NO.	THICKNESS OF PANEL - INCH (mm) (2)	LAMINATE DENSITY - PSI (gm/cm <sup>3</sup> )
	39, 40, 41, 42, 43, 51, 52, 53, 54	.029 - .032 (.74 - .81 mm)	TBD
	44, 45, 46, 55, 56, 57, 57, 58, 76, 77	.044 - .051 (1.12 - 1.30 mm)	
	47, 48, 49, 50, 59, 60, 61, 62, 78, 79	.055 - .072 (1.40 - 1.83 mm)	

- (1) ————— No. 143 KV29/5134  
 - - - - - 200-d Doweave, KV29/5134

- (2) Vacuum bag pressure cure.

Layup  
Description on  
Table V

0.1% OPEN  
(0.18 mm)  
0.007" Ti Foil Surface  
This Panel Only

3-PLY

#39

#40

5-PLY

#76

#77

6-PLY

#78

#79

Requested  
Hole Dia  
(In)

.004 (0.10mm) .008 (0.20mm)  
.135 (3.43mm) .243 (6.17mm)

0.5% OPEN

24 (typ)

#41

#42

#43

#44

#45

#46

#47

#48

#49

#50

.010 (.25mm) .018 (0.46mm)  
.135 (3.43mm) .243 (6.17mm)

1.0% OPEN

#51

#52

#53

#54

#55

#56

#57

#58

#59

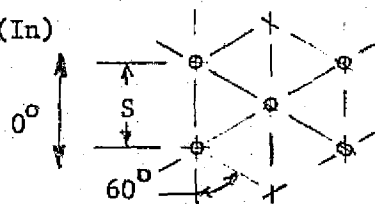
#60

#61

#62

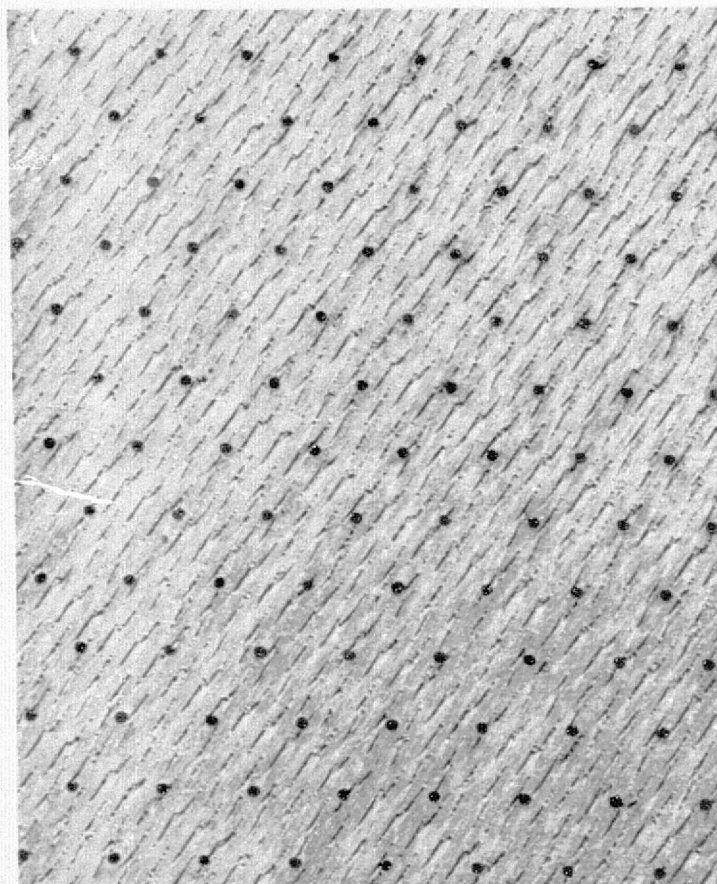
.014 (0.36mm) .026 (0.66mm)  
.135 (3.43mm) .243 (6.17mm)

Hole Spacing (In)

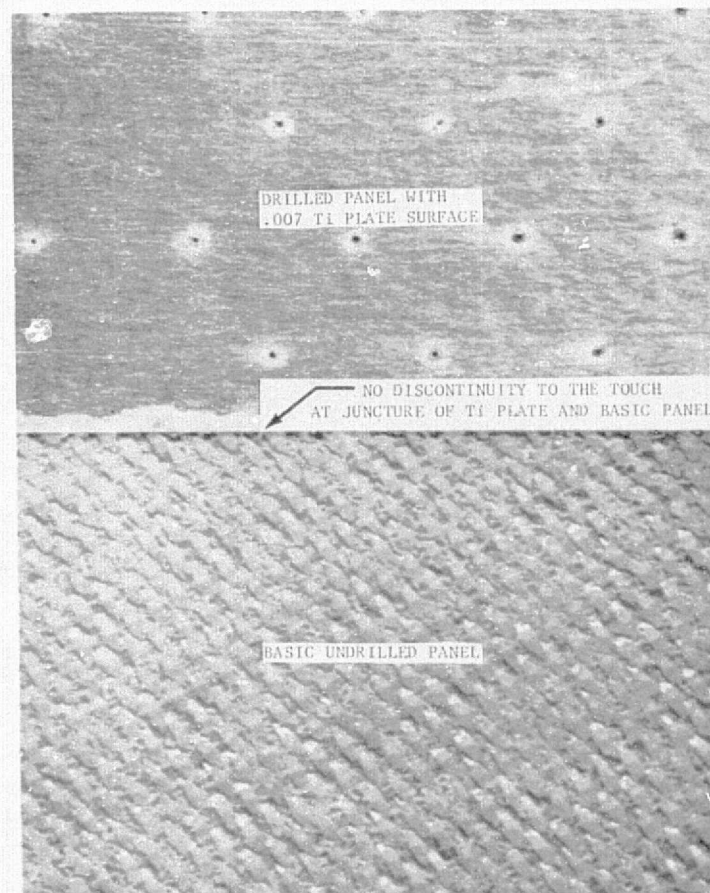


± 60 Array Hole Pattern

Figure 29. Electron Beam Perforated Panel and Panel No. Index



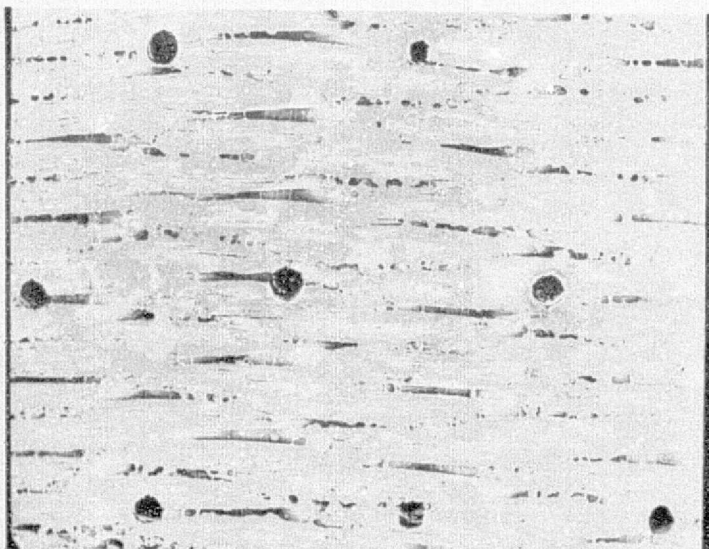
PANEL NO. 43  
 HOLE SIZE .018" (0.46mm)  
 HOLE SPACING .135" ~ 3.75X  
 (3.43mm)



PANEL NO. 40  
 HOLE SIZE .008 (0.20mm) ~ 3.75Δ  
 HOLE SPACING .243 (6.17mm)

Figure 30. Electron Beam Drilled Composite Panels  
 $[-60_{143}/0_D / 60_{143}]_T$

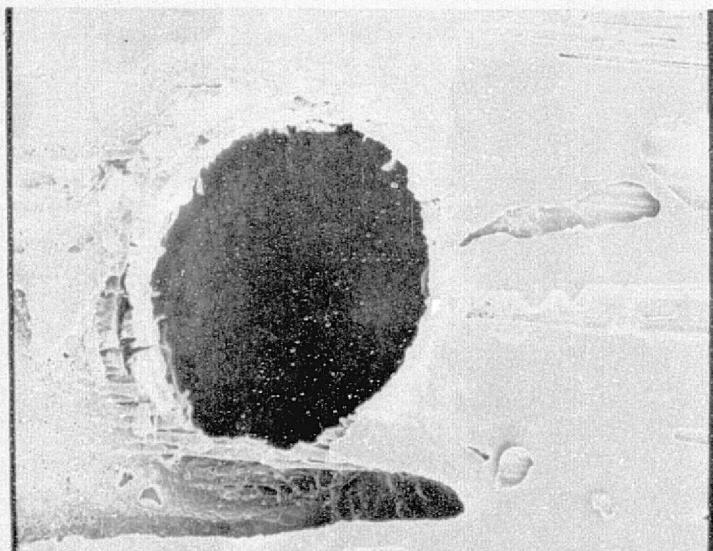




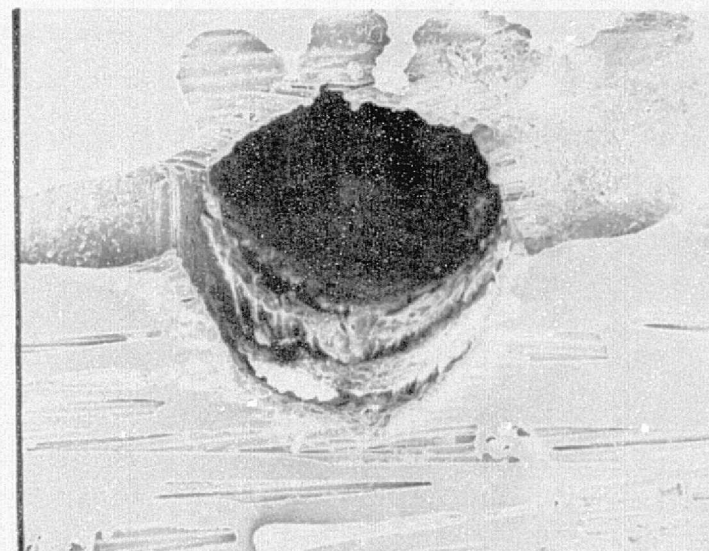
10X



20X



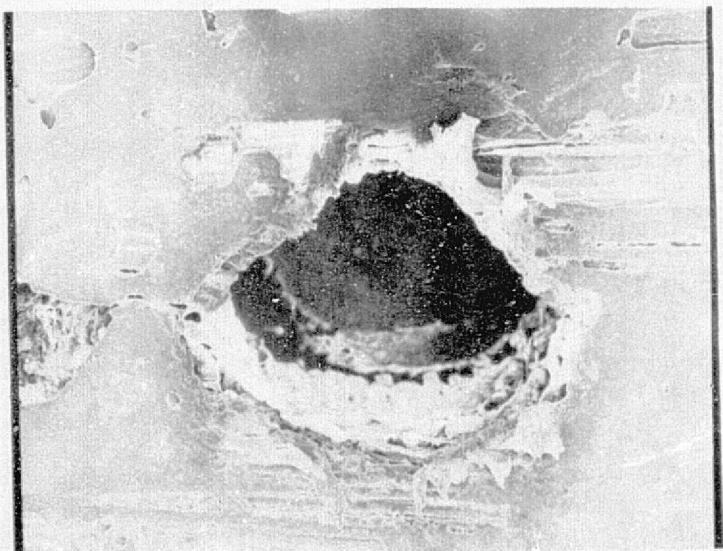
100X



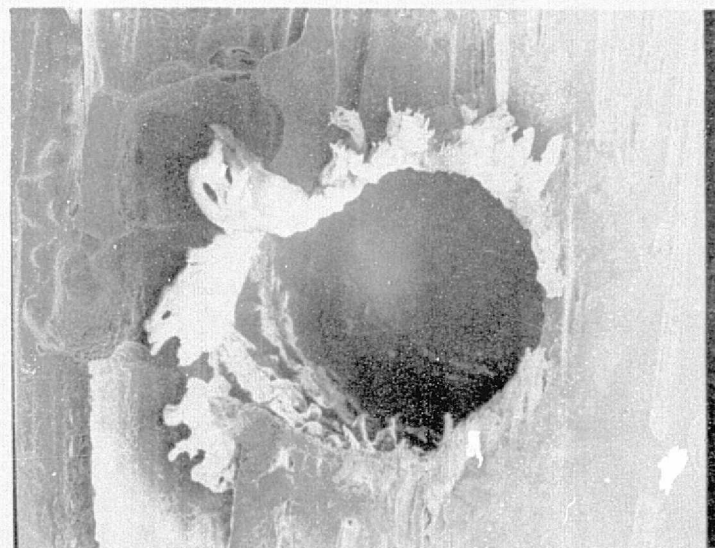
100X

Figure 31. Electron Beam Drilled Composite Panel (No. 149)  
 $\left[ -60_{143} / 60_{143} / 0_D / 0_D / 60_{143} / -60_{143} \right]_T$  Thickness = .055 Inch  
 (1.40 mm)

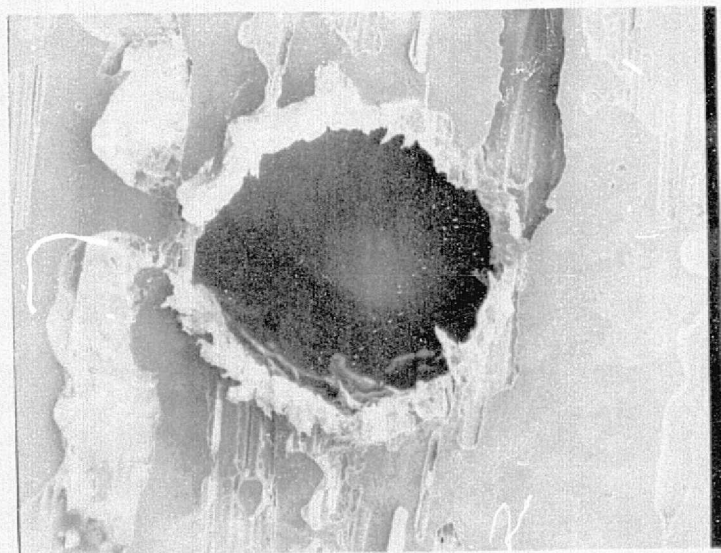




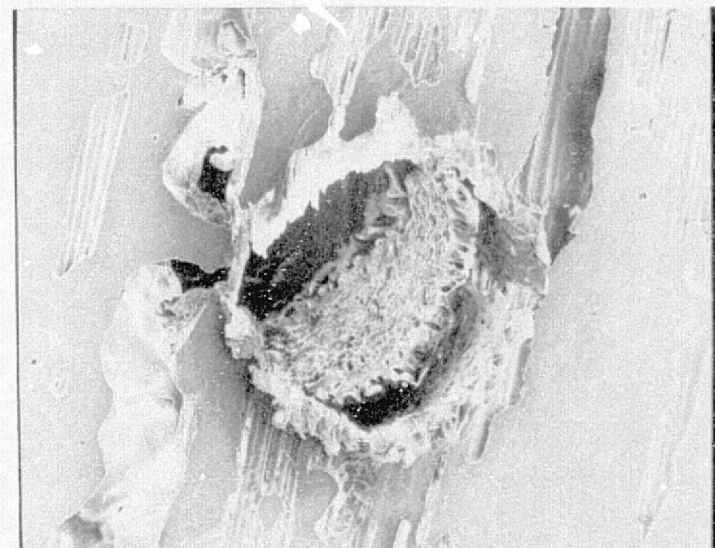
100X



100X



100X



100X

Figure 32. Electron Beam Drilled Composite Panel (No. 49)  
Normal and Oblique Views of Drilled Holes

examples of the "better" and "worst" cases of the drilled holes.

The correlation of the effective porosity of the electron beam drilled panels with geometric porosity required an assessment of the actual open area of the drilled panels. Such was obtained by use of the comparator, used by Douglas in their quality control work, whereby the panels could be sufficiently magnified to permit actual accurate measurement of the holes and evaluation of the regularity of the hole pattern. Transmission of light through the panels denotes air passage. Typical panels are thus shown in Figures 33 through 36. The panel number and magnification are noted in the left hand corner of the photograph. Effects of panel thickness, hole spacing, hole size, and the addition of titanium foil (Figure 33) are included in the above-mentioned photographs.

The geometrical properties of the electron beam perforated specimens as determined from the optical comparator inspection are given in Table VI. Since the entire flow area used in the test could not be inspected, the determination of hole size and porosity was made on the basis of a statistical sampling of a fraction of all the holes within the flow area. The average statistical population of hole sites examined was about 6 percent of the total within the flow area. There was appreciable variation in the quality of the hole size distributions. In an attempt to indicate possible geometric porosity data quality, Table VI indicates the relative dispersion of the hole diameters. This is the ratio of hole size standard deviation divided by the mean hole diameter. This parameter varies from a maximum of 117 percent to as low of 3.9 percent. For those specimens with missing holes, the porosity was determined by including the blank site in the determination (diameter)<sup>2</sup> but was excluded in determining the mean hole diameter. This allowed the mean value of diameter to represent only those holes that were present.

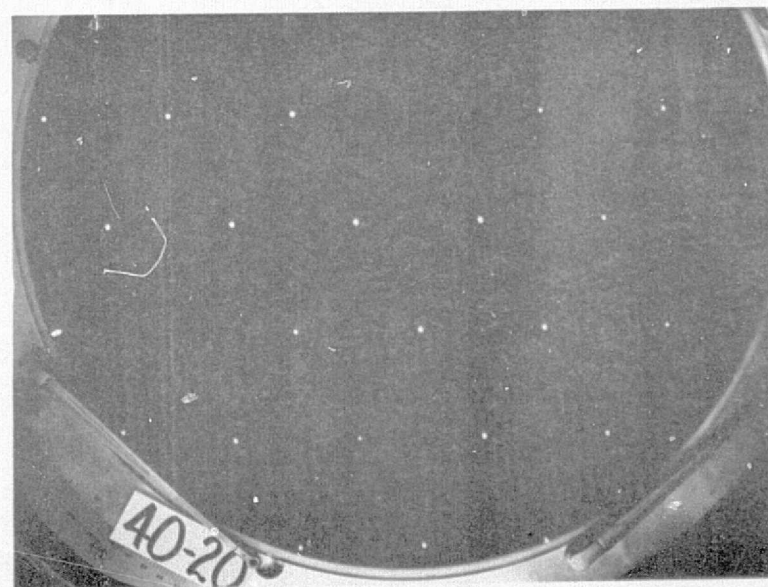
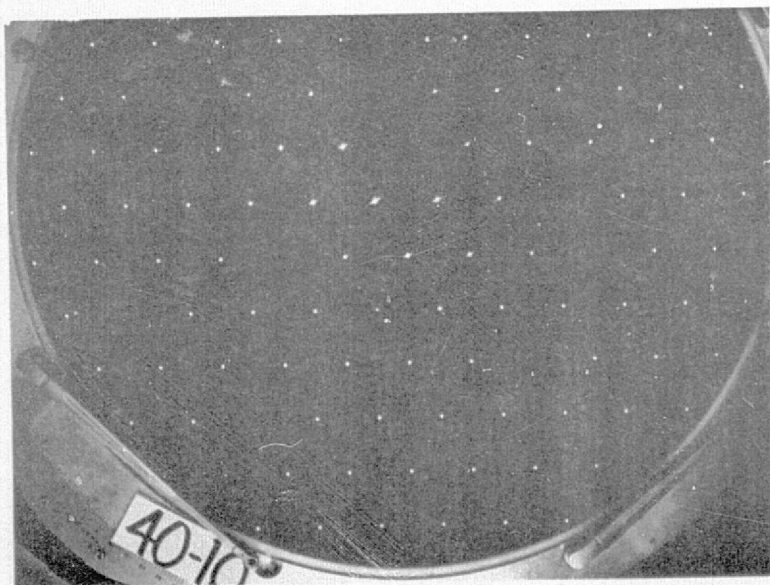
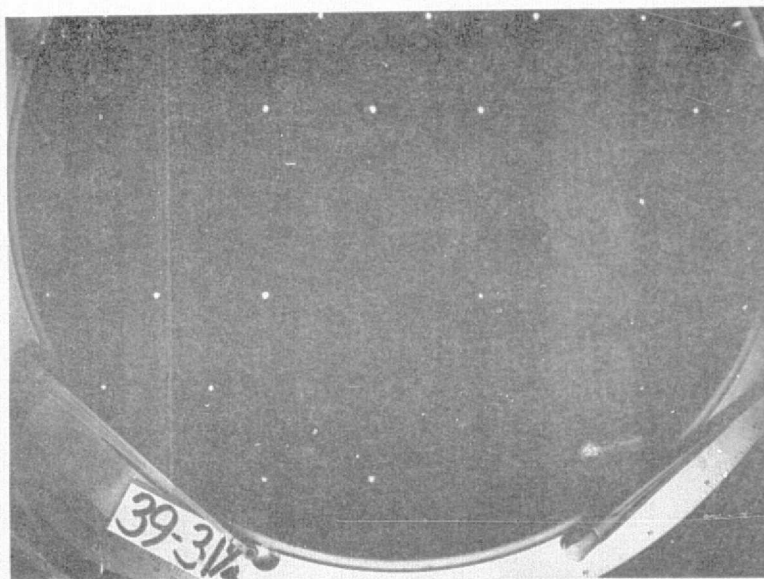
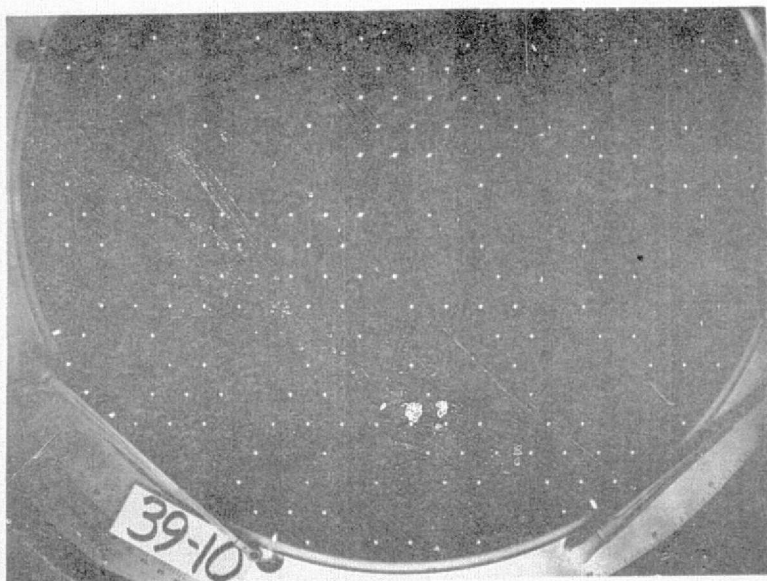
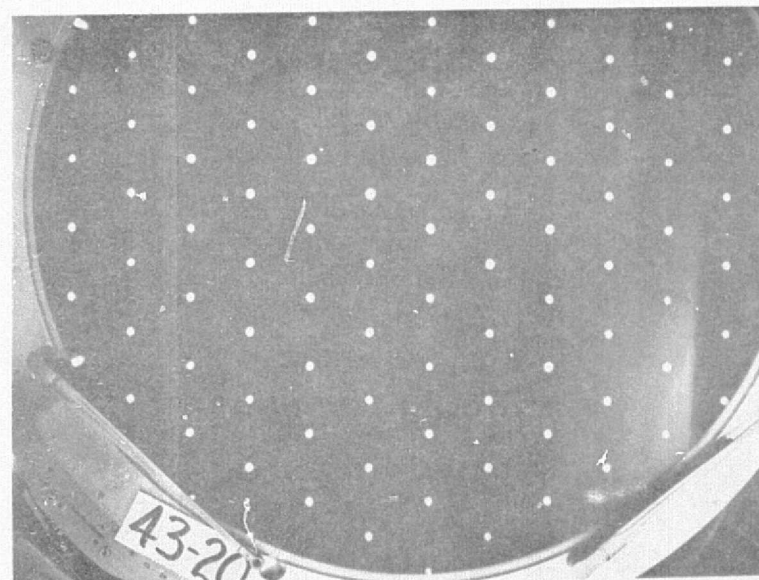
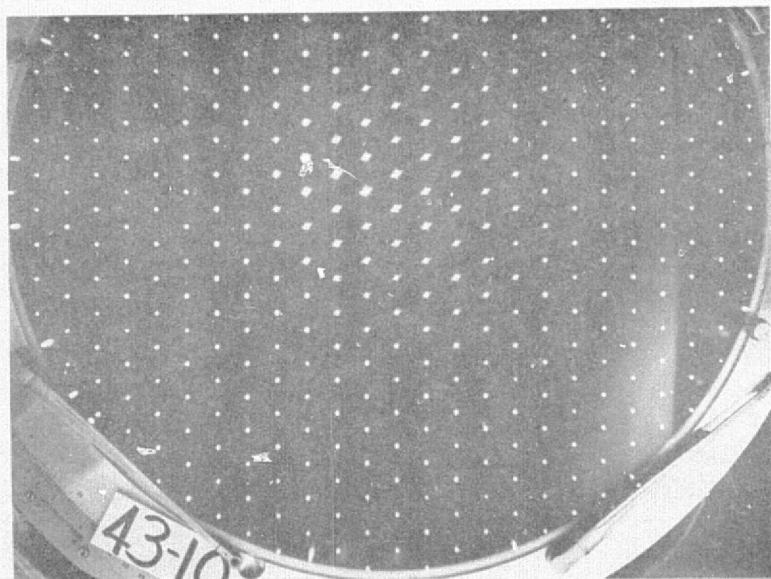
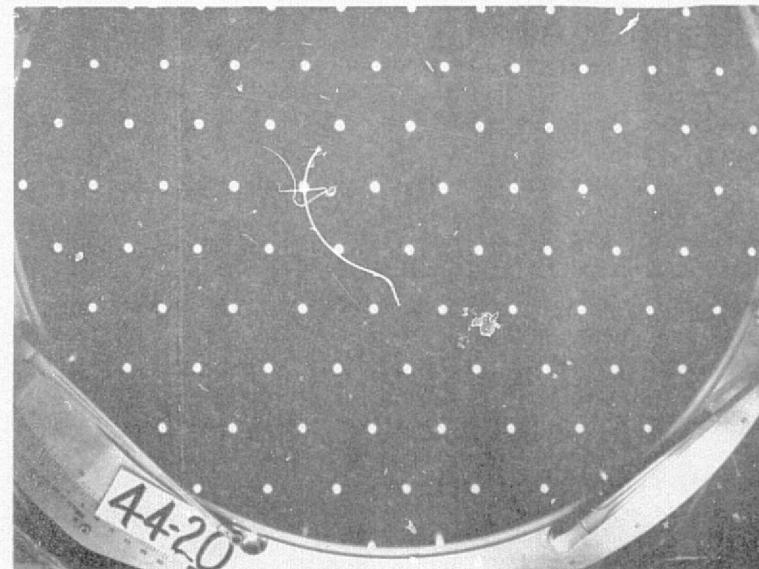
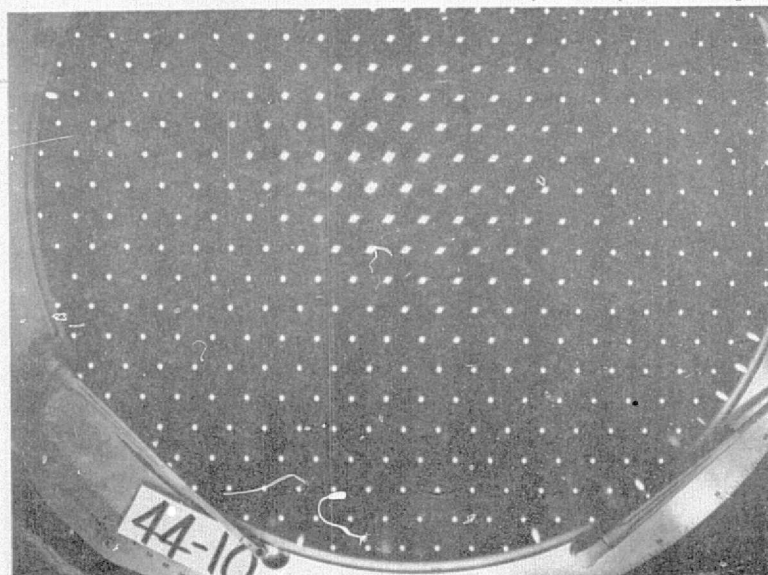


Figure 33. Hole Spacing .243 Inch (6.17mm) Hole Size .008 Inch (0.20mm)  
Electron Beam Drilled Panels + .007 In. (0.18mm) Ti Plate



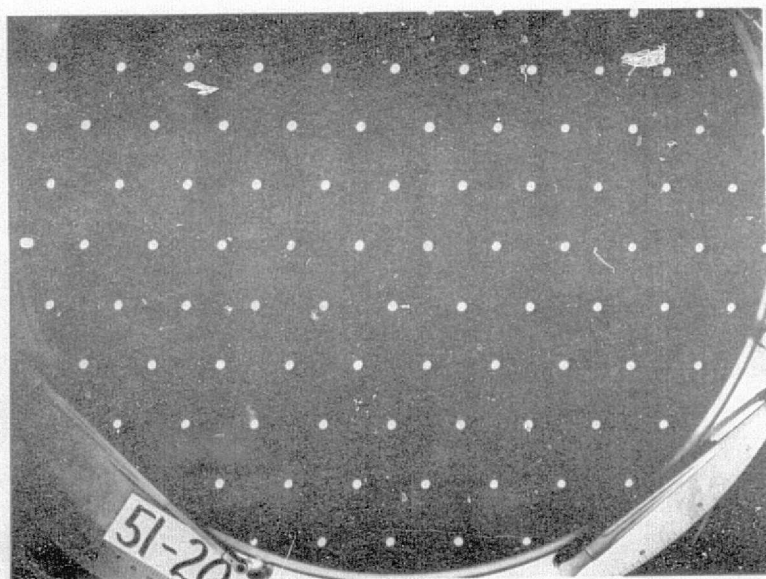


Thickness .029 Inch (.74mm) Hole Spacing .135 Inch (2.89mm) Hole Size .018 Inch (.457mm)

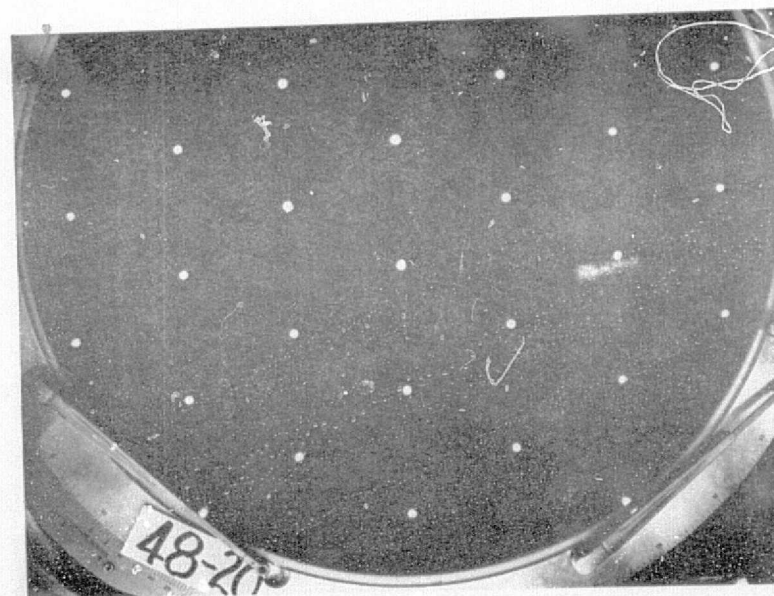


Thickness .044 Inch (1.12mm) Hole Spacing .243 Inch (6.17mm) Hole Size .018 Inch (0.46mm)

Figure 34. Electron Beam Drilled Panels



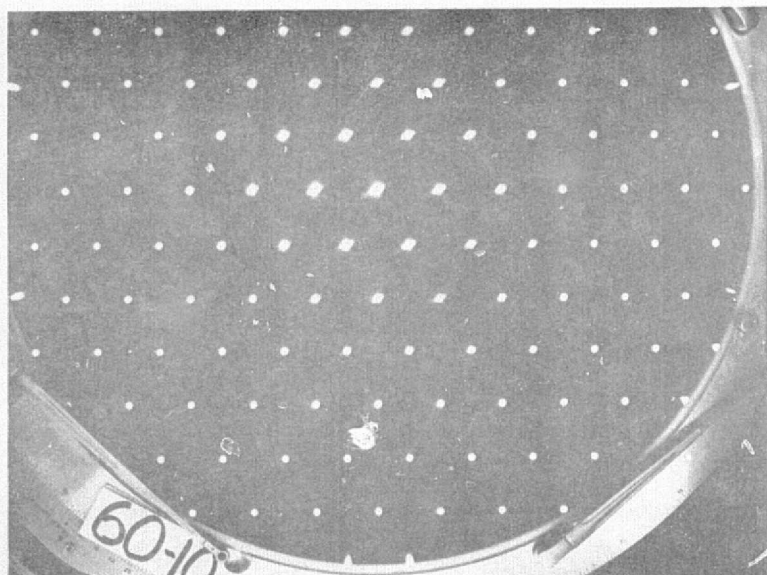
Thickness .032 Inch  
(0.81mm)      Hole Spacing .135 Inch (3.43mm)  
Hole Size .014 Inch (0.36mm)



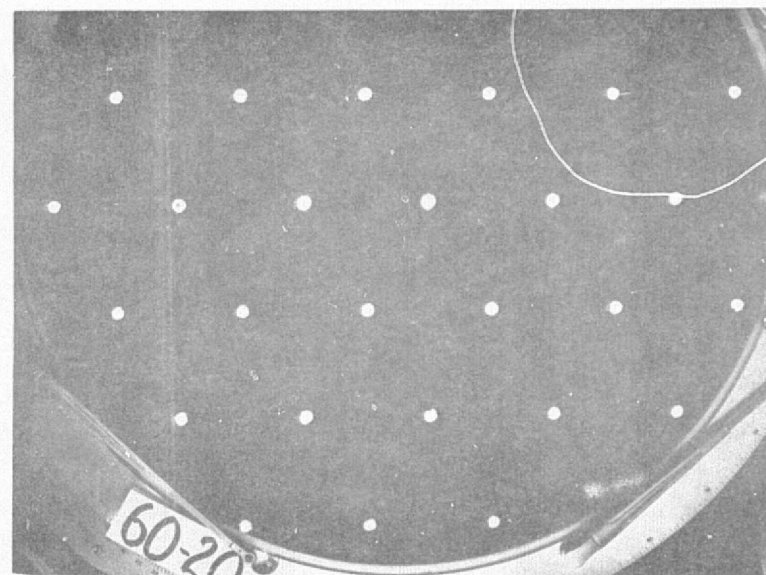
Thickness .055 Inch (1.40mm)  
Hole Spacing .243 Inch (6.17mm)  
Hole Size .018 Inch (0.46mm)

Figure 35. Electron Beam Drilled Panels



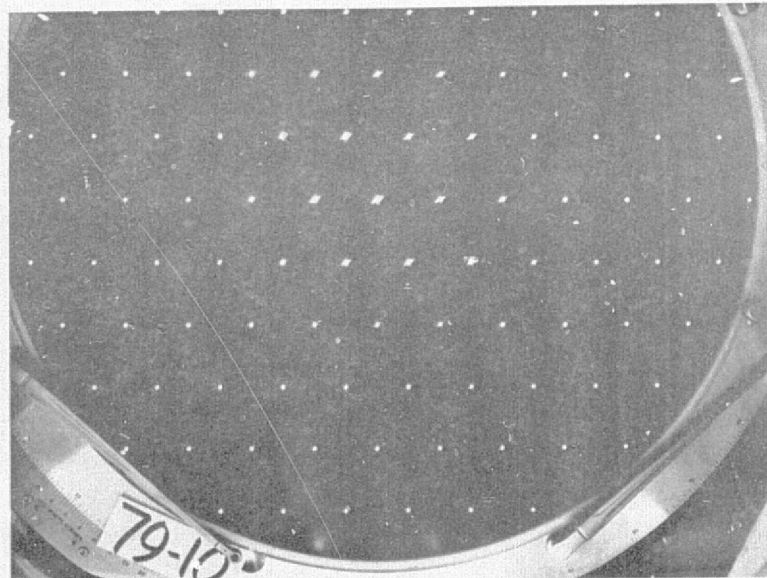


Thickness .072 In. (1.83mm)

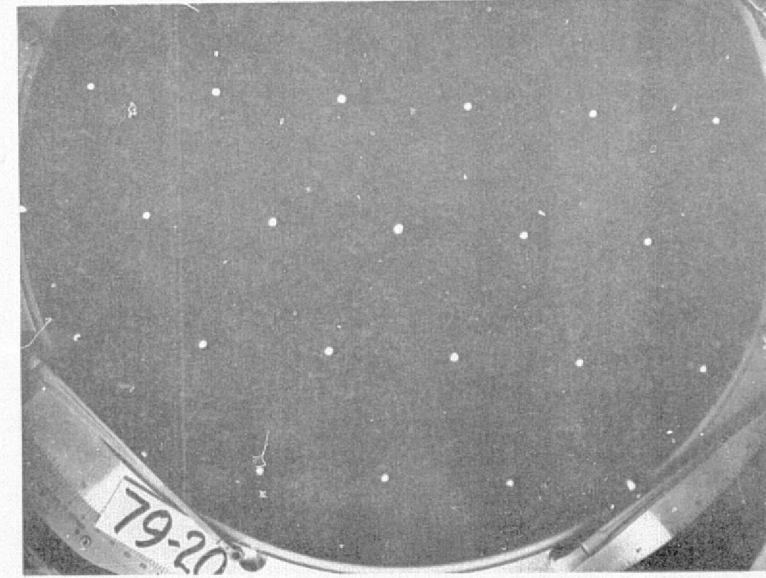


Hole Spacing .024 In. (0.62mm)

Hole Size .026 In. (0.66mm)



Thickness .061 In. (1.55mm)



Hole Spacing .243 In. (6.17mm)

Hole Size .014 In. (0.36mm)

Figure 36. Electron Beam Drilled Panels

TABLE VI  
AS INSPECTED PROPERTIES OF E.B. PERFORATIONS

SPEC. NO.	THICKNESS INCH (mm)	NO. HOLE SITES	NO. BLANKS	HOLE SPACING INCH (mm)	MEAN HOLE DIA. INCH (mm)	GEOMETRIC POROSITY $\sigma_g$	HOLE SIZE DISPERSION
*39	.032 (.81)	157	86	.135 (3.43)	.0075 (.19)	.00186	1.147
*40	.032 (.81)	68	7	.243 (6.17)	.0081 (.21)	.00109	1.173
41	.029 (.74)	42	0	.135 (3.43)	.0079 (.20)	.00414	.085
42	.029 (.74)	23	0	.243 (6.17)	.0121 (.31)	.00305	.139
43	.029 (.74)	43	0	.135 (3.43)	.0141 (.36)	.01331	.094
44	.044 (1.12)	44	0	.135 (3.43)	.0150 (.38)	.01487	.044
45	.044 (1.12)	21	0	.243 (6.17)	.0113 (.29)	.00264	.100
47	.055 (1.40)	42	0	.135 (3.43)	.0130 (.33)	.01131	.064
48	.055 (1.40)	19	0	.243 (6.17)	.0144 (.37)	.00428	.068
49	.055 (1.40)	50	0	.135 (3.43)	.0128 (.33)	.01094	.123
50	.055 (1.40)	22	0	.243 (6.17)	.0140 (.36)	.00404	.073
51	.032 (.81)	43	0	.135 (3.43)	.0145 (.37)	.01391	.063
52	.032 (.81)	22	0	.243 (6.17)	.0189 (.48)	.00734	.053
53	.032 (.81)	53	0	.135 (3.43)	.0115 (.29)	.00899	.134
54	.032 (.81)	22	0	.243 (6.17)	.0199 (.51)	.00820	.084
55	.051 (1.30)	57	0	.135 (3.43)	.0108 (.27)	.00782	.141
56	.051 (1.30)	21	2	.243 (6.17)	.0213 (.54)	.01036	.111
57	.051 (1.30)	52	0	.135 (3.43)	.0105 (.27)	.00748	.122
58	.051 (1.30)	22	0	.243 (6.17)	.0228 (.58)	.01062	.049
59	.072 (1.83)	55	5	.135 (3.43)	.0111 (.28)	.00921	.373
60	.072 (1.83)	22	0	.243 (6.17)	.0227 (.38)	.01057	.039
61	.067 (1.70)	62	5	.135 (3.43)	.0106 (.27)	.00872	.429
62	.067 (1.70)	20	0	.243 (6.17)	.0229 (.58)	.01076	.042
*76	.048 (1.22)	53	0	.135 (3.43)	.0086 (.22)	.00980	.098
*77	.048 (1.22)	20	0	.243 (6.17)	.0082 (.21)	.00139	.142
*78	.061 (1.55)	50	0	.135 (3.43)	.0112 (.28)	.00840	.076
*79	.061 (1.55)	21	0	.243 (6.17)	.0116 (.29)	.00277	.101

\* Denotes Titanium Foil Face

### Lock Core Test Panel

The Lock Core test panels (Panels 33-36, 92 and 93) were based on a sketch reproduced in Figure 37. The outer and inner facing of the basic panel was 8-ply Doweave,  $[0/90]_4$ , and the truss-web was 6-ply Doweave  $[0/90]_3$ . Core mandrels were an extruded silicone rubber with the extrusion dimensions shown. The webs were sewn to the facings for added strength. The panel back-face was divided into three areas. Back-face Area A was unaltered; Area B incorporated strips of a thin, densely woven prepreg intended to provide 50 percent flow reduction through the otherwise 8-ply back-face, and Area C incorporated a 3-ply #181 glass fabric rather than the 8-ply Doweave. The glass was chosen to allow ease of drilling clean holes, since Kevlar frays using most cutting methods except laser. Area C represents a non-porous back-face with discrete perforations for flow metering.

Subsequent to panel fabrication, discs were cut from Areas A, B and C, edge sealed, and tested for airflow through the entire panel. Figure 38 shows the hole pattern drilled in the glass back-facings of Area C, Panels 92 and 93. The figure shows only the 10 cm. test area diameter on which the theoretical back-face porosity (only) was calculated. Figures 39 and 40 show typical photographs of both the Lock Core face sheet and stiffened panels.

Other panels were fabricated to this design, and microperforated plate was cocured and bonded to the outer face to provide additional flow test panels numbered 95 and 96.



19

.07mm)

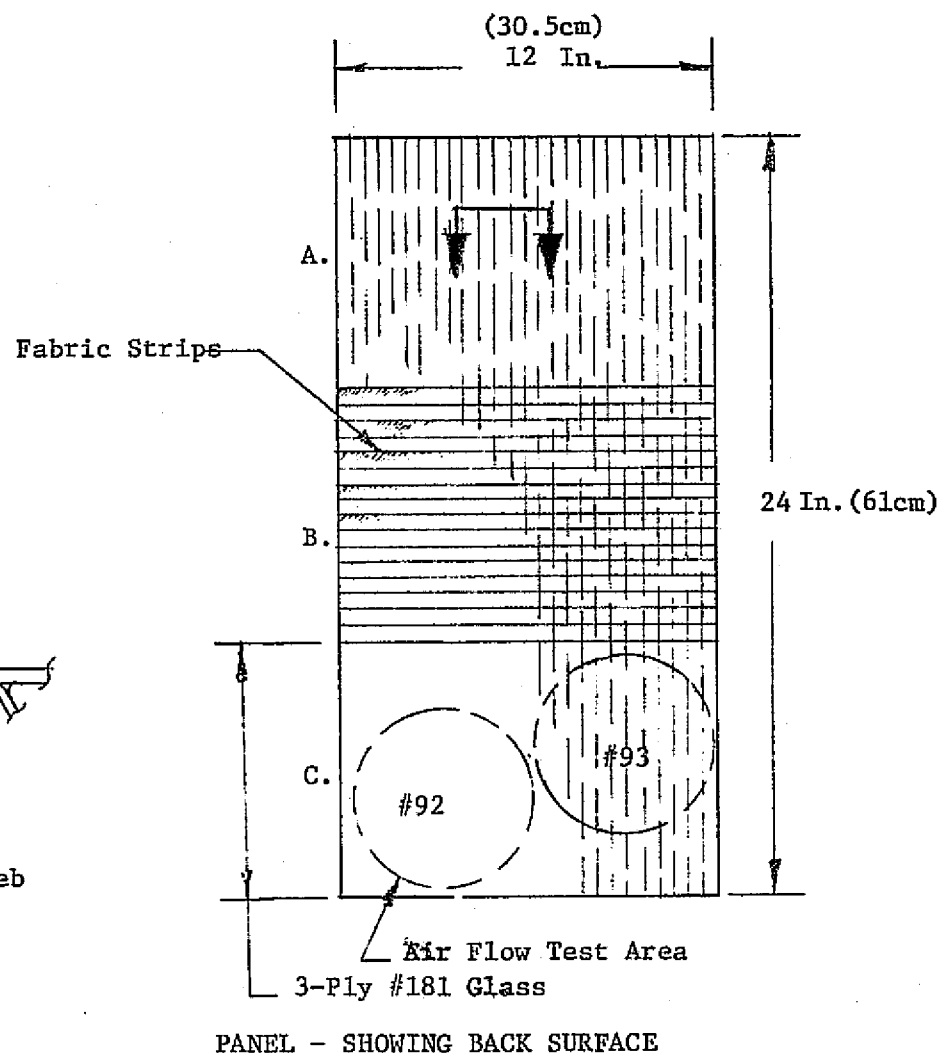
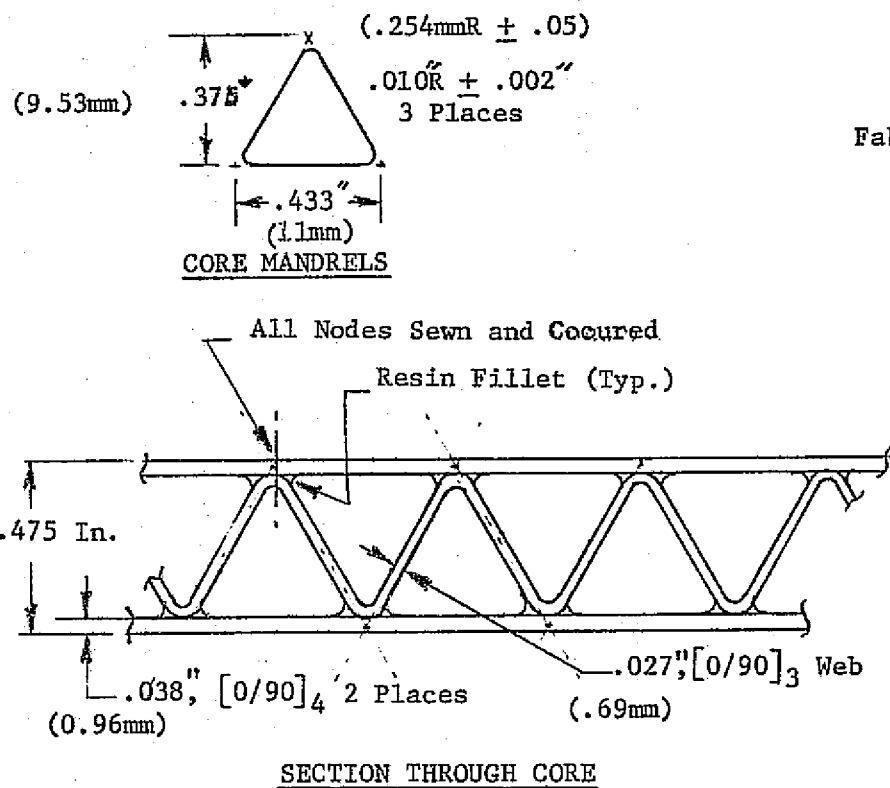


Figure 37. Lock Core Basic Panel Definition

SPECIMEN NO. 92

1.25 In.  
(31.75mm)  
TYP

1 1/4"  
(TYP)

5/8" (TYP)

.625 In.  
(15.88mm)  
TYP

(1.93mm)  
(2.08mm)

.076 In.  
.082 DIA. 14 HOLES . (  $\frac{5}{64}$  NOM. )

$\phi$  - SYMMETRY

.75-In.  
(19.05mm)  
TYP

CORE NODE LINES -  
CENTER HOLES  
BETWEEN JOINTS.  
+ 1/16" ON LOCATIONS. (1.57mm)

POROSITY

.00168  
.00202

(1.57mm).062 In.  
(1.73mm).068 DIA. 7 HOLES  
(1/16 NOMINAL)

POROSITY

.00505  
.00588

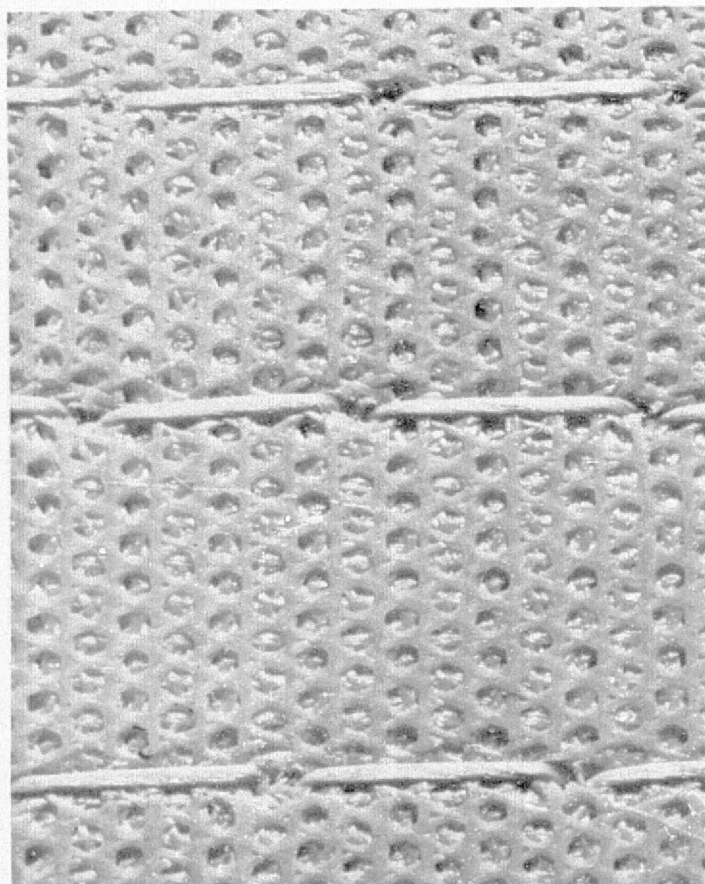
1.00 In.  
(25.4mm)  
TYP

3/4" (TYP)

1" (TYP)

SPECIMEN NO. 93

Figure 38. Backface Hole Patterns, Specimens 92 and 93.



~ 4.0X

Figure 39. Face Sheet of Lock Core Panel

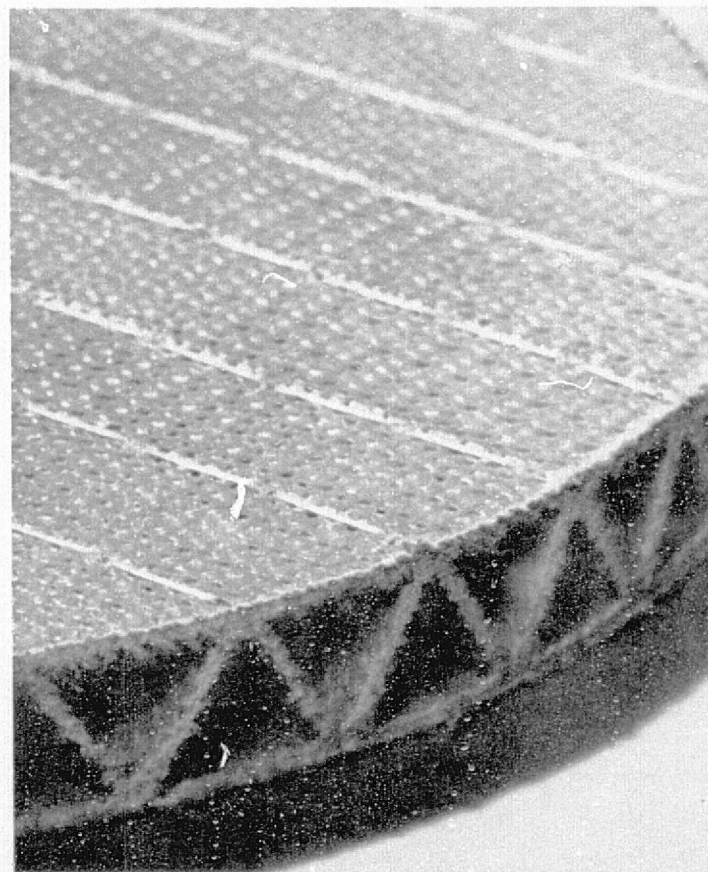


Figure 40. Lock Core Stiffened Panel

### Isogrid Test Panel

The isogrid-stiffened panels (specimens 94-98) were based on a sketch reproduced in Figure 41. It incorporates the same facing that was basic to the Lock Core Panels ( $[0/90]_4$  Doweave). Strength calculations had indicated that the 8-ply facing was stable to a critical buckling failure strain of 5200 micro-inches for the rather large 2.25 inch-grid triangle size. The panel itself was not stable in general stability to the same strain, but was not intended to be. The 1.95-inch triangle altitude is the required general stability support spacing and the complete panel design would have a parallel collection duct layer integrally bonded to this surface panel at each node bar. In anticipation of making the complete panel, the node bars were manufactured wider than the  $\pm 60^\circ$  crossing bars.

The sketch also shows a method for making an integral splice in the grid, since it is anticipated the grid would be made as relatively narrow but long segments using a filament winding procedure. Internal splices would thus be necessary to make a large panel with continuous porous facings.

It should be recognized that a thinner, stiffer facing on a grid, such as a Dynapore Monlayer facing working to the same 5200 micro-inch strains, would require a much more closely spaced grid. The grid depth would be increased to provide general grid stability between underlying supports.

Surface appearance of number 94 grid specimen (Figure 42) shows some waviness, corresponding to the grid triangle dimensions. It is not known if this waviness would exceed the aerodynamic waviness tolerance; at any rate, a stiffer microperforated plate surfacing on the Doweave, along with a closer grid spacing could obviate the apparent problem.

Since these panels did not achieve the targeted pressure drop in their design, even with a microperforated plate surface, future designs would incorporate a thin choker ply in the back facing similar to other airflow panels tested in this program.



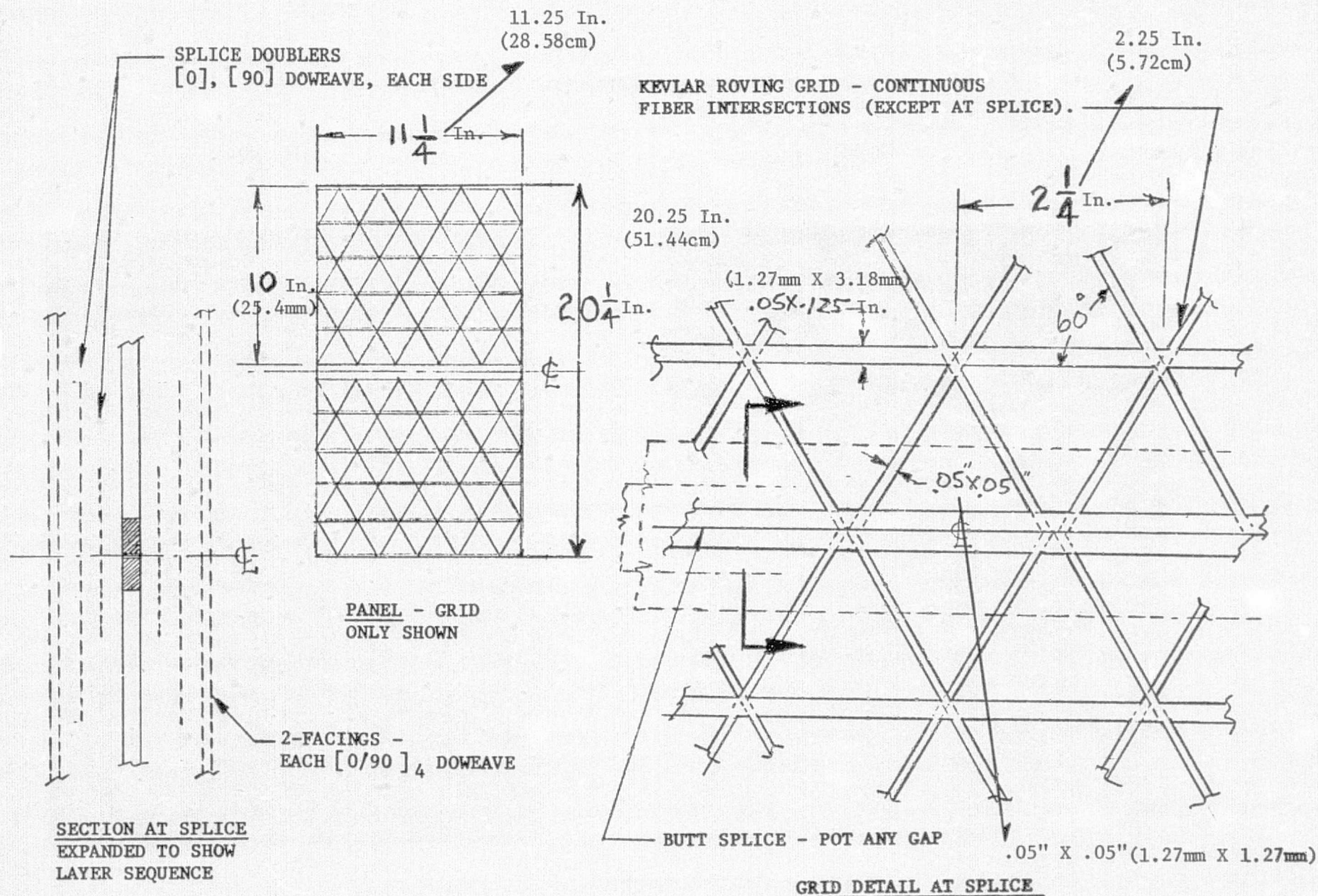
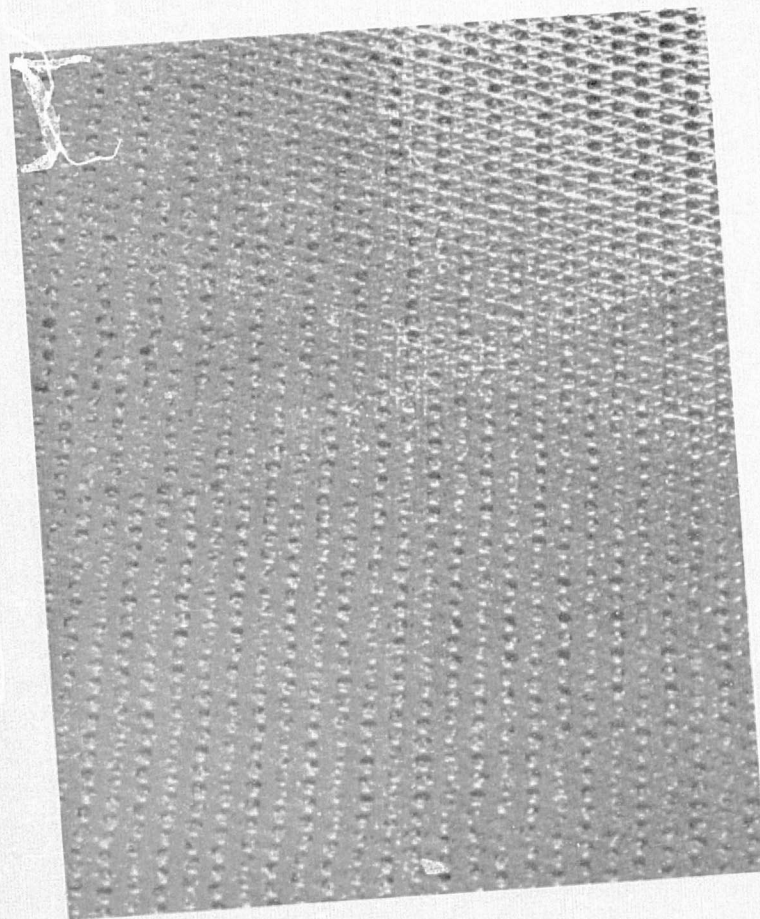
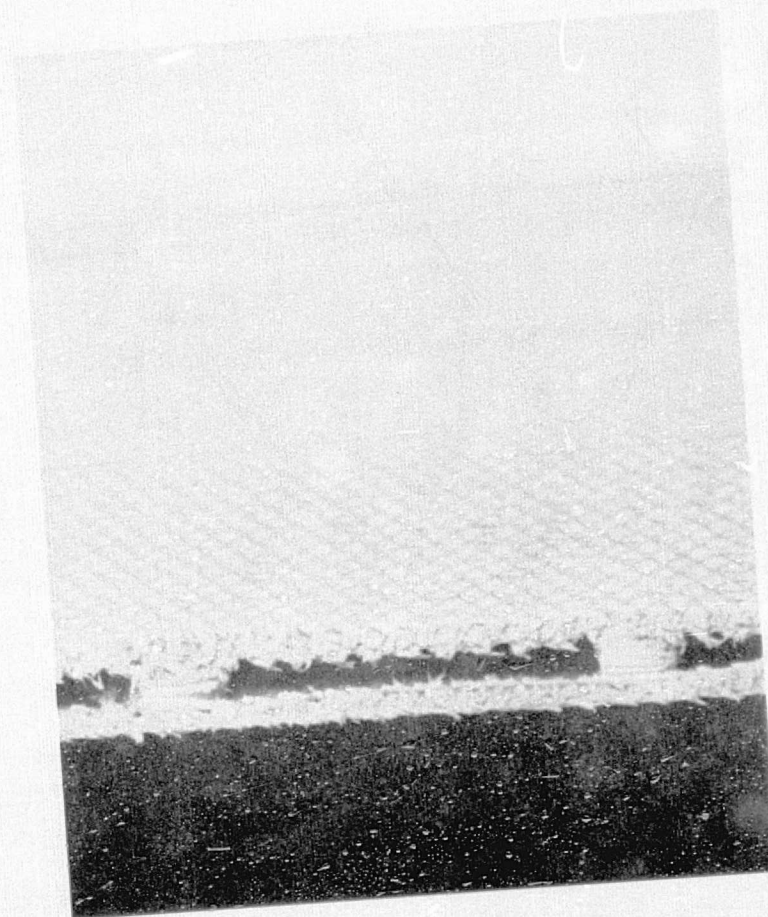


Figure 41. Scheme for No. 94 Grid Panel





TOP VIEW



END VIEW

Figure 42. Isogrid Stiffened Panel

## REPRODUCIBILITY OF COMPOSITE PANEL POROSITY

Materials and processing parameters effecting reproducibility of air flow test results are discussed in the following section.

The normal procurement time for special weaves that could optimize both structural and airflow properties was three months at the beginning of this contract. Such lead time was not available, thus it was necessary to purchase off-the-shelf items for all fabric and resin systems. For this reason the porous Kevlar fabrics were limited to 200 denier Doweave basic weave and #205 Leno weave. Corlar 5134F was selected as the resin system. This is a fire retardant version of the controlled flow Corlar 5134 epoxy approved for use at Douglas Aircraft Company under Douglas Material Specification (DMS) 1926. Preimpregnation of the cloth was done by Dupont since they were in the best position to surface treat Kevlar for resin adhesion. It was recognized at the time that for this fabric-resin combination, parameters such as resin content had not been established. Experience indicated however, that processing and choker plies could provide wide variations in porosity.

Actual resin content in the as-received material was 53.6 percent (200d Dow) and 53.2 percent (205 Leno).

The impregnation of the Doweave material was quite even, having a good surface appearance. The Leno weave, on the other hand showed considerable uneven resin distribution with open areas resin-covered in some instances. In order to correct this deficiency, an attempt at cure cycle variations and layup procedures was made for some test specimens. Air flow tests indicated that resin nonuniformity was too great and further work with this batch of Leno weave was discontinued. With the exception of the isogrid and Lock Core panels a standard cure of 250°F for 120 minutes was adopted.

Most porous faces and panels were fabricated in a short time span with specific configurations the main objective before it was realized from airflow tests, Figures 45 and 46, that this approach was not sufficiently reproducible, due primarily to high resin content. This resin content will also reduce observed strength properties of test specimens.



In order to verify that airflow can be repeatedly reproduced by proper control, three sheet laminates were fabricated and cured separately. The Doweave was hand impregnated to produce a final burn-out resin content of 25 percent. Eight ply with one center choker ply was used and the results are shown in Figure 43 . Repeatable porosity is considered an achievable production goal and will require close specification control of the material supplier's resin flow properties and impregnation parameters.

DMS 2054 silicone rubber mandrel material was selected for the Lock Core panels due to its relatively low expansion properties, i.e., 30 to 40 psi at 350°F which is compatible with low flow porosity control. Other mandrel materials are available but their high expansion can produce 100 to 1500 psi in a closed tool. These cures produce too much flattening of fiber and weave. DMS 2054 mandrels have their most effective expansion at 230°F. This is after the 5134 resin has started to gel and was an attempt to prevent bridging.

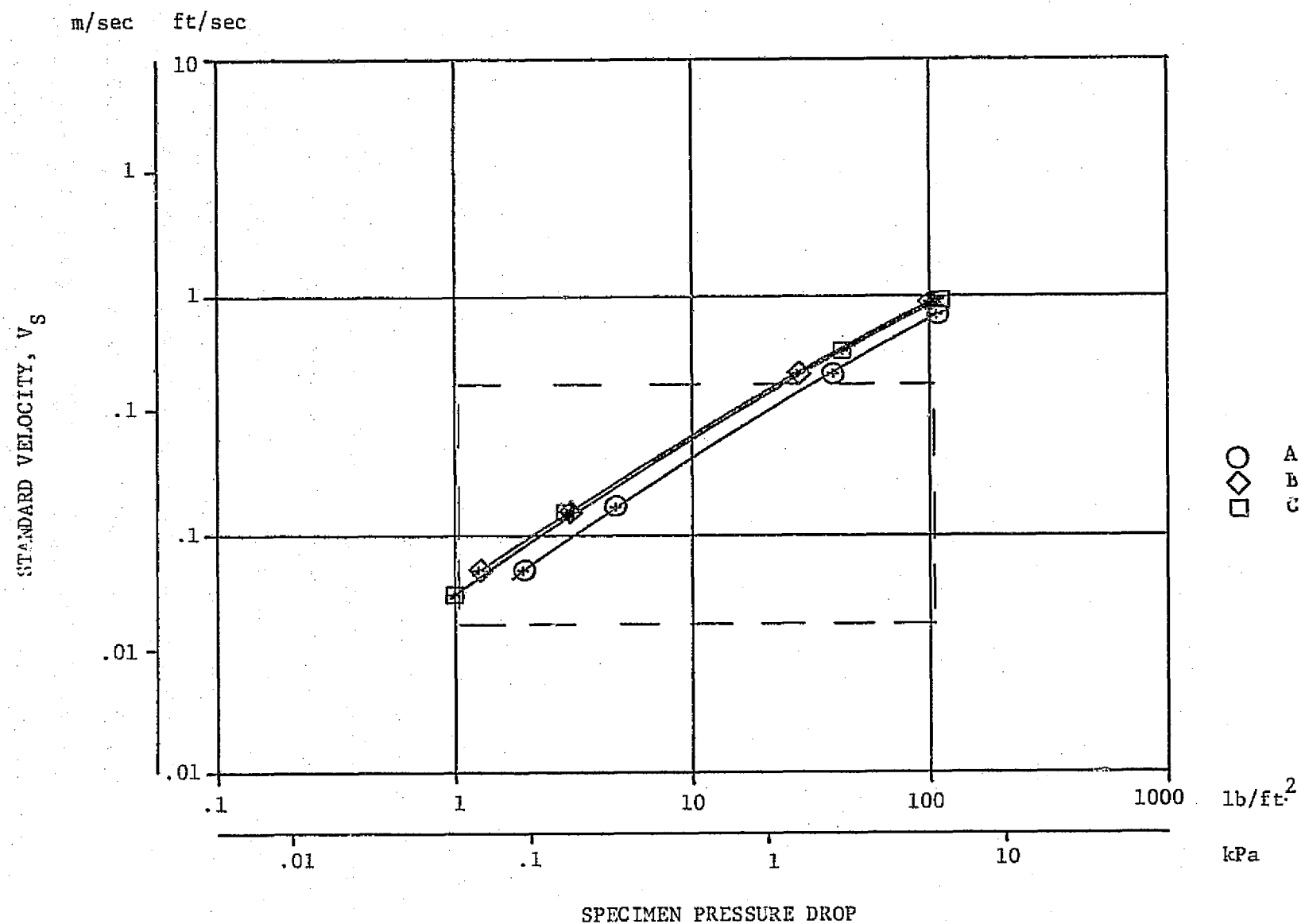


Figure 43. Demonstrated Reproducibility of  
Composite Panels Using Specific Resin Control  
[0/90]<sub>t</sub>, 120, [0/90]<sub>t</sub> Doweave

## AIRFLOW TEST RESULTS

### GENERAL

The airflow test results are presented in two different formats. The first, in terms of flow rate versus pressure drop, represents the data as directly measured on the test apparatus. This format has the advantage of presenting the results in easily understood physical parameters. In addition, it is useful when considering the effects of multiple layer systems since the pressure drop across each element of a system is directly additive for a constant flow rate.

The second presentation format is in terms of the effective porosity versus a unit Reynolds number based on the ideal velocity. The effective porosity,  $\sigma$ , is defined as the ratio of the measured flow rate to an ideal flow rate based on flow through an orifice with no losses having area equal to the total specimen area. For those specimen for which the geometric porosity can be determined, such as perforated materials, the ratio of effective porosity to geometric porosity is equivalent to a discharge coefficient. The ideal velocity is defined as the theoretical velocity achieved by a flow expanded isentropically through an orifice from the upstream pressure to the downstream pressure. This format is thought to be more useful for correlation of the data with theoretical or empirical prediction methods. The relationship between the two formats are summarized in Figure 44 for standard atmospheric test conditions. This figure shows the ideal flow rate versus pressure drop for an open area fraction equal to the indicated porosity.

The target airflow range is indicated by a dashed outline on each of the presentation plots.

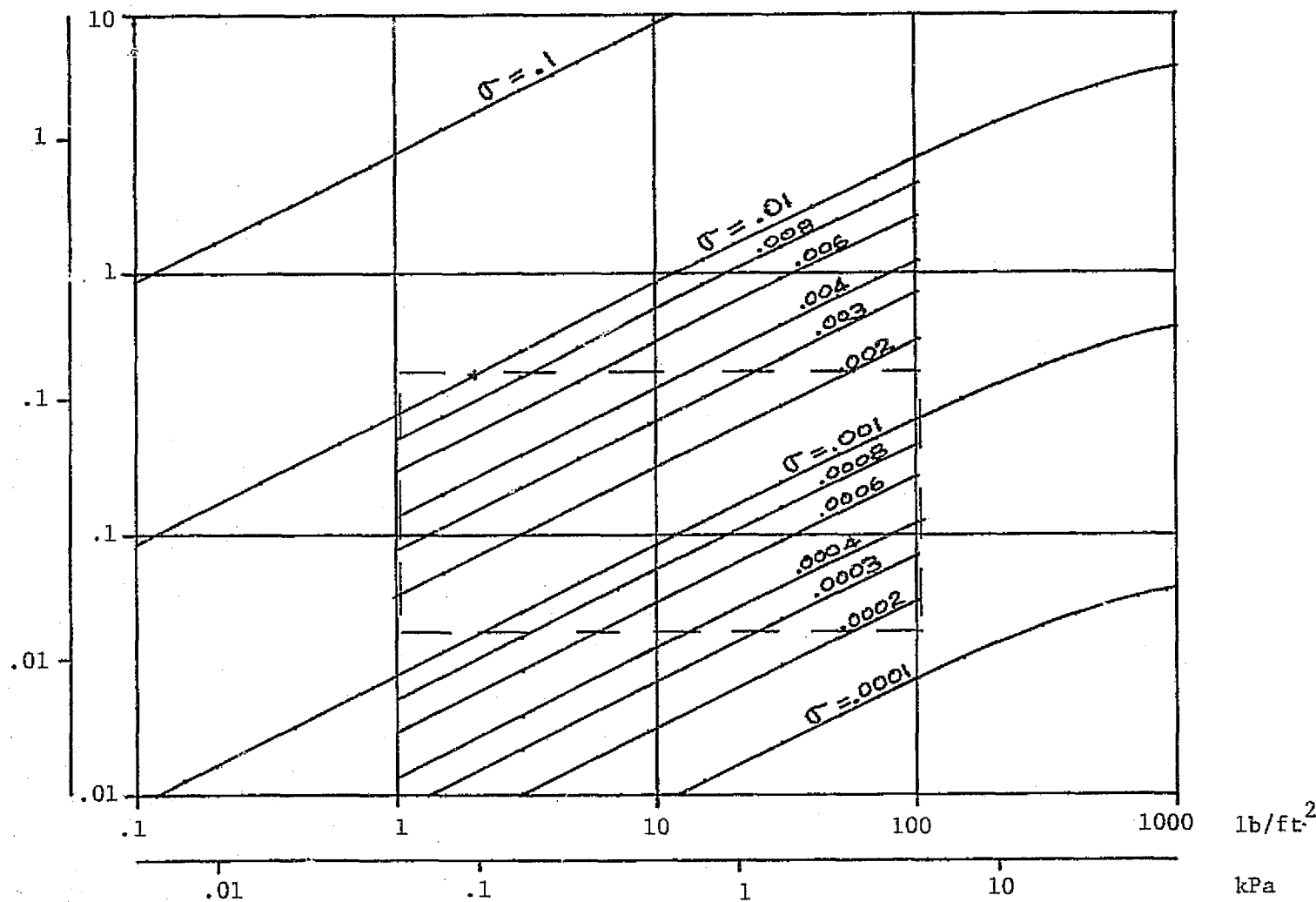
Presentation of the results is divided into three sections discussing the three distinctive types of materials: woven laminates, Dynapore, and electron beam perforated skins.

The Dynapore 316L stainless mon-layer results are included in the woven laminate section.



m/sec ft/sec

STANDARD VELOCITY,  $V_s$



SPECIMEN PRESSURE DROP

Figure 44. Relationship Between Pressure Drop Vs. Flow Rate and Effective Porosity at Standard Conditions

Configuration parameters of the particular specimens are summarized in the legend on each figure in an abbreviated manner. Complete details on the configuration or manufacturing process can be found in the Table D-1 for each specimen.

#### Derivation of Target Airflow Range

The range of airflows examined in this experiment is derived from the predicted flow coefficients for a typical design condition. The airfoil analysis indicates that the normal velocity coefficient,  $C_Q$ , should be between 0.0001 and 0.0003 over most of the airfoil surface and reaches values as large as 0.001 in localized areas. The range of  $C_Q$  is therefore selected to be between 0.0001 and 0.001. At a cruise Mach number of  $M = 0.8$  at 36,000 feet of altitude, the normal velocity,  $V_1$ , through the surface is

$$0.0775 \leq V_1 \leq 0.775 \text{ (ft/sec)}$$

The proper scaling of this velocity to the sea level test conditions depends on the means by which the air flowing through the porous material produces the pressure drop. Prior to any testing experience with the particular materials, this mechanism is unknown. It is reasonable to hypothesize that, at least for some types of materials, the pressure drop mechanism is a turbulent dissipation of energy much like that experienced by flow through a thin orifice. In this case the pressure drop depends on the total energy in the flow and so can be expressed as

$$\Delta P = \Delta \rho V^2$$

Following this hypothesis, then, results in a normal velocity scaling relationship of

$$V_{S.L.} = V_{alt} \sqrt{\frac{\rho_{alt}}{\rho_{S.L.}}} = .545 V_{alt}.$$

Therefore the target normal velocity for the experiment at sea level is

$$.0423 \leq V_1 \leq .423 \text{ (ft/sec)}$$

Conversely, determination of the flow rate through a particular specimen at a certain pressure drop at altitude is equal to the sea level test result divided by the square root of the density ratio.

The validity of this hypothesis is untested at this point. To verify this scaling behavior, experiments must be conducted over a range of simulated altitudes. Nevertheless, the results of the sea level tests, as is discussed in a subsequent section of this report, shows that most of the materials tested have a function relationship between pressure drop and velocity of close to

$$\Delta P = A V^2$$

Therefore the original hypothesis is considered reasonable, at least for those materials.

Determination of the optimum surface pressure drop is much more complex and depends on a careful suction pump and manifold cycle analysis. A simple criterion derived from X-21A flight experience (Ref.6 ) suggests the maximum pressure drop is about 0.2 times the design point dynamic pressure, or about 42 pounds per square foot. Another simple rule cited by Pfenniger mentions a value of 0.03 times the ambient pressure, or about 14 pounds per square foot. For the purpose of generality, in the test, this range was arbitrarily expanded to extend from 1 to 100 pounds per square foot.

## AIRFLOW DATA CORRELATIONS

### Woven Laminates

In attempting to correlate the airflow performance of the woven laminate materials with gross physical parameters such as number of plies, face sheets, ply orientation, etc., some difficulty was encountered. As stated previously, off-the-shelf materials and material suppliers' impregnation procedures were used for fabrication of the test panels. Within the limited manufacturing experience of the present program, many of the test specimens exhibited poor reproducibility and thus scatter in the airflow data. It appeared that small differences in manufacturing process produces large effects on the airflow characteristics. This problem was recognized; and Douglas research efforts, near the end of the program, on suitable thinner resins resulted in fabrication processes which demonstrated a high degree of reproducibility of panels. Unfortunately, this resin system was not available for the airflow test panel fabrication.

Some of this behavior is summarized in Figures 45 and 46. Airflow test results from specially prepared repeat specimens are compared with the original specimens for several different types of materials. In general, the materials with the greater pressure drop, or lower effective porosity, exhibit a greater susceptibility to poor manufacturing reproducibility. The greatest discrepancy amounts to a factor of six times in flow rate at a constant pressure drop. This degree of reproducibility must be kept in mind when attempting to discern the effects of configuration parameters. The more obvious trends are still quite evident, however.

The airflow test results for the various Doweave laminate specimens are shown in Figures 47.1 through 47.5. The effect of the number of plies is shown in Figure 47.1. Increasing the number of plies is shown to decrease the flow rate in a relatively smooth fashion.

The repeat specimens for the 10-ply and 12-ply configurations illustrate the reproducibility difficulty. The flow rate of the 4-ply laminate is much greater than the identified range of interest. The 10-ply and 12-ply material just begin to approach the proper range.

Figure 47.2 shows further scatter in the reproducibility for the 8-ply laminate, as well as the effect of a change in the manufacturing process, namely a different cure cycle.



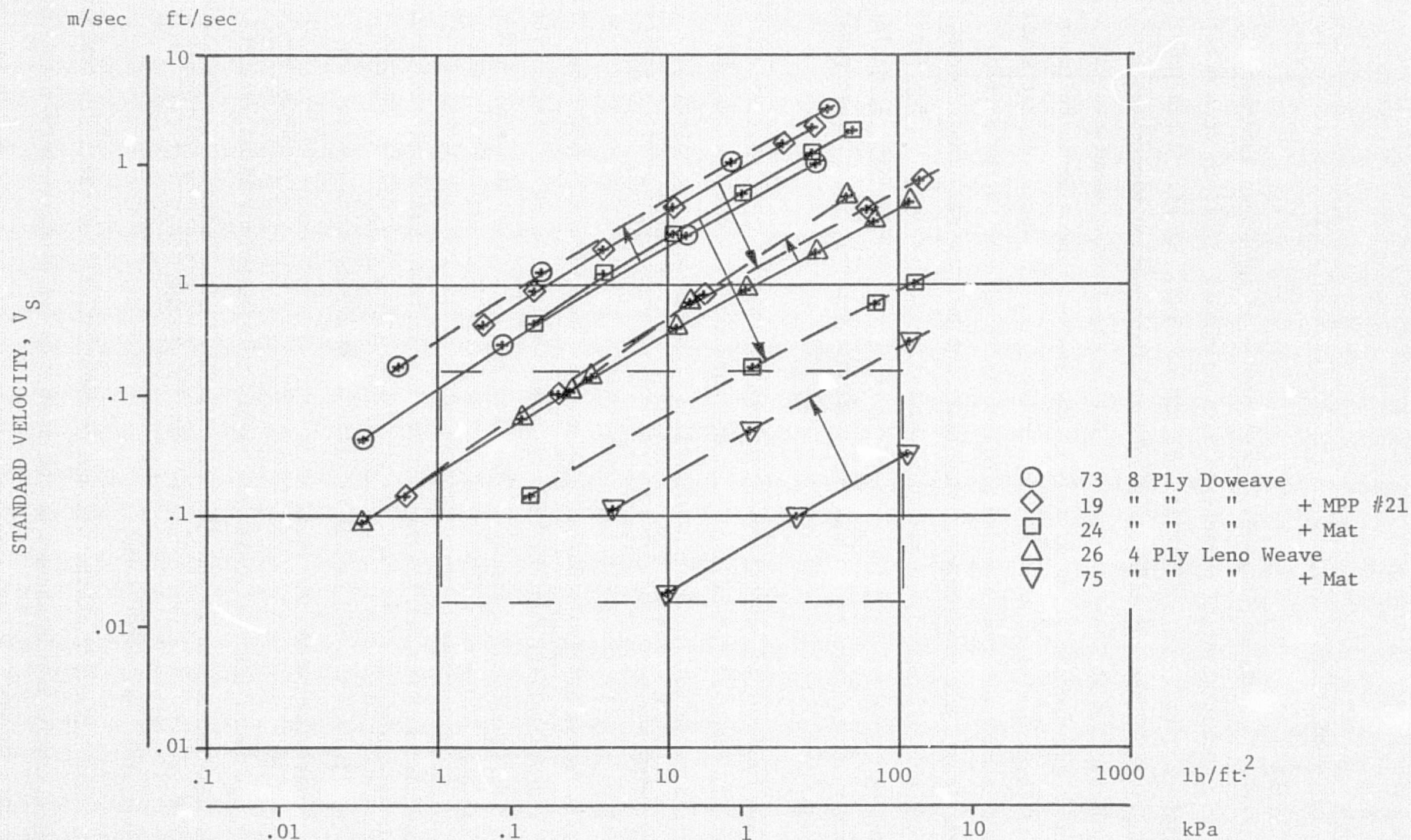
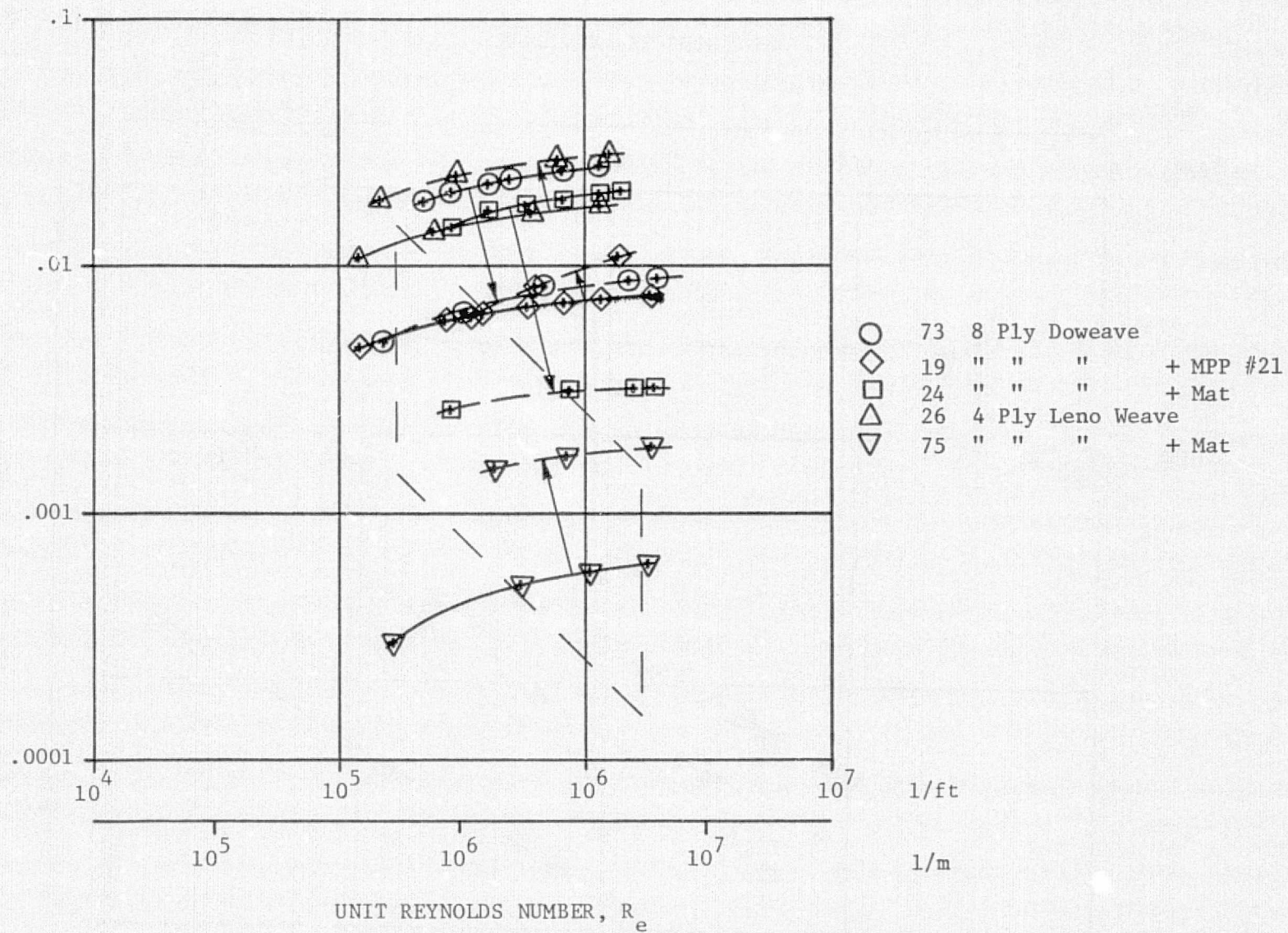


Figure 45. Effect of Specimen Reproducibility on  
 Airflow Characteristics



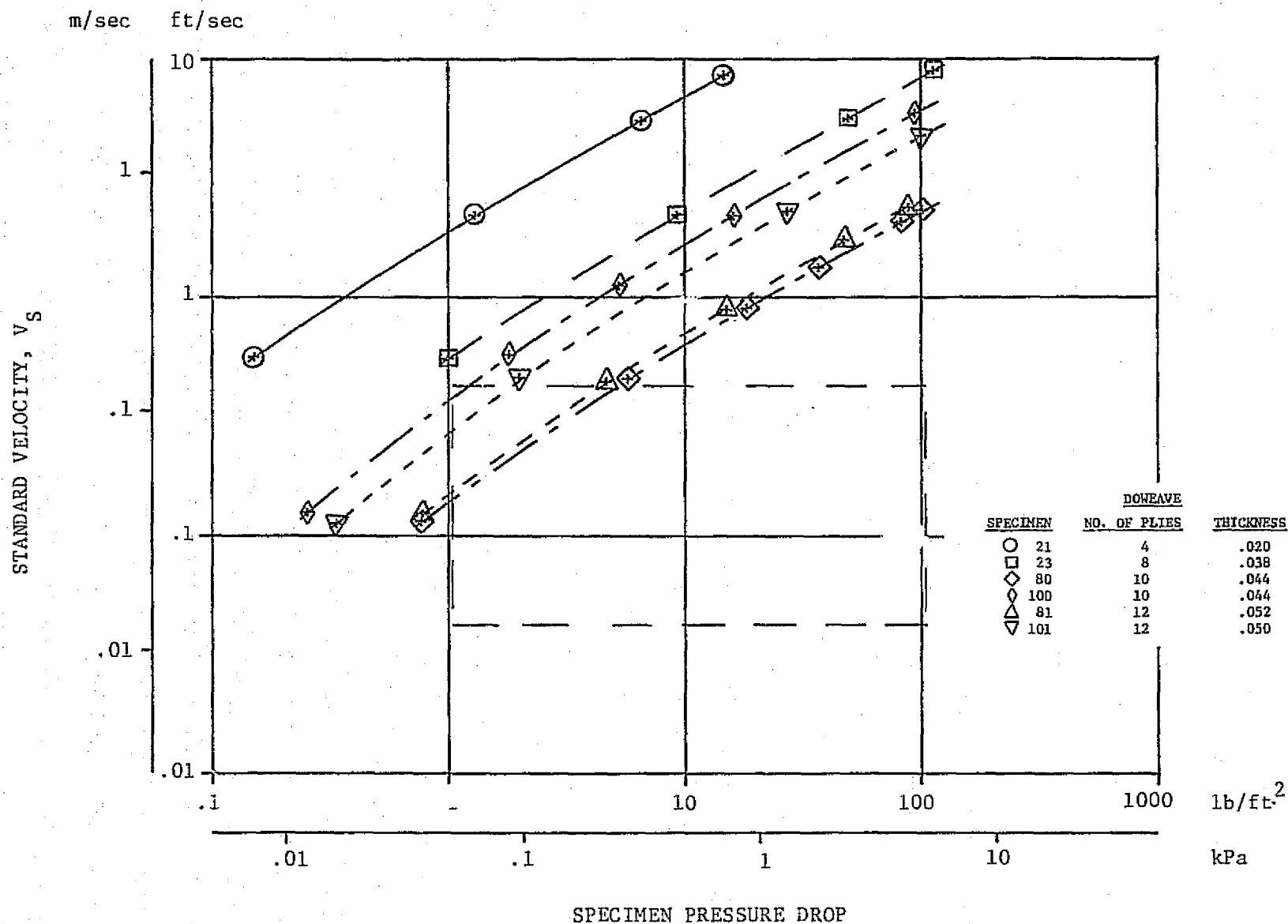


Figure 47.1. Pressure Drop Variations With Flow Rate

6L

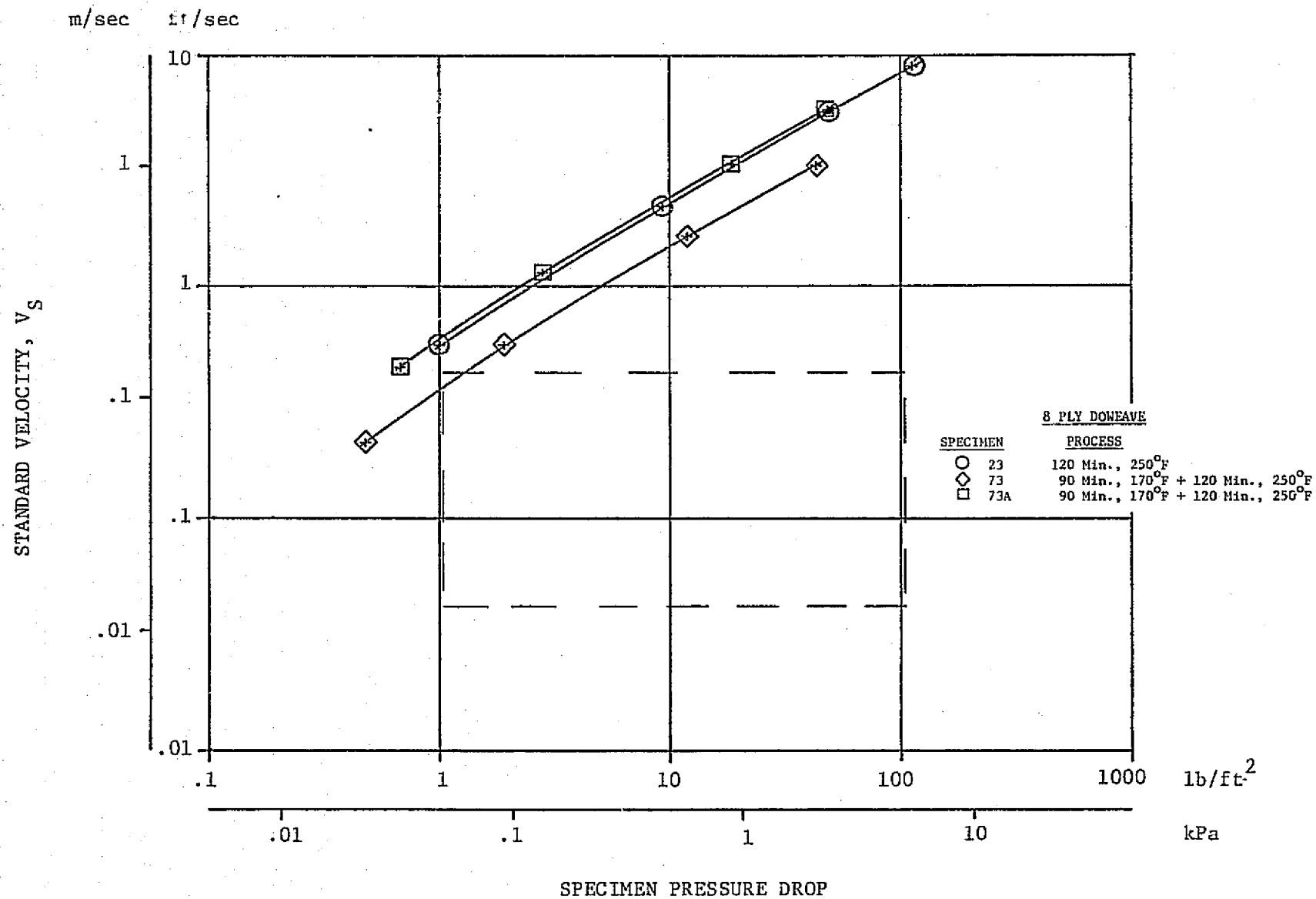


Figure 47.2. Pressure Drop Variations With Flow Rate



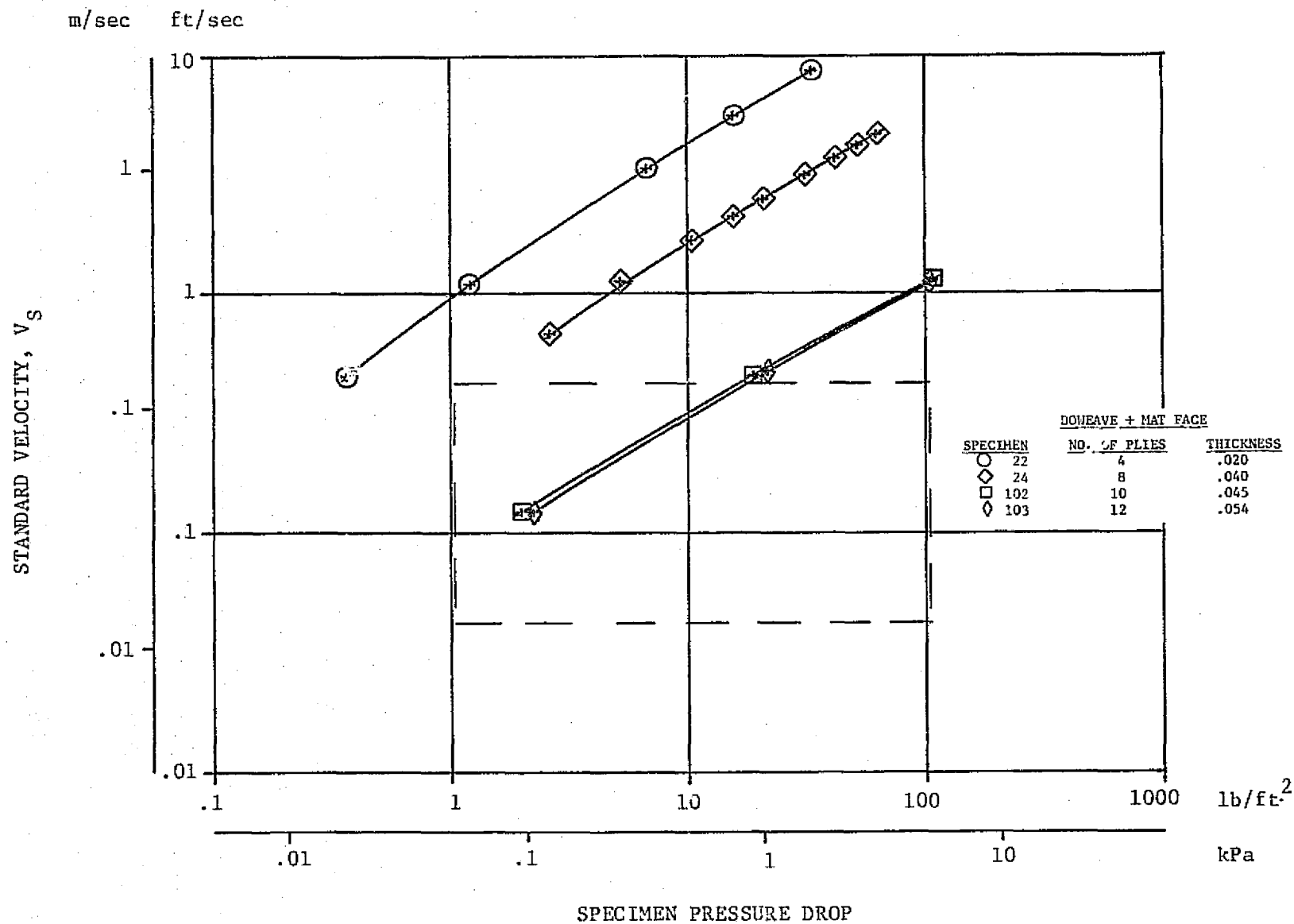


Figure 47.3. Pressure Drop Variations With Flow Rate

The effect of the number of plies on Doweave plus a mat face sheet is shown in Figure 47.3. Very similar trends are seen for these materials as were evident in Figure 47.1. The apparent similarity between the 10-ply and 12-ply materials is probably due to scatter in the reproducibility rather than a decrease in the ability of additional plies to produce further pressure drop.

These materials approach somewhat closer the target airflow range with the 10 and 12 ply specimens cutting through the upper half of the range of interest.

Figure 47.4 shows the effect of various face sheet materials on the 4 ply Doweave laminate. The mat face sheet is seen to produce the greatest blockage, about 60 percent reduction in flow rate at 10 pounds per square foot pressure drop. The two different micro-perforated plates show somewhat smaller effect. The 120 fabric face sheet is seen to produce a substantial reduction in flow rate on the 2 ply Doweave to make it similar to the 12 ply Doweave with mat face sheet.

The effect of face sheet on the 8 ply Doweave laminate is shown in Figure 47.5. Again there is a moderate reduction in flow rate due to the mat material and somewhat less effect of the micro-perforated plate.

The properties of the Leno weave laminates is illustrated in Figure 47.6 over a range of plies. The two ply laminate is well above the target airflow range while the six ply material is substantially less. The three different four ply specimens lie in the upper half of the target range and show the effect of different cure cycles.

Figure 47.7 shows the effect of various face sheets on two ply Leno weave. The micro-perforated plate and mat materials are much more effective in blocking the flow in this case than with the Doweave materials.

Figure 47.8 shows the effect of mat face material on four ply Leno weave with two different ply orientations. The magnitude of the flow decrease due to the mat face is close to that for the two ply material.

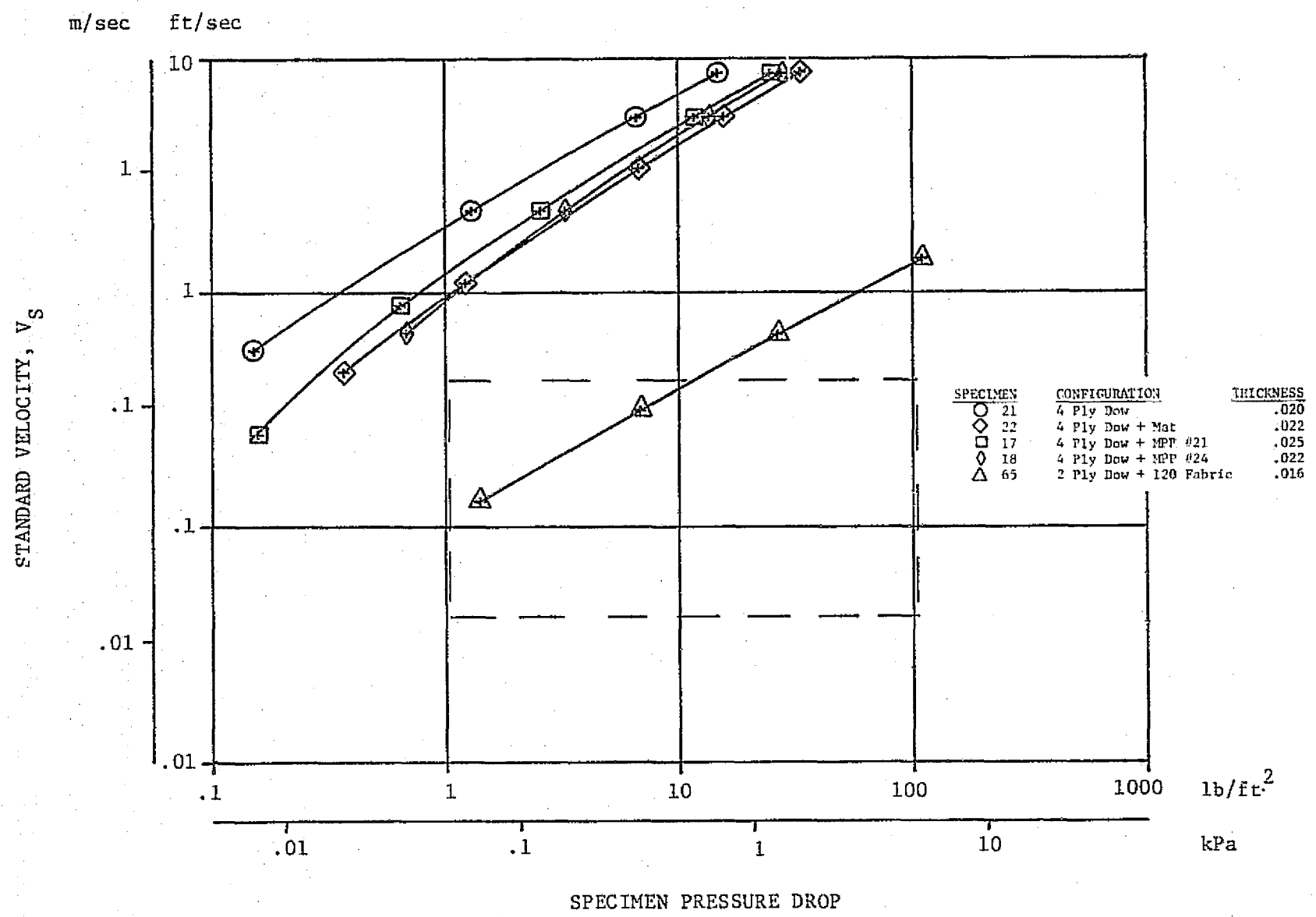


Figure 47.4. Pressure Drop Variations With Flow Rate

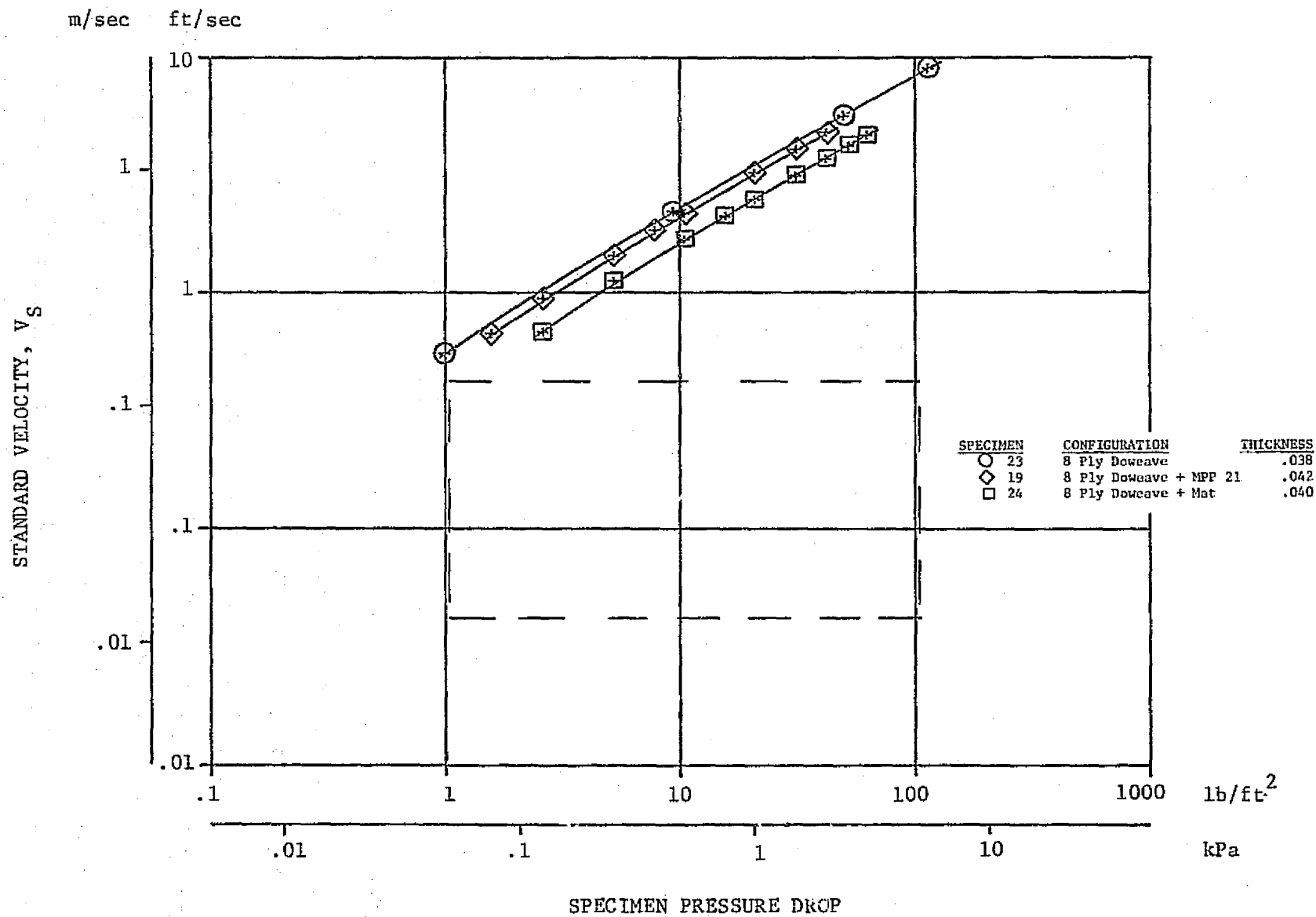


Figure 47.5. Pressure Drop Variations With Flow Rate



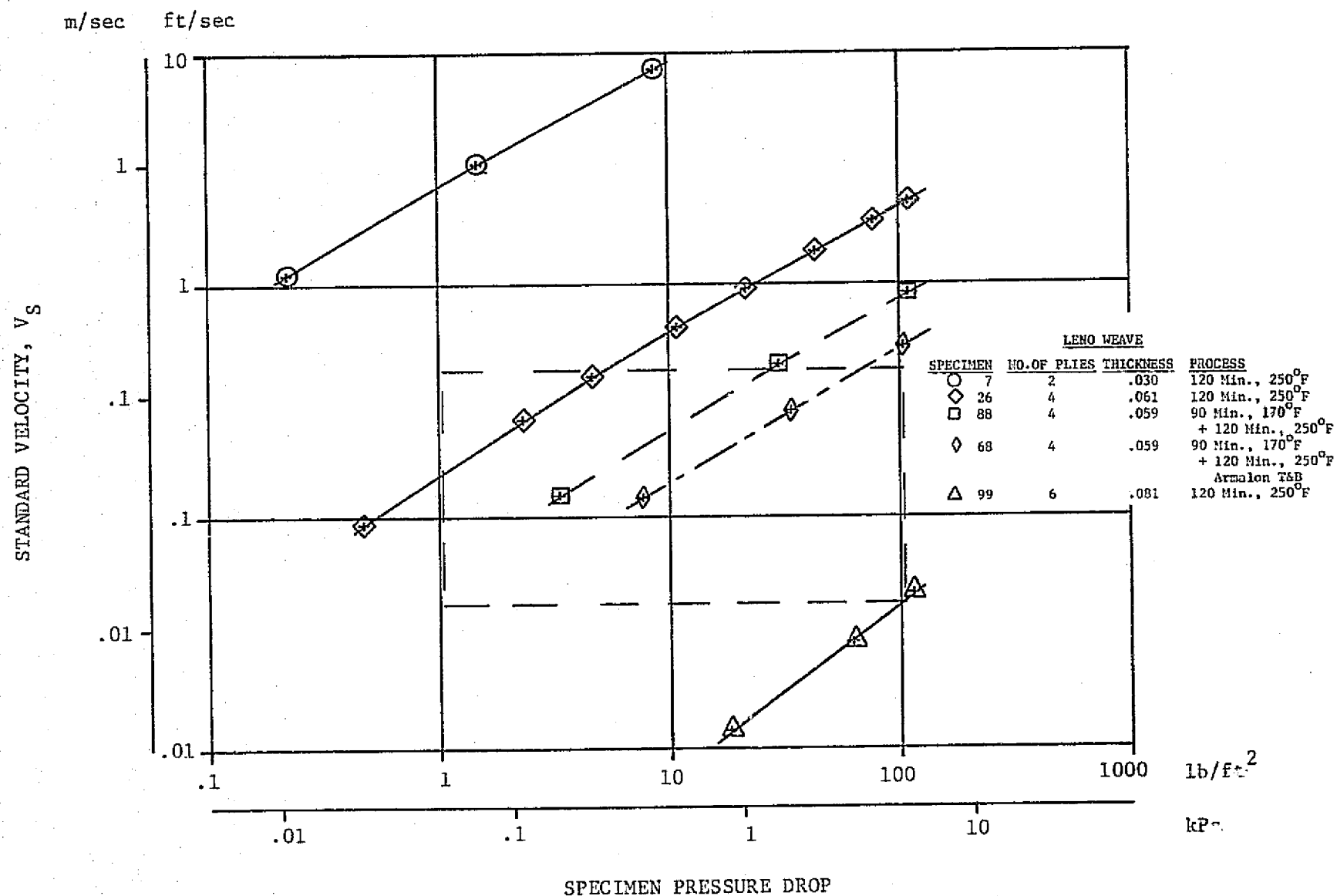


Figure 47.6. Pressure Drop Variations With Flow Rate

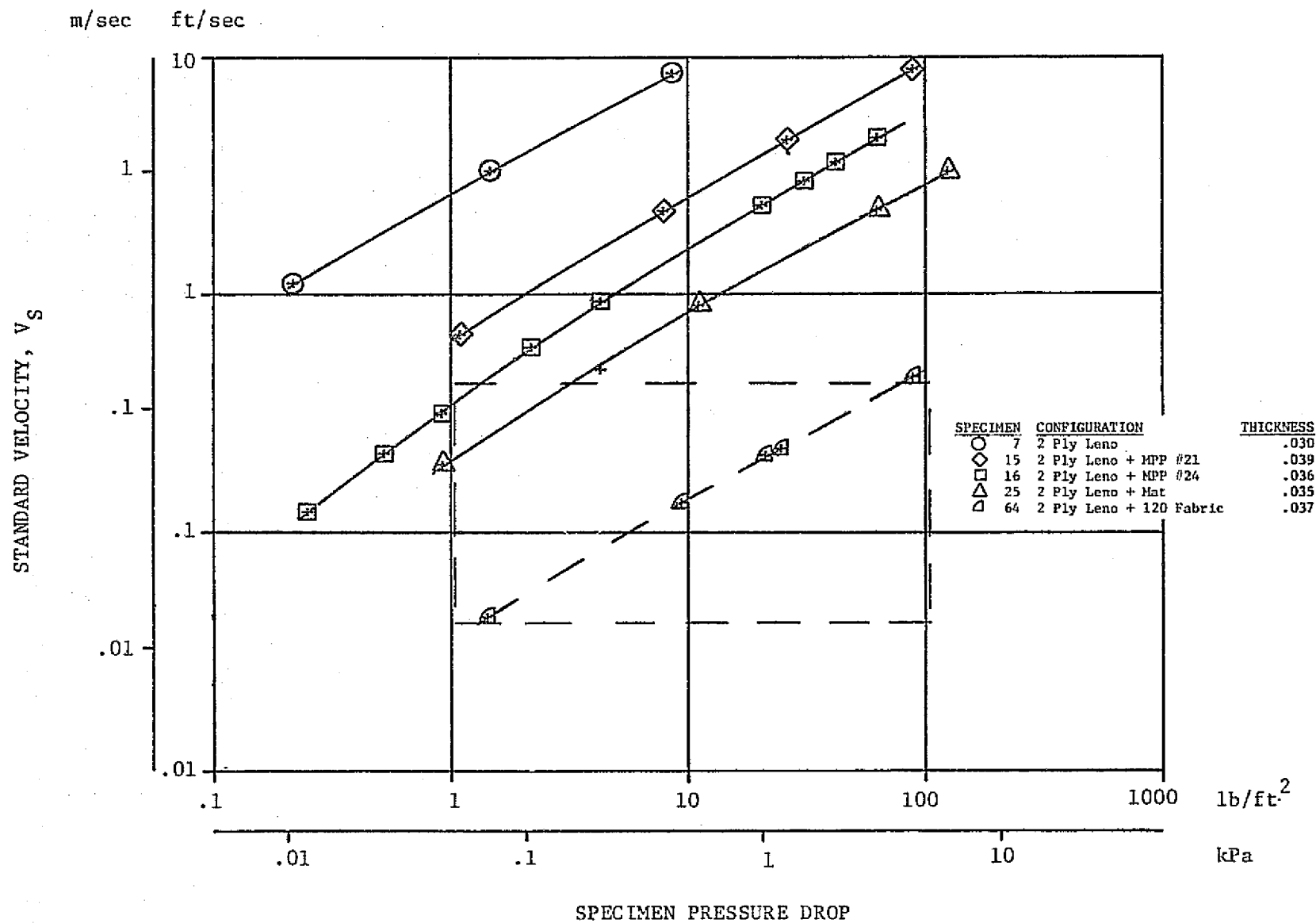


Figure 47.7. Pressure Drop Variations With Flow Rate

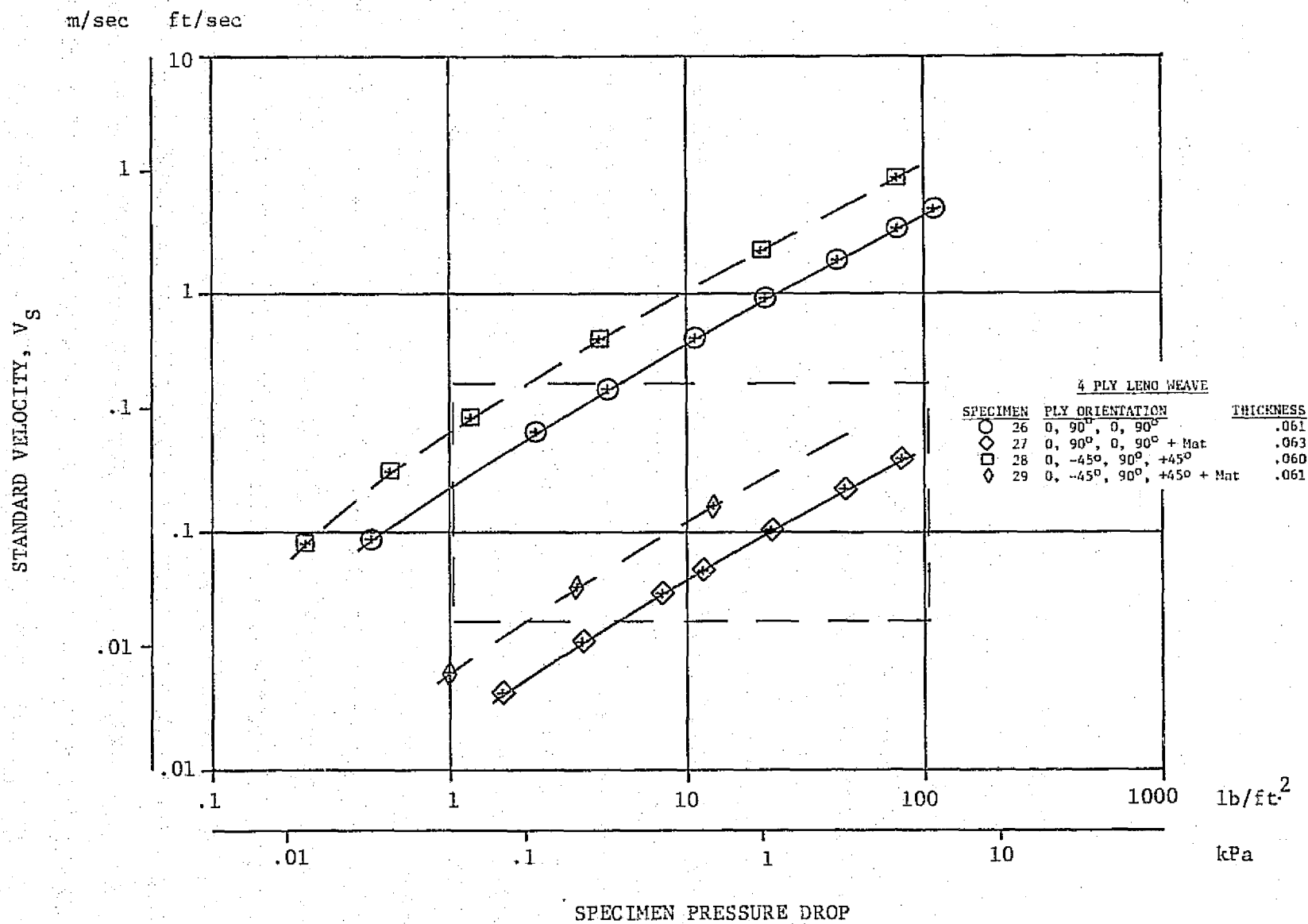


Figure 47.8. Pressure Drop Variations With Flow Rate

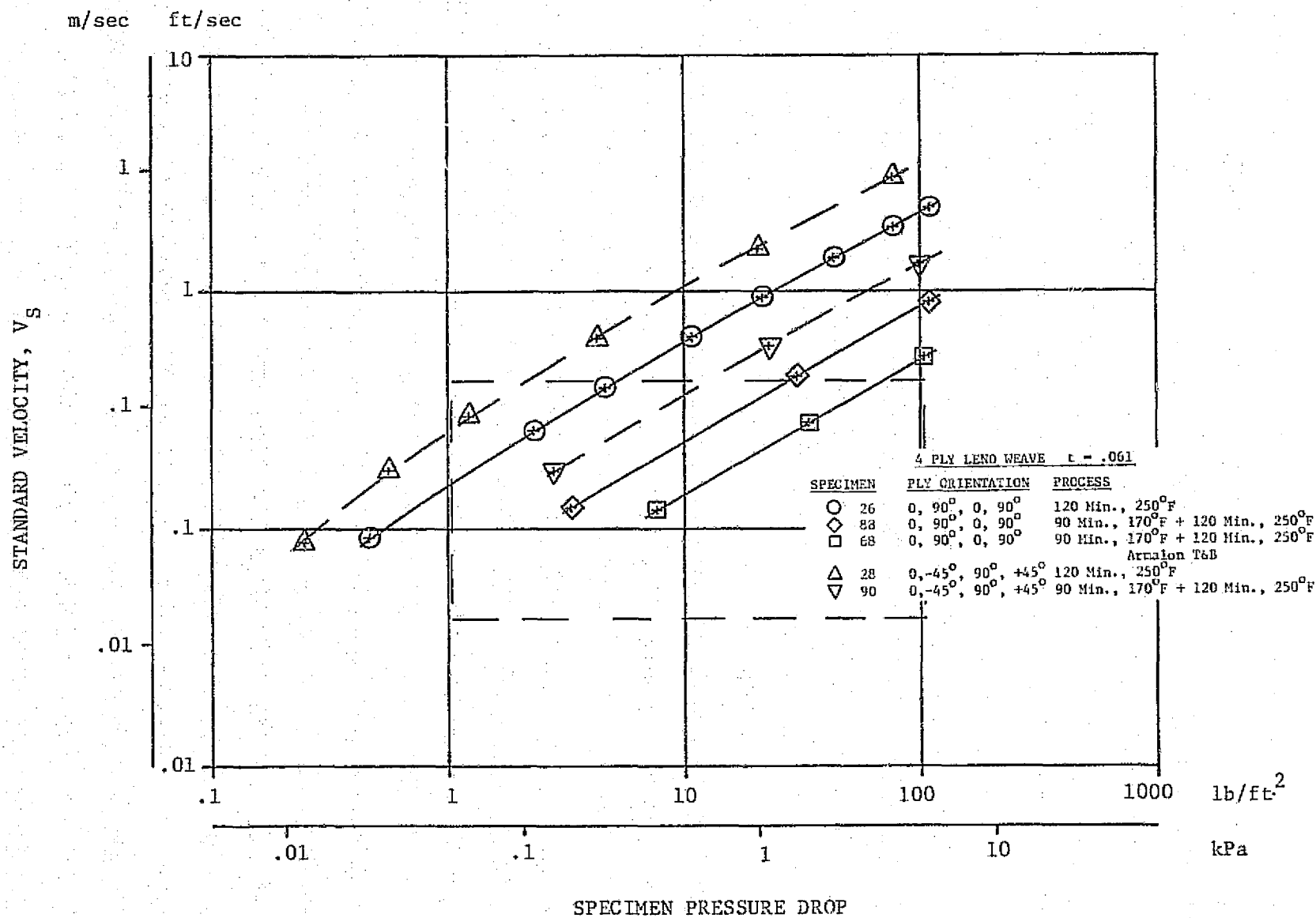


Figure 47.9. Pressure Drop Variations With Flow Rate

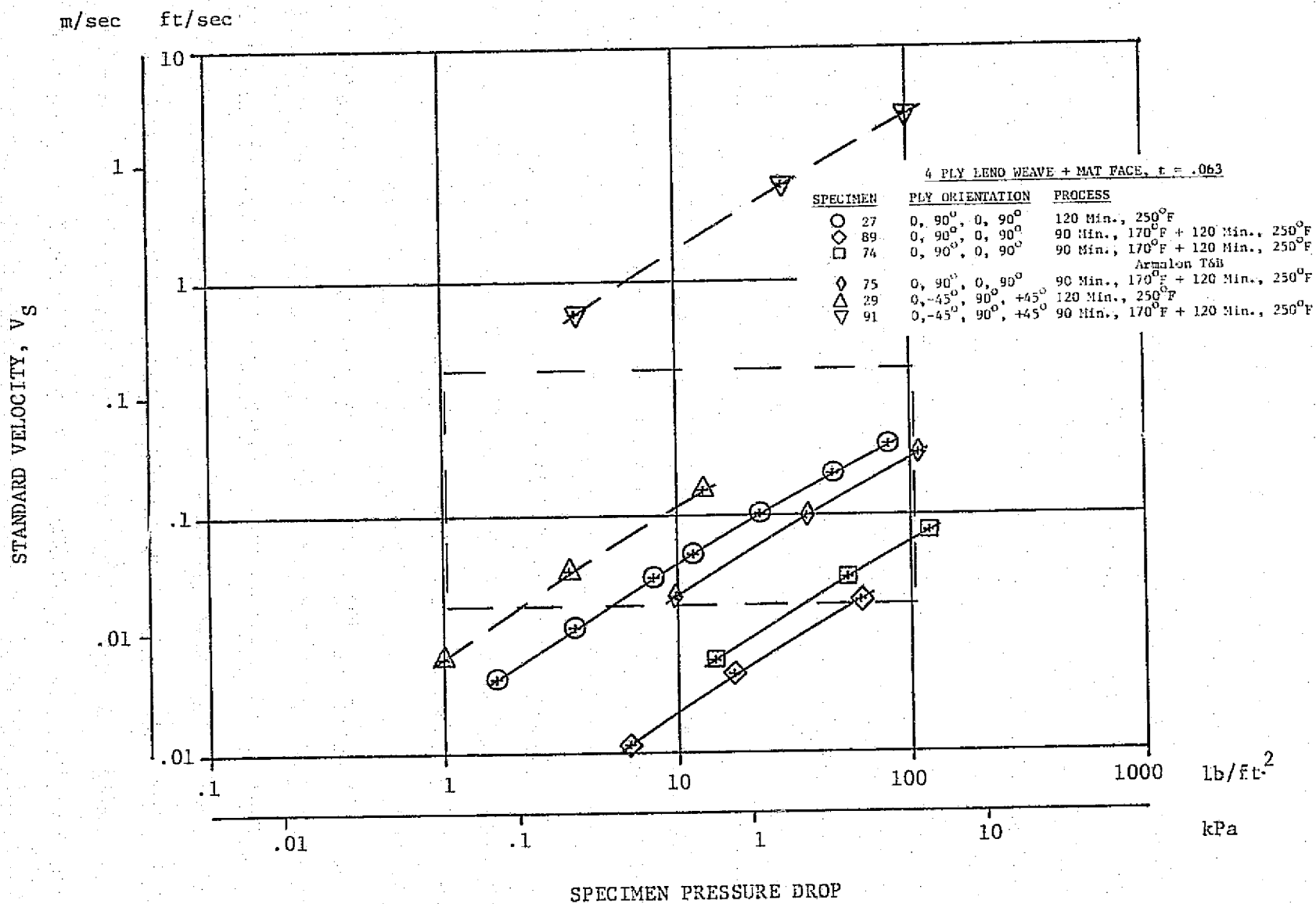


Figure 47.10. Pressure Drop Variations With Flow Rate



Figures 47.9 and 47.10 show the effects of ply orientation and cure cycle for four ply Leno weave with and without mat face sheet. The 45 degree ply orientation consistently exhibits less flow blockage than the 90 degree orientations. All of the four ply materials fall in the target airflow range.

All of the woven laminate materials exhibit one common distinctive feature. The slope and shape of the flow rate versus pressure drop curve remains much the same over a wide range of flow rate and pressure drop. The slope of the curve is steepest at the low pressure end and gradually approaches a nearly constant slope at the high pressure end. The value of the slope indicates a functional relationship between pressure drop and velocity of

$$\Delta P = A V^{1.9}$$

which is close to the behavior of high Reynolds number, inviscid type flow through an orifice which would be

$$\Delta P = A V^{2.0}$$

which represents the limiting condition for any material.

#### Dynapore

The airflow properties of the Dynapore monolayer material, shown in Figure 47.11, are distinctively different in this regard. Shown are three specimens for each of two different mesh sizes which differ in the extent of the calendaring received to tailor their flow rate properties. The slopes of all the specimens are much the same at the low pressure range, but at high pressures the coarse mesh 24 X 110 material deviates toward a shallower slope.

The magnitude of the initial slope is such that the relationship between flow rate and pressure drop is about

$$\Delta P = A V_s^{0.95},$$

while at the high pressure end of the curves

$$\Delta P = A V_s^{1.13}$$

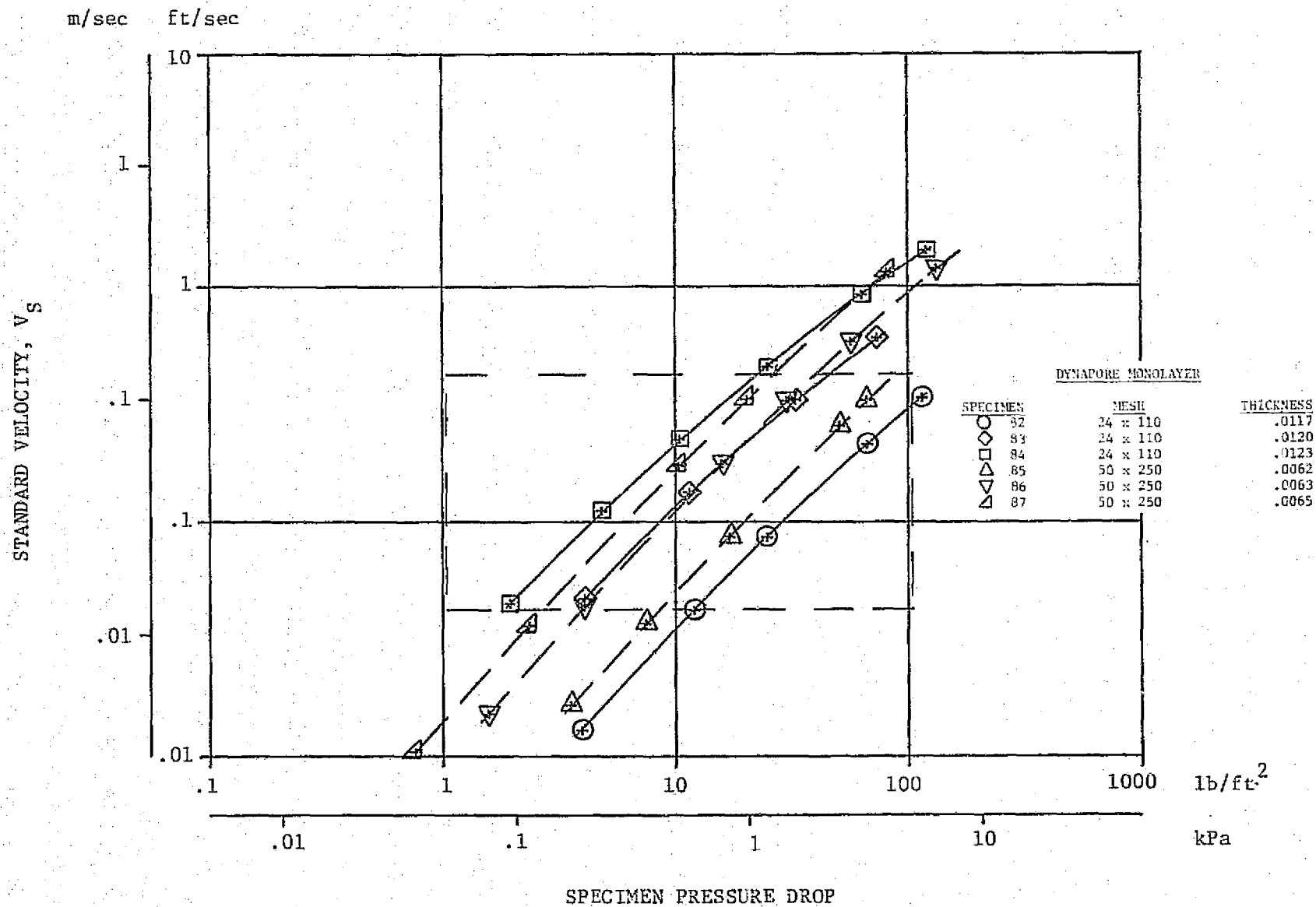


Figure 47.11. Pressure Drop Variations With Flow Rate

for the coarse mesh material and

$$\Delta P = A V_s^{1.15}$$

for the fine mesh Dynapore. The airflow properties of these materials fall squarely through the middle of the target airflow range.

The implication from this result is that the pressure drop mechanism for the Dynapore monolayer material is fundamentally different than for the woven laminate materials. The power of the velocity term for Dynapore, being very close to 1.0, suggests that the flow experiences energy loss as a result of low Reynolds number viscous dissipation in minute flow passageways. An example of this type of flow is found in the Hagen-Poiseuille flow where the Reynolds number is so low that the flow is completely laminate and distributes itself with parabolic velocity profile resulting in

$$\Delta P = A V^{1.0}$$

On the other hand a velocity power of close to 2.0, as seen for the woven laminates, implies flow through passageways at high enough local velocities and large enough dimensions that the flow is locally turbulent and exhibits full velocity profiles. Thus the pressure drop is more nearly proportional to the total energy of the flow which varies with the square of the velocity.

#### Electron Beam Perforations

The airflow test results for the electron beam perforated specimens are presented in Figures 48.1 to 48.3 in terms of flow rate versus pressure drop. Instead of also presenting the effective porosity, as was done for the woven laminates, a second data presentation format in Figures 49.1 to 49.4 is discharge coefficient,  $C_D$ , versus hole Reynolds number  $R_d$ . The discharge coefficient is defined as the ratio of the effective porosity to geometric porosity.

The results show airflow characteristics more or less uniformly distributed across the upper half of the target airflow range with a few test specimens lying in the lower half. A distinct trend is evidenced by relating the airflow results to geometrical porosity.

The other parameters which could be significant; hole diameter,  $d$ , material thickness,  $t$ , or thickness-to-diameter ratio,  $t/d$ , do not seem to present an obvious correlation with the airflow.

The individual curves in Figures 48.1 through 48.3 are very similar in slope and shape to those for the woven laminates except they are possibly slightly more uniform in slope. The magnitude of the slope approaches 1.9 indicating a functional dependence of pressure drop on flow rate of

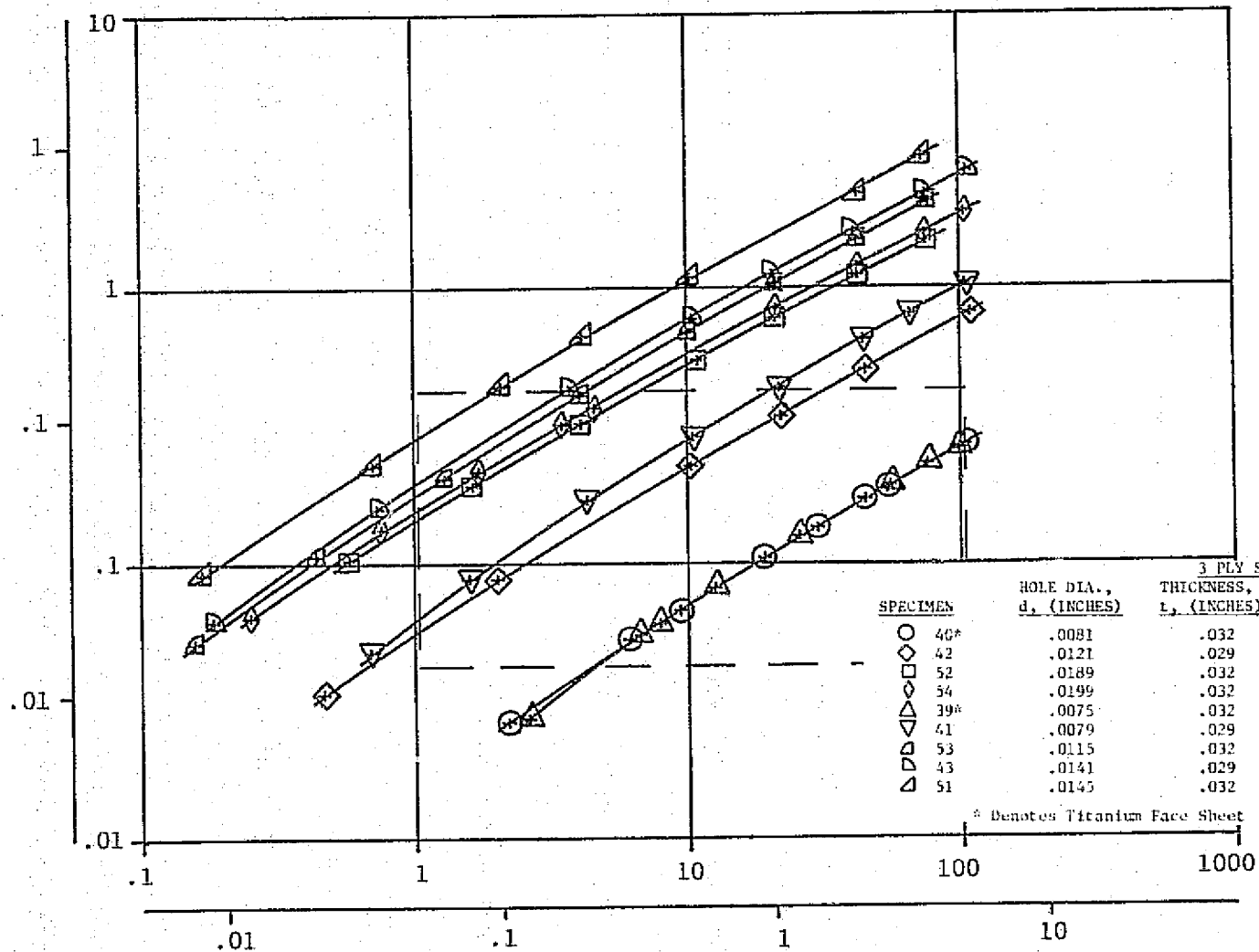
$$\Delta P = A V^{1.9}$$

as would be expected for high Reynolds inviscid type flow.

It was expected that the flow characteristics of the electron beam perforated specimens would be well correlated with theoretical orifice flow, but verification of this requires an accurate knowledge of the geometric porosity of the individual specimens. (See Table VI).

Figures 49.1 through 49.3 show the discharge coefficients for all the electron beam perforated specimens segregated according to material thickness, or number of plies. For each figure the data appear to delineate distinct bands if the most extreme curves are excluded. These apparent bands of discharge coefficient tend to level out at the high Reynolds number end of the range at nearly constant levels which seem to vary consistently with panel thickness.

m/sec ft/sec



SPECIMEN PRESSURE DROP

Figure 48.1.

Electron Beam Drilled Specimens  
Pressure Drop Variations With Flow Rate



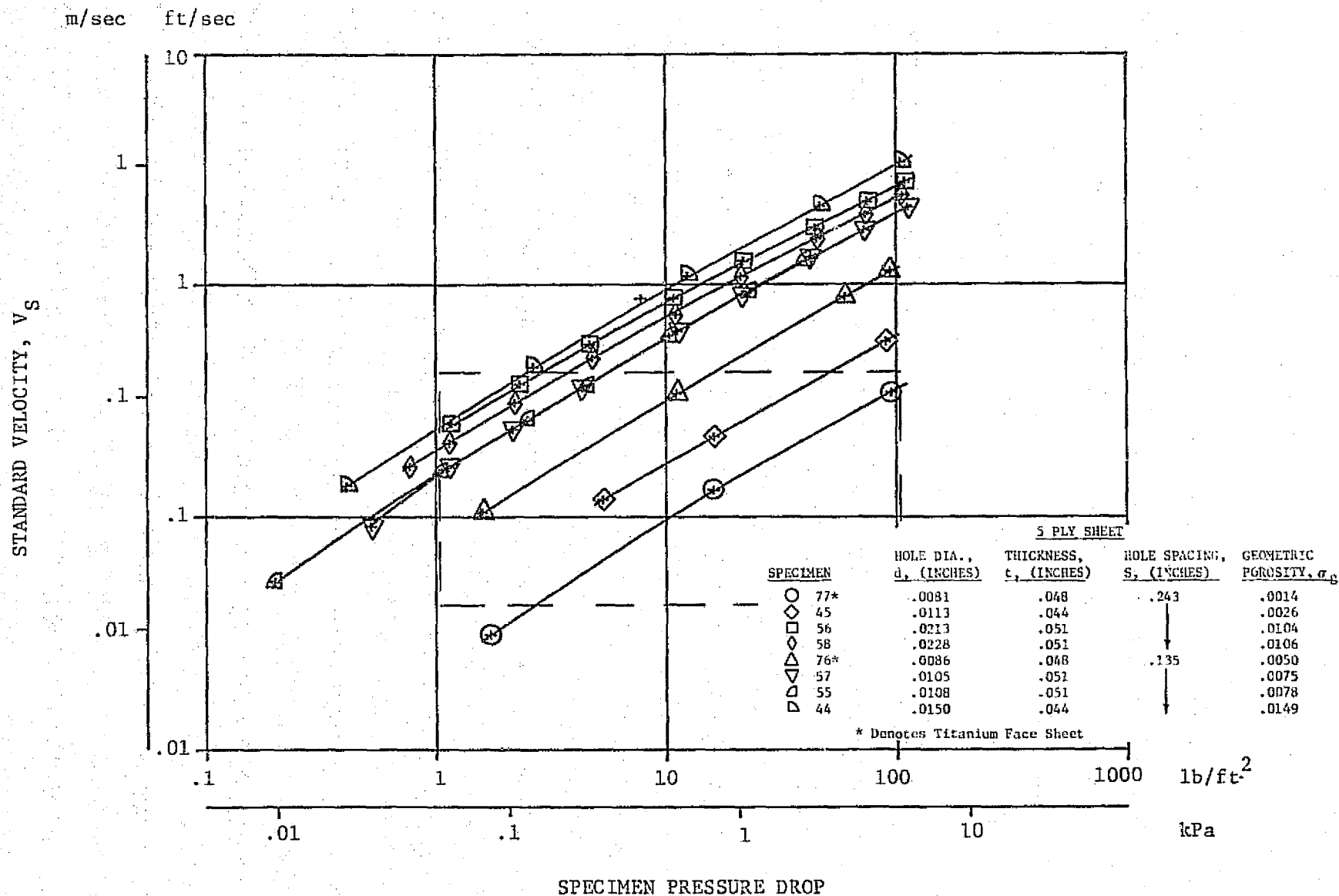


Figure 48.2. Electron Beam Drilled Specimens  
Pressure Drop Variations With Flow Rate

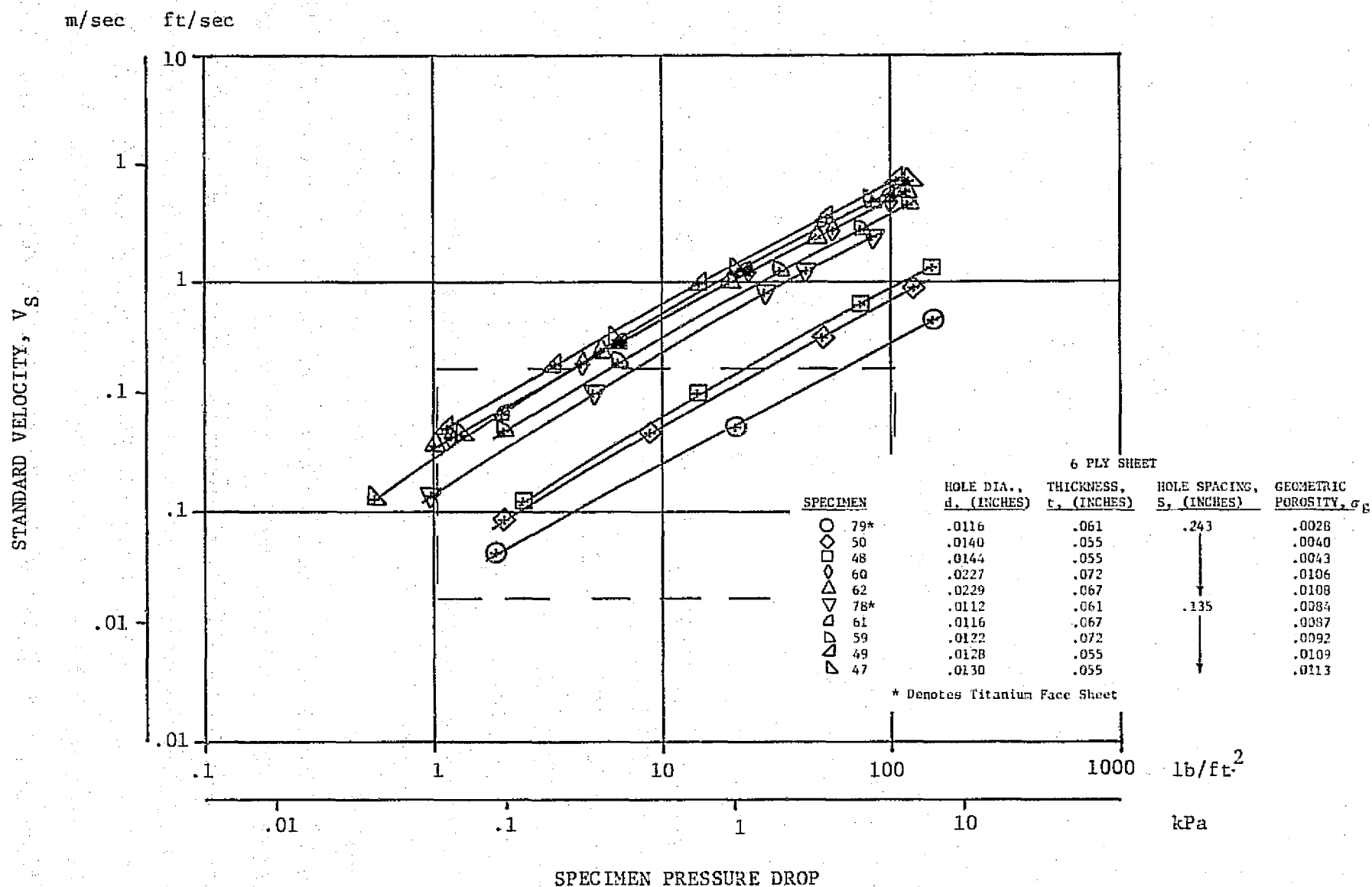


Figure 48.3. Electron Beam Drilled Specimens  
Pressure Drop Variations With Flow Rate

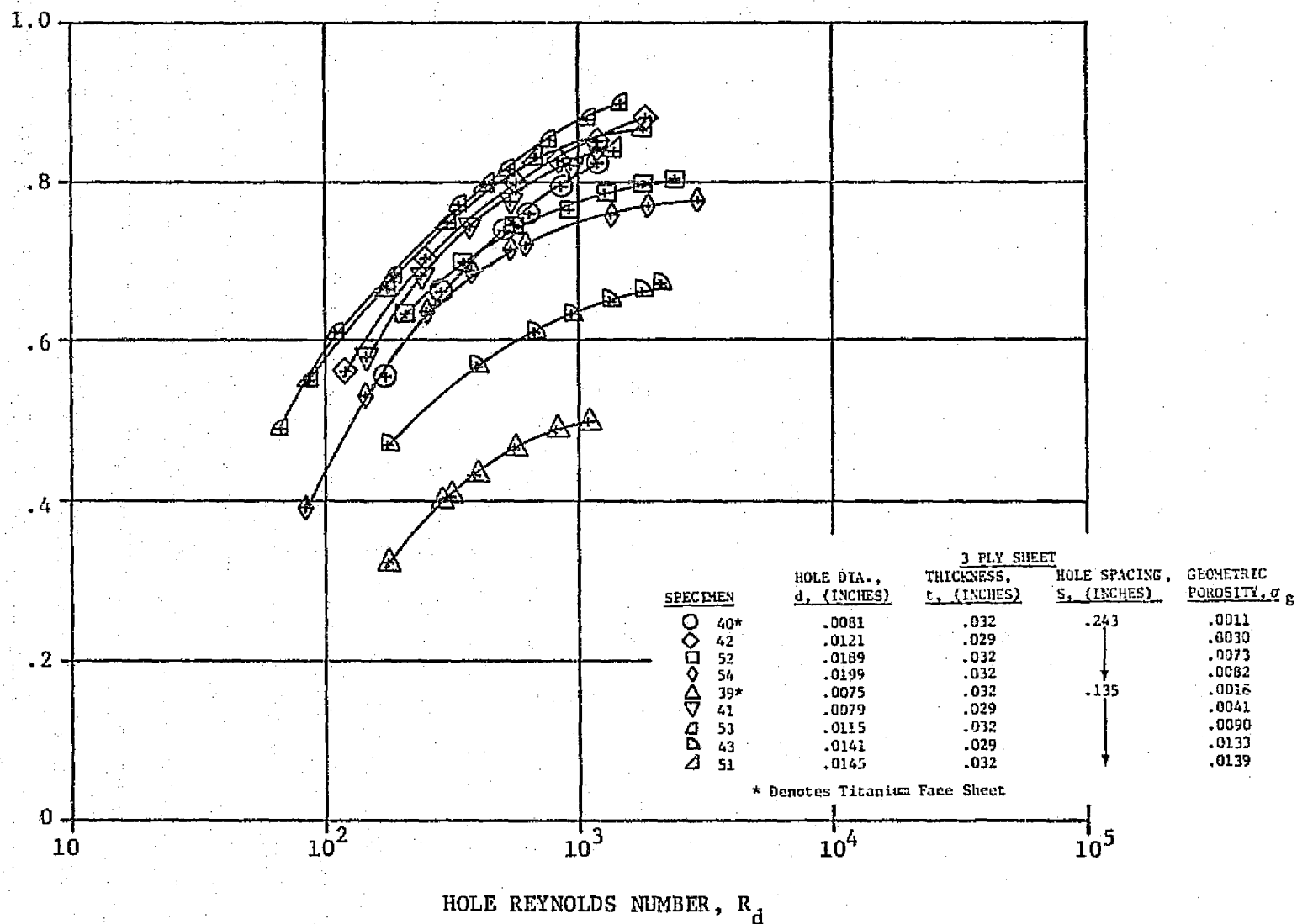


Figure 49.1. Electron Beam Drilled Specimens  
Discharge Coefficient Variations With Hole Reynolds Number

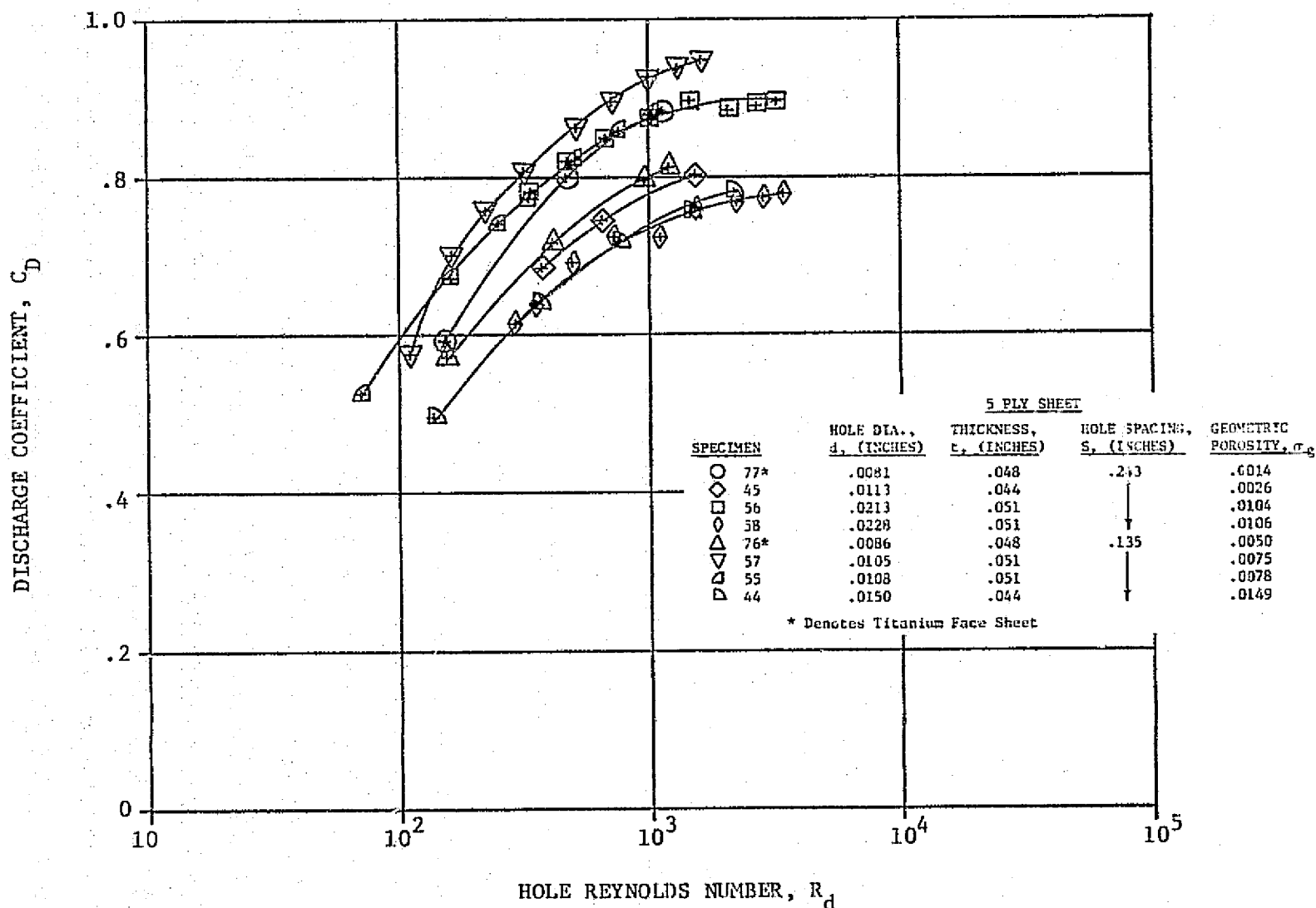


Figure 49.2. Electron Beam Drilled Specimens  
Discharge Coefficient Variations With Hole Reynolds Number

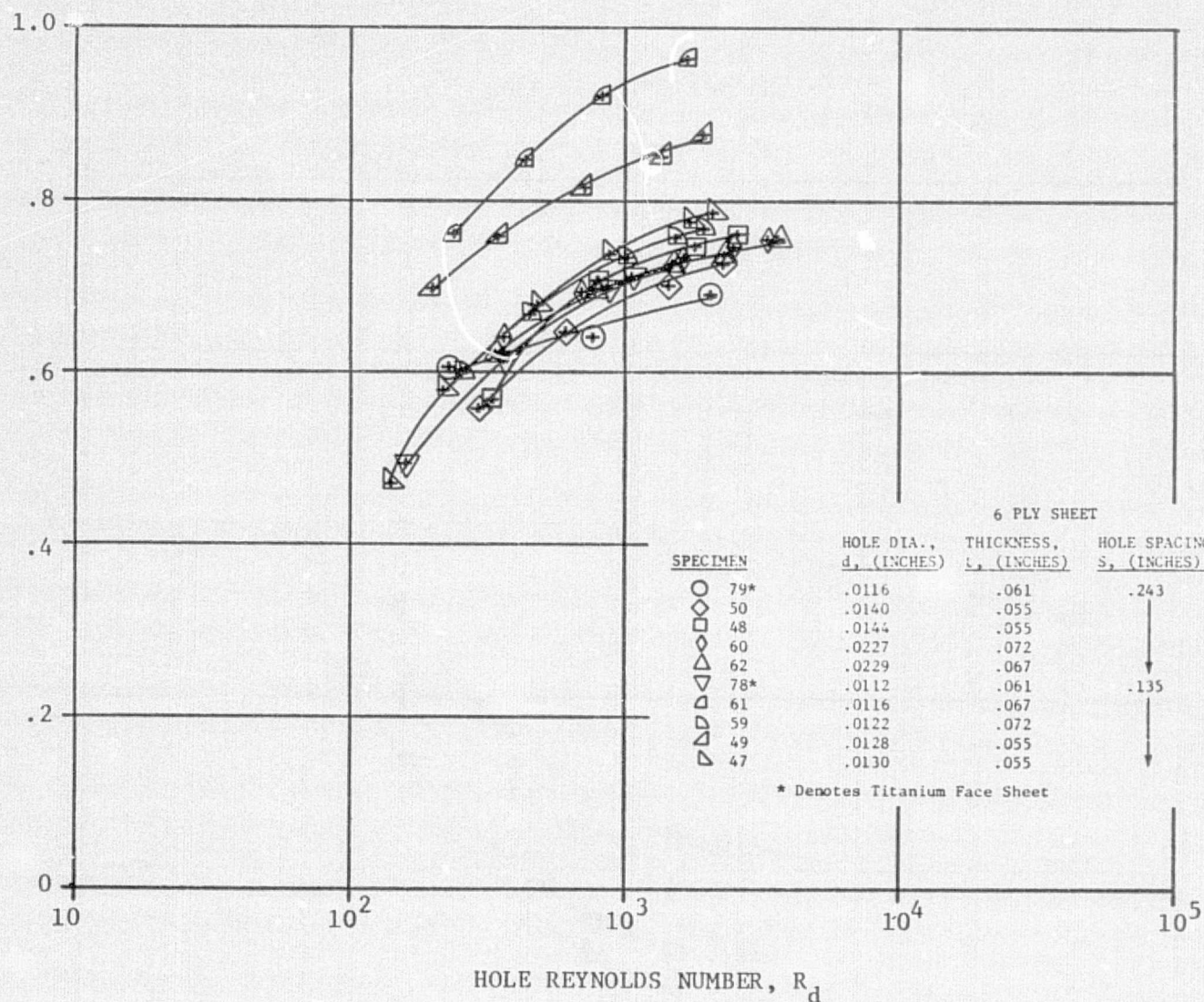


Figure 49.3. Electron Beam Drilled Specimens  
Discharge Coefficient Variations With Hole Reynolds Number



Thus the three ply specimens indicate a level of  $C_D = 0.85$ , the five ply specimens about  $C_D = 0.80$ , and the six ply specimens about  $C_D = 0.75$ . Such is a reasonable trend; the thicker materials show greater pressure drop. However, the data scatter band is large. If, on the other hand, all specimens with a hole diameter relative dispersion above a certain arbitrary level are excluded, a different conclusion results. Figure 49.4 shows the discharge coefficient for all specimens of hole diameter relative dispersion less than 0.08. The data still include a wide range of thickness/diameter ratio,  $t/d$ , hole diameter,  $d$ , and geometric porosity,  $g$ . They do not, however, indicate any consistent correlation with these parameters and, except for one specimen, are closely grouped into a relatively narrow band of discharge coefficient versus hole Reynolds number.

#### Stiffened Panels

The lock core panel results are shown in Figure 50 . The two specimen with the open edges should be identical with each other and comparable with the eight ply Doweave specimen of Figure 47.2, since the open edges allow the air to escape between the truss web without further resistance. Within the data scatter this seems to be the case. The closed edge specimen shows about twice the pressure drop as the open edge specimen which would be expected for flow through two face sheets. Depending on the porosity of the web material there may be additional pressure drop expected to account for that.

The specimen with 25 percent of the back face blocked shows an additional small decrease in flow rate while the two specimens with perforations on the solid back face have a greatly reduced flow rate so that they fall well within the target airflow range. This capability of flow metering is germane to specific aircraft applications.

The airflow test results for isogrid panels made from two Doweave laminates are shown in Figure 51 . All of the four specimens were part of a single panel so that uncertainty due to poor reproducibility should be minimized. The effect of one additional ply on the front laminate was to reduce the flow slightly, but addition of two different micro-perforated plates acted to apparently increase the flow. The small spread in the measured flow rate is

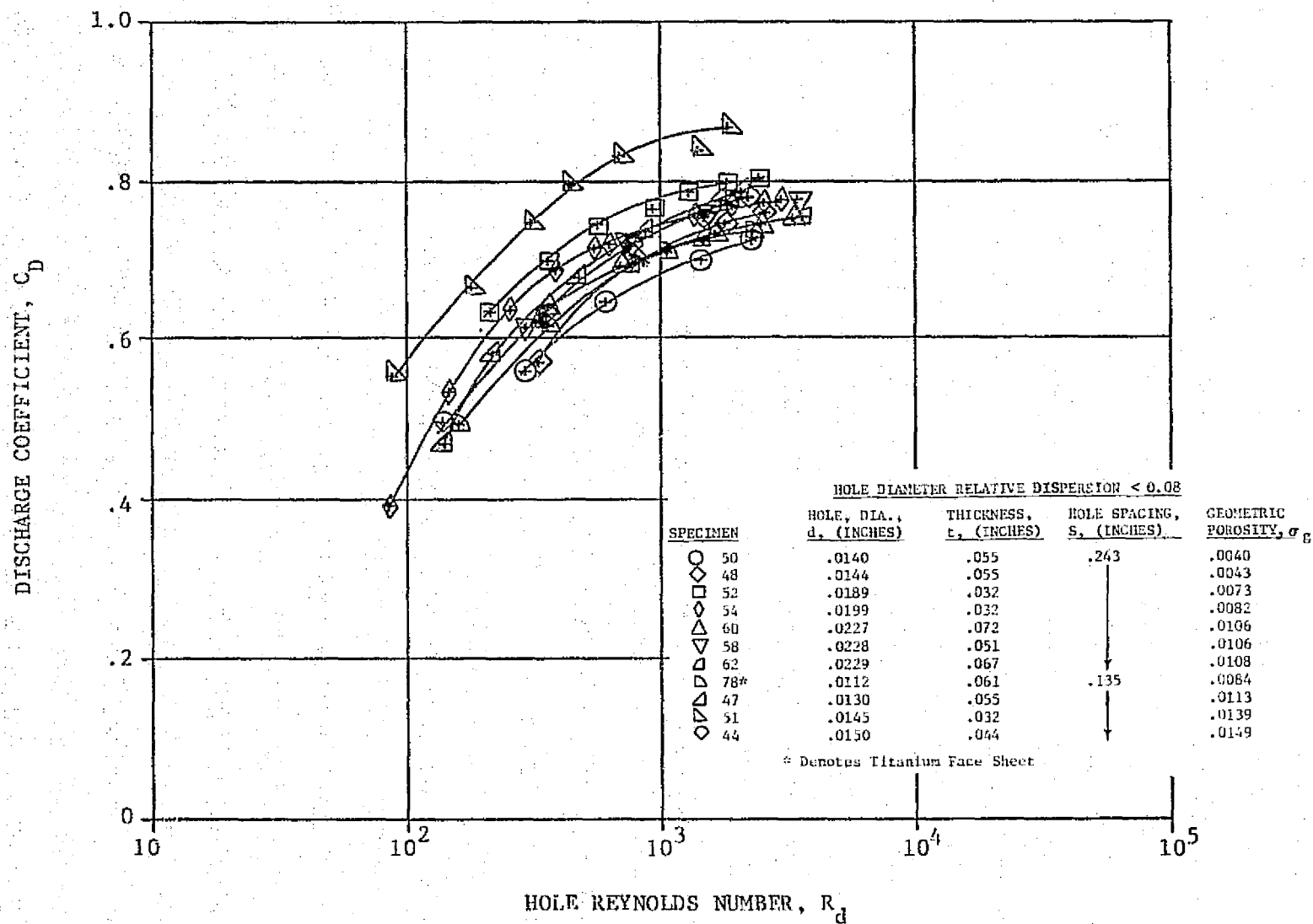


Figure 49.4. Electron Beam Drilled Specimens  
Discharge Coefficient Variations With Hole Reynolds Number

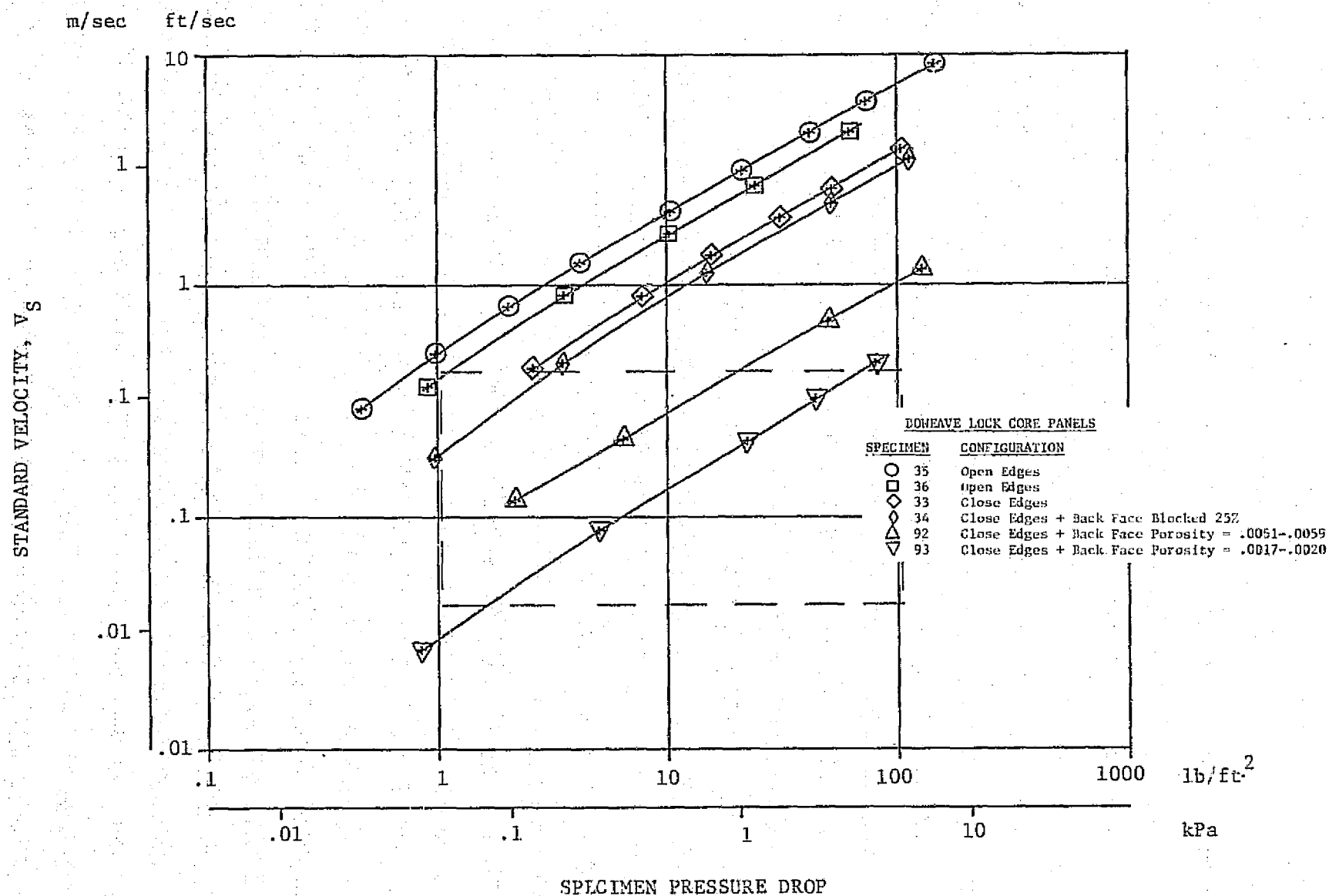


Figure 50. Pressure Drop Variation With Flow Rate

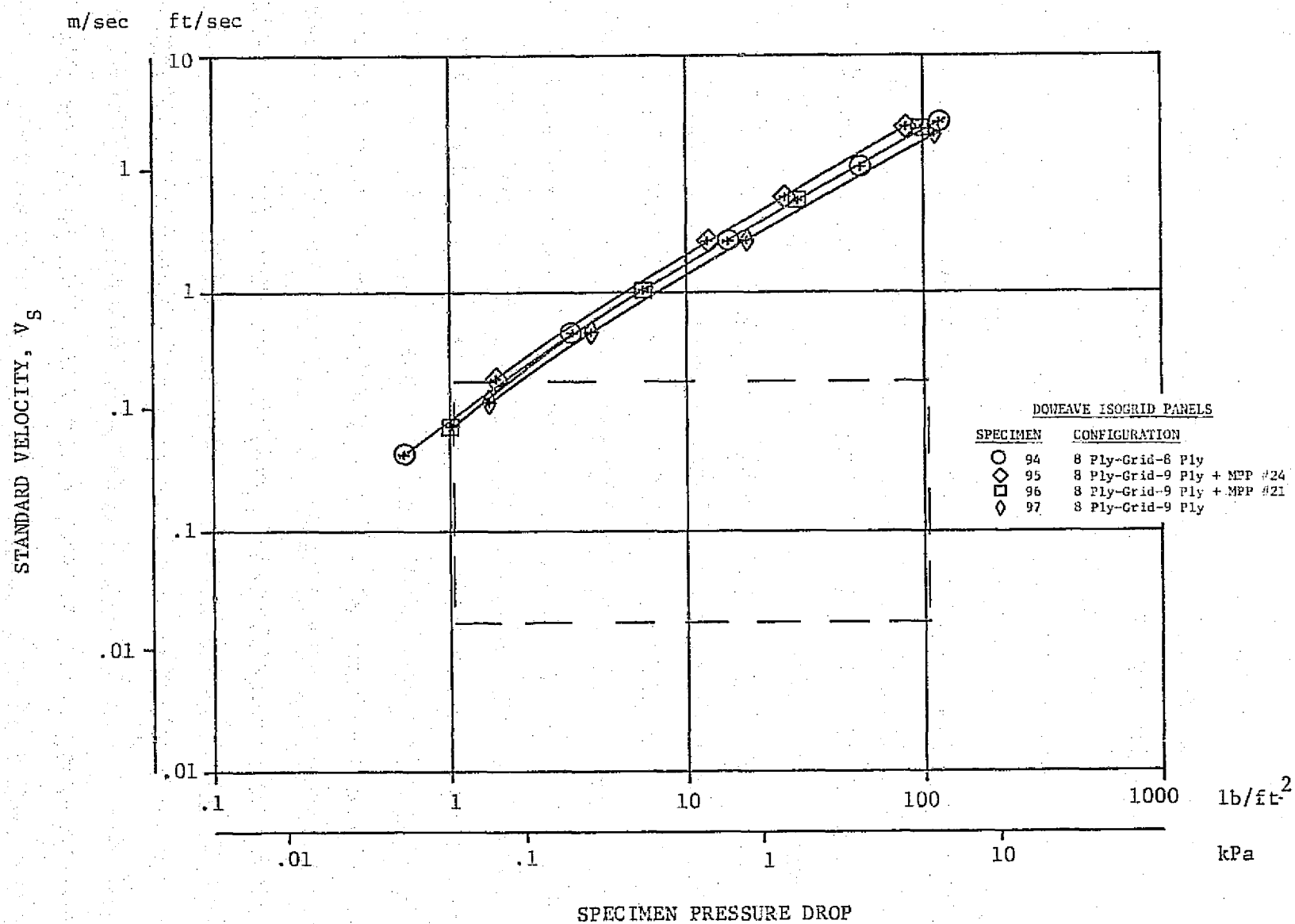


Figure 51. Pressure Drop Variations With Flow Rate

For those cases where this occurs, it may be convenient to use the apparent asymptotic value of  $\sigma$  as a descriptive parameter for each material.

The effective porosity results for the lock-core panel specimens with the perforated back are contained in Figure 53. Most of the pressure drop across the panel is produced by the perforations with front face and web material having relatively little effect. For example, specimen 92 (Figure 53), at a flow rate of 0.1 standard feet per second, produces a total pressure drop of 1.6 pounds per square foot. The Doweave face and web material is the same as specimen 35 (Figure 50). Extrapolating the test results to the same flow rate shows a pressure drop of 0.1 pounds per square foot. Allowing twice that pressure drop for two layers, the percentage of pressure drop for the back face is seen to be

$$\frac{1.6 - .2}{1.6} = 87.5\%$$



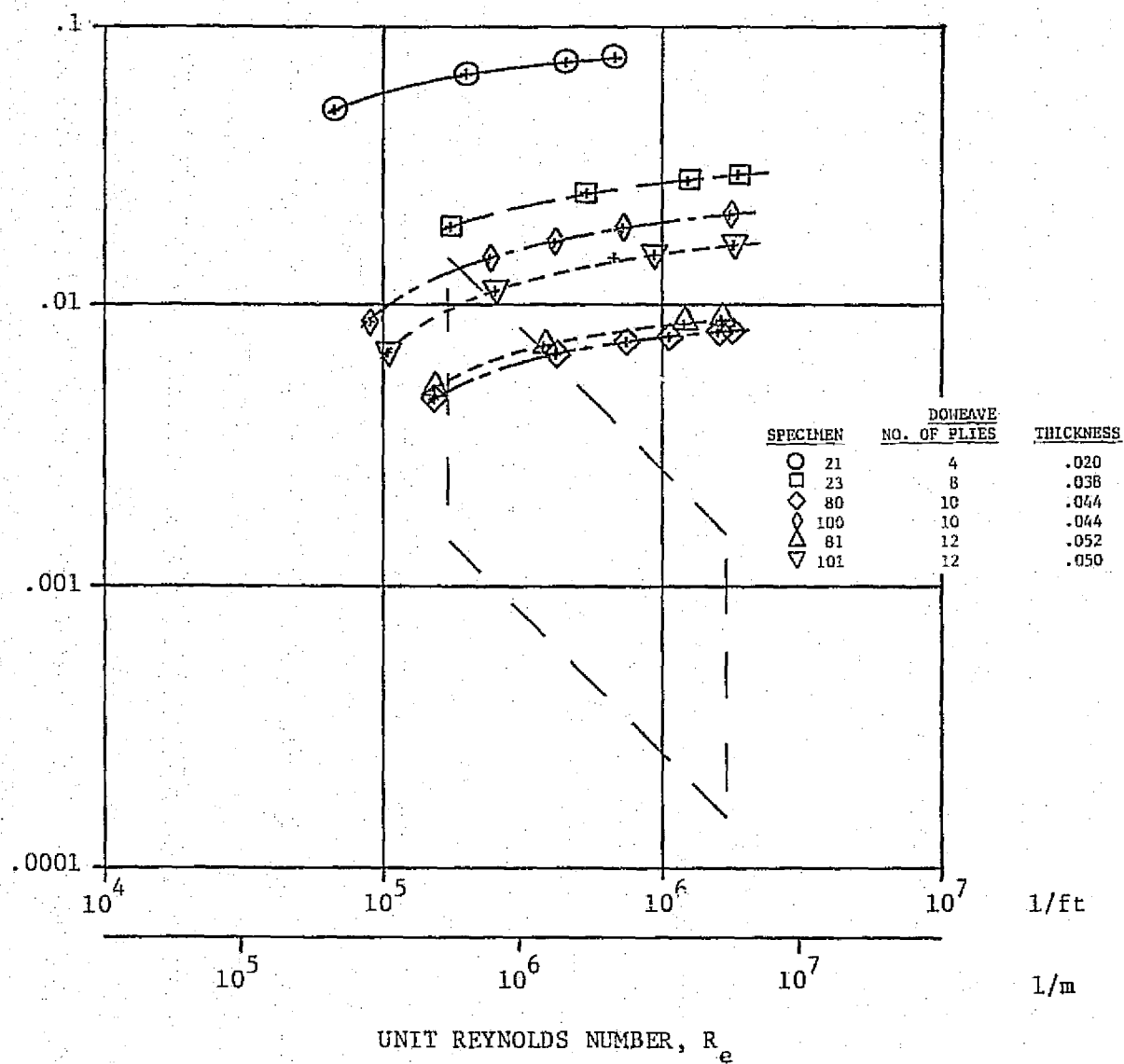


Figure 52.1. Effective Porosity Variations With Reynolds Number

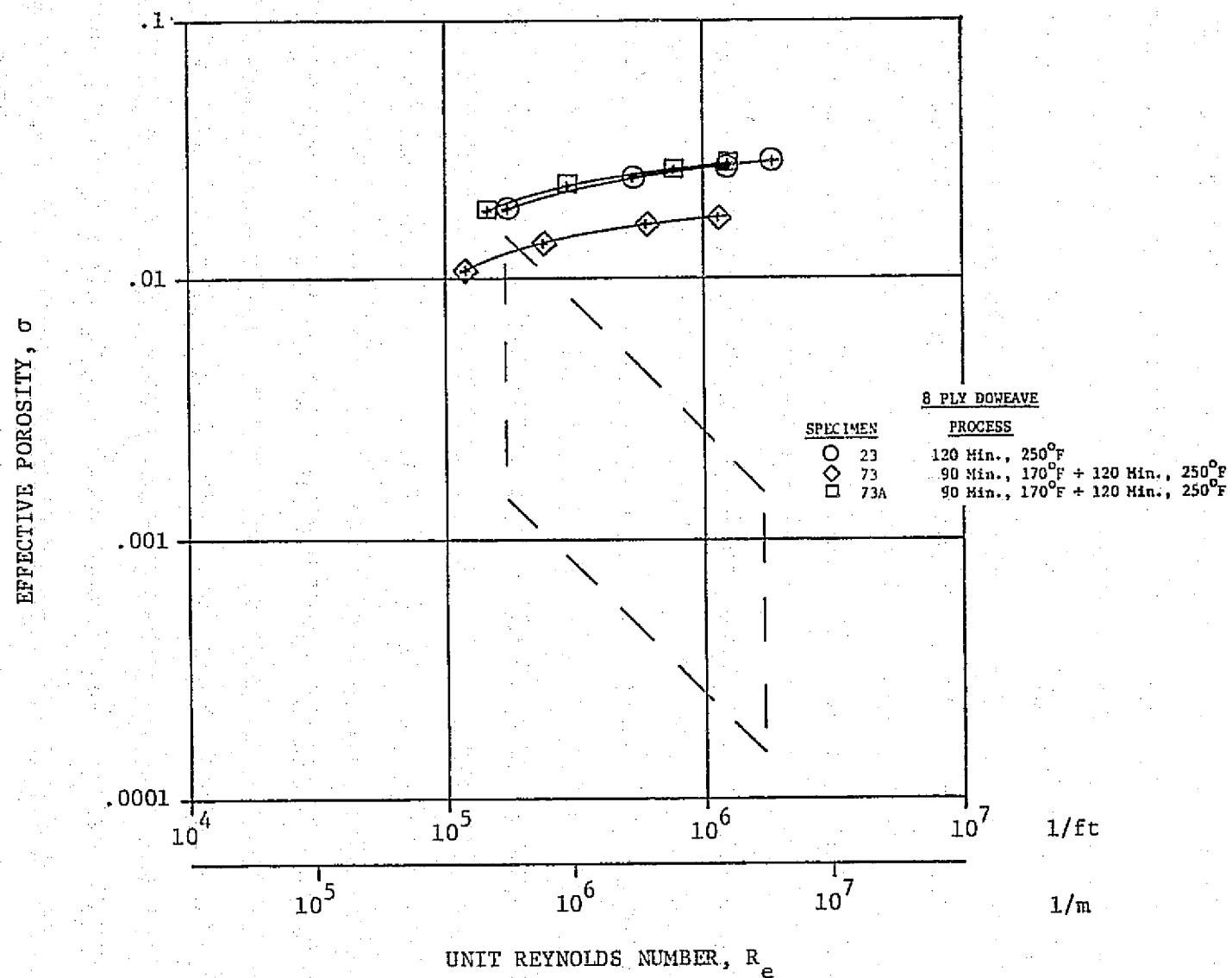


Figure 52.2. Effective Porosity Variations With Reynolds Number

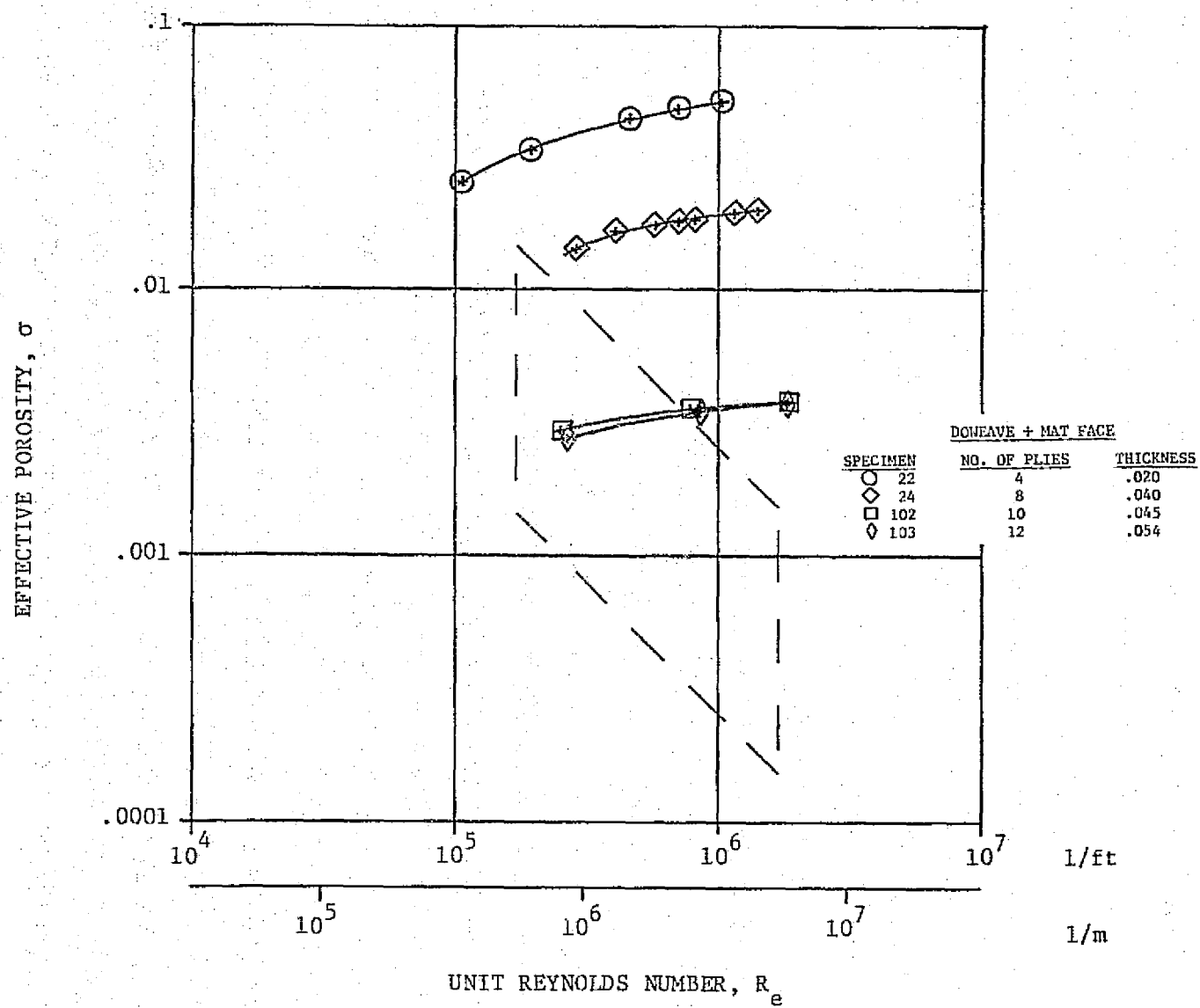


Figure 52.3. Effective Porosity Variations With Reynolds Number

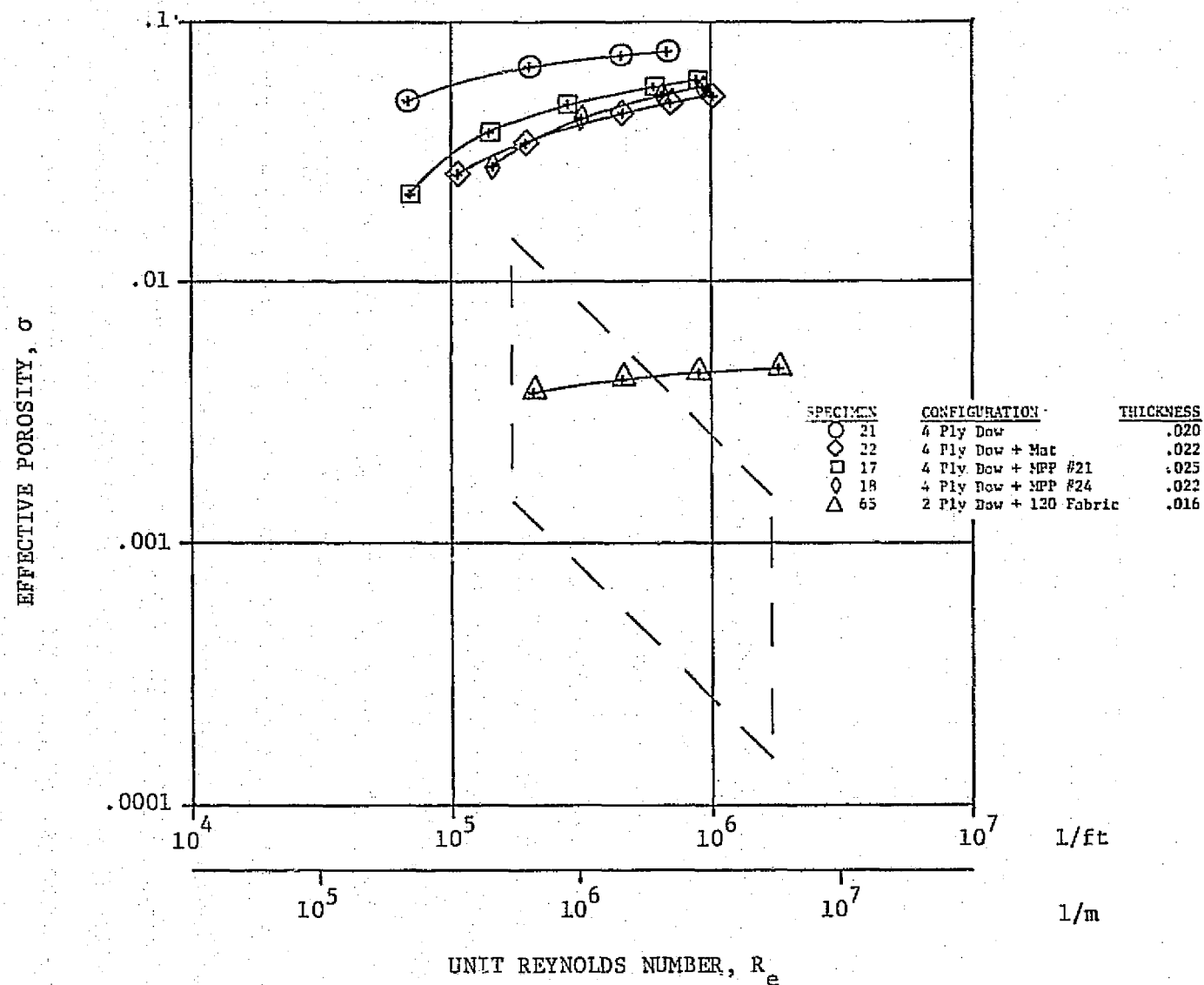


Figure 52.4. Effective Porosity Variations With Reynolds Number

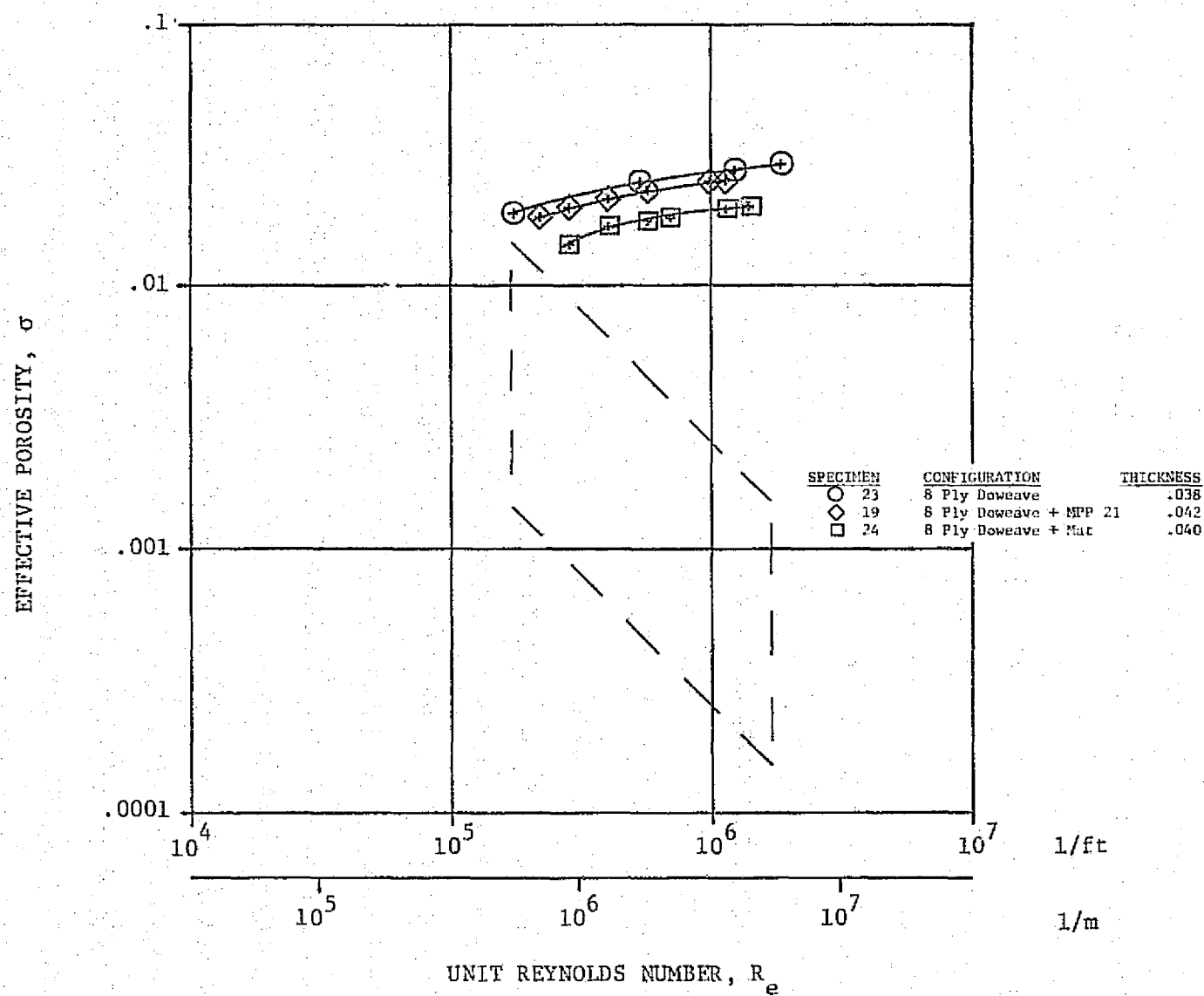


Figure 52.5. Effective Porosity Variations With Reynolds Number



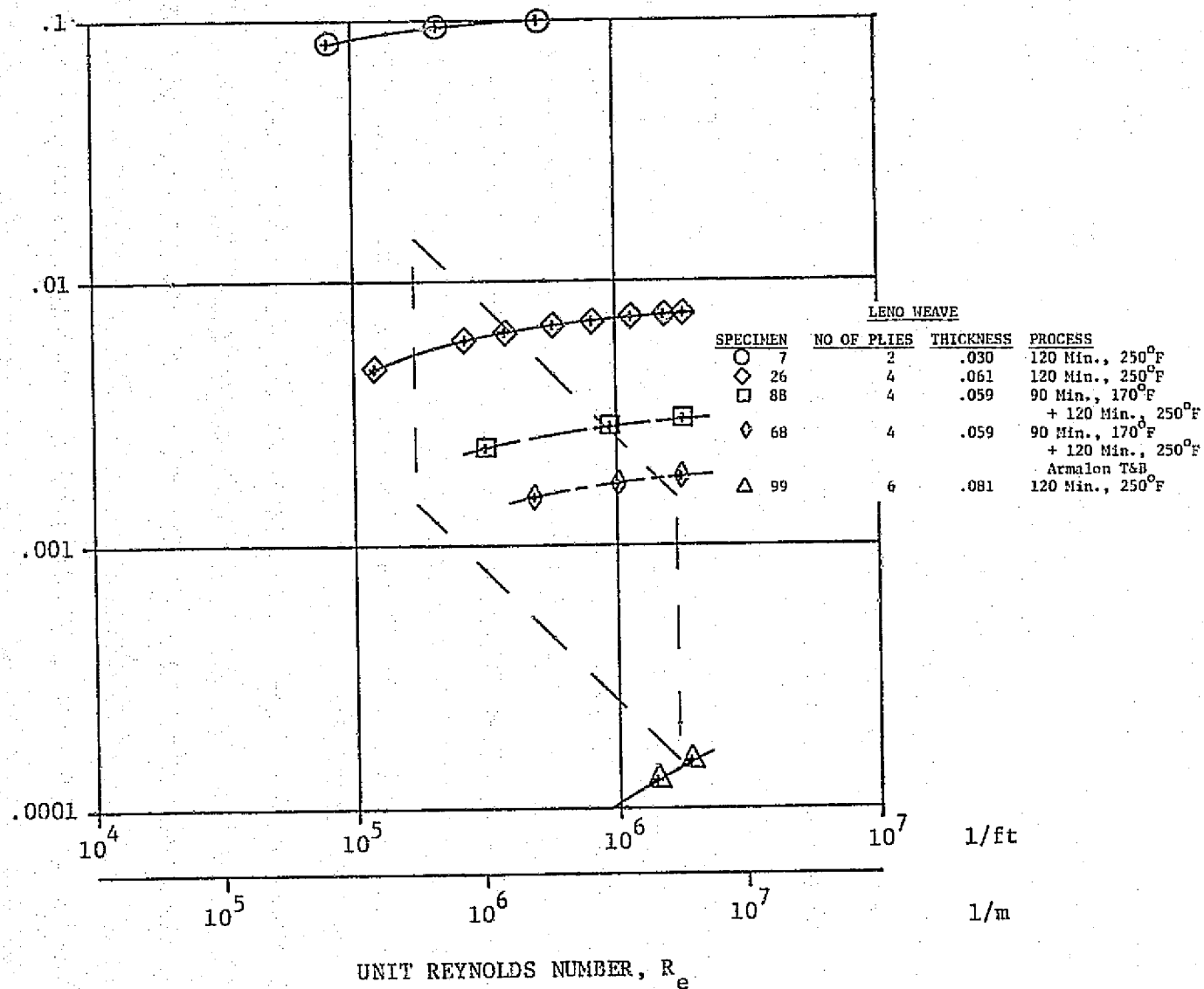


Figure 52.6. Effective Porosity Variations With Reynolds Number

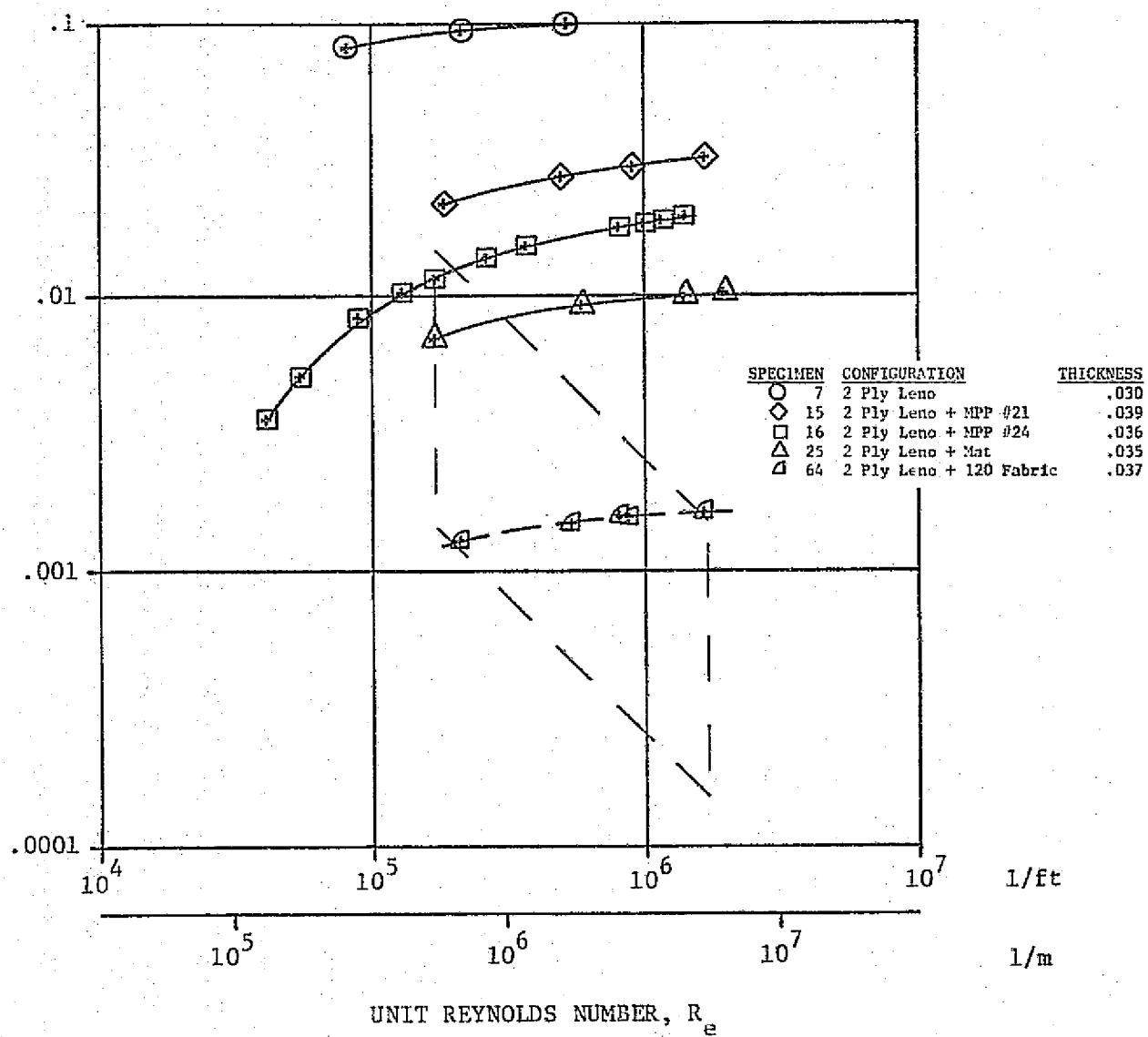


Figure 52.7. Effective Porosity Variations With Reynolds Number

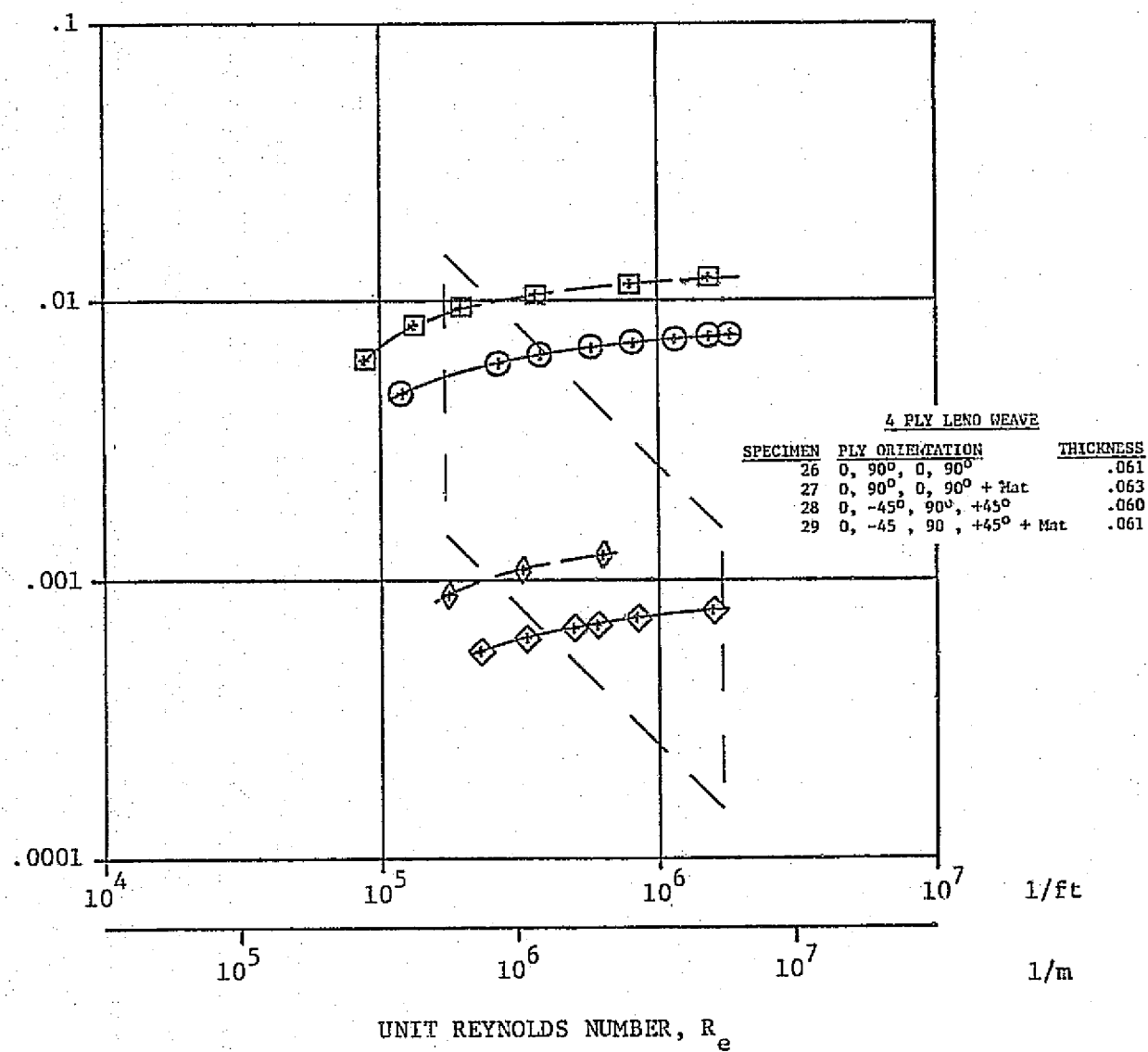


Figure 52.8. Effective Porosity Variations With Reynolds Number

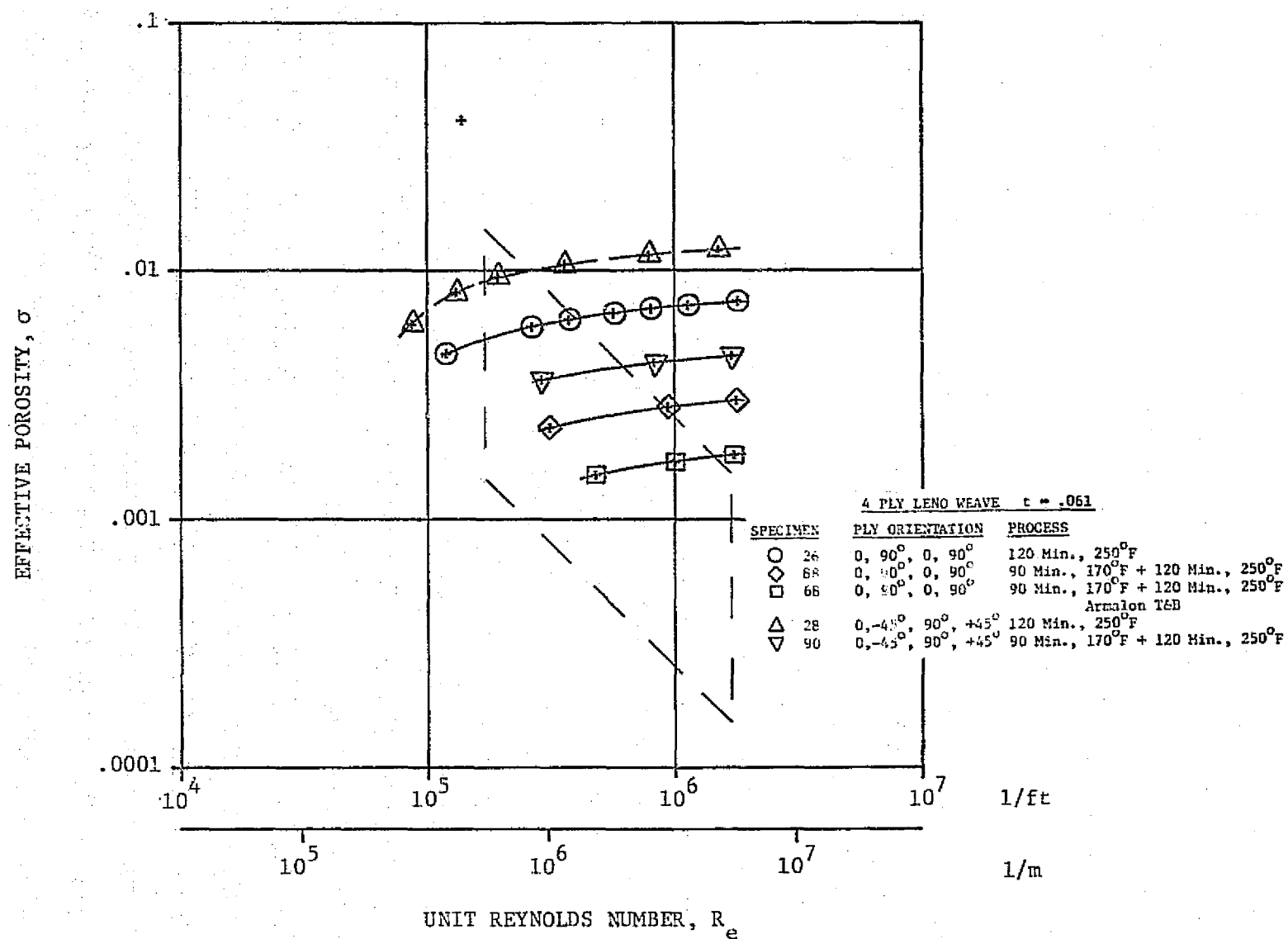


Figure 52.9. Effective Porosity Variations With Reynolds Number

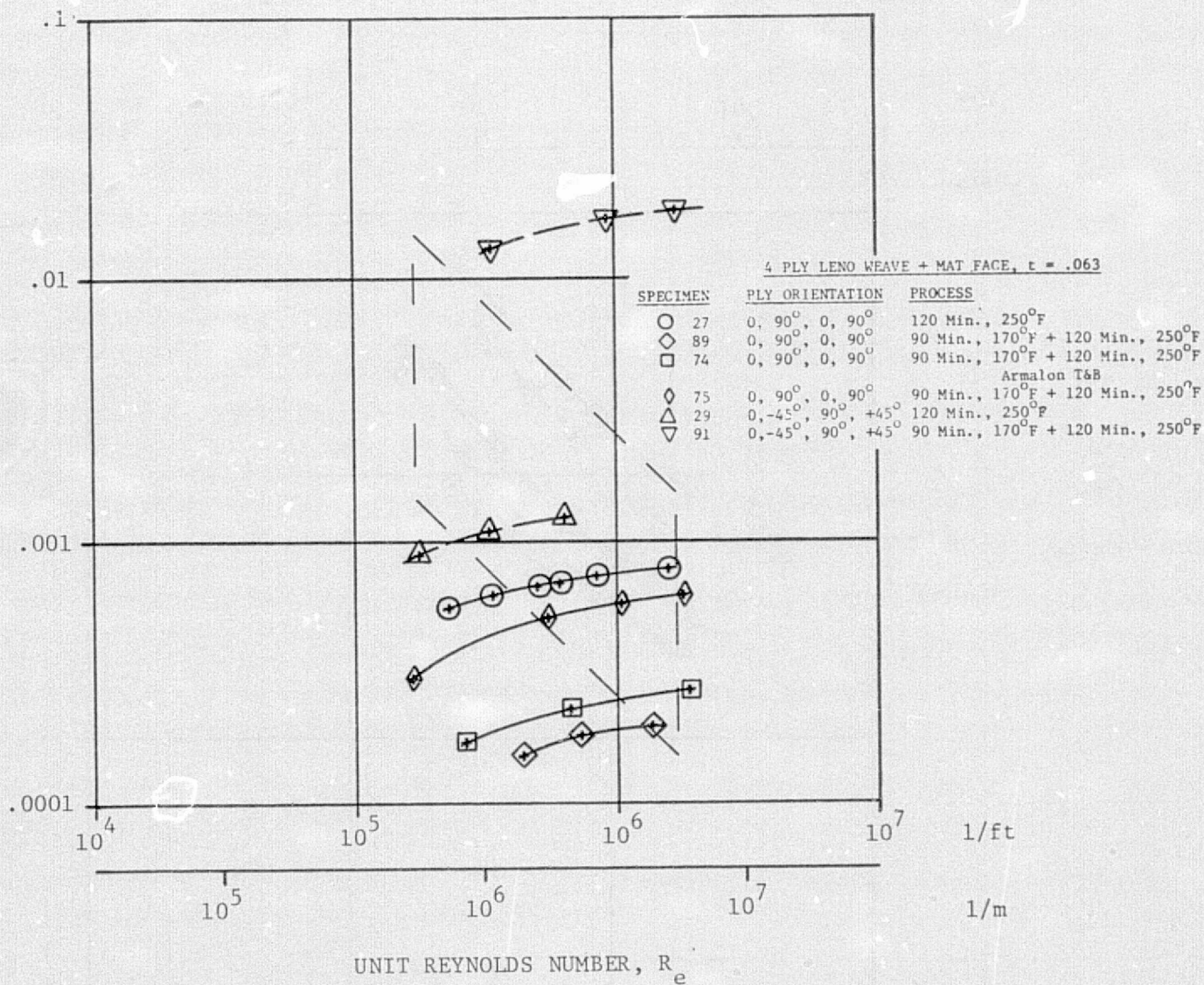
EFFECTIVE POROSITY,  $\sigma$ 

Figure 52.10. Effective Porosity Variations With Reynolds Number

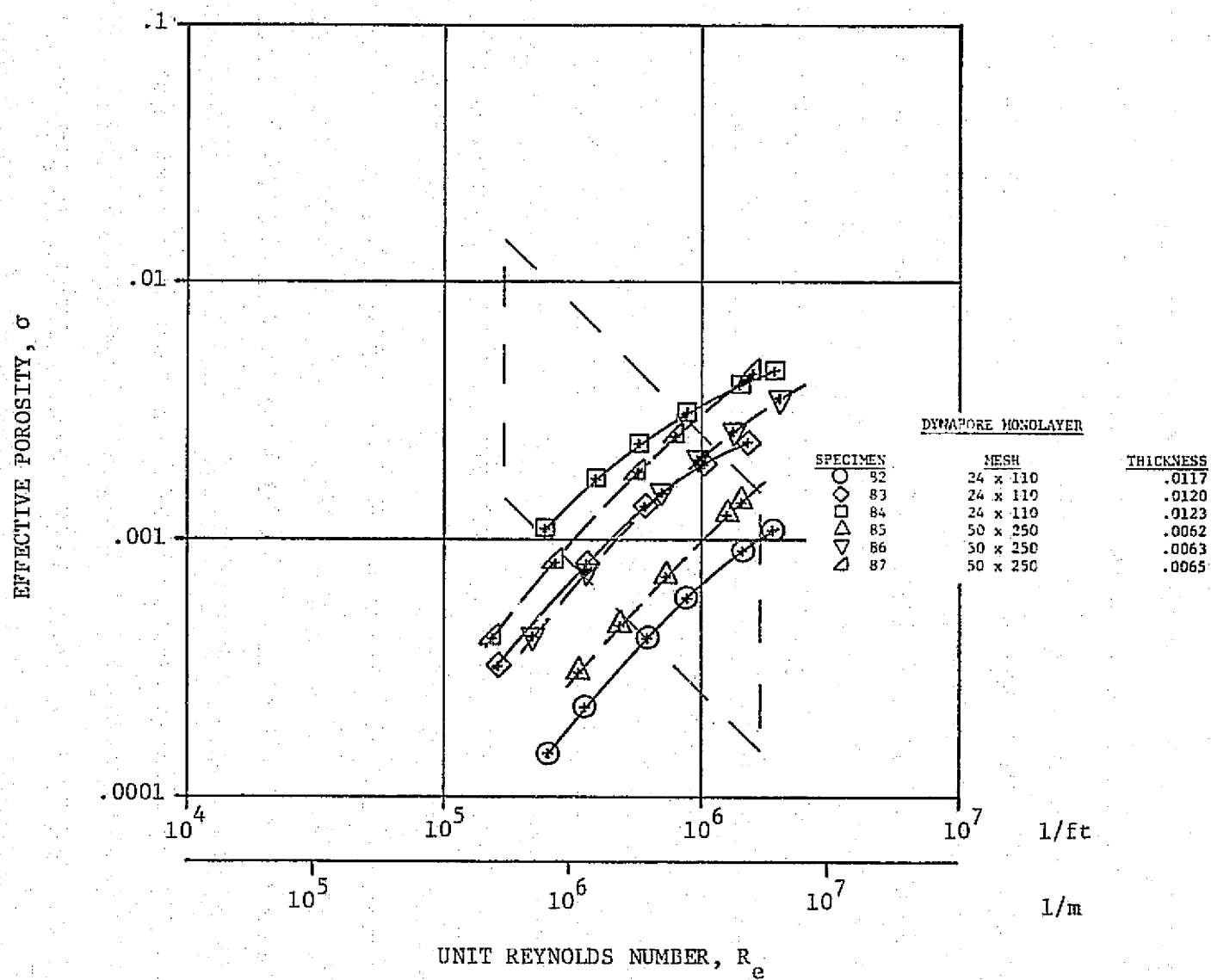


Figure 52.11. Effective Porosity Variations With Reynolds Number



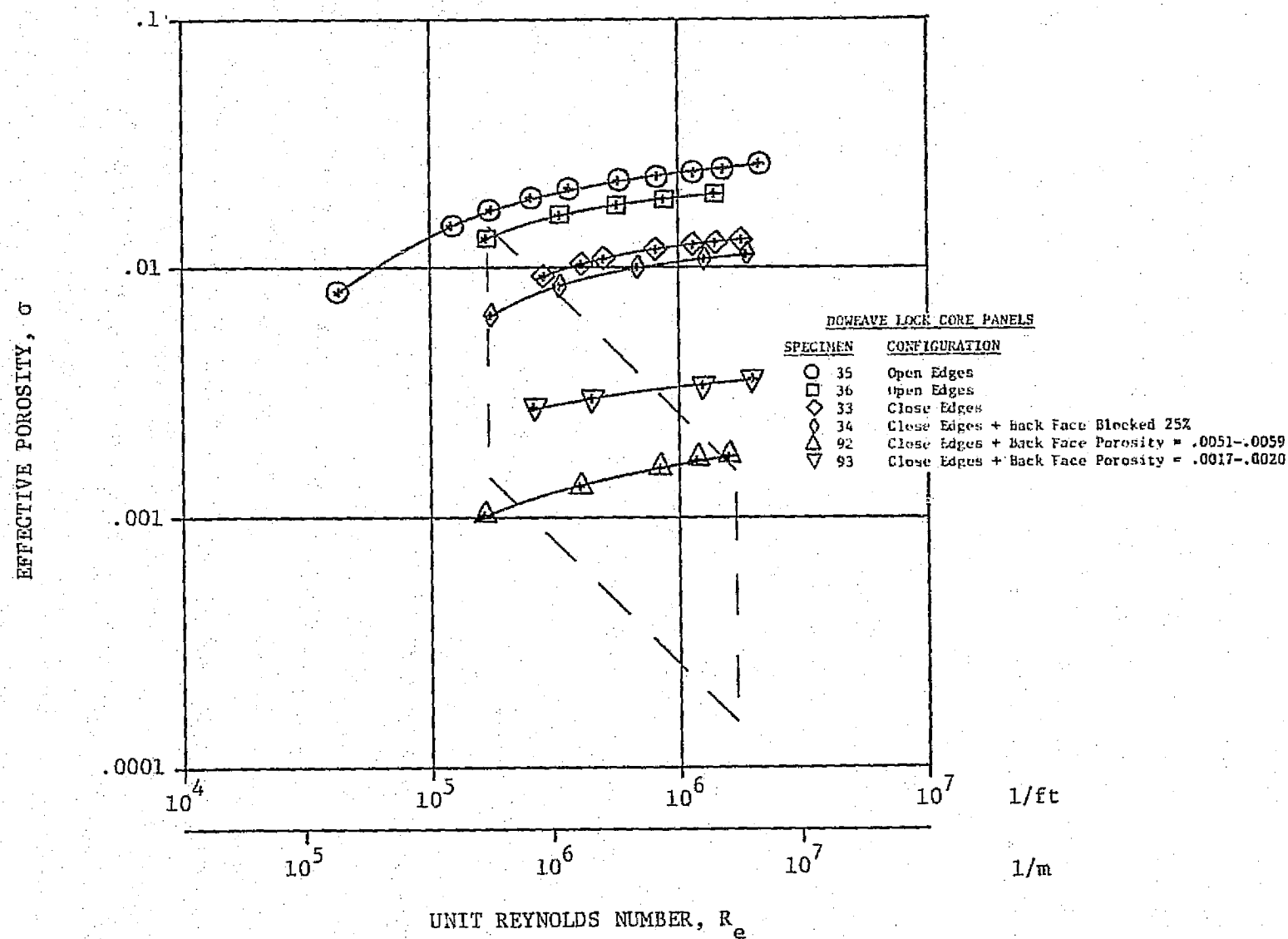


Figure 53. Effective Porosity Variations With Reynolds Number

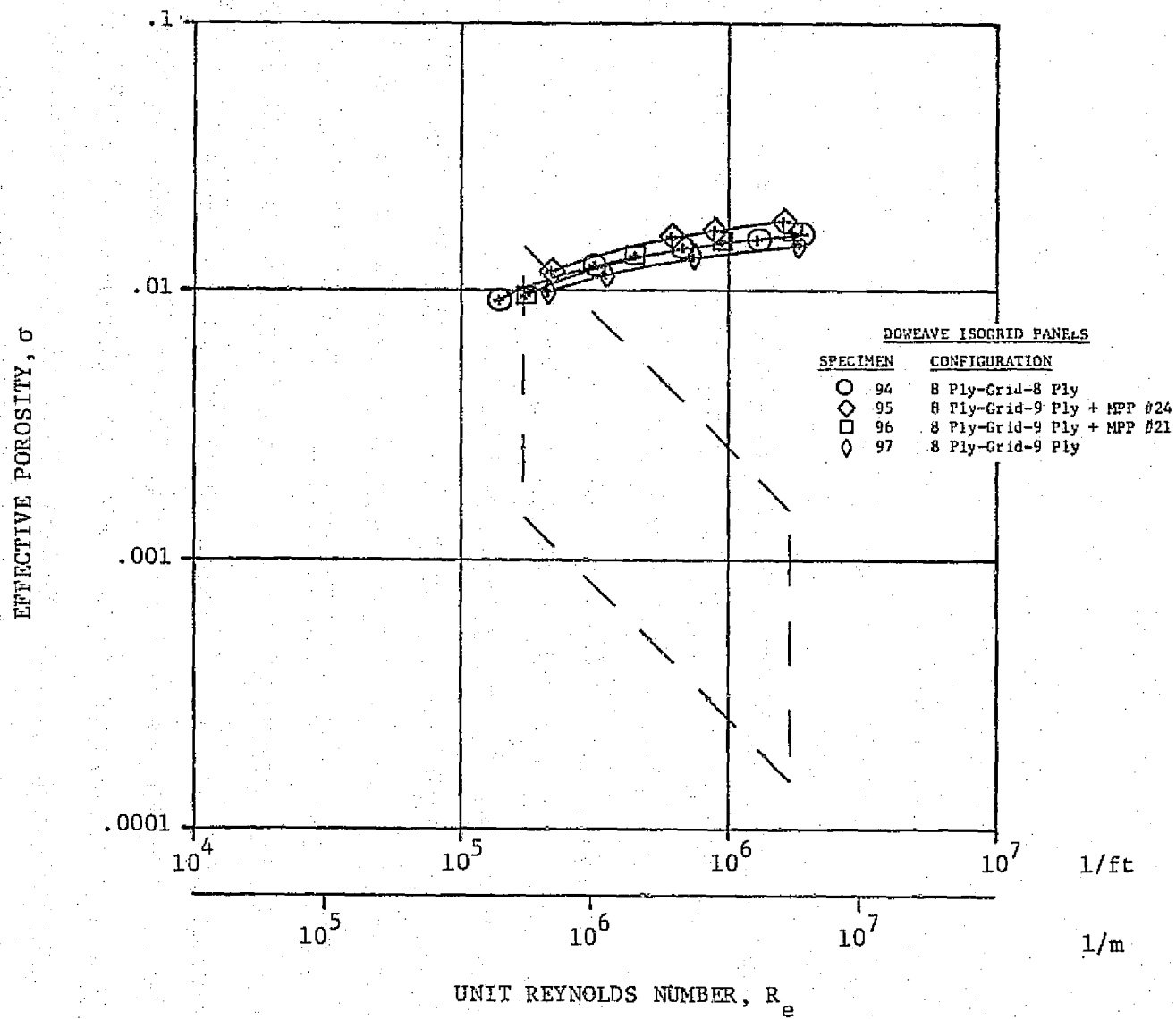


Figure 54. Effective Porosity Variations With Reynolds Number

A distinctive result is evident in Figure 52.11 which shows the effective porosity for the Dynapore mon-layer specimens. Instead of an asymptotic trend to a constant level, the curves have nearly constant slope with increasing Reynolds number. It does appear, however, that the coarse weave Dynapore may be curving over toward a constant level at the high Reynolds number end of the data. This is a reasonable trend, compared to the fine weave material, because the presumably larger pore size would be tending toward a high Reynolds number, inviscid type pressure drop mechanism.

#### CONTAMINATION TESTS

A convenient means of introducing a controlled contamination to selected test specimens was developed so that the existing test apparatus could be used with no modifications. This procedure amounted to recording the pressure drop characteristics of a specimen after it had been saturated with a contamination solution and blown dry with flow through the specimen. Typically the specimens required three to five minutes to blow dry. The flow characteristics after contamination are compared to those prior to contamination at the same flow rate in order to define an effective porosity ratio.

The contamination solution used was table salt in water with a small amount of wetting agent. The concentration of salt in the solution was varied from zero to 16 percent, which is close to the saturation level.

Figure 55 shows the results for six different specimens. The data points on the axis at zero salt concentration resulted from soaking the specimens with detergent solution in order to wet the material. Pure water would not soak

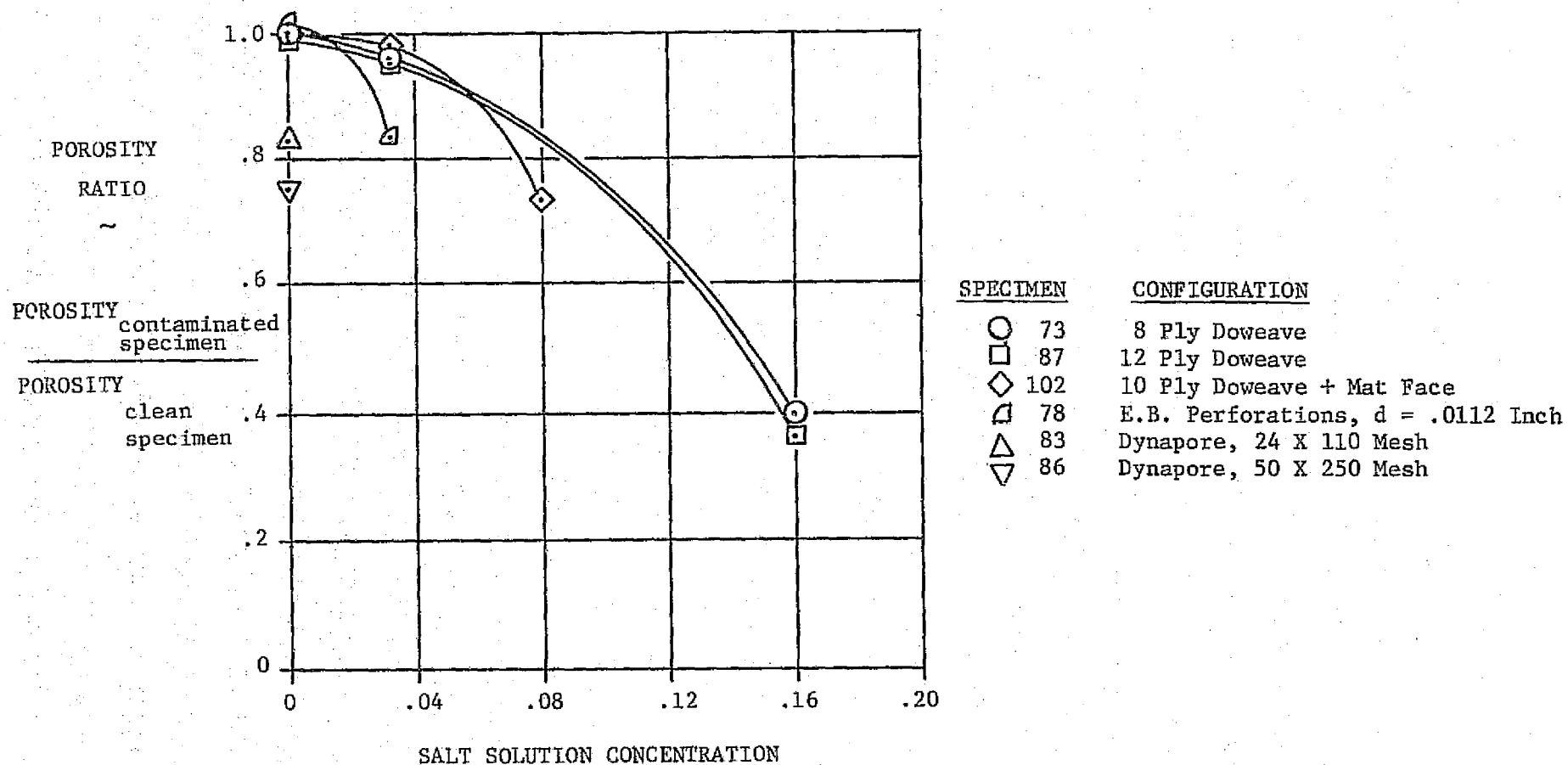


Figure 55. Effects of Contamination on Porosity

into any of the material because of its high surface tension. The Doweave specimens returned to within about one percent of their dry porosity after soaking with zero salt solution. The electron beam perforated specimen returned to a porosity almost two percent greater than the original level, raising the possibility that it had been somewhat contaminated to begin with and the detergent solution acted to clean it out. The two Dynapore specimens were permanently contaminated by 17 and 25 percent for the coarse mesh and fine mesh materials, respectively.

The effect of increasing the salt solution concentration was a steady decrease in the contaminated porosity. The electron beam perforated specimen appeared to be most strongly affected by the salt, followed next by the Doweave with mat face. The two Doweave specimens without the mat were affected to an identical extent. These materials, after a simple rinse with clear water, returned to the porosity levels, indicated by the shaded symbols, of over 90 percent. It is likely that they would have cleared further with a more thorough rinse. The Dynapore specimens are not tested with salt solution because of the drastic effect of the zero salt solution.

#### SUMMARY OF TEST RESULTS

The materials tested for airflow characteristics exhibit a wide range of flow rates exceeding the target range by an order of magnitude in each direction. The effects of number of laminate plies, surface face materials, ply orientation, cure cycle, and other factors in altering the airflow characteristics are well demonstrated. An accurate determination of these configuration parametric effects is not possible because of extraneous variations in the specimen properties caused by poor manufacturing reproducibility.

The Doweave materials show some difficulty in producing sufficient pressure drop with a reasonable number of plies, while the Leno weave laminates tend to produce an excessive pressure drop increment with each ply layer. The use of mat face material acts in a fairly consistent manner to produce additional pressure drop on the Doweave material and in a more effective and less well controlled manner on the Leno weave. The effects of microperforated plate on the woven laminates are less consistent. On the Doweave materials they

appear to have little or no effect, while on the Leno weave materials they are nearly as effective as the mat face material. This behavior seems to depend on the extent to which the microperforated plate becomes filled with resin, since the large porosity of the basic material would imply little effectiveness in producing flow blockage.

All the woven composite materials display a functional relationship between flow rate and pressure drop which tend toward

$$P = A V^{1.9}$$

at the high flow rates. This suggests a pressure mechanism controlled by high Reynolds number, inviscid type flow with the implication that the flow passageways are relatively large with high local velocities.

The Dynapore monolayer material, on the other hand, display a pressure drop relationship close to

$$P = A V^{1.0}$$

which suggests a low Reynolds number, viscous type pressure drop mechanism with low speed laminar flow through minute passageways. The magnitude of the pressure drop produced by the Dynapore specimens falls through the center of the target airflow range.

The electron beam perforated materials show flow rate characteristics scattered over a wide range above and within the target airflow range. The quality of the hole size distributions varies widely as well, which makes correlation of flow rate with hole parameters difficult. By discarding data from specimens with hole size relative dispersion above a certain arbitrary level, the flow rate data correlates well with measured geometric porosity. The flow appears to be independent of the other hole parameters such as hole diameter, thickness/diameter ratio, spacing, etc.

The data indicates a discharge coefficient trend extending from about  $C_D = 0.5$  at the low flow rates to a constant level at the high flow rates of about  $C_D = 0.75$ .



Contamination trials were conducted with selected specimens. The procedure developed entails saturating the specimen with a solution of table salt in water. The results are expressed in terms of the effective porosity after the liquid has been removed by flowing air through the specimen divided by the original dry effective porosity, to give a contaminated porosity ratio.

Doweave specimens indicated a consistent effect of salt solution concentration which varied from a porosity ratio of close to 99 percent for zero salt to a porosity ratio 30 to 40 percent for a nearly saturation salt solution of 16 percent concentration. A simple rinse with clear water restores the specimen porosity to greater than 90 percent. The Doweave plus mat face sheet specimen exhibits somewhat greater effect of salt concentration than those without the face sheet. The electron beam perforated specimen shows a small increase in porosity with zero salt solution indicating possible prior contamination which was washed away. The effect of salt solution acts at a greater rate than with the Doweave specimens.

The Dynapore monolayer specimens display substantial loss in porosity with just the zero salt solution.

#### ANALYTICAL PREDICTION OF FLOW CHARACTERISTICS THROUGH POROUS MATERIAL

In the present study, the development of an analytical prediction method for the pressure drop of gas flow through the porous materials being considered is viewed as an important achievement. Obviously such a method would be of great usefulness in designing LFC skins with controlled flow characteristics. Development of such an analytical method was identified as one of the tasks to be undertaken.

It was recognized from the outset, however, that a true analytical prediction method was precluded by the complexity of the flow paths through the porous material. Even if the equations of motion could be solved, the geometrical details of the boundary conditions are undefinable because of the randomness inherent in the construction of such materials. Therefore any prediction method would have to be an empirical method based on experimental data.

Several empirical methods for calculating pressure drop in porous systems have been developed and reported in the literature. The method of Ergun (Reference 3 ) successfully predicts the flow characteristics of packed particle beds over a wide range of flow rates. An extension of the Ergun equation to thin woven sheets is reported in Reference 4 .

The packed bed model amounts to a correlation of a friction factor, having the form of

$$C_f = \frac{\Delta P}{t} \frac{1}{\rho V^2} f(K)$$

with the Reynolds number

$$R = \frac{\rho V}{\mu} f(K)$$

The function,  $f(K)$ , is the characteristic dimension which must describe the geometrical features of the porous system. Derivation of this function is the fundamental problem in developing a prediction method.

The only way in which this function can be a predictable quantity is for the geometrical details of the porous material to be highly repeatable and preferably simple as well. This is the case for a packed bed of particles, which arrange themselves into a very regular matrix, or a woven mesh. This is far from being the case, however, for other porous materials such as sintered metals or matted fiber sheets. The materials under study in this instance, while being more regular than such completely random materials, nevertheless exhibit a relatively high degree of irregularity and therefore should probably be considered essentially unpredictable relative to materials pertinent to the Ergun equation.

In the light of these considerations, the most promising avenue for any degree of success, seemed to be the approach of Reference 4 , where a characteristic dimension for the porous material was derived from flow measurements at low rates and used to extend the prediction beyond the range of the initial measurements. This dimensional quantity is the square root of the D'Arcy permeability coefficient.

It was anticipated that the specimens tested would be grouped in distinct families and that hopefully the airflow characteristics, when expressed in terms outlined above, would correlate with physical features of the specimens. After examining some of the specimens, it became evident that not many of the complex physical features of the materials can be readily examined or described. The most obvious feature is the specimen thickness, which can be readily determined. The thickness can be thought of as the first order geometric parameter since the pressure drop is inversely proportional to it for isotropic materials.

The next most important, as well as readily determined, physical parameter is the solid void fraction. For an isotropic medium this is merely the ratio of the average density of the specimen to the bulk density of the material from which the specimen is made. As simple as this definition is, it remains very difficult to determine this quantity for the woven laminates studied here. This difficulty is illustrative of the general difficulty of developing analytic prediction methods for these materials. Since the woven laminates are comprised of unknown fractions of fiber and resin, the determination of the solid void fraction requires that the constituent components be separated to determine the relative mass fractions. Techniques to accomplish this are probably available, i.e. chemical or thermal decomposition, but would require considerable effort to develop to a reliable state. Such determinations for the specimens tested in this instance have not been attempted. This lack of convenient accessibility to such a fundamental physical parameter as the solid void fraction bodes ill for the development of empirical prediction methods with more than a very limited generality.

Use of the specimen thickness as a sole parameter for correlating material airflow characteristics may be possible for some restricted families of configurations (refer to Figure 47.1 or 47.3), but it appears that, in general, thickness is not at all sufficiently descriptive. Figures 47.6 and 47.10 illustrate the effect of cure cycle differences which affect the airflow characteristics far out of proportion to the small changes of thickness realized.

## STRUCTURAL TEST RESULTS

### DOWEAVE STRENGTH TEST RESULTS

Preliminary tensile characteristics of Doweave laminates are shown, Table VII. For economy reasons, the  $[0/90]_n$  laminate was not tested, in the belief that the "unidirectional" properties would bracket crossplied laminate values. The results show that the all- $90^\circ$  laminate, with no fibers in the load direction, displays a yield behavior when tested as a thin tensile strap without edge restraints. When tested as a beam, using 1/8-inch cell, 23-pound core, no facing or bond failure occurred but the core crimped, Figure 56. Specimen design accounted for this failure mode, but the 38 ksi stresses achieved at beam failure were considerably in excess of those achieved by the simple tension strap.

Compression failures of the  $[90]_6$  laminate were regular, Figure 57, and the 13.8 ksi strength values were lower than the tension values, as expected for Kevlar, and as expected for the unsupported fiber distances between tri-weave intersections. The tension value for  $[0]_6$  of 18 ksi is undoubtedly low, and represents the #1 direction (or  $0^\circ$ ) fibers only. The beam specimen provided "poisson effect" support for the #2 and #3 fiber directions and thus achieved higher strength. Since stresses are calculated on gross cross sections rather than actual fiber/resin area, the specific strengths and stiffnesses are included in the table for comparison with a standard graphite/epoxy laminate. In the case of the unfailed tension beams, a specific strength greater than the reference graphite laminate is indicated. The question remains, of course, just how strong is the  $[0/90]_n$  Doweave laminate selected for the airflow characterization. This should be determined at the earliest date.

Airflow and pressure drop tests through the laminate showed 12 plies or more of 200-denier Doweave are required to meet the targeted design conditions. Alternatively, inclusion of a ply of surfacing mat or #120 fabric produced the same result with fewer Doweave plies. Figure 58 displays airflow versus number of plies for a single pressure drop.\*

---

\*The wide scatter band of data is indicative of the variability of the controlled flow resin and impregnation of this batch. Improved process controls will narrow the scatter.

TABLE VII

STRENGTH AND STIFFNESS OF 200-DENIER DOWEAVE KEVLAR 29/EPOXY

MATERIAL <sup>(a)</sup>	LAYUP	t		F <sub>X</sub> <sup>1</sup>		E <sub>1</sub>		E <sub>S</sub>		DENSITY		F <sup>tu</sup> /ρ		E <sub>1</sub> /ρ		SPECIMEN TYPE
		IN.	MM	PSI	MPa	PSI x 10 <sup>-6</sup>	GPa	PSI x 10 <sup>-6</sup>	GPa	PCF	KG/M <sup>3</sup>	IN. x 10 <sup>-6</sup>	CM x 10 <sup>-6</sup>	IN. x 10 <sup>-6</sup>	CM x 10 <sup>-6</sup>	
KV20/5134	[0] <sub>6</sub>	0.030	(0.762)	18,015	(124.416)	0.939	(6.474)	0.804	(5.543)	0.030	(830)	0.601	(1.52)	31.30	(79.50)	1/2 IN. (12.7 MM) DOGDONE
								NOTE 1								
KV29/5134	[90] <sub>6</sub>	0.030	(0.762)	16,856	(116.218)	1.153	(7.949)			0.030	(830)	0.562	(1.43)	30.43	(97.61)	1/2 IN. (12.7 MM) DOGDONE
								NOTE 2								
KV20/5134	[90] <sub>6</sub>	0.030	(0.762)	37,897 <sup>(3)</sup>	(261.290)	NOT OBTAINED		—	—	0.030	(830)	1.264	(3.21)	—	—	BEAM
T300/5208	[0/45/90/-45]	0.044	(1.12)	60,033	(413.912)	8.110	(55.916)	—	—	0.057	(1577)	1.052	(2.67)	142.28	(361.39)	BEAM
				F <sub>X</sub> <sup>2</sup>												
				PSI	MPa											
KV29/5134	[90] <sub>6</sub>			13,756	(94.844)	NOT OBTAINED		—	—	0.030	(830)	—	—	—	—	BEAM

- NOTES: (1) SECONDARY MODULUS BEGINS AT 37 TO 38 PERCENT OF FAILURE LOAD AND EXTENDS TO 80 TO 98 PERCENT OF FAILURE WHERE A "YIELDING" BEHAVIOR BEGINS.  
(2) THE "90-DEGREE" DOWEAVE LAMINATE (FILL DIRECTION AT 90 DEG TO LOAD) DISPLAYED A YIELDING BEHAVIOR BEGINNING AT 25 TO 36 PERCENT OF FAILURE AND EXTENDS TO ABOUT 4300 MICRO-INCHES ELONGATION AT 97 TO 99 PERCENT OF FAILURE. (STRAIN NOT MEASURED TO FAILURE.)  
(3) NO FACING FAILURE, CORE CRIMPED BETWEEN REACTION AND LOAD.  
(4) DOWEAVE RESULTS ARE AVERAGE OF THREE SPECIMENS EACH. REFERENCE GRAPHITE LAMINATE IS FROM DC-10 GRAPHITE RUDDER CONTRACT NAS1-12954.

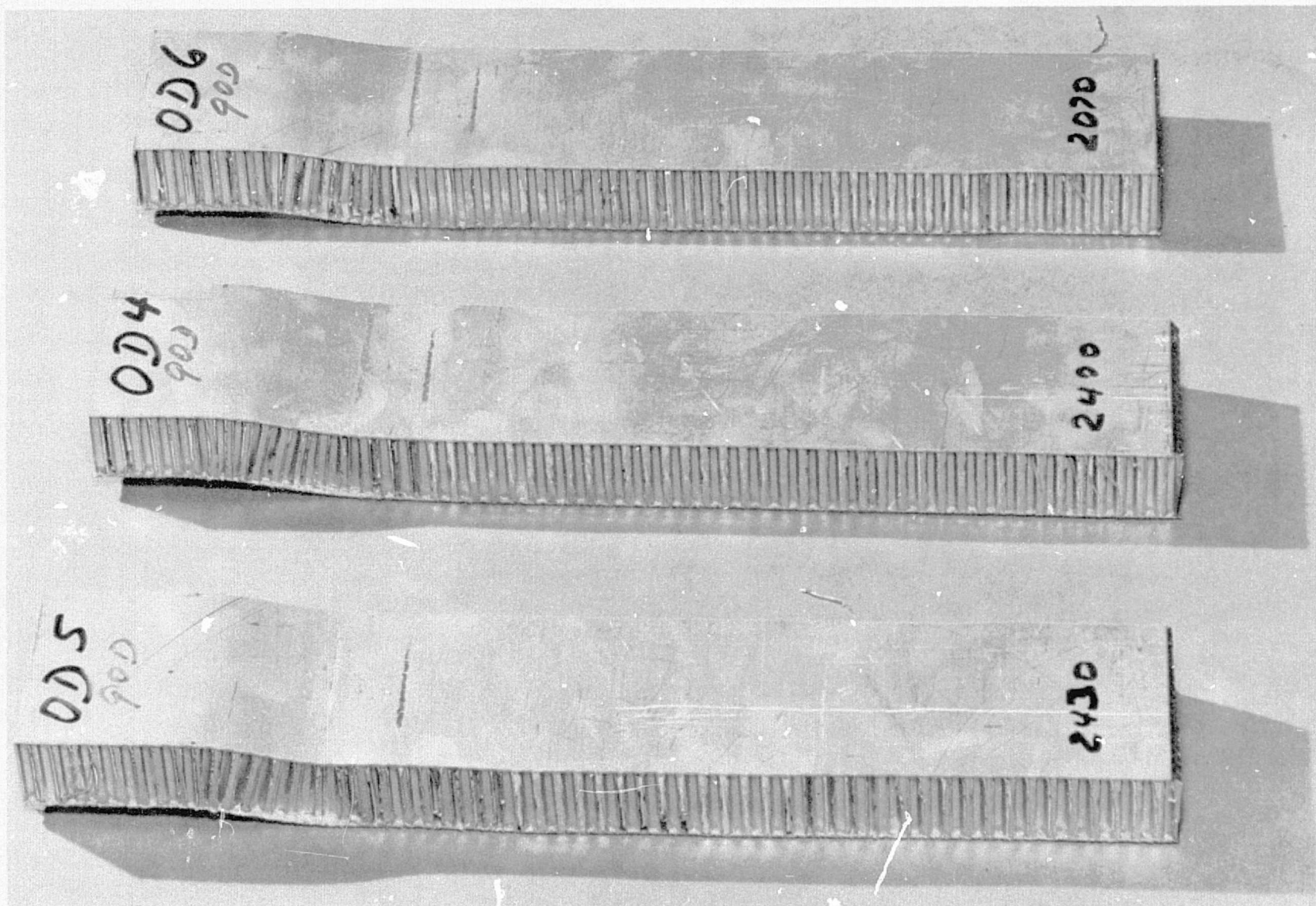


Figure 56. 90-Degree Doweave Beam Tension Test Failures



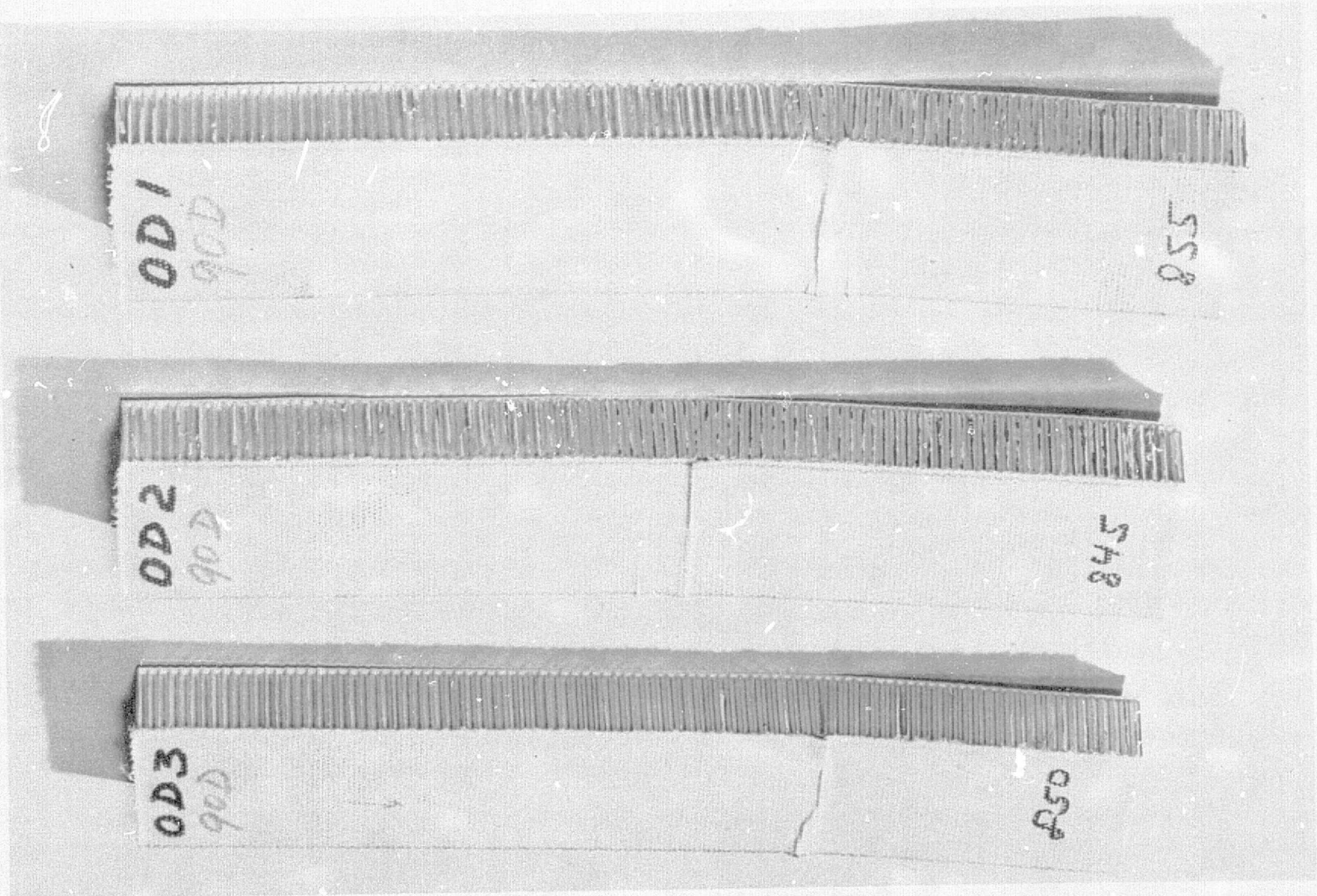


Figure 57. Dowave Beam Compression Specimens

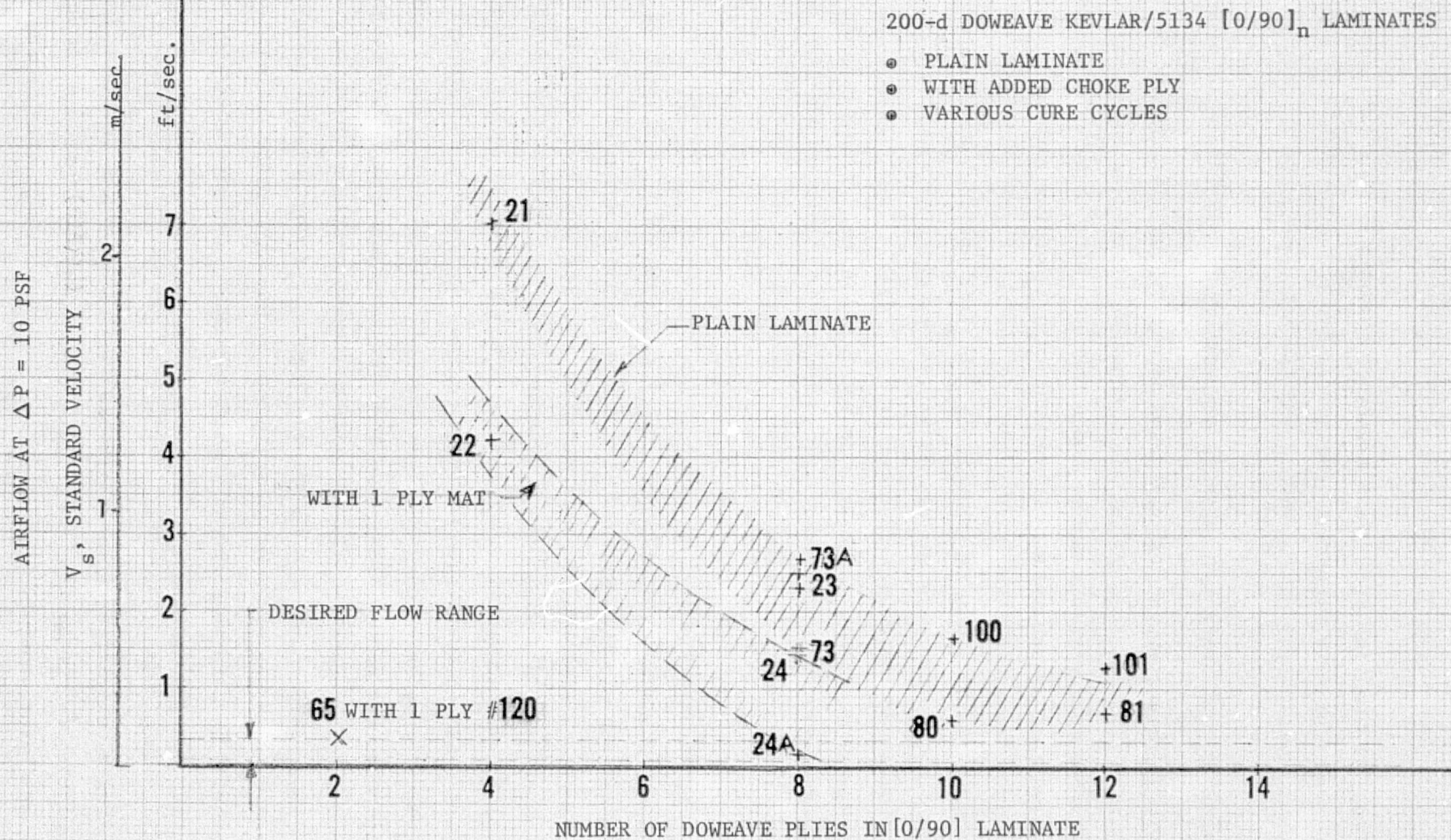


Figure 58. Trend Effect of Number of Doweave Plies on Airflow

Since the weaving pitch is a constant, a larger denier yarn should reduce the porosity per ply, allowing fewer plies for the same airflow. This would also be desirable from the standpoint of layup labor cost.

#### LENO NO. 205 WEAVE KEVLAR/EPOXY STRENGTH TEST RESULTS

Preliminary strength and stiffness of 4-ply Leno #205 laminates are shown in Table VIII. Because of the yield behavior of the dog bone tensile specimens, the recorded stresses may be lower than actually achievable; yet it should be noted that if one assumes 25 percent volume loading for the warp yarns of the  $[0/90]_s$  specimens, the warp yarns are working to 100 ksi, whereas one might expect 180 ksi. On the same basis, the compression beam specimen warp yarns are working to approximately 59 ksi, reflecting the typically lower compressive strength of the Kevlar 29 fiber or the probable lack of continuous support for compression fibers in these open-weave laminates. Figure 59 shows the  $[90]_4$  Leno compression beam failures and Figure 60 shows compression beam failures for the  $[0/90]_s$  laminate.

#### DYNAPORE MONOLAYER

Airflow and tensile strength characterization of 50 X 250 and 24 X 110 Dynapore Monolayer was accomplished at Michigan Dynamics and airflow was checked at Douglas. Table IX displays pertinent airflow and physical data for Dynapore Monolayer. The flow versus pressure drop data obtained by Douglas, Figure 47.11, for these two materials has a slope which indicates viscous losses are predominant at this low flow regime. This can be understood in terms of the pore paths which, in the uncompacted plain dutch weave, is an "S-path" through the mesh. These have been further distorted by the roughly 50 percent thickness reduction. These materials are normally used for higher flows at a lesser compaction. At the flows targeted for the LFC application, the material must be squeezed to nearly its point of non-uniformity as indicated by flow variation data measured at Michigan Dynamics. (Table IX). The targeted variation was  $\pm 25$  percent.

Preliminary strength and stiffness data is presented in Table X. Discussion of the low elongations at failure (approximately 5 percent is considered more normal for other Dynapore materials) centered about whether the values could



TABLE VIII

STRENGTH AND STIFFNESS OF NO. 205 LENO KEVLAR/EPOXY

		t		$F_X^t$		$E_i$		$E_S$	DENSITY		
MATERIAL	LAYUP	IN.	CM	PSI	MPa	PSI x 10 <sup>-6</sup>	GPa		PCI	KG/M <sup>3</sup>	SPECIMEN TYPE
KV29/5134 ↑ ↓ KV29/5134	[90] <sub>4</sub>	0.065	(0.165)	7,560	(52.124)	0.739	(5.095)	NOTE 1	0.036	(996)	<u>TENSILE</u> DOGBONE, 1/2-IN. (1.27-CM) WIDE NECKED DOWN SECTION, 2-IN. (5.08-CM) GAUGE LENGTH DOGBONE
	[0/90] <sub>S</sub>	0.065	(0.165)	24,945	(171.989)	1.731	(11.935)	NOTE 2	0.036	(996)	
				$F_X^C$							
					PSI	MPa					
		[90] <sub>4</sub>	0.065	(0.165)	12,499	(86.177)	NOTE 3		—	0.036	(996)
	[0/90] <sub>S</sub>	0.065	(0.165)	14,722	(101.504)			—	0.036	(996)	

- NOTES:
- (1) TENSILE SPECIMENS DISPLAYED A YIELD-LIKE BEHAVIOR AFTER REACHING 38 TO 44 PERCENT OF FAILURE LOAD. STRAIN RECORD OBTAINED TO ABOUT 0.28 PERCENT.
  - (2) YIELD-LIKE BEHAVIOR BEGAN AT 19 PERCENT FAILURE LOAD WITH EVIDENCE OF TRANSVERSE PLY FAILURES BEGINNING ABOUT 80 TO 85 PERCENT FAILURE LOAD. STRAIN RECORD OBTAINED TO 0.36 PERCENT (NEAR FAILURE).
  - (3) MODULI NOT OBTAINED.
  - (4) STRESSES ON NET CROSS SECTION. AVERAGE OF THREE SPECIMENS EACH REPORTED STRESS.

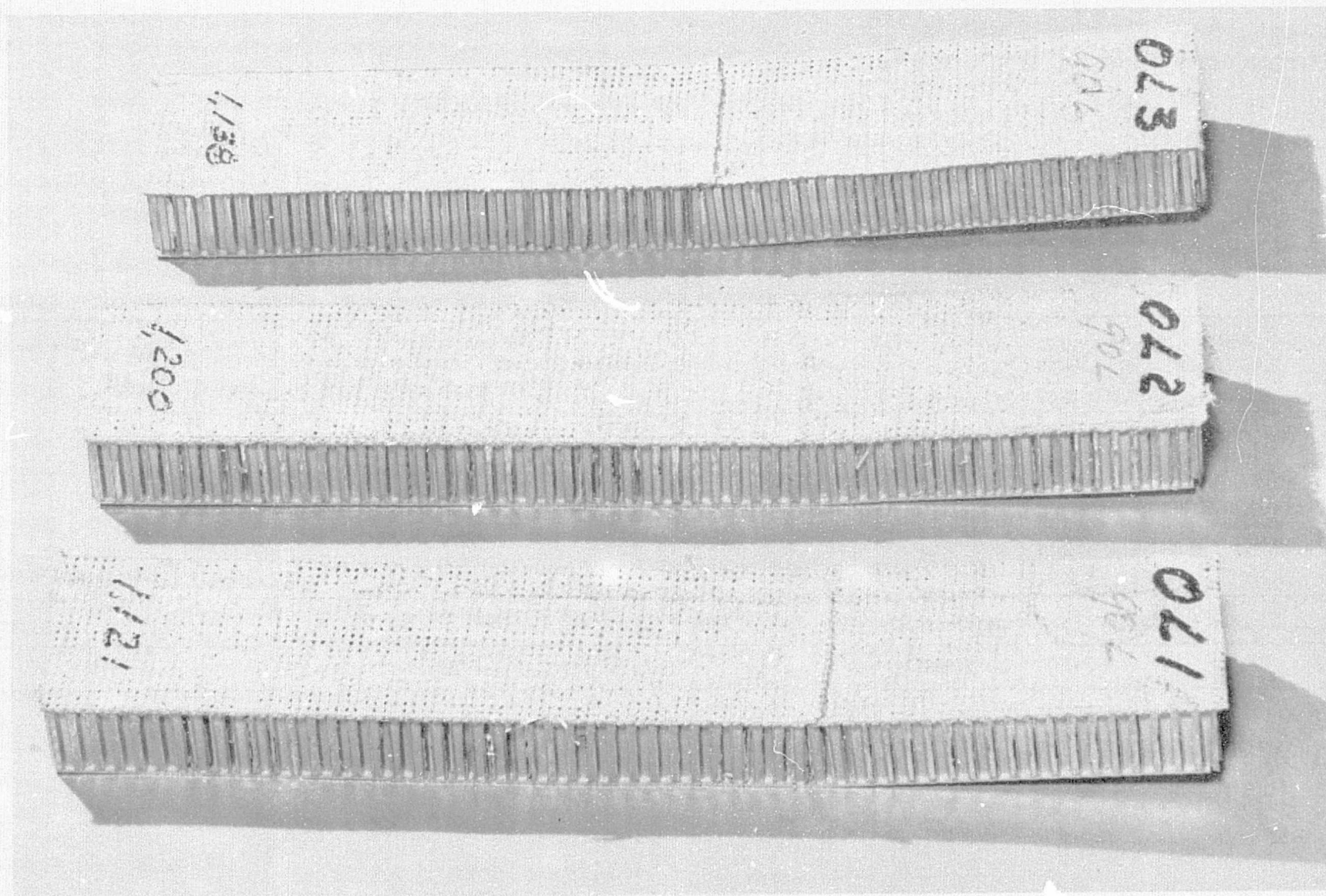


Figure 59.  $[90]_4$  #205 Leno  
Compression Beam Failures



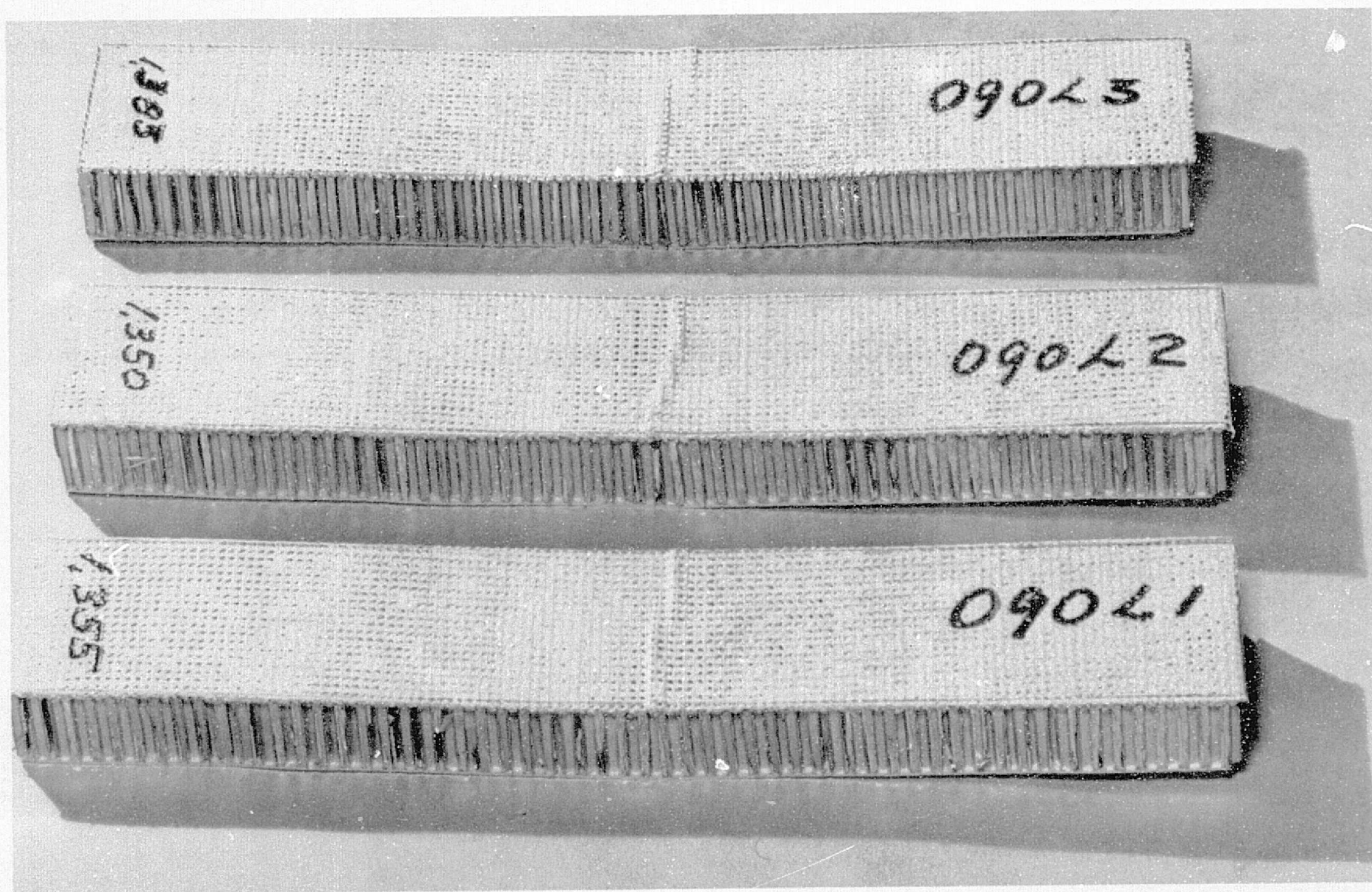


Figure 60.  $[0/90]_s$  #205 Leno  
Compression Beam Failures



TABLE IX  
DYNAPORE™ MONOLAYER – THICKNESS VERSUS AIRFLOW

MESH	t <sub>0</sub> AS WOVEN		PART NUMBER		AIRFLOW AT ΔP = 10 PSF (48.8 KG/M <sup>2</sup> )									
				DOUGLAS SAMPLE	DESIGN TARGET		MEASURED AT MICH. DYN. (1)		MEASURED AT DOUGLAS (2)		t <sub>FINAL</sub>		WEIGHT 316L	
	IN.	MM	MICH. DYN.	NO.	SCFM	M <sup>3</sup> /min	M <sup>3</sup> /min ± %	M <sup>3</sup> /min ± %	SCFM	M <sup>3</sup> /min	IN.	MM	PSF	KG/M <sup>2</sup>
24 x 110	0.030	(830)	603011-2	82	3.5	(0.099)	2.6 + 59 - 30	(0.074) + 59 - 30	2.1	(0.059)	0.0117	(0.297)	0.52	(2.54)
			603011-3	—	3.5	(0.099)	4.3 + 16 - 20	(1.22) + 16 - 20	—	—	0.0117	(0.297)		
			603012-1	83	7.0	(0.198)	7.7 + 19 - 18	(0.218) + 19 - 18	7.2	(0.204)	0.0120	(0.305)		
			603012-2	—	7.0	(0.198)	8.1 + 8 - 33	(0.229) + 8 - 33	—	—	0.0120	(0.305)		
			603013-1	84	14.0	(0.396)	13.7 + 27 - 33	(0.388) + 27 - 33	13.2	(0.374)	0.0123	(0.312)		
			603013-3	—	14.0	(0.396)	13.4 + 8 - 12	(0.379) + 8 - 12	—	—	0.0123	(0.312)		
50 x 250	0.012	(332)	603014-1	85	3.5	(0.099)	3.3 + 16 - 27	(0.093) + 16 - 27	3.0	(0.085)	0.0062	(0.157)	0.22	(1.07)
			603014-2	—	3.5	(0.099)	3.3 + 23 - 27	(0.093) + 23 - 27	—	—	0.0062	(0.157)		
			603015-1	86	7.0	(0.198)	6.9 + 25 - 24	(0.195) + 25 - 24	6.7	(0.190)	0.0063	(0.160)		
			603015-2	—	7.0	(0.198)	7.6 + 39 - 31	(0.215) + 39 - 31	—	—	0.0063	(0.160)		
			603016-1	87	14.0	(0.396)	13.9 + 25 - 19	(0.394) + 25 - 19	10.0	(0.283)	0.0065	(0.165)		
			603016-2	—	14.0	(0.396)	13.3 + 20 - 19	(0.377) + 20 - 19	—	—	0.0065	(0.165)		

NOTES: (1) 1-IN. (2.54-CM) DIAMETER TEST AREAS – 6 LOCATIONS/PANEL, 6 BY 12 IN. (15.24 BY 30.48 CM)  
(2) 4-IN. (10-CM) DIAMETER TEST AREA – 1 LOCATION/PANEL

ORIGINAL PAGE IS  
OF POOR QUALITY

TABLE X  
TENSILE STRENGTH AND STIFFNESS OF 316L DYNAPORE MONOLAYER

MESH	WARP WIRE DIAMETER		FILL WIRE DIAMETER		THICKNESS		LOAD <sup>(1)</sup>				STRESS								ELONGATION (%)	E		REMARKS
											GROSS AREA				NET WIRE AREA							
							YIELD		ULTIMATE		F <sup>LY</sup>		F <sup>TU</sup>		F <sup>LY</sup>		F <sup>TU</sup>					
	IN.	MM	IN.	MM	IN.	MM	LB/IN.	N/CM	LB/IN.	N/CM	KSI	MPa	KSI	MPa	KSI	MPa	KSI	MPa		PSI X 10 <sup>-6</sup>	GP <sub>a</sub>	
24 x 110	0.015	(0.381)	0.010	(0.254)	0.012	(0.305)	184	(322)	224	(392)	15.3	(105.5)	18.7	(128.9)	43.8	(302.0)	53.3	(367.5)	6.3	4.3	(29.64)	LOAD PARALLEL TO WARP 24/IN.
							310	(543)	334	(585)	25.8	(177.9)	27.8	(191.7)	36.0	(248.2)	38.8	(267.5)	1.1	6.6	(45.5)	LOAD PARALLEL TO FILL 110/IN.
50 x 250	0.0055	(0.139)	0.0045	(0.114)	0.0063	(0.160)	96	(168)	109	(191)	15.2	(104.8)	17.3	(119.3)	80.8	(557.1)	91.9	(633.6)	1.0	5.2	(35.9)	LOAD 11 TO WARP 50/IN.
							169	(296)	224	(392)	26.8	(184.8)	35.6	(245.4)	42.5	(293.0)	56.3	(388.2)	2.5	8.2	(56.5)	LOAD 11 TO FILL 250/IN.

NOTE: (1) YIELD SET AT 0.002 STRAIN OFFSET. LOAD VALUES ARE AVERAGES.

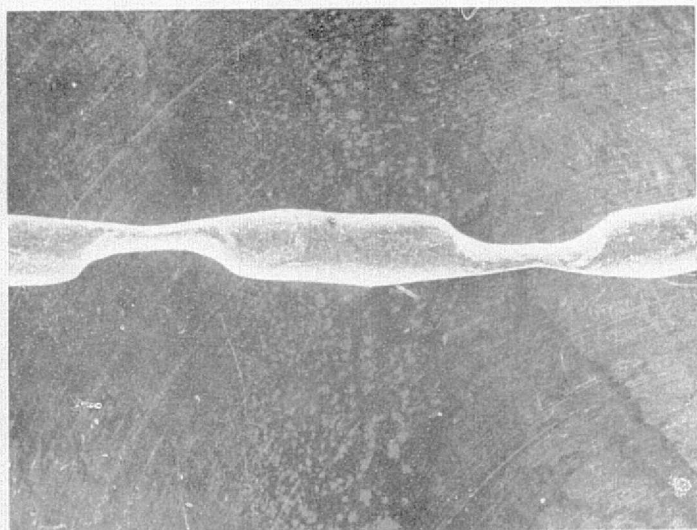
be due to slightly unsymmetrical loading of the very thin, one-half inch wide "dog bone" tensile specimens. Subsequent examination by scanning electron microscope (SEM), however, revealed the extent of deformation produced in both warp and fill wires by the compacting operation. In the case of 24 x 110 material, Figure 61 shows that the thickness reduction was 60 percent, the deformations in a warp wire and a peeled back fill wire is also shown. The deformations represent stress concentrations which can limit both elongation and ultimate strength. This is also suggested by net section stresses (based on original wire area since area is not removed by compaction, Table X ). It is not known how much thickness reduction was achieved after sintering; i.e., what percent of total thickness change can be called cold working. For comparison 316 steel sheet at 54 percent thickness reduction has  $F^{ty} = 140$  ksi and  $F^{tu} = 150$  ksi (Reference 5). 0.062-inch diameter drawn 316L wire in soft temper has  $F^{ty} = 75$  ksi and  $F^{tu} = 100$  ksi (Reference 5). Table X values are generally lower than these.

The static strengths and strains at the moduli indicated are just adequate to consider using in designs with other structural materials at extremes of temperature differential; however, its fatigue strength has not been investigated. It is apparent the strength potential of Dynapore Monolayer might be improved. Options for such strengthening include:

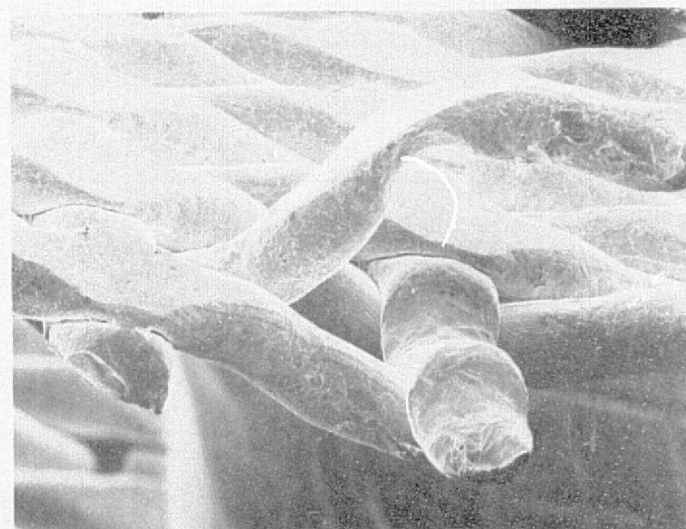
- Reduced total compaction.
  - Begin with a denser mesh such as 1WT 80 x 700.
  - Provide final airflow with some other operation such as moderate compaction plus electroless plating.
- Change to PH 17-7 or other material.
- Compaction/sintering process changes.
- Combination of above.

Reduced compaction would also reduce point to point airflow variations.

Since the strains at yield appear suitable, it is recommended further work with this material be pursued.



40X



100X

Figure 61. Extent of Wire Deformation  
During Compaction, Dynapore Monolayer

## STRUCTURAL ASSESSMENT

### LOAD/STRAIN ANALYSIS

The differing materials used for porous surface panels and primary structure raises the problem of whether these various materials will strain together without premature failure of some element. The lines of constant strain on Figure 62 indicates limit load strain levels accepted in current advanced design thinking and adopted, for purposes of this program, for primary wing structures of various materials. The required limit or yield strength of the LFC panel and facing, considered as straining with the primary structure, is shown as a function of its elastic modulus. The example, Figure 62, shows that a Dynapore Monolayer material working as an LFC surface on a graphite composite wing must have a minimum yield strength of 25 ksi if its effective (secant) modulus at yield is  $9.3 \times 10^{-6}$  psi. Actual Dynapore yield strain data is presented in Table XI, along with yield strength and elongations reported elsewhere. Referring these data to the criterion of Figure 62 shows Dynapore exceeds the minimum static strength requirement on all primary structure material except Titanium 8 Al 1 alloy. The ultimate strain can also be deduced to comfortably exceed ultimate strength requirements. For a given LFC material, the graphite/epoxy wing requires the least strain to failure. A titanium wing skin places the greatest strain requirement on an LFC material, unless the LFC panel is also of titanium.

A minimal amount of strength data was obtained for the Doweave and Leno porous composites, as presented in previous Tables. Comparison of the existing data for Doweave with the above strength criterion indicates limit compression and tension strengths of the  $[0/90]_n$  laminate should be satisfactory, assuming the initial elastic modulus is  $10^6$  psi. For the Leno #205,  $[0/90]_n$  pattern and initial modulus of  $1.7 \times 10^6$  psi, limit tension strength would be satisfactory, but limit compression strength probably does not meet the strain requirement of titanium. The  $0/\pm 45/90$  laminate pattern required for the Leno, if it is to be a shear-carrying panel would have reduced strengths and stiffnesses from the  $[0/90]_s$  pattern and requires further investigation.

All materials explored for airflow in this program require additional strength/stiffness characterization for structural design purposes.

PRECEDING PAGE BLANK NOT FILMED



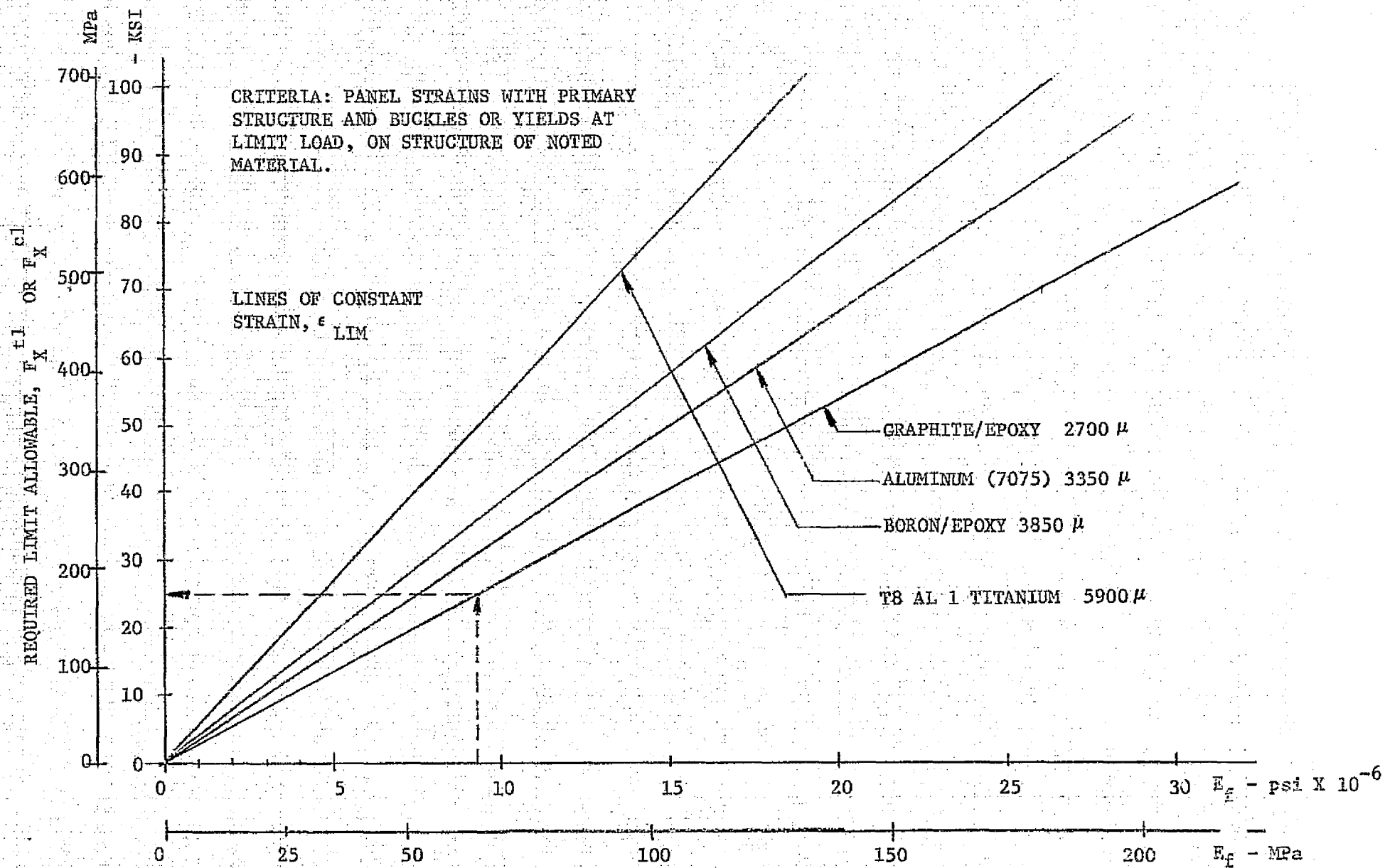


Figure 62. Required LFC Panel Limit Strains and Strengths



TABLE XI  
YIELD STRAIN DATA - DYNAPORE MONOLAYER

MESH	STRAIN AT YIELD	E <sub>secant</sub> YIELD X 10 <sup>-6</sup> psi (GPa)	YIELD STRENGTH .002 OFFSET KSI (MPa)	STRAIN AT FAILURE
24 X 110				
• WARP	5,560	(18.75) 2.72	(109.1) 15.1	63,000
• FILL	5,910	(29.65) 4.30	(175.1) 25.4	11,000
50 X 250				
• WARP	4,920	(24.06) 3.49	(118.6) 17.2	10,000
• FILL	5,270	(35.09) 5.09	(184.8) 26.8	25,000

## THERMAL STRAIN ANALYSIS

The above strength/strain criterion (Figure 62 ) presumes no pre-stress due to thermal strains present in dissimilar materials. A limited thermal strain assessment of dissimilar materials combinations for LFC panels and primary structures was conducted. The analysis used the method of one-dimensional bars of differing thermal expansion coefficients, cross-sectional areas and stiffnesses. For a given temperature change, the load necessary to bring each bar to the same length, as though they were intimately bonded together, is translated into interface load and bar internal stresses (or strains). If neither material yielded or failed over the temperature range ( $410^{\circ}\text{F}$  in the case of materials bonded at  $350^{\circ}\text{F}$  and taken to  $-60^{\circ}\text{F}$ ), the remaining strain capability of the material combination is examined for taking loads. This is necessarily a complex problem, and the following results should be viewed as indicating feasibility trends, pending further analyses utilizing the more accurate 2-dimensional thermal analysis procedures.

Table XII indicates many materials combinations are feasible if non-load bearing LFC panels are assumed. The problem there is to fabricate panels of dissimilar materials without warpage and fasten them to structure in such a manner that they do not pick up airframe loads other than normal pressures and maintenance loads. As mentioned earlier, however, the analytic feasibility of non-load-bearing LFC panels of reasonably large size is brought into question by the necessity for provision of large differential movements (typically  $\pm 1/8$  inch) at panel joints. This exceeds the capability of oversize holes and standard fastenings to adapt, so that load-sharing may prove to be the only reasonable alternative.

The latter portion of Table XII indicates certain materials combinations adaptable to loaded LFC panels. Specific and representative area ratios of LFC surface to LFC panel or of LFC panel to primary structure were examined. These areas were for a spanwise inch strip at a station of the wing designed to a load level of 22,000 lb/inch.

Design directions for load-shared panels by the thermal strain study are as follows:

TABLE 1

## THERMAL STRAIN COMPATIBILITIES OF DISSIMILAR MATERIALS (1)

			MATERIALS COMBINATIONS			ANALYTIC FEASIBILITY (2)	COMMENT
			LFC SURFACE	PANEL STIFFENING	PRIMARY STRUCTURE		
NON-LOAD BEARING PANELS (3)	Ti		Kv/E, Gr <sub>s</sub> /E	ANY	YES	-----	
	316L Dynapore		Kv/E, Gr <sub>s</sub> /E, Ti, Al.	ANY	YES	° Marginal feasibility on Kv&Gr. Need low temp. $\sigma$ , $\epsilon$ data or stress relieving after bonding. Area ratio limitation.	
	17-7 Dynapore		Gr <sub>s</sub> /E, Kv/E, Al	ANY	YES	° Need confirmation data.	
	Kv/E		Kv/E	ANY	YES	° Added surface protection needed.	
LOADED OR LOAD - SHARED PANELS	Ti		Kv/E, Gr/E	Gr <sub>s</sub> /E	YES	-----	
	Kv/E		Kv/E	Gr <sub>s</sub> /E	YES	-----	
	Kv/E		Kv/E	Al	MARGINAL	° Feasible if E, $\epsilon$ (allow) & area ratios O.K.	
	Dynapore	316L	316L	Ti	NO	° Dyna. won't strain as far as necessary at -60°F.	
		316L or 17-7	316L or 17-7	B/E	NO	° Dyna. strain limitation.	
		316L	316L	Al	MARGINAL	° 50 x 250 is a little too stiff. 24 x 110 is just adequate.	
		316L, ± 45°	316L, (4) ± 45°	Al	-	° Need data for investigation.	

- CONTINUED -

TABLE 1

	MATERIALS COMBINATIONS			ANALYTIC FEASIBILITY (2)	COMMENT
	LFC SURFACE	PANEL STIFFENING	PRIMARY STRUCTURE		
LOADED OR LOAD BEARING PANELS	Dynapore	17-7	A1	YES	° 17-7 must be 50% stronger but no stiffer than 316L.
		316L	Gr <sub>s</sub> /E	NO	° Panel bonded at 350°F.
		17-7	Gr <sub>s</sub> /E	YES	° Panel bonded at 350°F. Need confirmation data or stress relief technique after bonding.
		17-7	Gr <sub>s</sub> /E	YES	° Marginally feasible if E <sub>gr</sub> =10M
		17-7	Gr <sub>s</sub> /E	YES	° E <sub>gr</sub> = 13M, modulus of primary structure is significant.

NOTES: (1) Combinations not investigated are not listed.

(2) Feasibility: For unloaded panels, bond at 350°F, cool to -60°F without yield of surface,

For loaded panels,  $\Delta T = 160^\circ\text{F}$  unless specified otherwise.

(3) See comment in text regarding attachment feasibility.

(4)  $\pm 45^\circ$  refers to warp/fill orientation to span.

- Titanium perforated (or slotted) surface on a Kevlar panel directly tied to a graphite composite structure
- Kevlar porous or perforated panels on a graphite/epoxy or aluminum structure. In the case of Kevlar on aluminum, care in choosing structural area ratios must be exercised and the Kevlar panel stiffness kept below  $4 \times 10^6$  psi.
- 316L all-Dynapore panels are represented as marginal with aluminum structure, however a change to 17-7 steel Dynapore theoretically offers 50 percent greater strength, enough to more than overcome the increased thermal differential between 17-7 and aluminum.
- 17-7 steel Dynapore on graphite/epoxy primary structure is indicated feasible because of the reduced 17-7/graphite thermal differential, and, interestingly enough, the feasibility is enhanced if the graphite wing stiffness exceeds that of an aluminum wing.

#### PERFORATED PANEL STRESS CONCENTRATIONS

Open hole stress concentrations are, fortunately, less than those experienced at loaded holes (holes in which bolt bearing loads are transferred). Further, the theoretical stress concentration factor of 3.0 for an open hole in isotropic sheet holds for multiple holes spaced farther apart than 5 times the diameter. 5d represents a sheet 3.14 percent open - which is greater porosity than target porosities indicated from this program, therefore there should not be stress concentration penalties greater than 3 for LFC perforated surfaces. This should be significantly reduced for those woven constructions where material is not interrupted or where fiber directions may be aligned with the hole array geometry. Testing to ascertain stress concentration values is recommended.

#### COST AND WEIGHT COMPARISON

Table XIII shows present Kevlar Doweave raw material costs (1976 dollars) and unit weights compared with fabricated Dynapore Monolayer sheet on an equal area, equal airflow, and relatively small quantity basis. Doweave costs do not include labor to fabricate the 2 X 4 foot panels. Hand layup and vacuum bag curing would be additive cost for Doweave as would the additional surface treatment necessary for equivalent environmental resistance and smoothness. The Dynapore, of course, would also incur additional labor costs required to form it and join it into stiffened panels. At present, it would appear on this very

ORIGINAL PAGE IS  
OF POOR QUALITY

TABLE XIII

RELATIVE COSTS AND WEIGHTS - KEVLAR DOWEAVE VERSUS 316L DYNAPORE

BASIS: 2-BY 4-FT (0.61M x 1.22M) FLAT PANELS, 1976 DOLLARS, EQUAL AIRFLOW  
PREIMPREGNATED FABRIC (1700 YARD [1554M] /ROLL QUANTITIES)

LAMINATE (RAW MATERIAL ONLY)		COST/100 PIECES				COST/1000 PIECES					
		BY AREA		BY WEIGHT		BY AREA		BY WEIGHT		FINISHED WEIGHT	
NO. PLIES	DOWEAVE DENIER	\$/FT <sup>2</sup>	\$/M <sup>2</sup>	\$/LB	\$/KG	\$/FT <sup>2</sup>	\$/M <sup>2</sup>	\$/FT <sup>2</sup>	\$/KG	LB/FT <sup>2</sup>	KG/M <sup>2</sup>
14	200	11.47 <sup>(1)</sup>	(123.46) <sup>(1)</sup>	41.56 <sup>(1)</sup>	(91.62) <sup>(1)</sup>	11.47	(123.46)	41.56	(91.62)	0.418 <sup>(3)</sup>	(2.041) <sup>(3)</sup>
8	500	7.63 <sup>(1)</sup>	( 82.13) <sup>(1)</sup>	27.65 <sup>(1)</sup>	(60.96) <sup>(1)</sup>	7.63	( 82.13)	27.65	(60.96)	0.418 <sup>(3)</sup>	(2.041) <sup>(3)</sup>
DYNAPORE MONOLAYER <sup>(2)</sup>		100 PIECES (FABRICATED)				1000 PIECES (FABRICATED)					
50 BY 250		9.60	(106.56)	43.64	(96.21)	6.62	(71.26)	30.09	(66.34)	0.22 (REF)	(1.074) (REF)
24 BY 110		10.52	(113.24)	20.23	(44.60)	7.32	(79.79)	14.08	(31.04)	0.52 (REF)	(2.539) (REF)

NOTES: (1) DOWEAVE COST DOES NOT INCLUDE LAYUP LABOR, UTILIZATION FACTOR, G&A, OVERHEAD, OR PROFIT.

(2) ESTIMATED BY MICHIGAN DYNAMICS FOR ENGINEERING PURPOSES ONLY.

(3) DOWEAVE LAMINATE WEIGHT INCLUDES NO. 21 MICROPERFORATED PLATE SURFACE AT 0.116 PSF (0.556 KG/M<sup>2</sup>)



preliminary analyses, the Dynapore has a cost/weight advantage.

Future developmental efforts to increase the strength of Dynapore at the expense of pressure drop could remove a present cost advantage. Options also exist to reduce Doweave laminate cost and weight for equal airflow, such as insertion of a thin choker ply in a laminate of fewer plies. A high quantity production basis would produce much lower materials costs for both materials. Both materials are available today. Relative lead times for procurement favor the Dynapore since availability of Doweave triaxial weaving machinery is limited at present.

This cost comparison should be an on-going effort extended to fully designed panels in future studies.

#### PRELIMINARY DESIGN SKETCHES

In accordance with panel design directions suggested in previous sections, three conceptual designs for integrated LFC panel/wing cover structure are portrayed in Figures 63, 64 and 65. All three are conceived for graphite/epoxy composite primary structure, although the same general geometries could be accomplished for an aluminum wing. These figures illustrate the nature of the LFC panel/structure design integration problem.

Figure 63, a porous sandwich LFC panel on a blade-stiffened wing cover, was sized for an area of the wing upper surface with a load level of roughly 20,000 pounds/inch. Sandwich depth is 1/4-inch and the minimum depth for attaching the panel to chordwise standoffs is used for collection duct space, approximately 3/8-inch. Penetration of the wing cover with multiple fasteners is thus avoided. The unsymmetric LFC sandwich panel is attached to strain with the wing without buckling until above limit load. Panel deflections due to unsymmetrical loading should not be large, but would be calculated if aerodynamic waviness tolerance is found to be restrictive. It is recognized that the integrated collection ducting would not be as efficient as the structure shows in this arrangement.

Another arrangement, Figure 64, seeks both structural efficiency and surface air collection efficiency. To do this, spanwise stringers are turned upside

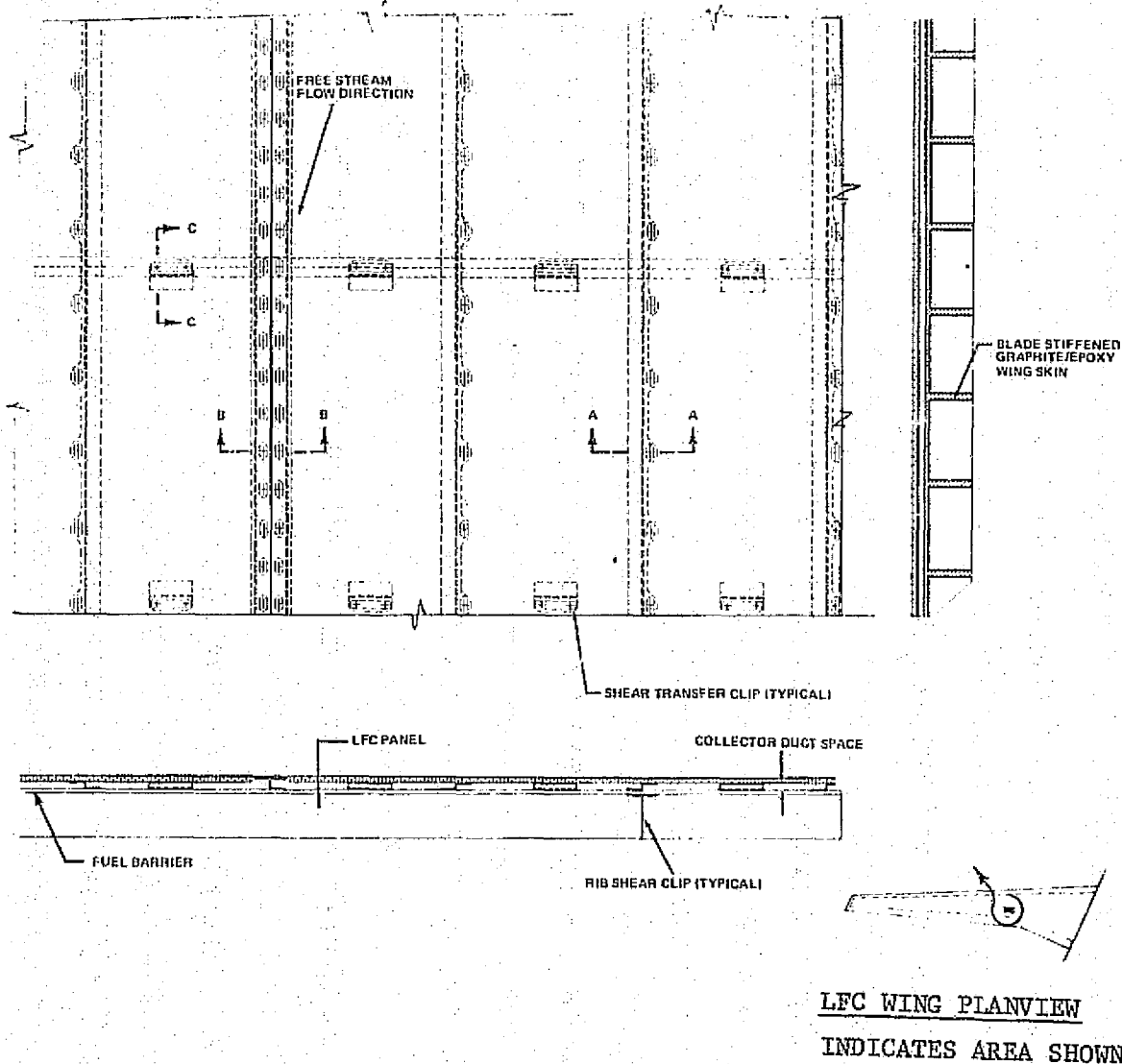
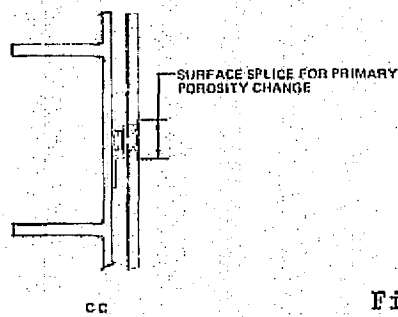
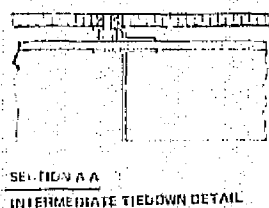
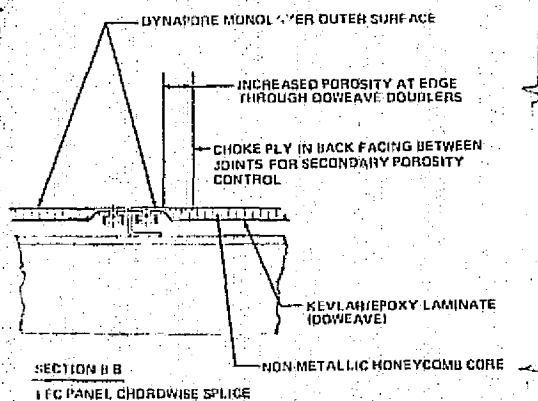
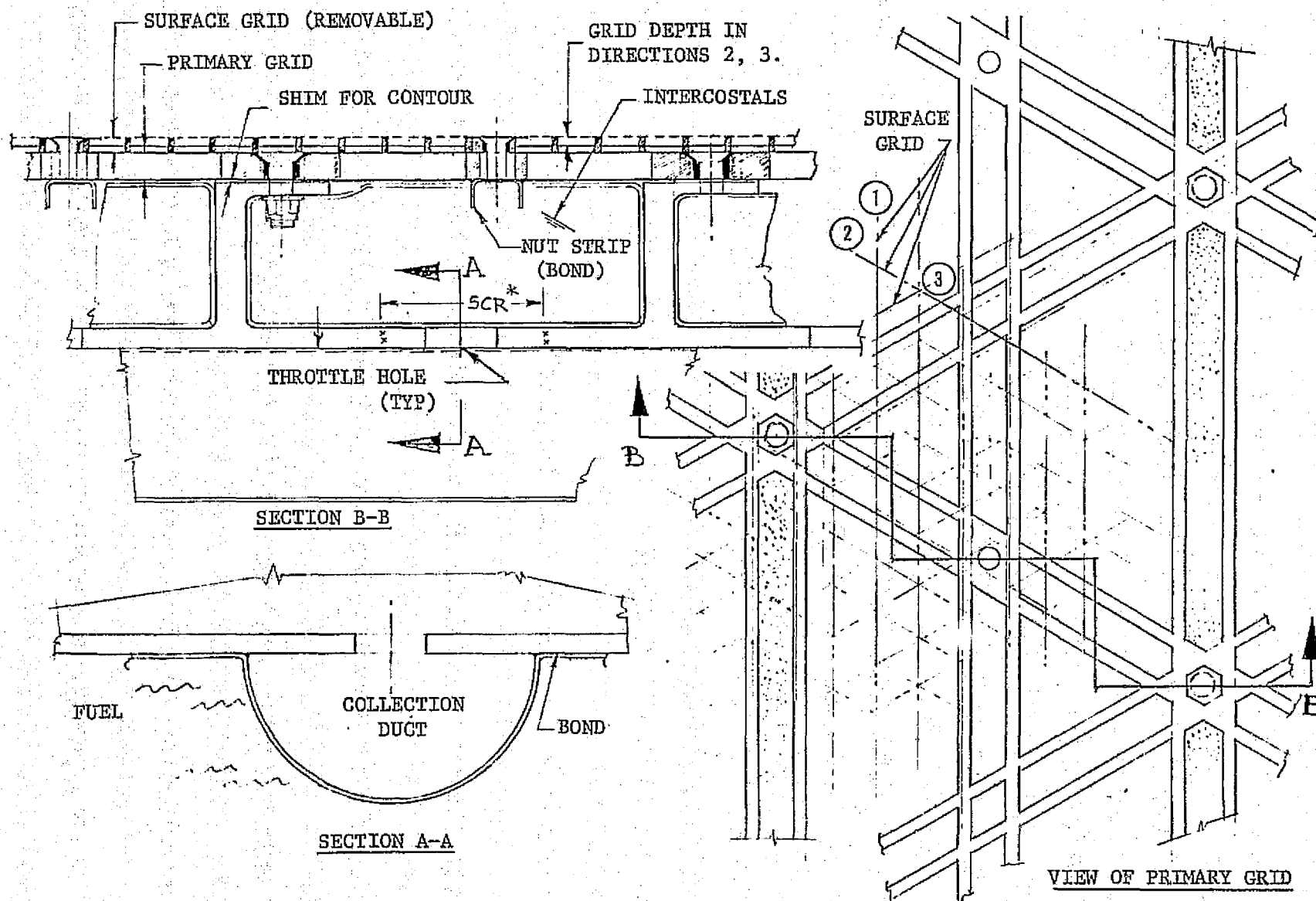


Figure 63. Sandwich LFC Panel on Blade-Stiffened Wing Cover

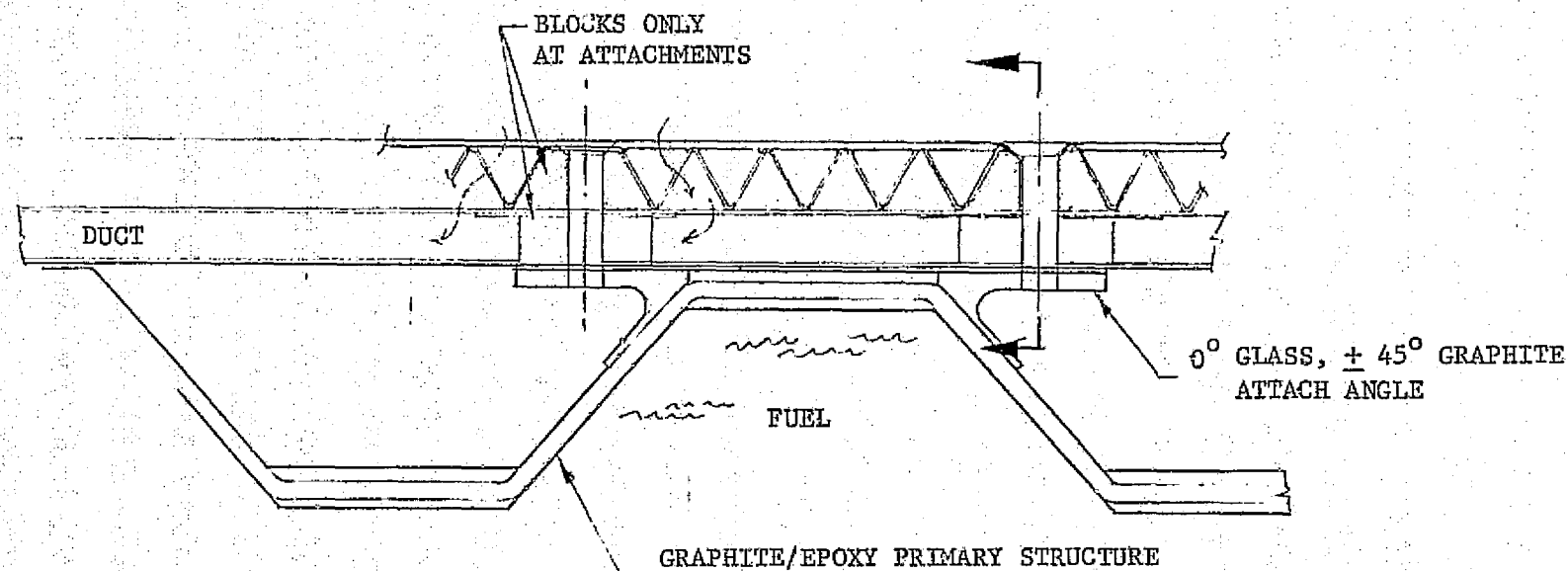


\*SCR - STRESS CONCENTRATION RELIEF AT HOLES

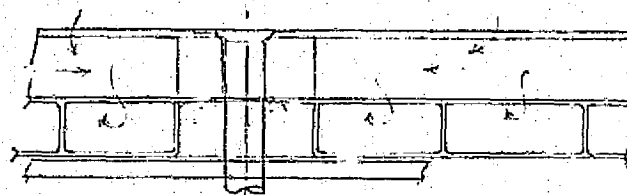
Figure 64. Skin and Stringer with Double Grid Concept

down to provide plenum space under a double grid. The outer grid, similar to that produced in this program, is close-spaced to support a thin Dynapore porous facing. It is removable for inspection and servicing of structure underneath. The primary structural grid is permanently attached to the spanwise stringers. The collected air is drawn entirely through the structure to chordwise collection passages formed by a continuous molded and sealed sheet that also acts as a fuel barrier.

In the arrangement of Figure 65, the air is conducted chordwise by a double sandwich LFC panel, the outer layer of which is a porous truss-core, such as explored in this program. Flow metering would occur through the middle sheet of this double sandwich panel. It is tempting to consider the spanwise spaces of the corrugated wing cover as distributed collection ducts, if spanwise collection can be realized in a practical manner.



- DUCT LAYER CONTRIBUTES TO EI, GJ STIFFNESS
- STRUCTURE INSPECTABLE AND ACCESSABLE
- MAXIMIZES FUEL VOLUME



SECTION SHOWING INNER LAYER COLLECTION DUCTING

Figure 65. Double Sandwich Panel on Corrugated Primary Structure

# 1

## REFERENCES

1. Douglas Aircraft Company, "Conceptual Design Studies of Composite AMST". Report AFML-TR-74-164, October 1974.
2. Douglas Aircraft Company, "TRAD Interim Report Manufacturing Techniques for Composites". MDC Report J6924/01, January 1975.
3. Ergun, Sabri, "Fluid Flow Through Packed Columns". Chemical Engineering Progress, Volume 48, No. 2, February 1952.
4. Armour, James C. and Cannon, Joseph N., "Fluid Flow Through Woven Screens". AIChE Journal, Volume 14, No. 3, May 1968.
5. Air Force Materials Laboratory, "AFML Aerospace Structural Metals Handbook". Volume I, AFML-TR-68-115, 1975 Publication. 316L Steel Wire Data in Code 1307, Pages 6 and 7.
6. Nenni, J.P., and Glynas, G. L., "Aerodynamic Design and Analysis of an LFC Surface", Astronautics and Aeronautics, Pages 52-55, July 1966.

PRECEDING PAGE BLANK NOT FILMED



## Appendix A

### AIRFLOW TEST APPARATUS

The airflow tests were conducted on the Douglas Flow Resistance Test Rig. This apparatus had been previously developed and utilized for quality control monitoring of pressure drop characteristics of porous sheet materials used for engine inlet duct acoustic treatment. At the time the present program started, this equipment had been idle and was available full time for these tests. The apparatus was well suited for the present application and required no modification except for the addition of another flow meter and supply line to accommodate lower flow rates for some of the specimens.

Photographs of the test rig are presented in Figures A-1 and A-2 showing front and rear views of the apparatus. All controls and data readout equipment are situated on the rear panel as shown in Figure A-2. A schematic diagram of the apparatus is shown in Figure A-3.

The air supply comes from the plant compressed air system, delivered at a pressure of about 100 pounds per square inch. The air is passed through a moisture trap to remove large suspended water and oil droplets. The air is further treated with a five micron filter and passed through a pressure regulator. The air supply line branches into separate parallel circuits for each of the two flow meters. A third, high capacity, flow meter and supply circuit was left installed in the apparatus, but was not used in the present series of tests. Each supply circuit incorporates parallel coarse and fine control valves.

Thermocouple temperature sensors are installed in each supply line downstream of the control valves. The thermocouple leads are connected, through a rotary switch, to a D.C. galvanometer type readout device.

The flow meters utilized in the apparatus are laminar flow type meters manufactured by the Merriam Instrument Company. These are differential pressure devices that utilize a matrix of capillary channels through which the metered flow is directed. The result is a nearly linear relationship between differential pressure and the volumetric flow rate. This depends on the fact that, within the range of the instrument, the Reynolds number within each capillary channel



Figure A-1. Douglas Flow Resistance Test Rig - Front View

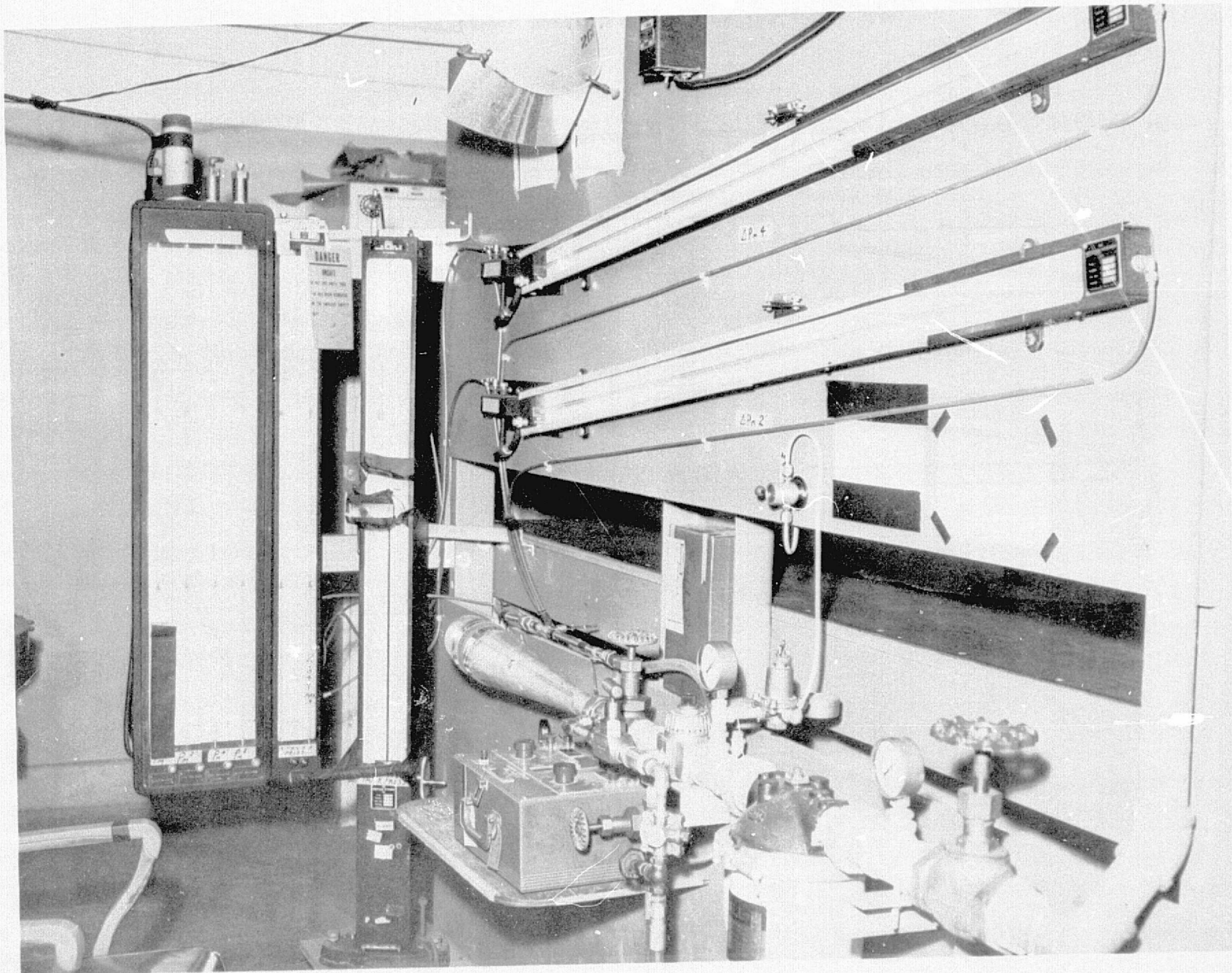


Figure A-2. Douglas Flow Resistance Test Rig - Rear View



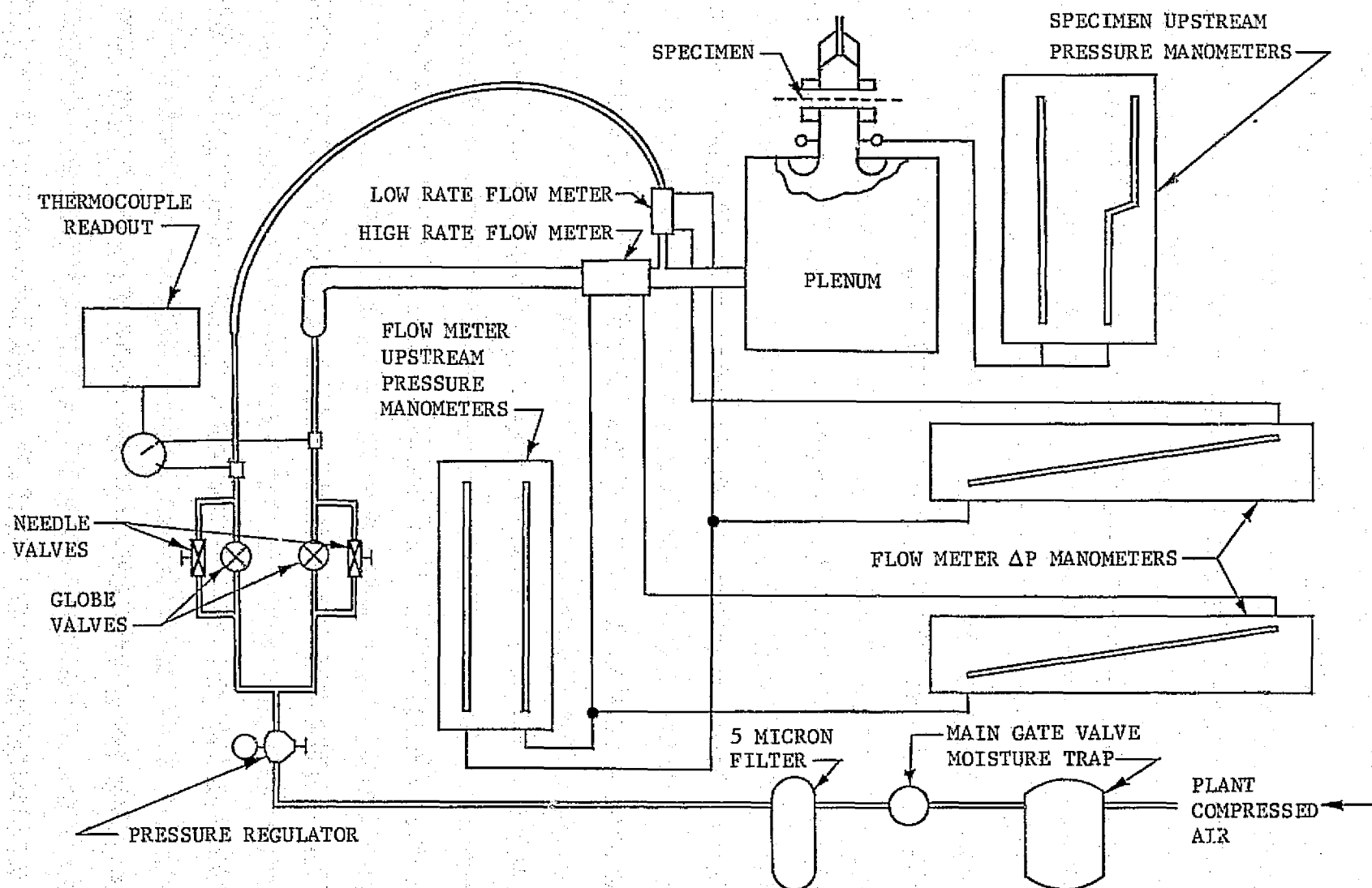


Figure A-3. Schematic Diagram of Airflow Test Apparatus

is so low that the so-called Hagen-Poiseuille equation of laminar flow pertains which holds that the pressure drop depends only on the product of velocity times the viscosity. The result is a flow metering device that produces a differential pressure that is almost linearly proportional to the volumetric flow rate, independent of pressure, and only weakly dependent on temperature. Because of the near linearity, the device maintains nearly constant sensitivity over the entire range, unlike orifice flow meters which depend on velocity squared.

The particular flow meters used, designated respectively low rate and high rate, are Merriam Model Numbers 50 MJ10 and 50 MW20-2. The low rate flow meter has a maximum flow capability of 1.5 cubic feet per minute, while the high rate meter will accommodate a maximum of 40 cubic feet per minute. The low rate meter is installed with one-half inch pipe fittings, and the high rate is installed with two-inch pipe fittings.

Both flow meters develop a maximum differential pressure of eight inches of water. The differential pressure for each flow meter is read on a Merriam inclined water manometer with a full scale reading of eight inches. The manometer scale graduations are 0.01 inch increments.

The flow meters are supplied with calibration curves of Actual Cubic Feet per Minute (ACFM) versus differential pressure at a temperature of 70°F. To determine the ACFM flow rate at the test condition, the calibration reading must be multiplied by a viscosity correction factor. To determine the mass flow rate, given in Standard Cubic Feet per Minute (SCFM), the volumetric flow rate, ACFM, must be multiplied by a density correction factor. Details of these correction factors are provided in Appendix C of the report.

After passing through either one of the flow meters, the air enters a cylindrical plenum tank having dimensions five feet in diameter and five feet long. The outlet duct is situated in the center of the top plate of the tank. The outlet duct diameter is 3.93 inches (0.10 m). A bell-mouth fairing is located tangent to the outlet to prevent separation from the corner. Static pressure taps surrounding the outlet duct are manifolded to a piezometer ring which is connected to manometers measuring the specimen upstream pressure. A flange

at the end of the outlet duct mounts a two-inch wide annular seal made from closed cell foam rubber on which the test specimen rests. A mating annular seal is clamped tightly onto the specimen from above with a pneumatic power cylinder. The air flows directly to ambient pressure.

The manometers used to measure the specimen upstream pressure consist of a conventional 30 inch vertical water manometer, reading in increments of 0.1 inches, and a null-reading micro-manometer, capable of indicating increments of 0.001 inches of water. The micro-manometer is used at low specimen upstream pressures, usually less than five inches of water, while the vertical manometer is used at higher pressures.

All data reading are manually recorded on paper. The flow meter upstream pressures and the specimen upstream pressure manometers are referenced to ambient pressure. Ambient pressure is read from a mercury barometer situated nearby.



## Appendix B

### AIRFLOW TEST PROCEDURE

Prior to each specimen test, all the manometers are checked and adjusted for zero reading. The specimen is checked for cleanliness and placed on the outlet duct flange with the exterior surface facing down. The upper sealing ring is then pressed on to the specimen with the pneumatic cylinder.

The independent test parameter is specimen pressure dropped with a nominal range of 1 to 100 pounds per square foot. This amounts to a range of specimen upstream pressure of from about 0.2 to 20 inches of water.

Depending on the material being tested, one or the other flow meter is selected. The test commences at the lowest flow rate by manually adjusting the control valve to an arbitrary flow rate indication until the specimen upstream pressure reaches a value close to the desired level. When all the readings have stabilized, the manometer and thermocouple readings are recorded. The control valve is then manually adjusted to achieve the next test point.

The supply pressure is sufficiently well regulated that no discernable fluctuations are evident during several minutes of operation at any one test point. The temperature is mostly constant and occasionally changes by one or two degrees during the course of a specimen test. The ambient barometric pressure is read every three to four hours.

The time required to conduct one specimen test depends strongly on the properties of the specimen. A high porosity specimen with large flow rates can be tested over the range of pressure with five or six test points in as many minutes. However, a specimen with very low porosity may require over one hour of test time.

It was an unexpected result that at very low flow rates, the time required for the pressure in the plenum to reach an equilibrium value becomes very large.

The situation appears to be analogous to the well known properties of a direct current electrical circuit known as an R-C (for resistance, capacitance) network. In this analogy the tank volume corresponds to the capacitance, the flow rate

to the current and the resistance to the inverse of the porosity of the specimen. The solution of such a network shows that the voltage across the capacitor, which in this case would correspond to the plenum pressure, rises exponentially toward an asymptotic value. The rate at which the current rises is described by a characteristic time constant.

Without performing a solution of the analogy, it appears that for the combination of flow rate and pressure drop of some of the low porosity specimens, the volume of the plenum tank is unnecessarily large. It was not possible to alter the tank for the present series of tests. Therefore the situation was tolerated and allowance made for additional pressure stabilization time. In future test series, however, careful consideration should be given to reducing the effective volume of the tank. This could be accomplished by partially filling the tank with sealed tin cans or ping-pong balls, etc. Such an operation will require that the screen covering the exit duct be removed, however.

Prior to the test program there was some concern about efficiency of the annular foam sealing rings in preventing leakage laterally. Two aspects appeared possible. First, rough surface texture may preclude a sufficiently good seal and leakage may occur between the foam rubber and the specimen. Second, leakage may occur within a specimen. Periodic checks were made during the test program to monitor this problem. The checks were performed by wetting the outside perimeter of the sealing rings with leak detecting solution. This is a soap solution that indicates air leaks by presence of bubbles. No leaks were detected in any of the checks.

During the initial trials with the apparatus, a determination of the pressure drop from the down stream end of each flow meter to the plenum was made. For the flow rate ranges being used, this difference in pressure was always less than about 0.3 inches of water. It was therefore decided to refrain from recording the flow meter upstream pressure as a test parameter and instead calculate it as the sum of the plenum pressure and flow meter  $P$ . This quantity is only used to calculate the density correction for the mass flow rate. An error of 0.3 inches of water, compared to the ambient pressure amounts to an error of 0.07 percent, which is considered negligible.

## Appendix C

### DATA REDUCTION PROCEDURES

The data recorded during the test consist of the following parameters:

Specimen Upstream Pressure,  $P_1$  (inches  $H_2O$ , differential)

Flow Meter Differential Pressure,  $\Delta P_1$ ,  $\Delta P_2$  (inches  $H_2O$ )

Air Flow Temperature,  $T$  (degrees Fahrenheit)

Ambient Pressure,  $P_2$  (inches Hg, absolute)

The flow meter calibration curves are supplied as a function of  $\Delta P$  in inches of water, so the calibration functions are determined to be:

1) Low Rate Flow Meter

$$\Delta P_1 \leq 2 \text{ (in. } H_2O)$$

$$Q_1 = 0.224 \Delta P_1 \text{ (inches } H_2O)$$

$$\Delta P_1 > 2 \text{ (inches } H_2O)$$

$$Q_1 = 0.224 \Delta P_1 \text{ (inches } H_2O) - 0.002139 (\Delta P - 2)^2$$

2) High Rate Flow Meter

$$Q_2 = 5.7386 \Delta P_2 \text{ (inches } H_2O)$$

The remaining data reduction is carried in English units, pound, feet, second,

$^{\circ}R$ , so the raw data is converted to:

$$P_1 \text{ (lb/ft}^2, \text{ abs.)} = 5.197 P_1 \text{ (inches } H_2O) + P_2 \text{ (lb/ft}^2)$$

$$P_2 \text{ (lb/ft}^2, \text{ abs.)} = 70,527 P_2 \text{ (inches Hg)}$$

$$T(^{\circ}R) = T(^{\circ}F) + 459.6$$

The volumetric flow rate is calculated by

$$Q \text{ (ACFM)} = (Q_1 \text{ or } Q_2) \times \frac{\mu}{\mu_o}$$

and the mass flow rate by

$$q \text{ (SCTM)} = Q \text{ (ACFM)} \frac{P_o}{P_a} \frac{T}{T_o}$$

Where

$$\frac{\mu}{\mu_o} = \left( \frac{T}{T_o} \right)^{3/2} \left( \frac{T_o + 216}{T + 216} \right)$$

$$T_o = 529.6^\circ R$$

$$P_o = 2116.2 \text{ (lb/ft}^2\text{)}$$

$$P_a = \text{Flow meter upstream pressure} = P_1 + (\Delta P_1 \text{ or } \Delta P_2) \text{ (lb/ft}^2\text{)}$$

The mass flow rate is presented in this report as the standard velocity  $V_s$ , defined as the mass flow rate per unit area. For the outlet duct diameter of 3.93 inches,

$$A = .08451 \text{ (ft}^2\text{)}$$

$$V_s = \frac{q}{60A} \text{ (ft/sec)}$$

The specimen pressure drop is  $(P_1 - P_2)$

These two quantities are used for the presentation of most of the data. An alternative presentation format is given in terms of the effective porosity,  $\sigma$ , versus unit Reynolds number  $R_e$ . The parameter,  $\sigma$ , is defined as the ratio of mass flow rate,  $q$ , to the ideal flow rate,  $q_i$ , through the outlet duct at the pressure ratio  $P_1/P_2$ .

$$\sigma = q/q_i$$

$$q_i = \frac{60A P_1}{35.01 \sqrt{T}} \frac{M}{(1 + .2M^2)^{3/2}} \text{ (SCFM)}$$

where

$$M = \sqrt{5 \left[ \left( \frac{P_1}{P_2} \right)^{1/3.5} - 1 \right]}$$

The unit Reynolds number,  $R_e$ , is defined with the ideal velocity  $V_i$

$$R_e = \frac{\rho V_i}{\mu} \quad (1/\text{ft})$$

Where

$$V_i = 49 \sqrt{T} \quad M$$

$$\rho = \frac{P_o}{P_1} \frac{T}{T_o} \quad 0.002378 \quad (\text{lb sec}^2/\text{ft}^4)$$

$$\mu = \frac{\mu}{\mu_o} \quad 3.808 (10)^{-7} \quad (\text{lb sec}/\text{ft}^2)$$

## Appendix D

### BASIC AIRFLOW PRESSURE DROP TEST DATA AND PANEL DESCRIPTIONS

Detailed plots of the airflow pressure drop test data are presented in Appendix D, Figures D-1 through D-18. The associated description of the individual panel construction is also included in Table D-I. This detailed information permits the reader to make additional comparisons of the various panels, if such is desired. As stated previously, all of the panels constructed, described in Table D-I, were not airflow tested; those which were obviously too open or too opaque were not included in the test specimens.

Table D-II, D-III and D-IV describe the construction of those panels which were submitted, in compliance with the contract, to NASA Langley for structural testing.

PRECEDING PAGE BLANK NOT FILMED



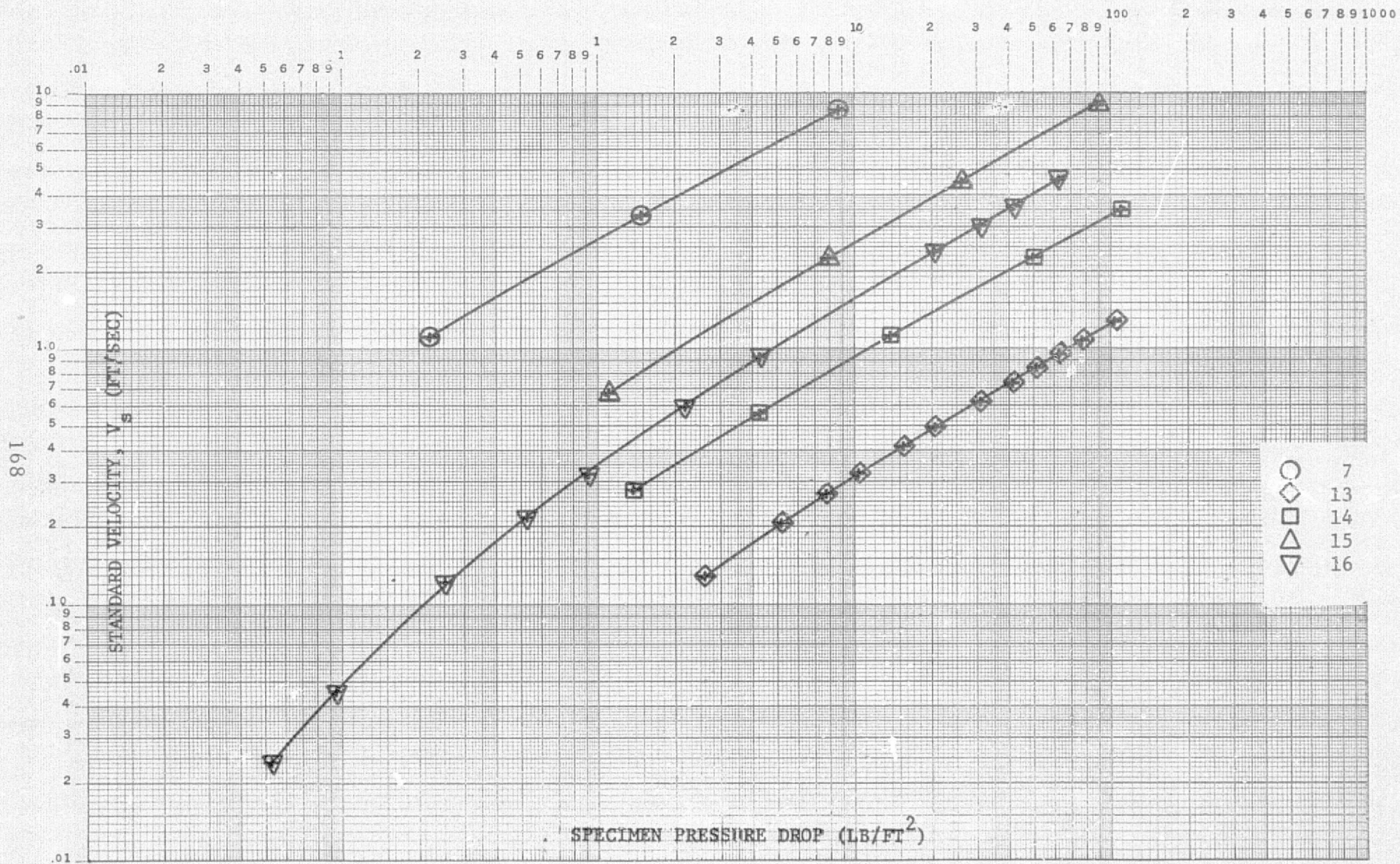


Figure D-1. Airflow Test Results



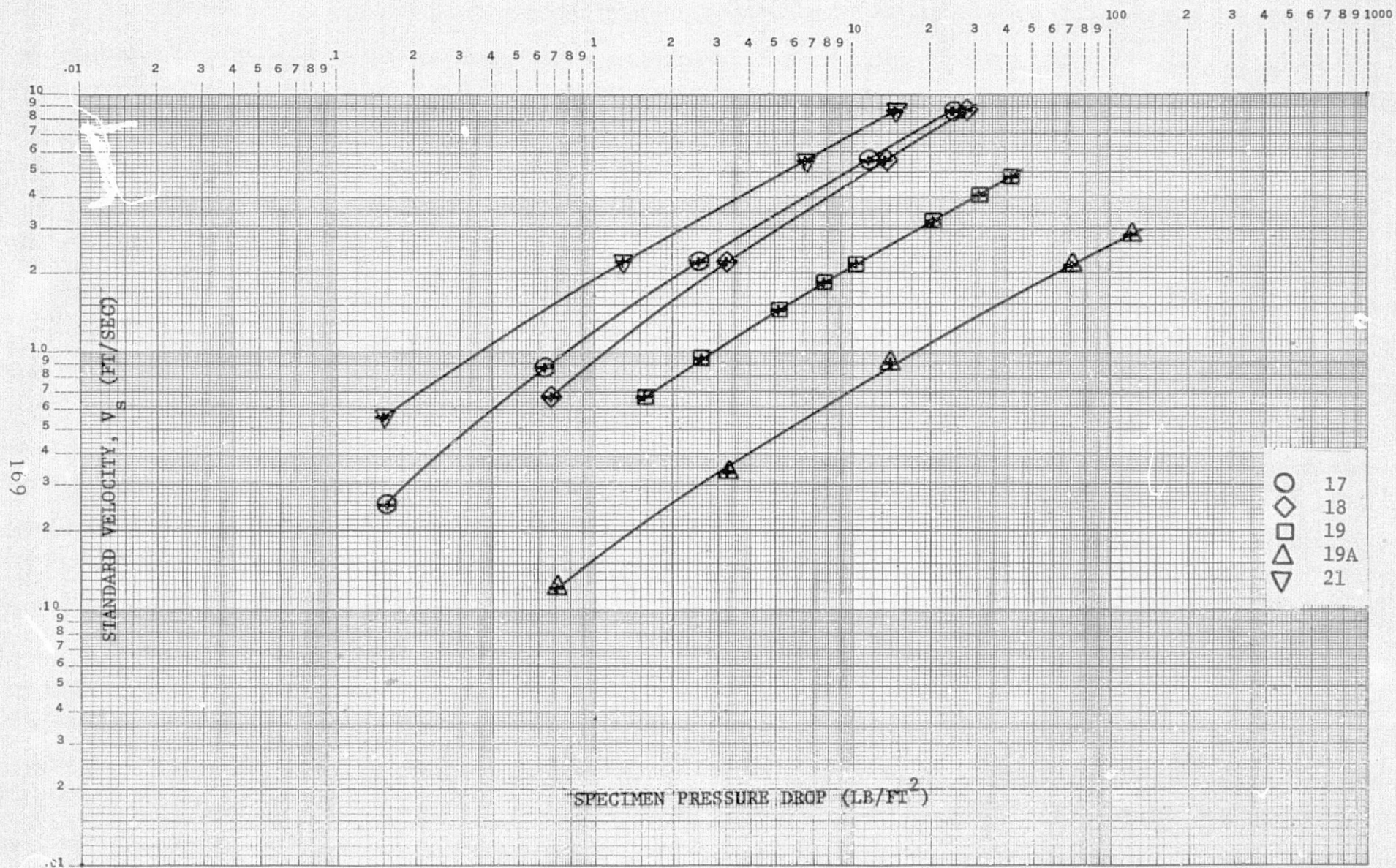


Figure D-2. Airflow Test Results

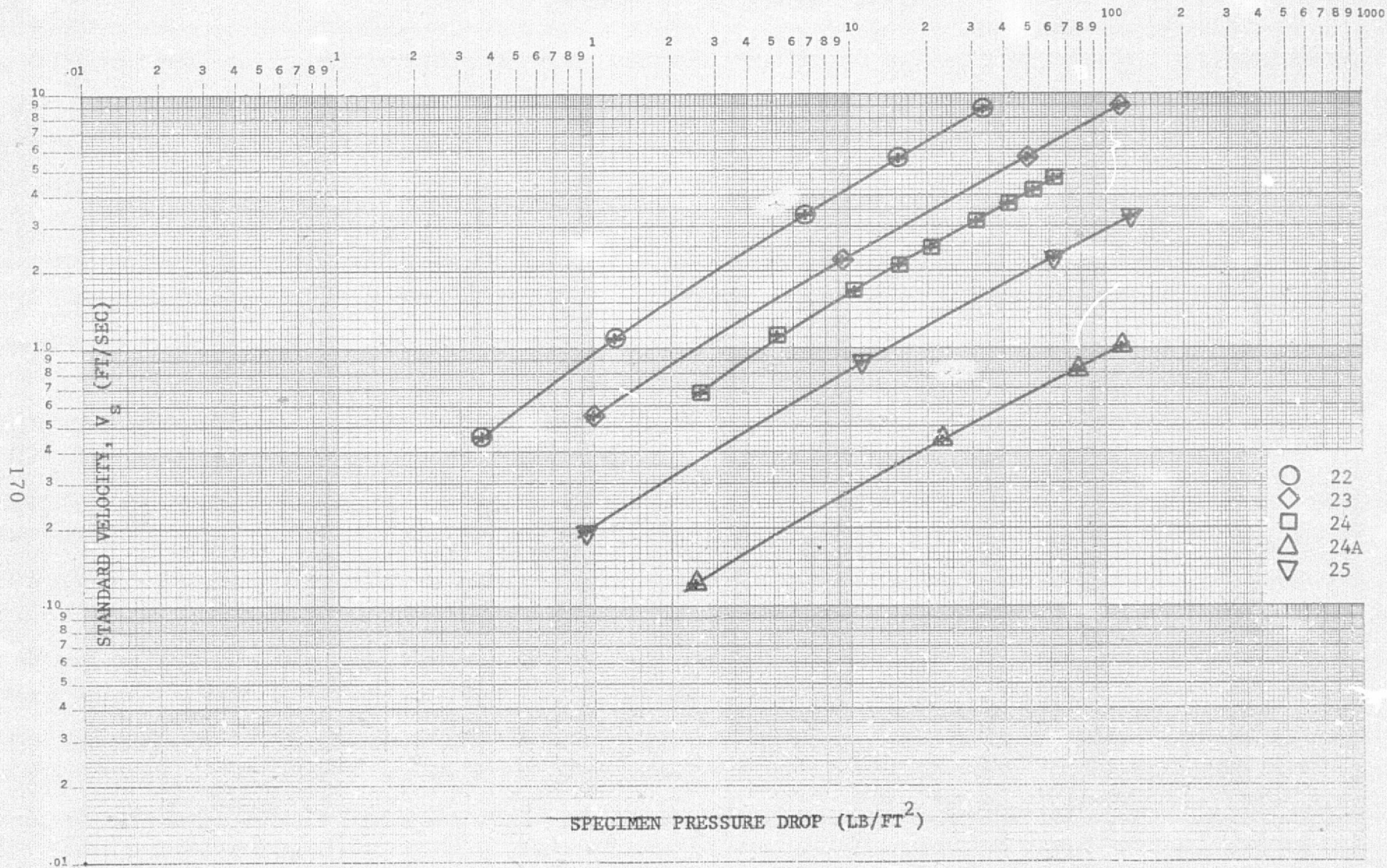


Figure D-3. Airflow Test Results



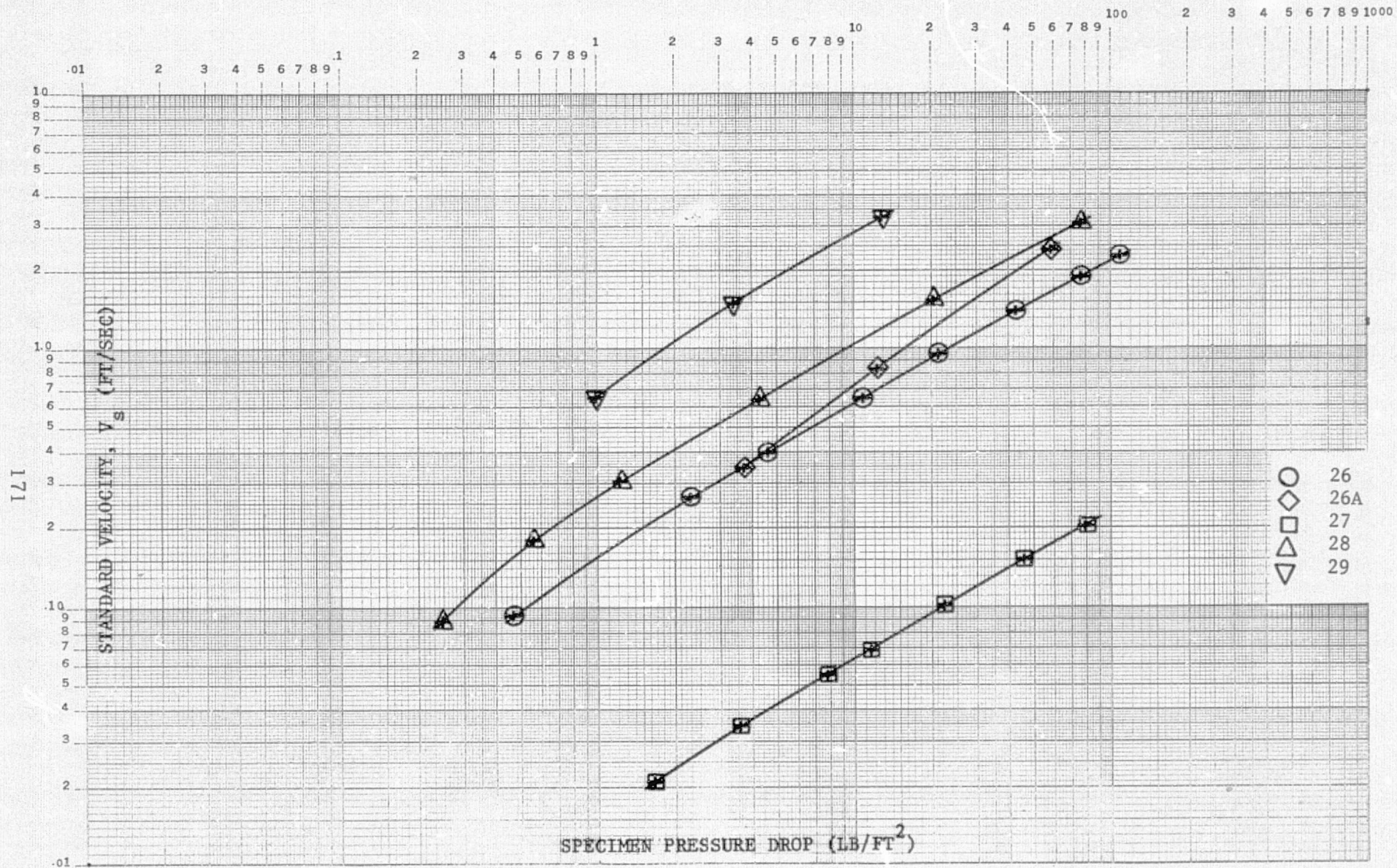


Figure D-4. Airflow Test Results

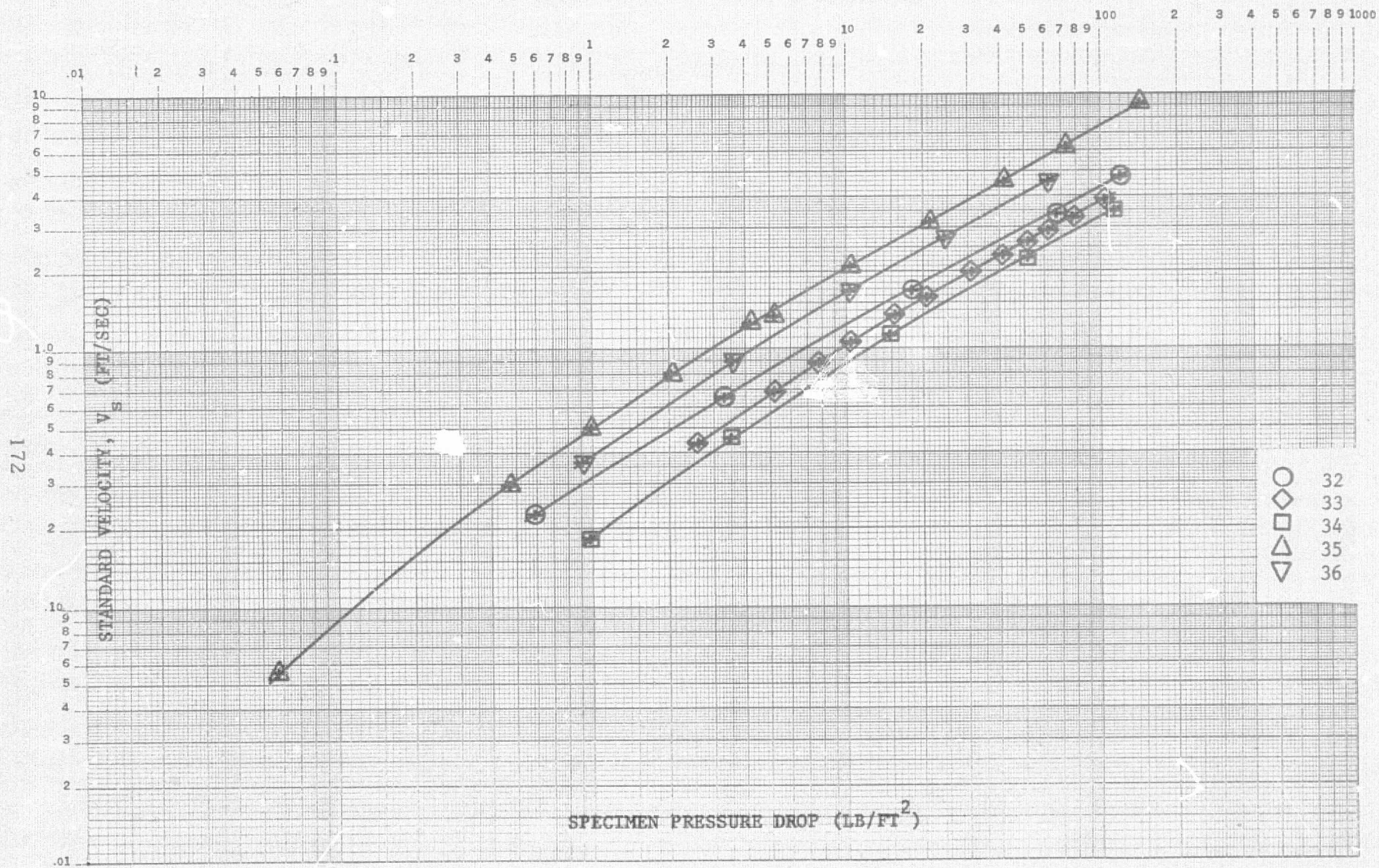


Figure D-5. Airflow Test Results



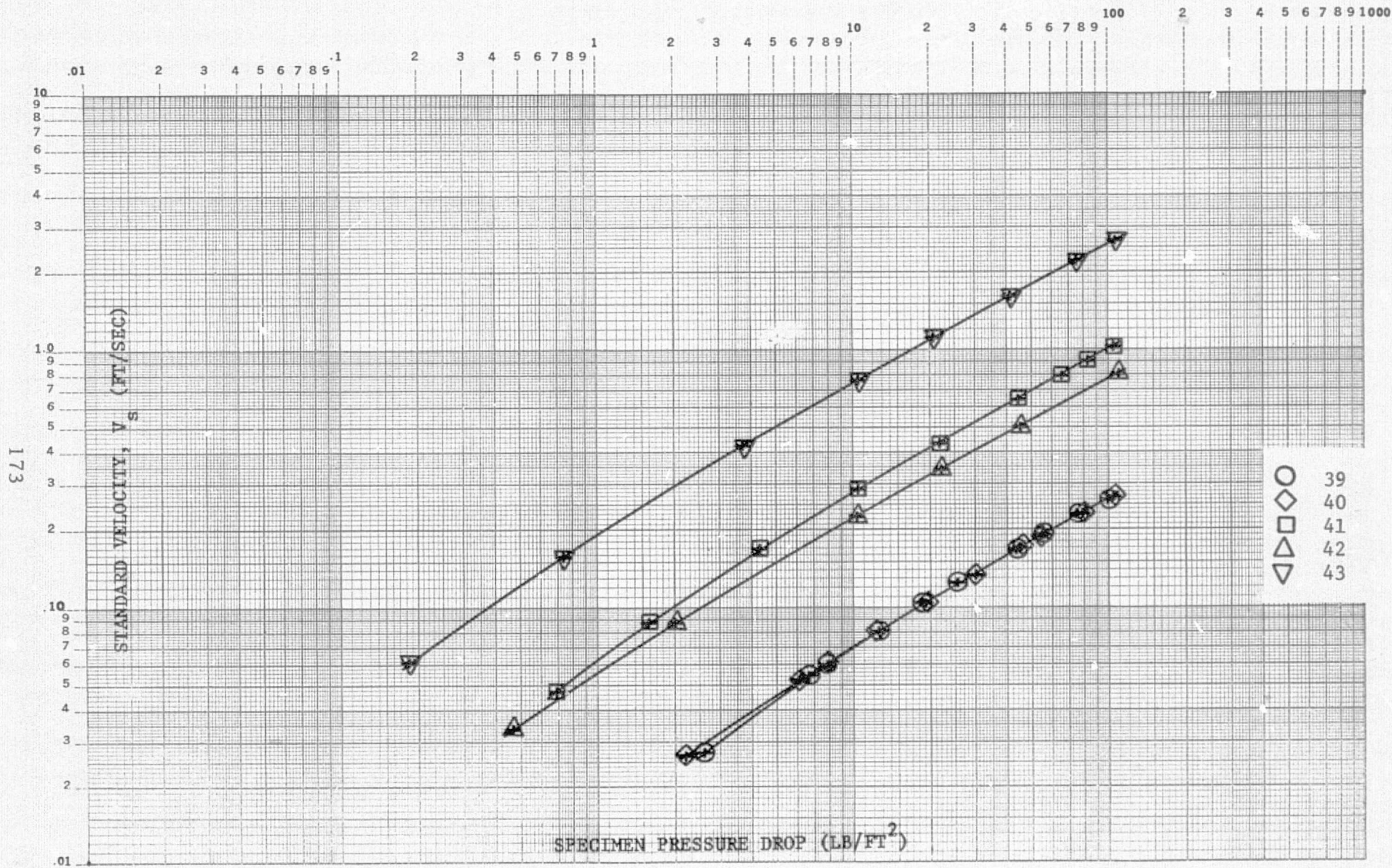


Figure D-6. Airflow Test Results



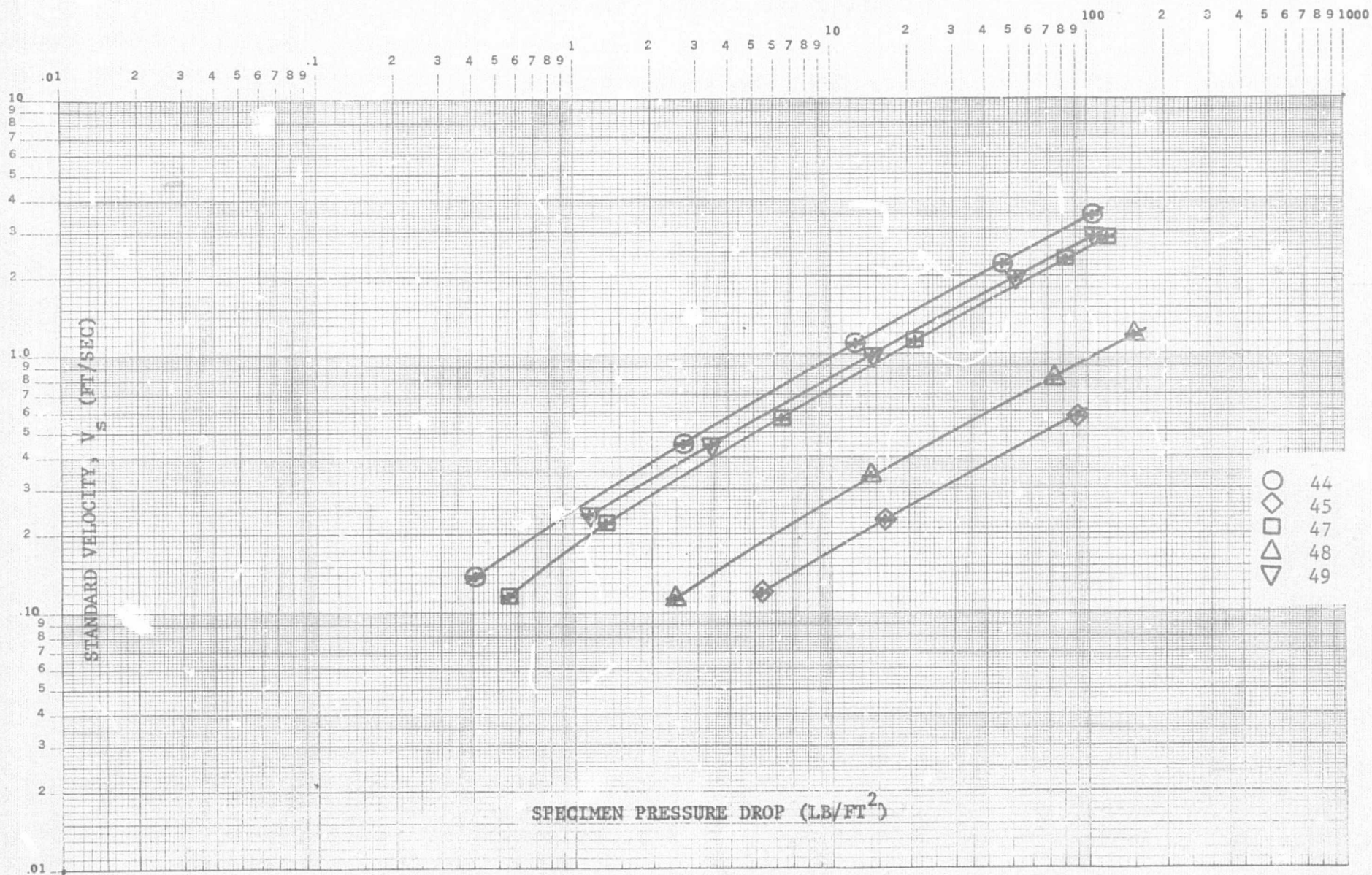


Figure D-7. Airflow Test Results

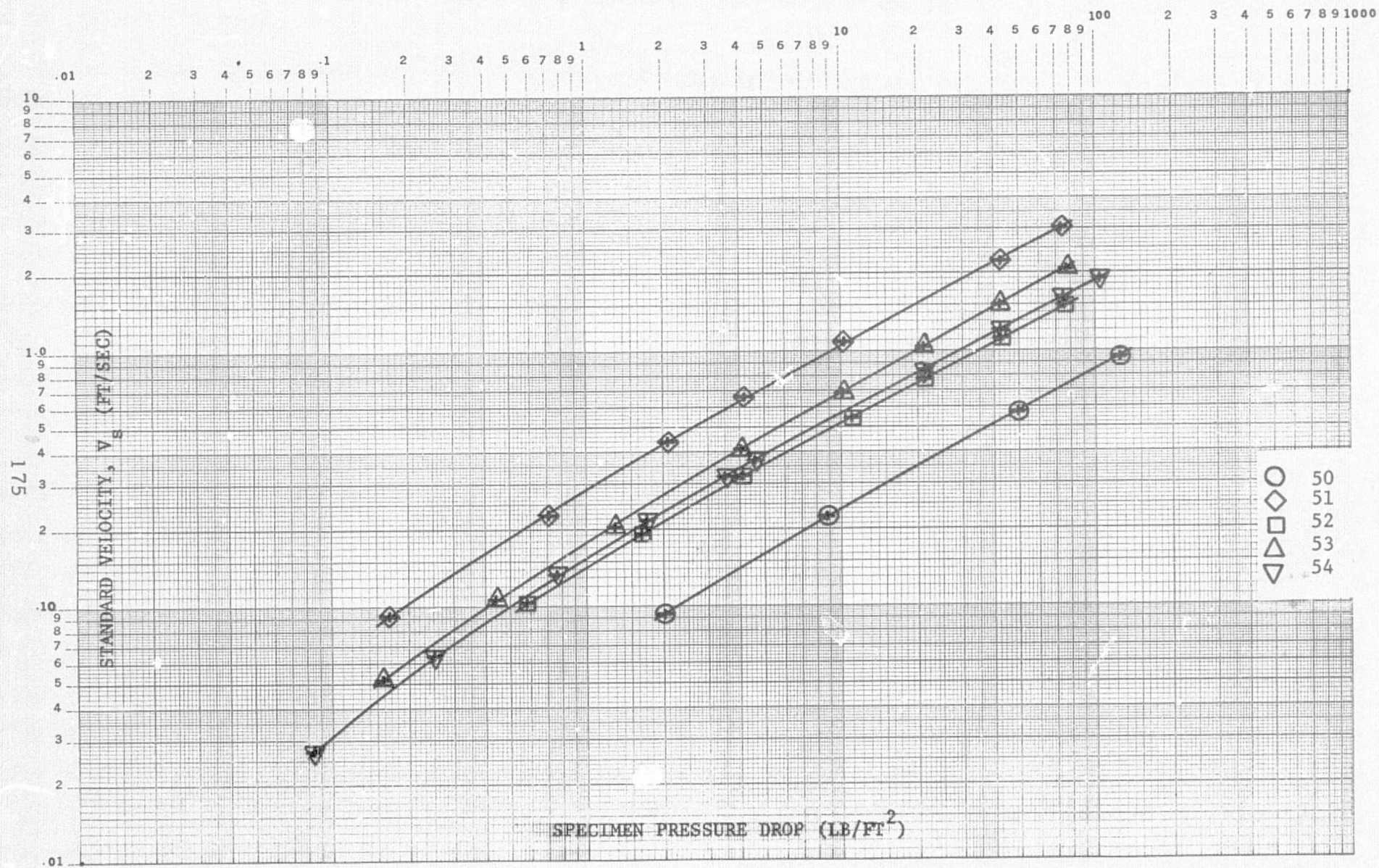


Figure D-8. Airflow Test Results



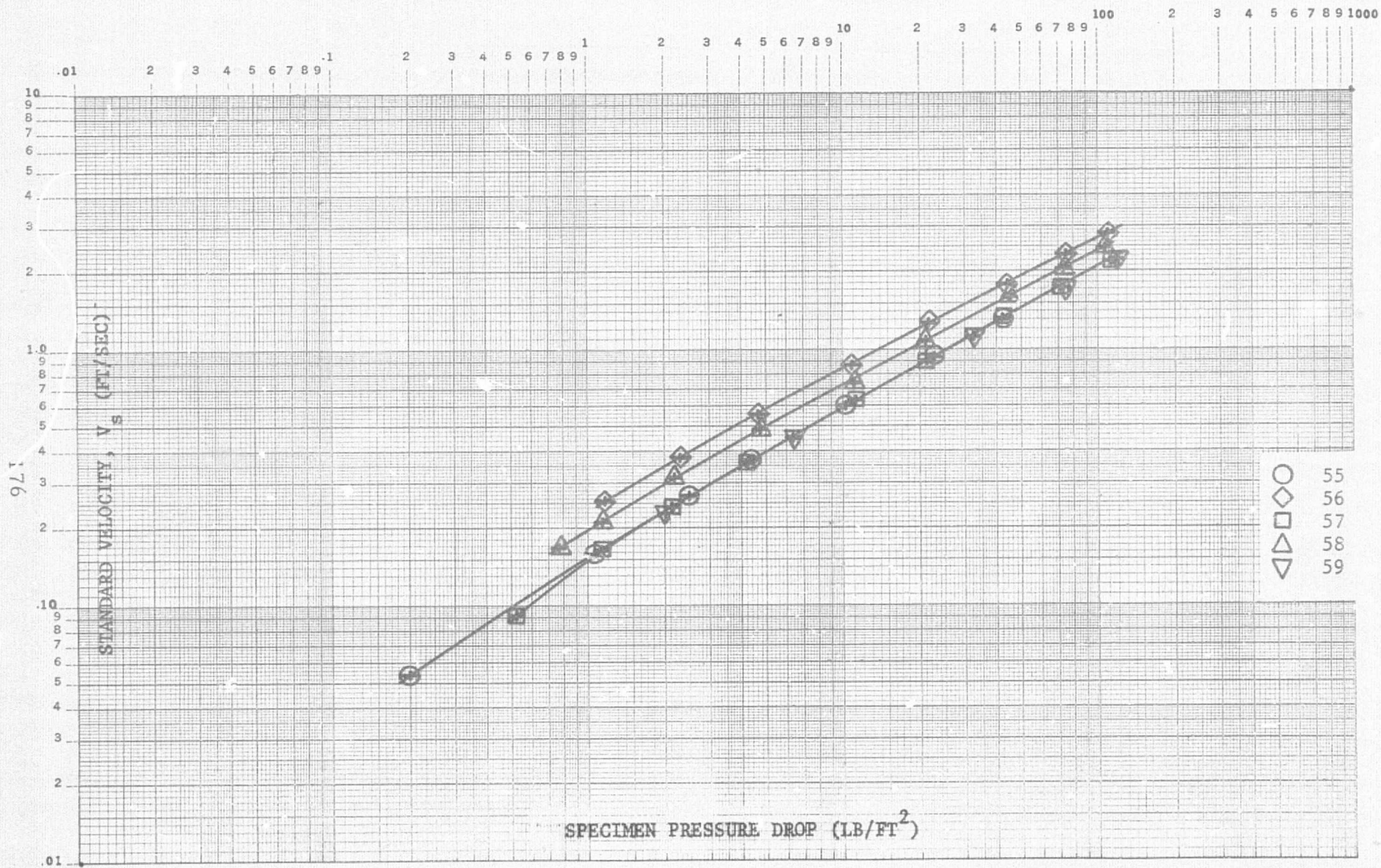


Figure D-9. Airflow Test Results

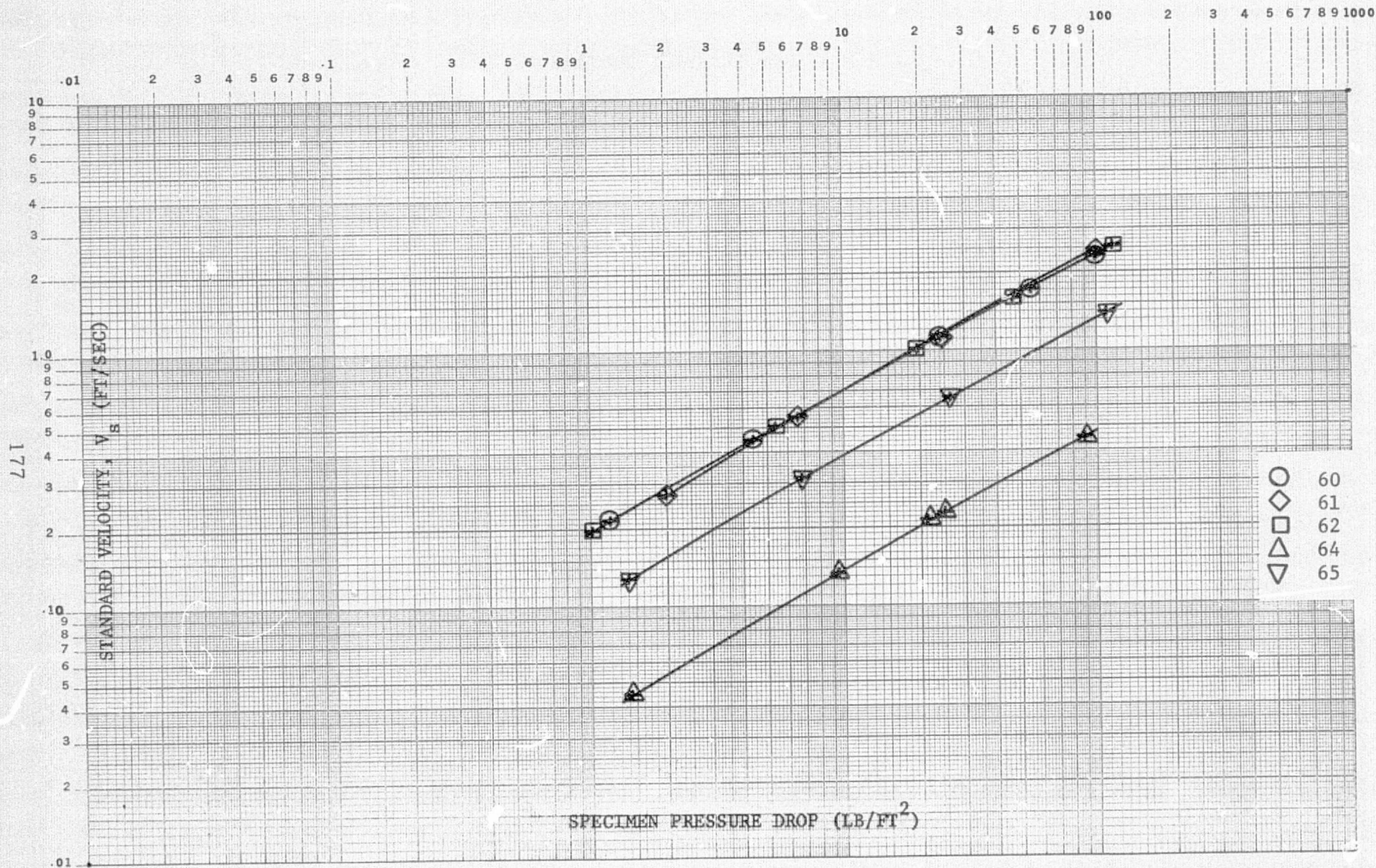


Figure D-10. Airflow Test Results



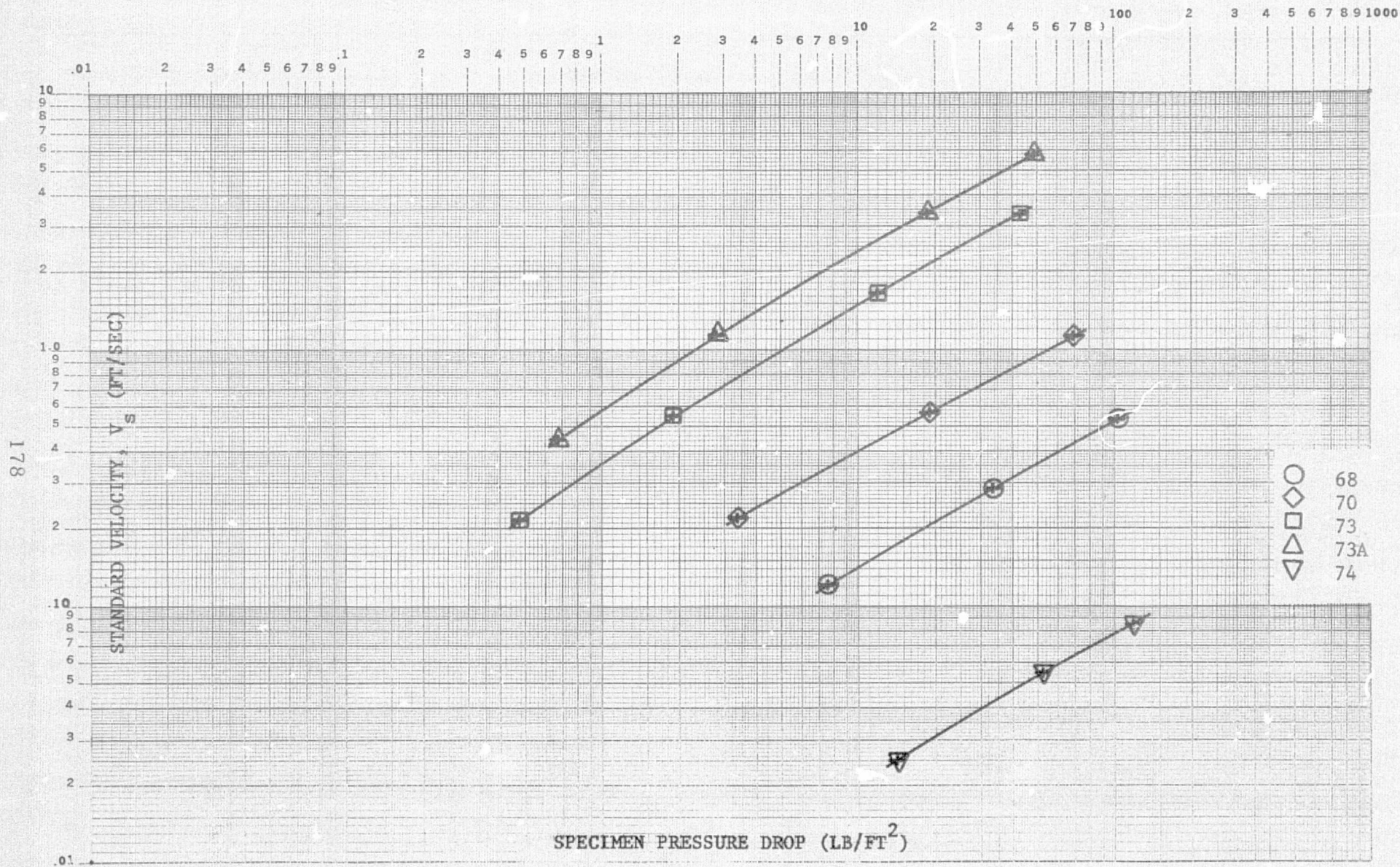


Figure D-11. Airflow Test Results

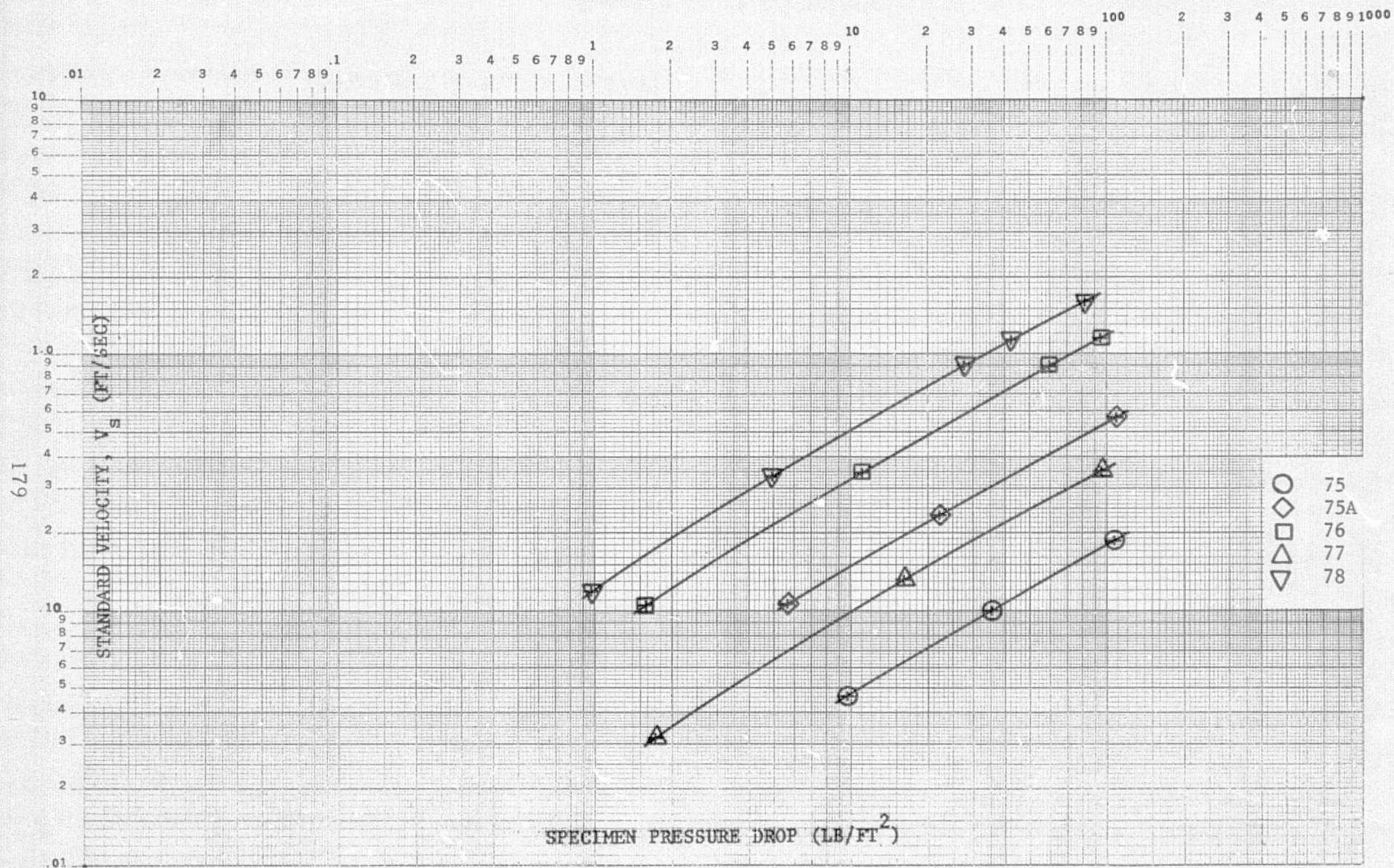


Figure D-12. Airflow Test Results



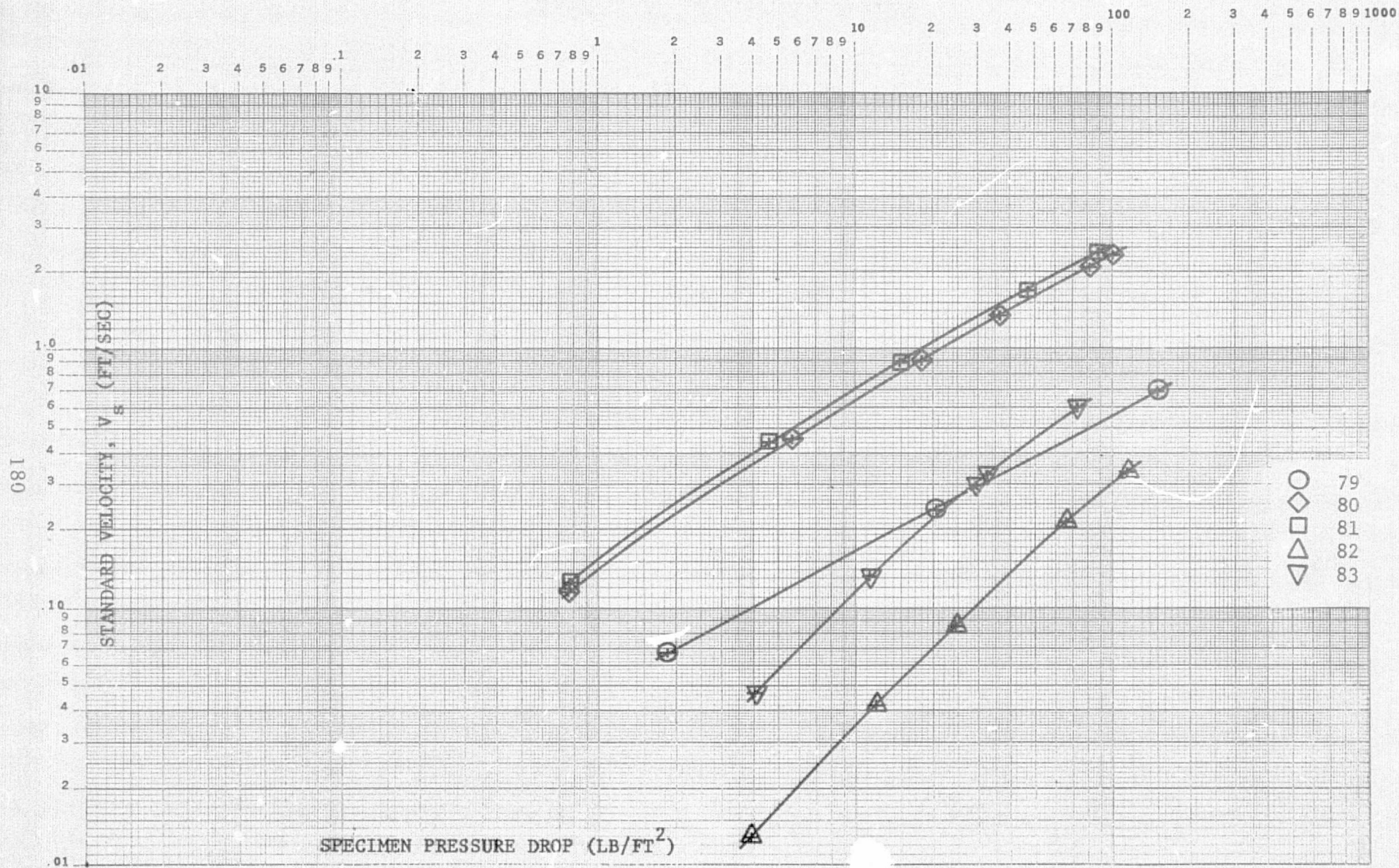


Figure D-13. Airflow Test Results

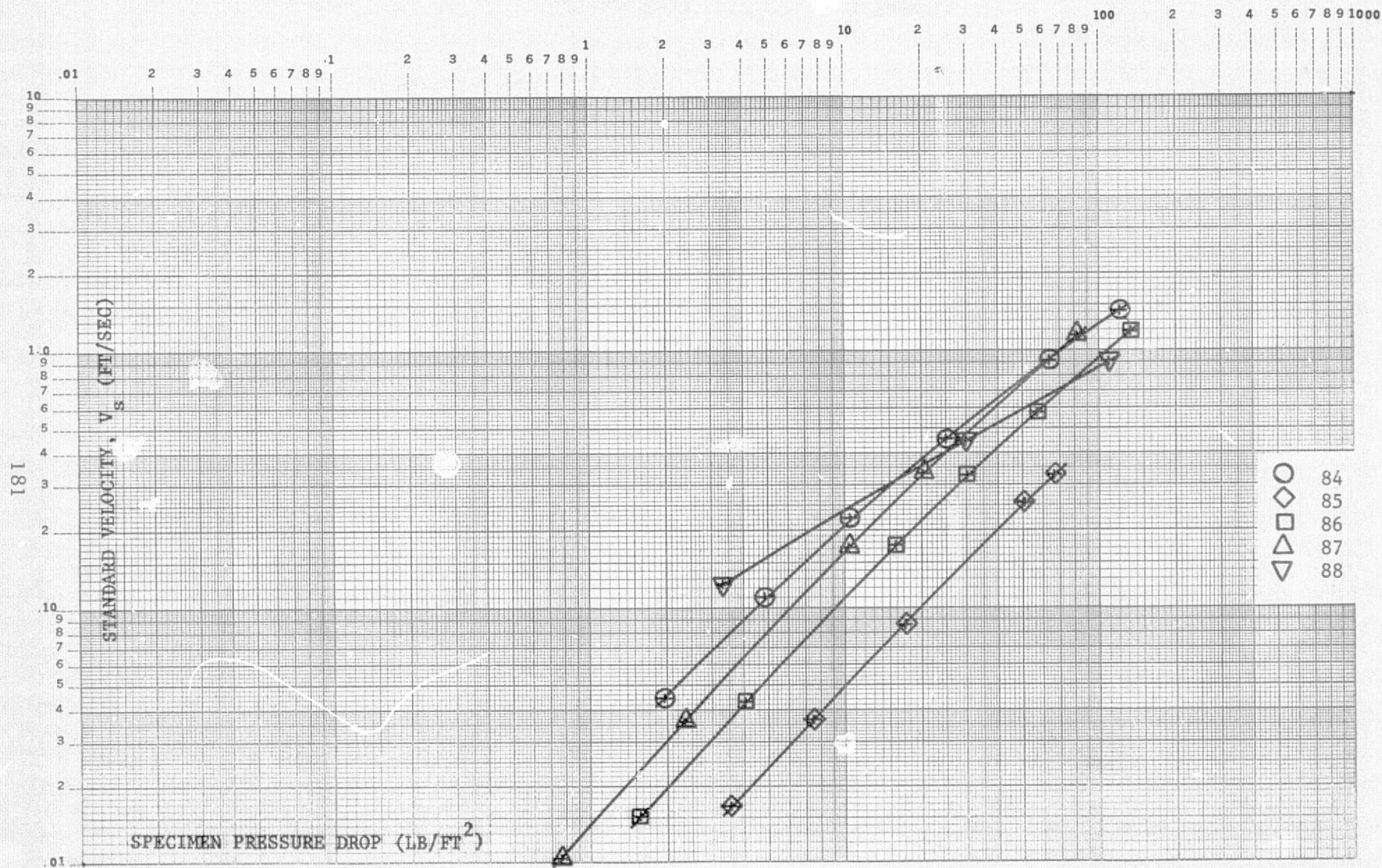


Figure D-14. Airflow Test Results



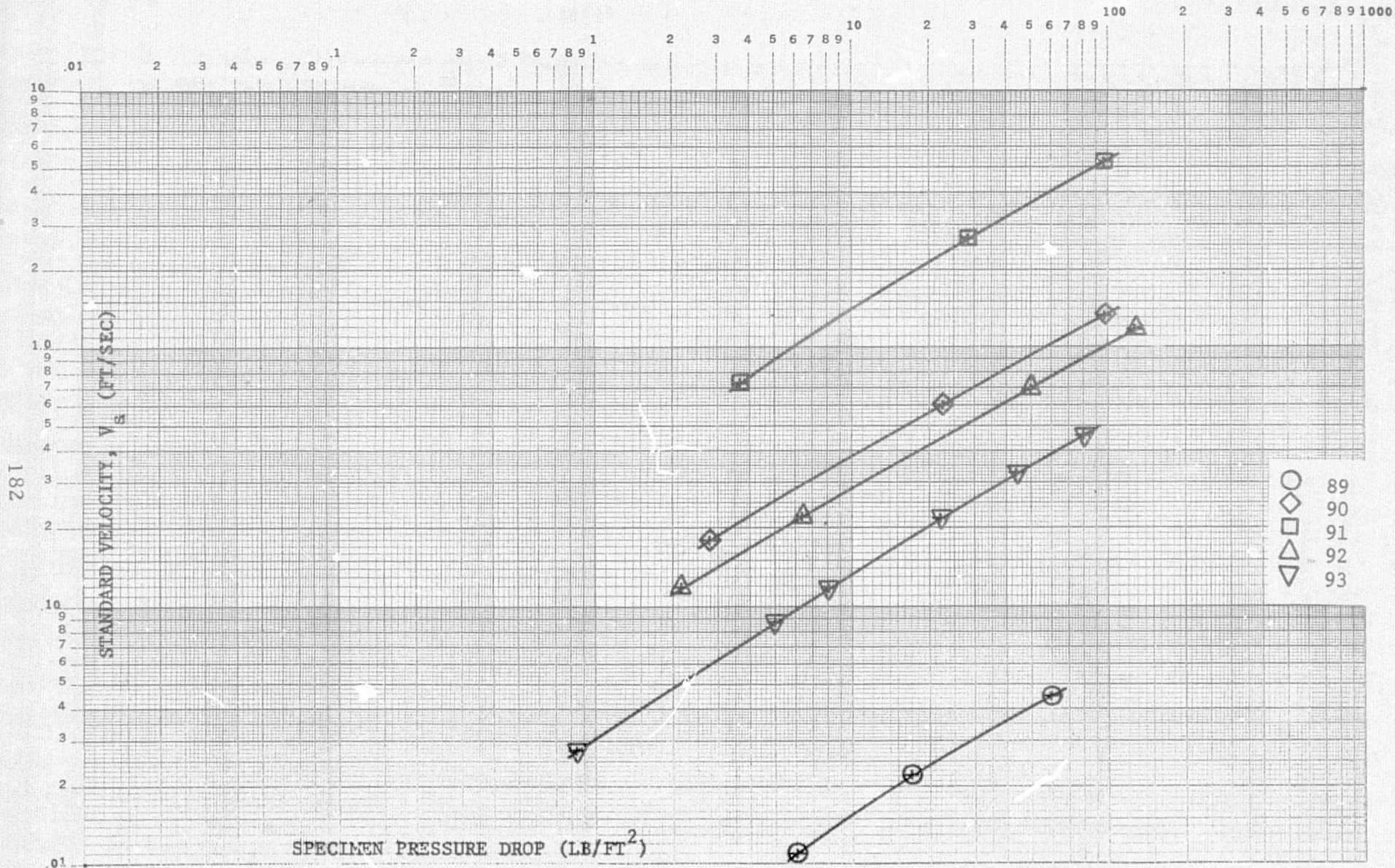


Figure D-15. Airflow Test Results

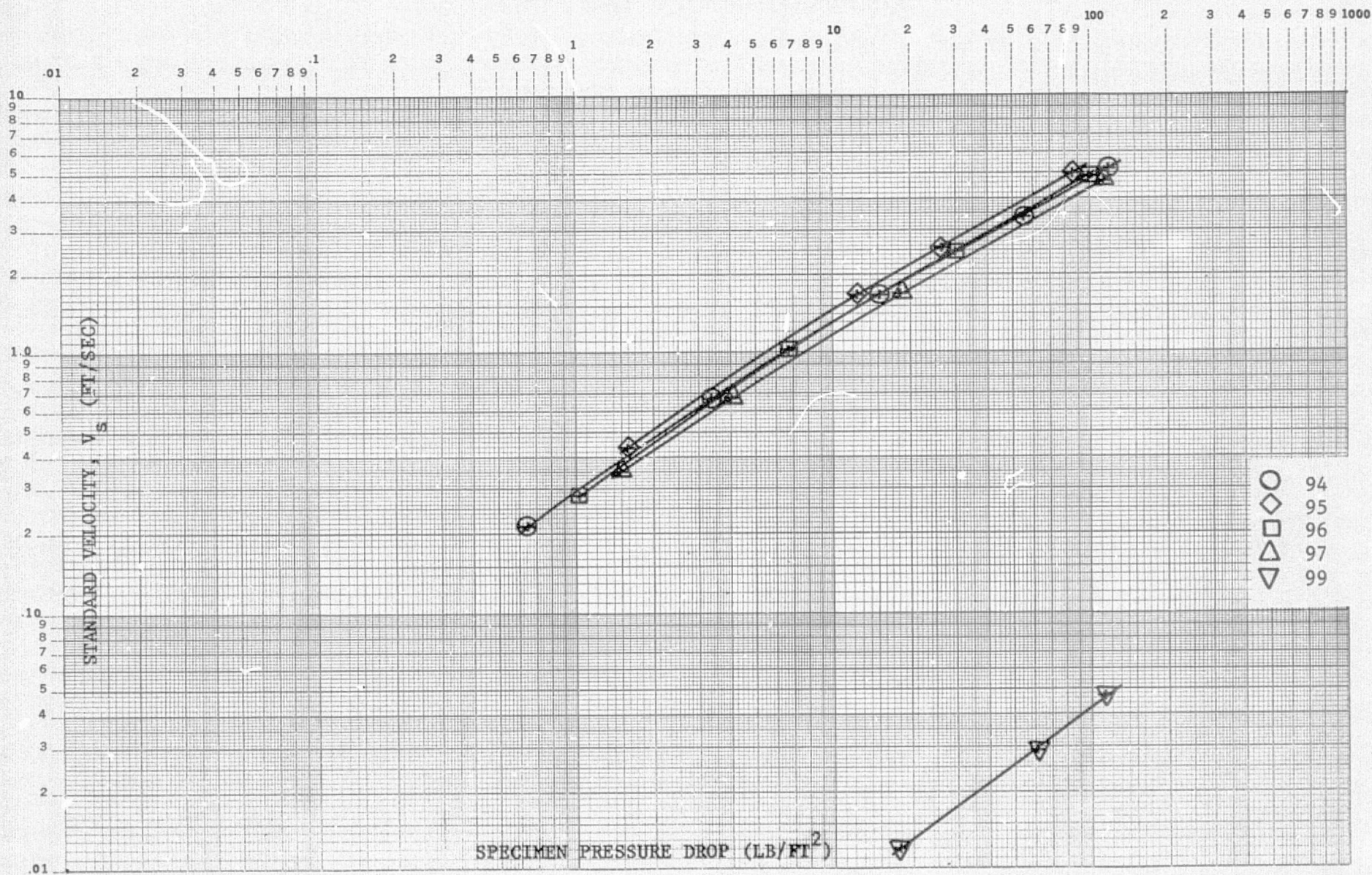


Figure D-16. Airflow Test Results



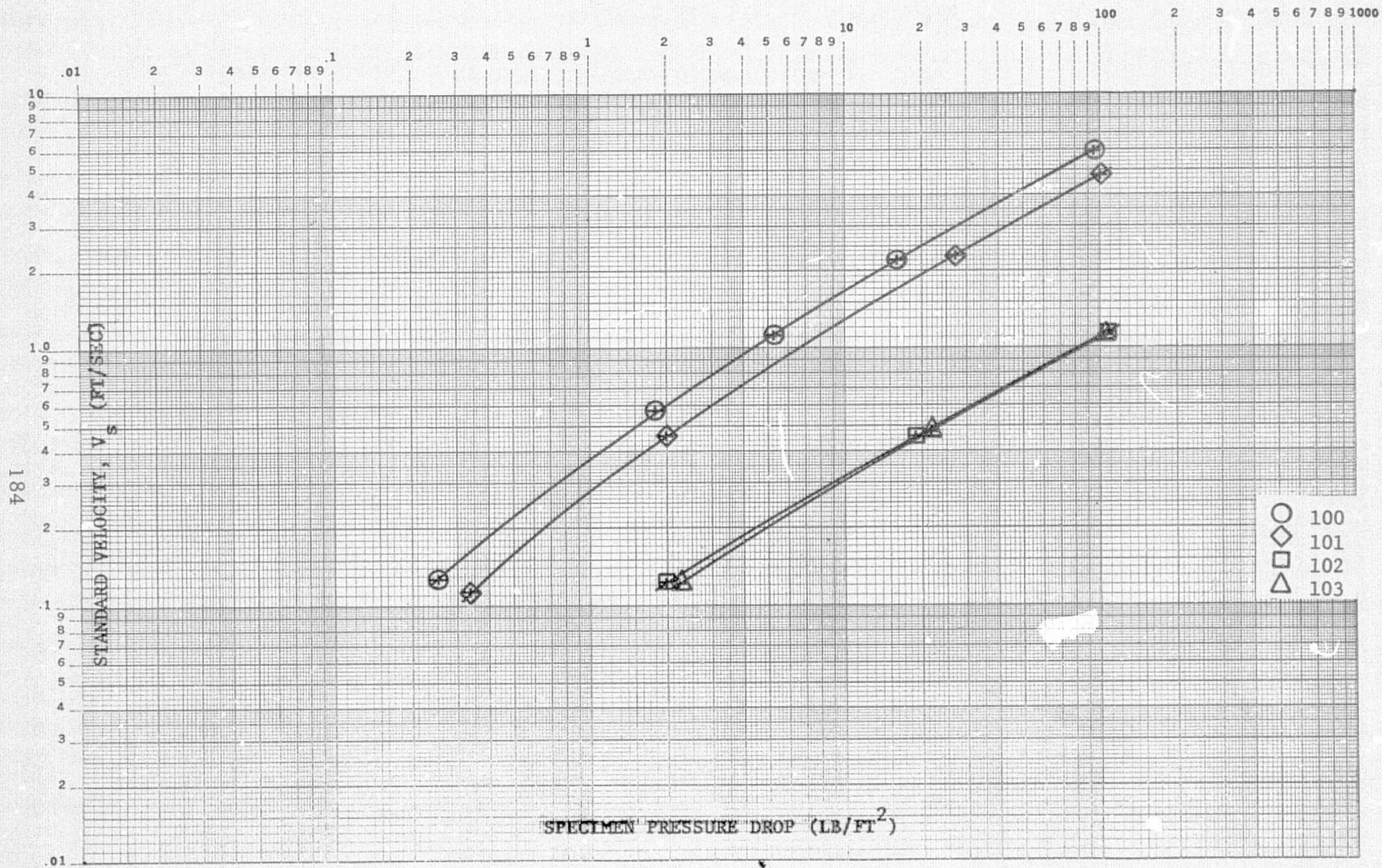


Figure D-17. Airflow Test Results

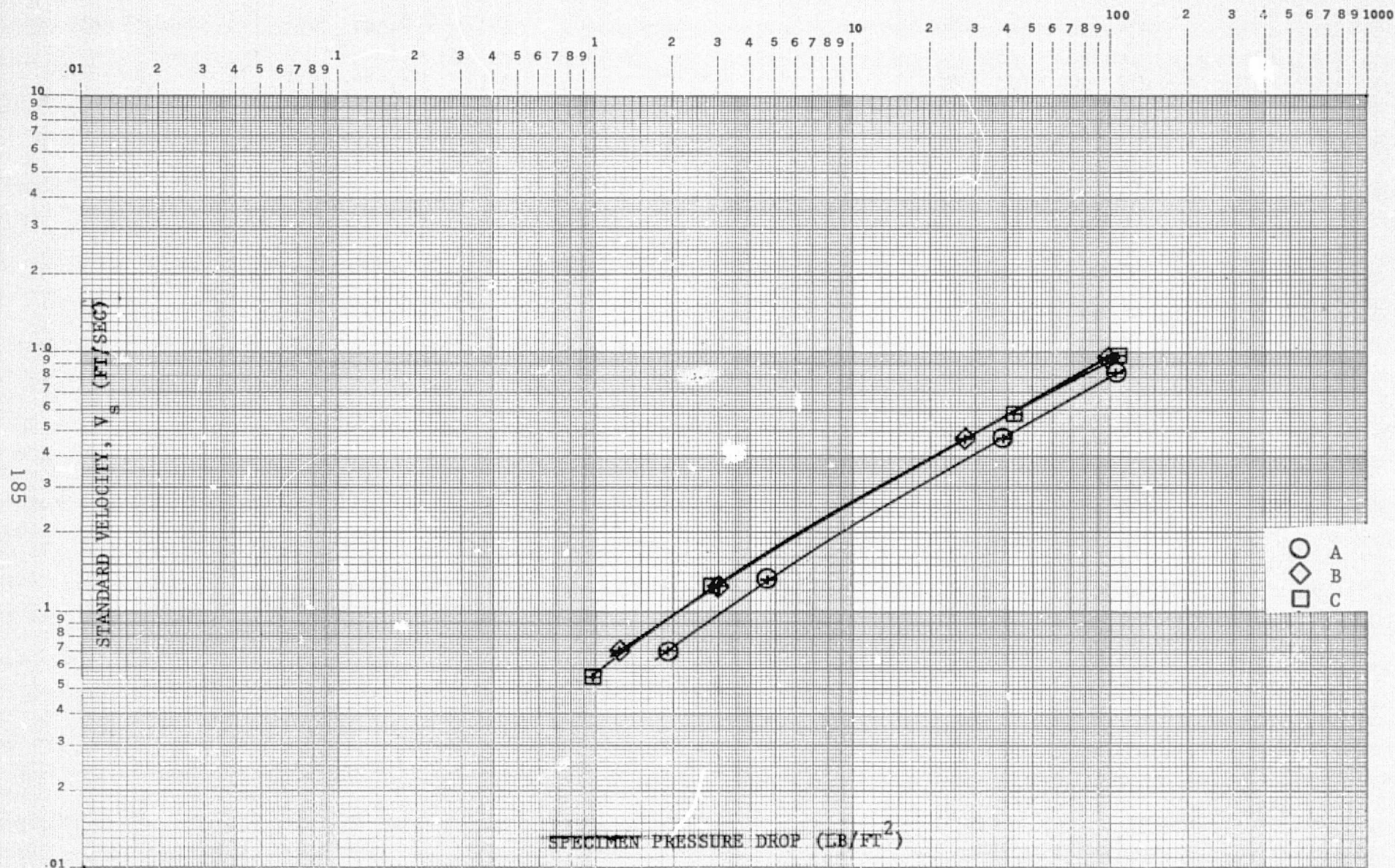


Figure D-18. Demonstrated Reproducibility of  
Composite Panels Using Specific Resin Control  
[0 90<sub>4</sub>] 120 [0 90<sub>4</sub>] Doweave



TABLE D-I  
DESCRIPTION OF PANEL CONSTRUCTION

PANEL NO. IDENTIFICATION	CONSTRUCTION D = NOW L = LENO M = MAT SUBSCRIPTS 181, 120, 143 DENOTE FABRIC	PLIES	THICKNESS (IN)	REMARKS
1	$[0_D / 30_D / -30_D / 90_D]_T$	4	.018	Cure 2 Hours 250°F
2	$[0_D / 45_L / -45_L / 90_D]_T$	4	.036	
3	$[0_D / 90_L / 0_L / 90_D]_T$	4	.034	
4	$[0_D / 30_D / 45_D / -45_D / -30_D / 90_D]_T$	6	.026	
5	$[0_D / 90_L / 45_L / -45_L / 0_L / 90_D]_T$	6	.056	
6	$[0_L / 30_L / 60_L / -60_L / -30_L / 90_L]_T$	6	.072	
7	$[0_L / 90_L]_T$	2	.030	
8	$[0_D / 30_D]_T$	2	.010	Cure 2 Hours 250°F
9	$[0_L / 45_L / -45_L / 90_L]_T$	4	.047	Cure 60M RT, 75M 175, 60M 265, 60M 350
10	$[0_L / 45_L / -45_L / 90_L]_M$	5	.048	
11	$[0_D / 45_D / -45_D / 90_D]_T$	4	.017	
12	$[0_D / 45_D / -45_D / 90_D]_M$	5	.018	60M RT, 75M 175, 60M 265, 60M 350
13	$[0_{181} / 90_{181}]_T$	2	.022	EB .008
14	$[0_{181} / 90_{181}]_3$	6	.062	EB .022

PANEL NO. IDENTIFICATION	CONSTRUCTION D = DOW L = LENO M = MAT SUBSCRIPTS 181, 120, 143 DENOTE FABRIC	PLIES	THICKNESS (IN)	REMARKS
15	$\left[0_L/90_L\right]_T$ MPP 21	3	.039	Cure 120M @ 250°F ↓
16	$\left[0_L/90_L\right]_T$ MPP 24	3	.036	
17	$\left[0_D/90_D\right]_2 + \text{MPP 21}$	5	.025	
18	$\left[0_D/90_D\right]_2 + \text{MPP 24}$	5	.022	
19	$\left[0_D/90_D\right]_4 + \text{MPP 21}$	9	.042	
20	$\left[0_D/90_D\right]_T + \text{M}$	3	.013	
21	$\left[0_D/90_D\right]_2$	4	.020	
22	$\left[0_D/90_D\right]_2$	5	.022	
23	$\left[0_D/90_D\right]_4$	8	.038	
24	$\left[0_D/90_D\right]_4$	9	.040	
25	$\left[0_L/90_L\right]_T + \text{M}$	3	.035	
26	$\left[0_L/90_L\right]_2$	4	.061	
27	$\left[0_L/90_L\right]_2$	5	.063	
28	$\left[0_L/-45_L/90_L/45_L\right]_T$	4	.060	



PANEL NO. IDENTIFICATION	CONSTRUCTION D = DOW    L = LENO    M = MAT SUBSCRIPTS 181, 120, 143 DENOTE FABRIC	PLIES	THICKNESS (IN)	REMARKS	
29	$\left[0_L / -45_L / 90_L / 45_L\right]_T^M$	5	.061	120M @ 250°F	
30	$\left[0_L / 90_L\right]_4$	8	.110		
31	$\left[0_L / -45_L / 90_L / 45_L\right]_2$	8	.113		
32	$\left[0_D / 90_D / 0_L / 90_D / 0_D / 90_L / 0_D / 90_D\right]_T$	8	.057		
80	$\left[0_D / 90_D\right]_5$	10	.044		
81	$\left[0_D / 90_D\right]_6$	12	.052		
LOCK CORE PANELS					
33	AVI #5 Section A #1 Edge Sealed		.469	180M @ 250°F	
34	AVI #5 Section B #2 Edge Sealed		.475		
35	AVI #5 Section A #3		.470		
36	AVI #5 Section B #4		.475		
37	AVI #5 Section C Top		.456		
38	AVI #5 Section C Bottom		.456		
92	AVI #9A Specimen C1 Edge Sealed		.456		
93	AVI #9A Specimen C2 Edge Sealed		.456		
ELECTRON BEAM DRILLED PANELS					
39	$\left[-60_{143} / 0_D / 60_{143}\right]_T^+ .007$ Titanium	4	.032	<u>SPACING</u> .135	<u>HOLE SIZE</u> .004
40	$\left[-60_{143} / 0_D / 60_{143}\right]_T^+ .007$ Titanium	4	.032	.243	.008

PANEL NO. IDENTIFICATION	CONSTRUCTION D = DOW L = LENO M = MAT SUBSCRIPTS 181, 120, 143 DENOTE FABRIC	PLIES	THICKNESS (IN)	REMARKS	
				<u>SPACING</u>	<u>HOLE SIZE</u>
41	$[-60_{143}/0_D / 60_{143}]_T$	3	.029	.135	.010
42	$[-60_{143}/0_D / 60_{143}]_T$	3	.029	.243	.018
43	$[-60_{143}/0_D / 60_{143}]_T$	3	.044	.135	.010
44	$[-60_{143}/0_D / 0_{143}/0_D / 60_{143}]_T$	5	.044	.243	.012
45	$[-60_{143}/0_D / 0_{143}/0_D / 60_{143}]_T$	5	.044	.135	.010
46	$[-60_{143}/0_D / 0_{143}/0_D / 60_{143}]_T$	5	.055	.135	.010
47	$[-60_{143}/+60_{143}/0_D]_s$	6	.055	.135	.010
48	$\begin{array}{c} \updownarrow \\ \downarrow \end{array}$		.055	.135	.018
49			.055	.135	.010
50		6	.055	.243	.018
51		3	.032	.135	.014
52	$\begin{array}{c} \downarrow \\ \downarrow \\ \downarrow \end{array}$		.032	.243	.026
53			.032	.135	.014
54			.032	.243	.026
55		5	.051	.135	.014
56			.051	.243	.026
57			.051	.135	.014
58			.051	.243	.026

PANEL NO. IDENTIFICATION	CONSTRUCTION D = DOW L = LENO M = MAT SUBSCRIPTS 181, 120, 143 DENOTE FABRIC	PLIES	THICKNESS (IN)	REMARKS
59	$[-60_{143} / 60_{143} / 0_D]_B$	6	.072	.135 .014
60			.072	.243 .026
61			.067	.135 .014
62			.067	.243 .026
63	$[0_L / 90_L]_T + M$	3	.034	90M 170°F + 120M 250°F
88	$[0_L / 90_L]_2$	4	.059	
89	$[0_L / 90_L]_2^M$	5	.060	
90	$[0_L / -45_L / 90_L / 45_L]_T$	4	.058	
91	$[0_L / -45_L / 90_L / 45_L]_T + M$	5	.059	
66	$[0_L / 90_L]_4$	8	.108	
67	$[0_L / -45_L / 90_L / 45_L]_2$	8	.109	
73	$[0_D / 90_D / 0_D]_T$	3	.036	90M 170°F + 120M 250°F
65	$[0_{120} / 90_D / 0_D]_T$	3	.016	90M 170°F, 120M 250, Arm Bot.
64	$[0_L / 45_L / 90_{120}]_T$	3	.037	90M 170°F, 120M @ 250°F
68	$[0_L / 90_L]_2$	4	.059	90M 170, 120 @ 250, Arm T&B
74	$[0_L / 90_L]_2 + M$	5	.060	



PANEL NO. IDENTIFICATION	CONSTRUCTION D = DOW L = LENO M = MAT SUBSCRIPTS 181, 120, 143 DENOTE FABRIC	PLIES	THICKNESS (IN)	REMARKS	
71	$\left[0_D/90_D\right]_{143T}$	3	.023	90M 170, 110M 250 BL. T&B	
72	$\left[0_D/90_D/143/90_D/0_D\right]_T$	5	.032		
69	$\left[0_L/90_L\right]_2$	4	.059		
75	$\left[0_L/90_L\right]_2 + M$	5	.060		
70	$\left[90_D/45_L/90_{120}\right]_T$	3	.026	90M 170, 120M 250 BL. T&B	
<u>ELECTRON BEAM DRILLED PANEL</u>				<u>SPACING</u>	<u>HOLE SIZE</u>
76	$\left[-60_{143}/0_D/0_{143}/0_D/60_{143}\right]_T + .007 \text{ Titanium}$	6	.048	.135	.012
77	" " " "		.048	.243	.012
78	$\left[-60_{143}/60_{143}/0_D\right]_S + .007 \text{ Ti.}$	7	.061	.135	.014
79	" " " "		.061	.243	.014
<u>DYNAPORE</u>	<u>PANEL NO.</u>				
82	603011 24 X 110 Mesh -2		.0117		
83	603012 24 X 110 Mesh -1		.0117		
84	603013 24 X 110 Mesh -1		.0120		

PANEL NO. IDENTIFICATION	CONSTRUCTION D = DOW L = LENO M = MAT SUBSCRIPTS 181, 120, 143 DENOTE FABRIC	PLIES	THICKNESS (IN)	REMARKS
85	603014 50 X 250 Mesh -1		.0062	
86	603015 50 X 250 Mesh -1		.0063	
87	603016 -1		.0065	
<u>ISOGRID PANEL</u>				
94	$\left[ 0_D / 90_D \right]_4$ , $\left[ 90_D / 0_D \right]_4$	16	.146	See Description in Sample Writeup.
95	$\left[ 0_D / 90_D \right]_4$ , $\left[ 90_D / 0_D \right]_4$ + MPP 21	17	.154	
96	$\left[ 0_D / 90_D \right]_4$ , $\left[ 90_D / 0_D \right]_4$ + MPP 24	17	.162	
97	$\left[ 0_D / 90_D \right]_4$ , $\left[ 90_D / 0_D \right]_4$	16	.158	
98	$\left[ 0_D / 90_D \right]_4$ , $\left[ 90_D / 0_D \right]_4$	16	.144	
107	$\left[ 0_D / 90_D \right]_4$ , $\left[ 0_D / 90_D \right]_4$	16	.140	
99	$\left[ 0_L / 90_L \right]_3$	6	.081	120M @ 250°F
100	AVI #10 Item 2 $\left[ 0_D / 90_D \right]_5$	10	.044	

PANEL NO. IDENTIFICATION	CONSTRUCTION D = DOW    L = LENO    M = MAT SUBSCRIPTS 181, 120, 143 DENOTE FABRIC	PLIES	THICKNESS (IN)	REMARKS
101	AVI #10 Item 2 $\left[ \begin{smallmatrix} 0_D / 90_D \end{smallmatrix} \right]_5$	10	.044	120M @ 250°F  ↓
102	AVI #10 Item 4 $\left[ \begin{smallmatrix} 0_D / 90_D \end{smallmatrix} \right]_5 + M$	11	.045	
103	AVI #10 Item 5 $\left[ \begin{smallmatrix} 0_D / 90_D \end{smallmatrix} \right]_6 + M$	13	.054	
<u>LOCK CORE</u>				
104	AVI # 4 and 5 Section A	22	}	Autoclave Cure
105	AVI # 4 and #5 Section C	19		90M @ 170°F
106	AVI #4 and #5 Section C + MFP #21	20		120M @ 250°F at 50 PSI.

DEVELOPMENT OF THE TECHNOLOGY FOR THE FABRICATION OF RELIABLE LAMINAR FLOW CONTROL PANELS  
IDENTIFICATION OF LAMINAR FLOW CONTROL SURFACE MATERIAL PANELS SUBMITTED TO NASA LANGLEY  
IN COMPLIANCE WITH CONTRACT NAS1-14408 - FOR PRELIMINARY STRUCTURAL TESTING

TEST PANEL NO.		PLIES	THICK- NESS (IN)	HOLE SIZE	HOLE SPACING	MAT/ PLATING	PROCESSING
<u>ELECTRON BEAM DRILLED</u>							
43A	$\left[ -60_{143}^{\circ} / 0_D^{\circ} / 60_{143}^{\circ} \right]_T$	3	.029	.018	.135		120 Min @ 250°F
47A	$\left[ -60_{143} / 60_{143} / 0_D \right]_S$	6	.055	.010	.135		
48A	" " "	6	.055	.018	.243		
53A	$\left[ -60_{143} / 0_D / 60_{143} \right]_T$	3	.032	.014	.135		
54A	" " "	3	.032	.026	.243		
57A	$\left[ -60_{143} / 0_D / 0_{143} / 0_D / 60_{143} \right]_T$	5	.051	.014	.135		
58A	" " "	5	.051	.026	.243		
61A	$\left[ -60_{143} + 60_{143} 0_D \right]_S$	6	.067	.014	.135		
62A	" " "	6	.067	.026	.243		
39A	$\left[ -60_{143} / 0_D / 60_{143} \right] + .007 \text{ Ti}$	4	.032	.004	.135	.007 Ti	
40A	" " "	4	.032	.008	.243	.007 Ti	
see page two							

TEST PANEL NO.		PLIES	THICK- NESS (IN)	HOLE SIZE	HOLE SPACING	MAT/ PLATING	PROCESSING
<u>DYNAPORE</u>							
82A	24 X 110 Mesh	1	.0117	NA	.042 X 809		Compaction/Sinter/Compaction
83A		1	.0120				
84A		1	.0123				
85A	50 X 250 Mesh	1	.0062		.020 X .004		
86A		1	.0063				
87A		1	.0065				
<u>LENCE LEAVE</u>							
7A	$[0_L/90_L]_T$	2	.030				120 Min. @ 250°F (1)
26A	$[0_L/90_L]_2$	4	.061				
28A	$[0_L/-45_L/90_L/45_L]_T$	4	.060				
63A	$[0_L/90_L]_T^M$	3	.034				90 Min @ 170°F + 120 Min @ 250°F (1)
68A	$[0_L/90_L]_2$	4	.059				90 Min @ 170°F + 120 Min @ 250°F (2)
74A	$[0_L/90_L]_2^M$	5	.060				
75A	$[0_L/90_L]_2^M$	5	.060				90 Min @ 170°F + 120 Min @ 250°F (3)
88A	$[0_L/90_L]_2$	4	.059				90 Min @ 170°F + 120 Min @ 250°F (1)
89A	$[0_L/90_L]_2^M$	5	.060				
90A	$[0_L/-45_L/90_L/45_L]_T$	4	.058				
91A	$[0_L/-45_L/90_L/45_L]_T^M$	5	.059				
99A	$[0_L/90_L]_3$	6	.081				120 Min @ 250°F (1)



TEST PANEL NO.		PLIES	THICK- NESS (IN)	HOLE SIZE	HOLE SPACING	MAT/ PLATING	PROCESSING
<u>DOWEAVE</u>							
17A	$[0_D/90_D]_2$ MPP #21	5	.025				120 Min @ 250°F <sup>(1)</sup>
18A	$[0_D/90_D]_2$ MPP #24	5	.022				
19A	$[0_D/90_D]_4$ MPP #21	9	.042				
20A	$[0_D/90_D]_T^M$	3	.013				
21A	$[0_D/90_D]_2$	4	.020				
22A	$[0_D/90_D]_2^M$	5	.022				90 Min @ 170°F + 120 Min @ 250°F <sup>(2)</sup>
23A	$[0_D/90_D]_4$	8	.038				
24A	$[0_D/90_D]_4^M$	9	.040				
65A	$[0_{120}/90_D/0_D]_T$	3	.016				
71A	$[0_D/90_D/143]_T$	3	.023				
73A	$[0_D/90_D]_4$	8	.036				90 Min @ 170°F + 120 Min @ 250°F <sup>(3)</sup>
100A	$[0_D/90_D]_5$	10	.044				90 Min @ 170°F + 120 Min @ 250°F <sup>(1)</sup>
101A	$[0_D/90_D]_6$	12	.050				120 Min @ 250°F <sup>(1)</sup>
102A	$[0_D/90_D]_5^M$	11	.045				
103A	$[0_D/90_D]_6^M$	13	.054				

TEST PANEL NO.		PLIES	THICK- NESS (IN)	HOLE SIZE	HOLE SPACING	MAT/ PLATING	PROCESSING
<u>STIFFENED PANELS</u>							
35A	Lock Core* (#73 Face Sheet Both Sides).						180 Min @ 250°F
36A	Lock Core* (#73 Face Sheets One Side, 3 Ply 181 Glass Fabric To Be Drilled).						
38A	Lock Core* (#73 Face Sheet Both Sides + #120 Fabric Strips).						
104A	(Duplicate of 35A).						Autoclave (See Attached Writeup) 90 Min @ 170°F 120 Min @ 250°F 50 psi
105A	#73 Face Sheet, One Side 3-Ply 181 Glass Fabric.						Autoclave Cure
106A	Lock Core* (#73 Face Sheet One Side, 3 Ply 181 Glass Fabric +MPP on One Side).						Autoclave Cure
107A	Isogrid** (#73 Face Sheet, On Both Sides).						
NOTE: (*) $\left[ \begin{matrix} 0/90_D \end{matrix} \right]_3$ Doweave Truss Webs. (**) .05 X .05 Kevlar Roving Grid CSA @ h = 2.25 inch.							

SAMPLE  
NO.

A	Plain Leno Material
B	Plan Dow Material
C	Preimpregnated Leno Material (Uncured)
D	Preimpregnated Dow Material (Uncured)
E	Microperforated Plate #24 316 Stainless (Michigan Dynamics #406251)
F	Microperforated Plate #21 316 Stainless (Michigan Dynamics #406121)
G	120 Kevlar Preimpregnated (Uncured)
H	143 Kevlar Preimpregnated (Uncured)
I	.07 Nylon Mat Calendared.

---

Superscript (1) Armalon and bleeder top only.  
(2) Armalon top and bottom, bleeder top only.  
(3) Armalon and bleeder top and bottom.

TABLE D-III

## PANELS ASSOCIATED WITH TYPICAL COMPARISONS

ELECTRON BEAM DRILLED PANELS  
THICKNESS EFFECTS AND HOLE SIZING

<u>Panel No.</u>	<u>Thickness</u>	
43	.029	} .135 hole spacing .010 hole size
47	.055	
53	.032	} .135 hole spacing .014 hole size
57	.051	
61	.067	
54	.032	} .243 hole spacing .026 hole size
58	.051	
62	.067	
47	.055	} .135 hole spacing .010 hole size
48	.055	
		} .243 hole spacing .018 hole size

DYNAPORE  
THICKNESS EFFECTS AND HOLE SPACING

82  
83  
84  
85  
86  
87

LENO WEAVE PANELS  
THICKNESS EFFECTS

7	.030	} No Mat
26	.061	
99	.081	
63	.034	} Mat
89	.060	

LENO WEAVE PANELS  
EFFECT OF DIRECTION OF LAYUP

<u>Panel No.</u>	<u>Thickness</u>
88	} ~ .060 thick
89	
90	
91	

LENO WEAVE PANELS  
EFFECT OF CURE CYCLE

89  
74  
75

DOWEAVE PANELS  
THICKNESS EFFECTS

21	.020	} With Mat
23	.038	
100	.044	
101	.050	
20	.013	
22	.022	
24	.040	}
102	.045	
103	.054	

DOWEAVE PANELS  
MICROPERFORATED PLATE EFFECTS

17	.025	} 5 Ply
18	.022	
19	.042	} 9 Ply

DOWEAVE PANELS  
PROCESSING EFFECTS

20  
65  
71



TABLE D-IV  
PANEL FABRICATION DESCRIPTION

The material used for this program was Dupont's Kevlar impregnated with Dupont's Corlar 5134 F, a modified epoxy system. Due to limited availability within the span of the contract the choice of weaves was limited to two types:

- Kevlar 49 Leno Weave #205  
as shown by Sample #A.
- Basic Doweave 200 Denier Kevlar 29 as  
shown by Sample #B.

Both materials were preimpregnated by Dupont with Corlar 5134 F, a modified epoxy system. This resin is flame-retardant, cures at 250°F and is flow controlled. Sample C shows the impregnated Leno 205 weave. Note the uneven resin distribution which occurred due to the shortage of available fabric as well as the limited available time.

The resin distribution on the 200 Denier Doweave is more even as shown on Sample D.

For the grid structure of the isogrid, Sample #107A, Kevlar 29 Roving, 7100 Denier was used. The impregnating material for the roving was Corlar 5134F Resin. The impregnated Roving was staged for 2 minutes at 235°F prior to use.\*

Several of the samples require explanations:

Lock Core Samples #104A, #105A and #106A are the only samples cured in an autoclave under 50 psi for 90 minutes at 170°F and 120 minutes at 250°F. Due to the higher pressure the porosity was reduced considerably. The samples were finished in time for complete airflow testing.

Samples #105 and #106A were not separated to show the smooth transition where the microperforated plate was added.

The splotchy appearance of Samples #57A, #58A, #61A and #62A was caused by chem-milling off the aluminum caul sheet which accidentally did not release from the laminate. A scheduled vacation shutdown at Farrel Co. precluded fabrication of a new laminate on time.

The facing mat used on some of the samples is:

Cerex Nylon Mat, Calendared 0.7 Oz/Yd<sup>2</sup>  
from Monsanto, St. Louis.

---

Note (\*): The grid was cured for 4 hours at 350°F in order to obtain sufficient pressure with the silicone rubber mold. Although both face skins consist of 8 plies 0° 90° Downave 6 ply layers of each face were precured under vacuum pressure at 250°F for 2 hours. The remainir : 2 plies of each skin were used to bond the precured faces to the precured grid under vacuum pressure at 250°F for 2 hours.